IMPACT OF NOMINAL SIGNAL DEFORMATIONS
ON SATELLITE NAVIGATION SYSTEMS

A DISSERTATION
SUBMITTED TO THE DEPARTMENT OF ELECTRICAL ENGINEERING
AND THE COMMITTEE ON GRADUATE STUDIES
OF STANFORD UNIVERSITY
IN PARTIAL FULFILLMENT OF THE REQUIREMENTS
FOR THE DEGREE OF
DOCTOR OF PHILOSOPHY

Gabriel Hoong Wen Wong

June 2014

This dissertation is online at: http://purl.stanford.edu/wy655jp2867

I certify that I have read this dissertation and that, in my opinion, it is fully adequate in scope and quality as a dissertation for the degree of Doctor of Philosophy.

(Per Enge) Principal Adviser

I certify that I have read this dissertation and that, in my opinion, it is fully adequate in scope and quality as a dissertation for the degree of Doctor of Philosophy.

(Joseph M Kahn)
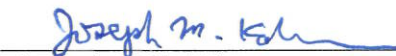
I certify that I have read this dissertation and that, in my opinion, it is fully adequate in scope and quality as a dissertation for the degree of Doctor of Philosophy.

(Todd Walter)

Approved for the Stanford University Committee on Graduate Studies

ABSTRACT

Global Navigation Satellite Systems (GNSS), of which GPS is the standard-bearer, are ubiquitous and widely used in various applications including aviation, agriculture, automobile navigation, search and rescue, and recreation. GNSS are steadily being improved with the addition of new constellations, new frequencies, and new signals. Future multi-frequency GNSS will eliminate one of the largest error sources (ionosphere) and promises even better performance: improving accuracy from approximately 5 meters to 1 meter.

Unfortunately, the new frequencies and signals will have small but unavoidable biases relative to one another. The impact of these biases increases as other error sources are eliminated. Nominal satellite signal deformations − deviations of broadcast GPS satellite signals from ideal − result in tracking errors, range biases, and position errors in GPS receivers. It is thus imperative that these errors are quantified, to enable the design of appropriate error budgets and mitigation strategies for various application fields.

Traditional measurement methods for these signal deformations can be broadly classified into two categories. The first category uses large antenna dishes paired with high-resolution, high-bandwidth measurements and is limited to short time intervals (seconds) due to data storage constraints. However, these measurements could be subject to time-varying effects that are unobservable between data sets. The second category uses lower-resolution, lower bandwidth measurements over long continuous

time periods, but less effectively attenuates error sources such as multipath that obscure the signal deformations of interest.

The major contribution in this dissertation is the development of an innovative measurement method that combines the merits of both past approaches while mitigating the disadvantages, rendering nominal signal deformations measurable. Furthermore, these measurements were repeatable over long time periods of hours, days, and months. A good estimate of the position error impact on user receivers could be obtained using these highly consistent measurements. A mitigation strategy was developed in response and verified using this measurement method. The results show that the position error impact could be substantial, but could also be effectively mitigated with the use of an appropriate mitigation strategy. This work is a critical component toward the successful implementation of future dual-frequency GNSS-based landing systems for aviation.

ACKNOWLEDGEMENTS

My research accomplishments would have been difficult, if not impossible, without the generous help of the many wonderful people I have been blessed to know.

My heartfelt gratitude starts with Prof Per Enge. Prof Enge has been like the GNSS signals he researches: always there to provide inspiration and guidance from on high to the lost. Through his guidance, I have learnt how not to lose sight of the big picture and how to carry out impactful research. I could not have asked for a better advisor, both to work for and to emulate.

I would also like to thank Dr Todd Walter, who has so generously shared with me his encyclopedic knowledge and experience in WAAS. Dr Walter operates on a literally open door policy - always available to provide suggestions, insights and perspectives.

I am also grateful to Prof Joseph Kahn, who first introduced me to the fascinating world of Signals and Systems during my undergraduate days, and for agreeing to be my oral defense committee member and thesis reader.

I also want to show my appreciation to Prof Teresa Meng and Prof Thomas Kenny for agreeing to be in my oral defense committee. Thank you, Prof Meng, for providing precious feedback to my research during the defense, and to Prof Kenny, for chairing the committee.

CONTENTS

LIST OF TABLES

LIST OF FIGURES

Chapter 1

Introduction

1.1 Overview

Global Navigation Satellite Systems (GNSS), particularly the Global Positioning System (GPS), are widely used today in various applications such as agriculture, automobile navigation, search and rescue, and recreation.

To enable GPS to be safely used for aviation, augmentation systems are necessary. In the US, the Wide Area Augmentation System (WAAS) serves this function, enabling GPS to meet stringent standards of accuracy, availability, continuity, and integrity. Pilots can now rely on the augmented system for all phases of flight, from en route down to airport approach [1].

WAAS requires that the different error sources are measured, corrected, or otherwise mitigated. This ensures that error residuals are bounded to extremely high levels of confidence (99.99999%). A summary of these errors, and their mitigation, are found in Table 1-1; they are discussed in greater detail in Chapter 2.

Category	Error	Mitigation
Receiver-independent	Clock Ephemeris Ionosphere Troposphere	Differential-GPS
Receiver-dependent	Radio Frequency Interference (RFI) Receiver White Noise	Time-Averaging
	Multipath	Time-Averaging Antenna/ Environment
	Measurement Equipment Time-varying errors (Seen mainly in dish antennas)	Calibration Repeated measurements Cross-verification
	Signal Deformation Range Biases (Signal of Interest)	**Specially-Configured Receivers**

Table 1-1: Measurement Errors and Mitigation

One of the largest error sources is the ionospheric error. These errors can be as large as 1-10 m at mid-latitudes, and even up to 30 m (slant range) in equatorial regions in the midst of an ionospheric storm. In the near future, GPS satellite signals will be transmitted at the L5 (1176.45 MHz) frequency, in addition to the current L1 (1575.42 MHz) frequency. A linear combination of these dual-frequency ranges eliminates the ionospheric error, since this error is a known function of frequency.

Unfortunately, this linear combination will also amplify the satellite signal deformation range biases, a previously small error originating from on-board satellite transmission hardware. With the removal of the ionospheric errors, and the resultant amplication of the satellite signal deformation range biases, these biases are now a significant contributor to the overall error budget. These biases will need to be quantified and mitigated to avoid limiting the future performance of WAAS.

Past measurement methods for satellite signal deformation range biases contained limitations such as time-varying drift effects, short-term noises, and insufficient attenuation of multipath. This necessitated the development of an innovative hybrid method, overcoming past limitations, to render satellite signal deformation range biases observable and measurable (Chapter 3).

Using the measured range biases, the unmitigated impact on user position errors could be quantified (Chapter 4). A mitigation method is proposed and verified to be effective using the new measurement method (Chapter 5).

In the rest of this introductory chapter, Section 1.2 highlights why it is important, yet difficult, to measure and mitigate satellite signal deformation range biases, particularly in aviation applications. Section 1.3 details past work by other researchers in this research area, and Section 1.4 describes the contributions of this dissertation. Section 1.5 outlines how satellite signal deformation range biases will be measured and mitigated in the rest of this dissertation.

1.2   Motivation and Challenges

For the current single-frequency L1-only GPS positioning (Figure 1-1), WAAS assumes that the nominal satellite signal deformation range biases are small. This is a reasonable assumption as the worst case ionospheric errors are much larger and dominant.
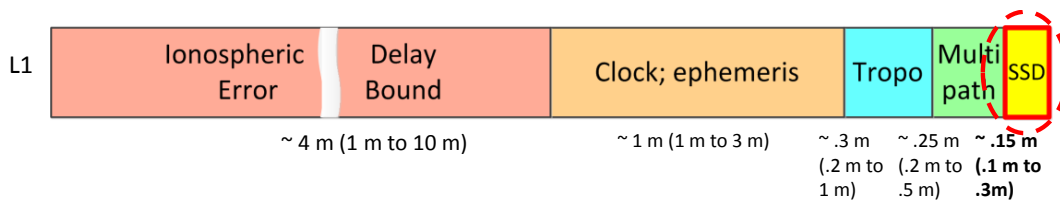
Figure 1-1: Range Error Contributions for single frequency L1-only GPS signal

Future dual-frequency WAAS allows aviation users to use dual-frequency ranging to eliminate the ionospheric error. However, in so doing, the impact of these range biases will be amplified by the dual-frequency ionosphere-error-removal scale factor of 2.6

or larger (Refer to Section 2.4.4 Equations (2.29) and (2.32)). Satellite signal deformation range biases now make up a larger proportion of a smaller error budget. Left unquantified and unmitigated, future WAAS performance may be limited by these biases (Figure 1-2).
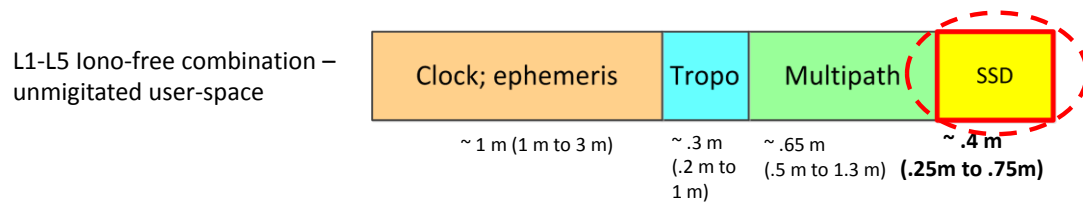
Figure 1-2: Range Error Contributions for unmitigated dual frequency L1/L5 GPS

The goal of this research is to measure and mitigate the satellite signal deformation range biases, to reap the benefits of dual-frequency navigation without paying the penalty of increased vulnerability to these biases (Figure 1-3). This requires overcoming some thorny challenges.
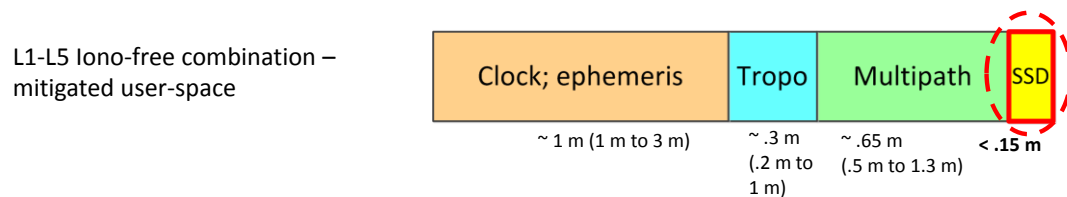
Figure 1-3: Range Error Contributions for mitigated dual frequency L1/L5 GPS

1.2.1   Measurement Challenges

Measuring the satellite signal deformation range biases is challenging for a number of reasons. Low multipath measurements from the actual, airborne environment are relatively inaccessible; instead, what are accessible are ground measurements that contain higher levels of multipath. As a result, the satellite signal deformation biases are often concealed by the multipath. Furthermore, the biases may vary with different antennas, receiver filters, and correlator spacings, further complicating the measurement process.

1.2.2   Mitigation Challenge

One of most effective ways to reduce user range errors, including satellite signal deformation range biases, is to constrain user receiver configurations to closely, if not identically, match that of WAAS reference receivers. In this case, differential-GPS would eliminate much of the error (Section 2.4.4).

Unfortunately, many of the legacy user receivers were designed and deployed before the research community was aware of the satellite signal deformation threat; these legacy user receivers have configurations that could be quite different from that of the WAAS reference receivers [2].

In the mitigation of satellite signal range biases, the challenge is to enable the largest user receiver design space, while preserving accuracy, availability, and integrity for

both single-frequency L1-only legacy users as well as new dual-frequency L1/L5 users (Refer to Section 2.5).

1.3   Previous Work

The research community was first alerted in 1993 to satellite signal anomalies caused by faulty satellite hardware [3], [4], [5].. Vertical position errors as large as 8 m resulted when the faulty signal from SVN 19 was used in position computation by ground GPS receivers [6], [7].

This new phenomenon, then widely known as (Satellite) Signal Deformation, sparked much new research [8], [9], [10], [11], [12], and [13] which continues today [14]. Alexander Mitelman carried out detailed investigations into the likely causes of the fault [7]. Eric Phelts and Per Enge postulated a second order threat model (2OS) with analog and digital satellite distortion fault modes [15]. Eric Phelts analyzed the anomalous satellite signal deformations and their worst case effects on WAAS receivers, and proposed effective fault monitoring and mitigation strategies which would require minimal modifications to existing GPS hardware [16].

The use of large satellite dish measurement instruments was key to the investigation efforts. Dennis Akos and Alexander Mitelman developed efficacious techniques combining the use of the satellite dishes with specialized low-noise, high bandwidth

vector spectrum analyzers [17]. Marco Pini and Dennis Akos demonstrated the use of innovative techniques to enhance observability of satellite signal distortions [18], [19].

Researchers also observed analog and digital satellite signal distortions present under regular, unfaulted working conditions. These distortions would result in range biases and position errors. Mitelman provided early satellite dish measurements of nominal analog and digital satellite signal distortions [20]. Chris Hegarty analyzed the effects of digital distortions on range biases for receivers with different correlator spacings and proposed recommended distortion requirements [21].

Concurrently, Honeywell researchers Mats Brenner and Liu Fan published early observations of nominal analog and digital satellite signal distortions using hemispherical, "all-in-view," low-multipath antennas connected to conventional receivers [8], [22], [23]. More recently, Ohio University researchers Sanjeev Gunawardena and Frank van Graas observed nominal distortions, also using hemispherical, "all-in-view," low-multipath antennas, but connected to software GNSS receivers [24], [14].

However, evaluation of these methods showed that there were inherent time-varying effects in large satellite dishes (Section 3.5.2), and multipath magnitudes on the order of the nominal range biases (Section 3.6.2) in hemispherical antenna measurements, which these methods were not directed at mitigating. As a consequence, it was a challenge to quantify how large the biases were and their resultant impact on user

position errors. Without an accurate measurement method, it was also difficult to propose and verify the effectiveness of mitigation strategies.

1.4   Contributions

The research contributions are as follows:

- <u>Render nominal satellite signal deformation measurable</u>

The main goal of this research was to render nominal satellite signal deformation range biases measurable. This required:

  - o   Determining the nature of the measurement errors inherent in legacy methods
  - o   Developing innovative hybrid "Measure-and-Verify" method to mitigate these measurement errors

The resultant measurement method produced results that showed reduced multipath and demonstrated repeatability over almost a year.

- <u>Quantify Impact on Aviation</u>

The satellite signal deformation range bias measurements were used to analyze and determine the unmitigated impact of nominal satellite signal deformation on aviation users. These included single-frequency L1-only, single-frequency L5-only, and dual-frequency L1/L5 users.

- Demonstrated an effective mitigation strategy

The novel "Measure-and-Verify" measurement technique also facilitated the demonstration of an effective mitigation strategy, which reduced errors by up to an order of magnitude.

The hybrid measurement technique and mitigation strategies are further extendible to signals from multi-frequency, multi-GNSS configurations. This will be useful given the ubiquity of such signals in the near future.

1.5   Dissertation Outline

In the rest of this dissertation, Chapter 2 introduces the use of GNSS for Aviation, focusing particularly on the senior GPS system. The basic signal structure, receiver operations, error sources, and common mitigation techniques are described. In particular, Chapter 2 discusses how nominal satellite signal deformation would result in range biases, which in turn cause position errors. These position errors are discussed keeping in mind the stringent requirements imposed on GNSS for aviation applications; these stringent aviation requirements are also introduced.

Chapter 3 articulates the main contribution of the dissertation – the accurate quantification of Satellite Signal Deformation range biases. Measurement results, errors, and limitations of the two legacy measurement methods as well as the novel hybrid measurement method are discussed. Consistent and repeatable measurement

results are presented for the single-frequency L1-only, single-frequency L5-only, and dual-frequency L1/L5 signals.

Chapter 4 analyzes and determines the resultant user vertical position errors from the measured individual satellite signal deformation range biases. Both average (95%) and worst case errors are quantified.

Chapter 5 addresses various strategies to mitigate the impact of satellite signal deformation range biases. A simple yet practical strategy is found to be effective in mitigating the impact of the range biases. The mitigated range biases are analyzed and the resultant mitigated position errors are compared to the unmitigated case, demonstrating considerable improvement.

Chapter 6 summarizes the major contributions in this dissertation regarding the effective measurement and mitigation of satellite signal deformation biases. It also presents further possible research in this area.

Chapter 2

GNSS for Aviation

2.1   Overview

Global Satellite Navigation Systems (GNSS) work on the idea of trilateration. If the satellite positions are known, and the distances from them are also known, the principle of trilateration can be used to combine them to determine the location of the user receiver (Figure 2-1).
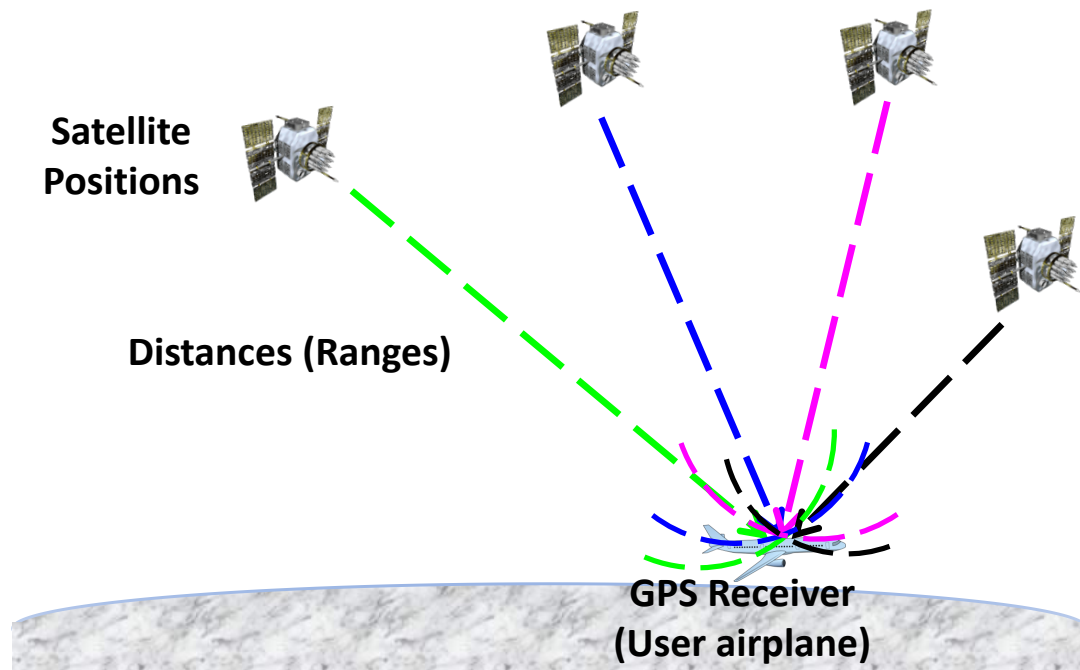
Figure 2-1: Trilateration: Computation of user position from distances and satellite

positions

Position computation requires a minimum of three satellite ranges to compute a three dimensional position fix. Typically user receivers contain inexpensive user receiver clocks, and require four or more satellite ranges to fix both the user position and the additional unknown clock bias of the user receiver.

Each satellite transmits signals that contain ephemeris data, in the form of orbital elements of the satellites, and timing information. Once the user receiver acquires and tracks the signal, it decodes the ephemeris data and determines the time of transmission of each signal. With this information, the receiver is able to compute the satellite positions, user position, and user clock bias [Refer to Section 2.3.5].

In addition, satellite signals at multiple frequencies enables the removal of the largest error source (Section 2.4.4), thus providing additional robustness (Section 2.5.2).

This dissertation focuses on the Global Positioning System (GPS), which is currently senior amongst GNSS systems. Other systems – Glonass, Galileo, and Beidou – are in varying stages of development and deployment [25], [26]. GPS satellites transmit two signals at 1575.42 MHz (L1) and 1176.42 MHz (L5) which are in the highly protected Aeronautical Radio Navigation Service (ARNS) band [27], [28] to be used for civil aviation. Special attention is paid to the L1 frequency signal, which is the most widely used civil signal today. This dissertation will also explore the L5 frequency civil signal which will be available in the near future.

2.2   Signal Structure Basics

This section introduces the basics of the GPS signal structure. 50 bps navigation data bits containing time and orbital parameters are modulated using Binary Phase Shift Keying (BPSK) onto a Direct Sequence Spread Spectrum (DSSS) signal. The modulated spread spectrum signals are in turn further modulated onto carriers at three frequencies, L2-frequency at 1227.6 MHz, L1-frequency at 1575.42 MHz, and L5-frequency at 1176.45 MHz. The military L2-P(Y) signals are encrypted and have unknown code modulations, while civilian L2C signals are not fully available. More importantly, the L2-frequency signal is not in the protected Aeronautical

Radionavigation Service (ARNS) frequency band [29], unlike the L1 and L5 frequency bands. For these reasons, this dissertation will focus primarily on the signals at the latter two frequencies, L1 (1575.42 MHz) and L5 (1176.45 MHz).

2.2.1 Satellite Vehicle Signal Generation and Transmission

Figure 2-2 and Figure 2-3 (adapted from [30], [31], [32], [33], [34]) show the signal modulation and transmission hardware chains for the transmitted signals at the GPS L1 and L5 frequencies, respectively. The two hardware chains are similar: the low-rate (50 bps) navigation data is modulated onto a spread spectrum Gold code signal ([35]; Section 2.2.2), and then further modulated in stages onto a carrier in the L-band (1-2 GHz).

The main differences between the two signals are:

1. The spread spectrum code rate is 1.023 Mbps for the L1 civil signal. For the L5-signal, the code rate is 10.23 Mbps, or 10 times higher.

2. Differences in the navigation data contained in the L1-frequency and L5-frequency signals: [36], [37].

   a. Additional rate 1/2 convolutional encoder to 100 symbols per second, modulated onto I5 (L5-in-phase) code, which is called the L5-Data Signal.

   b. The Q5 (L5 quadraphase) carrier has no data and is called the L5 Pilot signal.

3. The L1-frequency signal is transmitted at 1.57542 GHz, while the L5-frequency signal is transmitted at 1.17645 GHz.
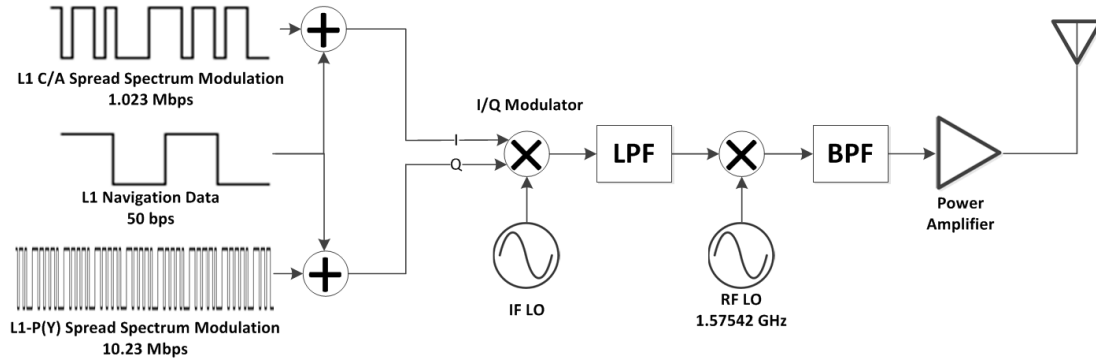
Figure 2-2: Modulation and Transmission of L1-Frequency GPS Satellite Signal (Civil Signal Only)
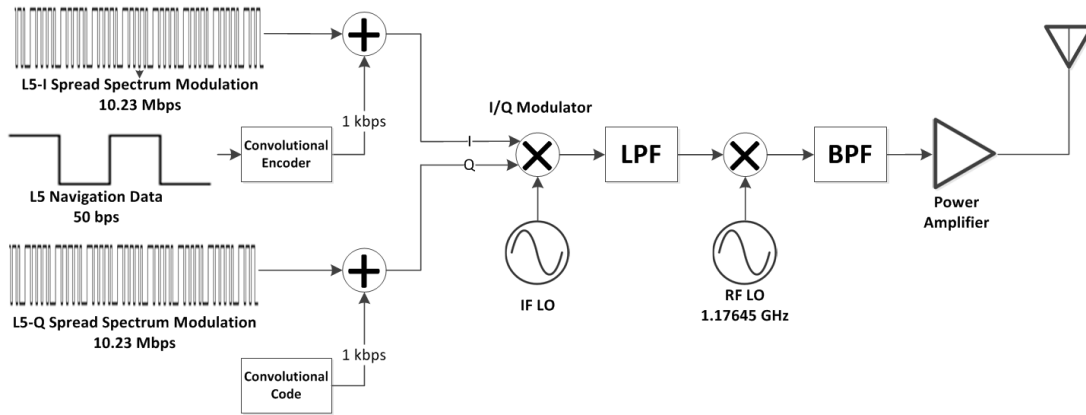
Figure 2-3: Modulation and Transmission of L5-Frequency GPS Satellite Signal

The civil signals are transmitted on the in-phase channels, and are mathematically represented as follows:

Equation for L1-Frequency Civil Signal:

$$x_{L1,I}(t) = \sqrt{2P_{L1,I}}\, D_{L1,I}(t)\, C_{L1,I}(t)\cos[2\pi f_{L1,I}t + \phi_{L1,I}] \tag{2.1}$$

where

$X_{L1,I}(t)$: Transmitted in-phase signal from GPS satellite at L1 frequency

$P_{L1,I}$: Power of transmitted in-phase signal from GPS satellite at L1 frequency

$D_{L1,I}(t)$: Navigation Data Message (50 bps) in transmitted in-phase signal at L1 frequency

$C_{L1,I}(t)$: Linear-Feedback Shift Register (LFSR) Pseudorandom Noise (PRN) Spread Spectrum Gold Code (1.023 Mbps) for transmitted in-phase signal at L1 frequency

f_{L1} : Center frequency of carrier of transmitted in-phase signal at L1 frequency, 1575.42 MHz

$\Phi_{L1,I}$: Carrier phase offset of transmitted in-phase signal at L1 frequency

Equation for L5-Frequency Civil Signal – InPhase:

$$x_{L5,I}(t) = \sqrt{2P_{L5,I}}\, D_{L5,I}(t)\, C_{L5,I}(t)\cos[2\pi f_{L5,I}t + \phi_{L5,I}] \tag{2.2}$$

where

$X_{L5,I}$: Transmitted in-phase signal from GPS satellite at L5 frequency

$P_{L5,I}$: Power of transmitted in-phase signal from GPS satellite at L5 frequency

$D_{L5,I}$: Navigation Data Message (100 symbols per second) for transmitted in-phase signal at L5 frequency

$C_{L5,I}$: Linear-Feedback Shift Register (LFSR) Pseudorandom Noise (PRN) Spread Spectrum Gold Code (10.23 Mbps) for transmitted in-phase signal at L5 frequency

f_{L5} : Center frequency of carrier of transmitted signal at L5 frequency, 1176.45 MHz

$\Phi_{L5,I}$: Carrier phase offset of transmitted in-phase signal at L5 frequency

Equation for L5-Frequency Civil Signal – Quadrature:

$$x_{L5,Q}(t) = \sqrt{2P_{L5,Q}}\,C_{L5,Q}(t)\cos[2\pi f_{L5}t + \phi_{L5,Q}] \tag{2.3}$$

where

$X_{L5,Q}$: Transmitted quadrature signal from GPS satellite at L5 frequency

$P_{L5,Q}$: Power of transmitted quadrature signal from GPS satellite at L5 frequency

$C_{L5,Q}$: Linear-Feedback Shift Register (LFSR) Pseudorandom Noise (PRN) Spread Spectrum Gold Code (10.23 Mbps) for transmitted quadrature signal at L5 frequency

f_{L5} : Center frequency of carrier of transmitted quadrature signal at L5 frequency, 1176.45 MHz

$\Phi_{L5,Q}$: Carrier phase offset of transmitted quadrature signal at L5 frequency

2.2.2   Pseudorandom Code Modulation

The L1 C/A Spread Spectrum Code Generators use two 10-bit Linear Feedback Shift Registers (LFSRs) whose outputs are added modulo-2. Both shift-registers are maximal-length, i.e., they have code periods of exactly 1023 bits or chips. The resultant spread spectrum codes are known as Gold Codes [35]. They are clocked at 1.023 Mbps, and repeat every millisecond (or 1023 chips) [36].

The L5 Spread Spectrum Code Generators use two 13-bit Linear Feedback Shift Registers (LFSRs) whose outputs are added modulo-2., generating maximal-length Gold Codes [35] of code periods of exactly 8192 bits or chips. When 8192 chips have passed, the spread-spectrum codes are allowed to repeat, until a total of 10,230 chips have been generated. The spread spectrum codes are clocked at 10.23 Mbps, and repeat every millisecond (or 10,230 chips) [37].

2.2.3   Navigation Frequencies and Spectra

Figure 2-4 [38] and Figure 2-5 [39] show frequency spectra of the signals at the L1 transmission frequency of 1575.42 MHz and L5 transmission frequency of 1176.45 MHz, respectively.
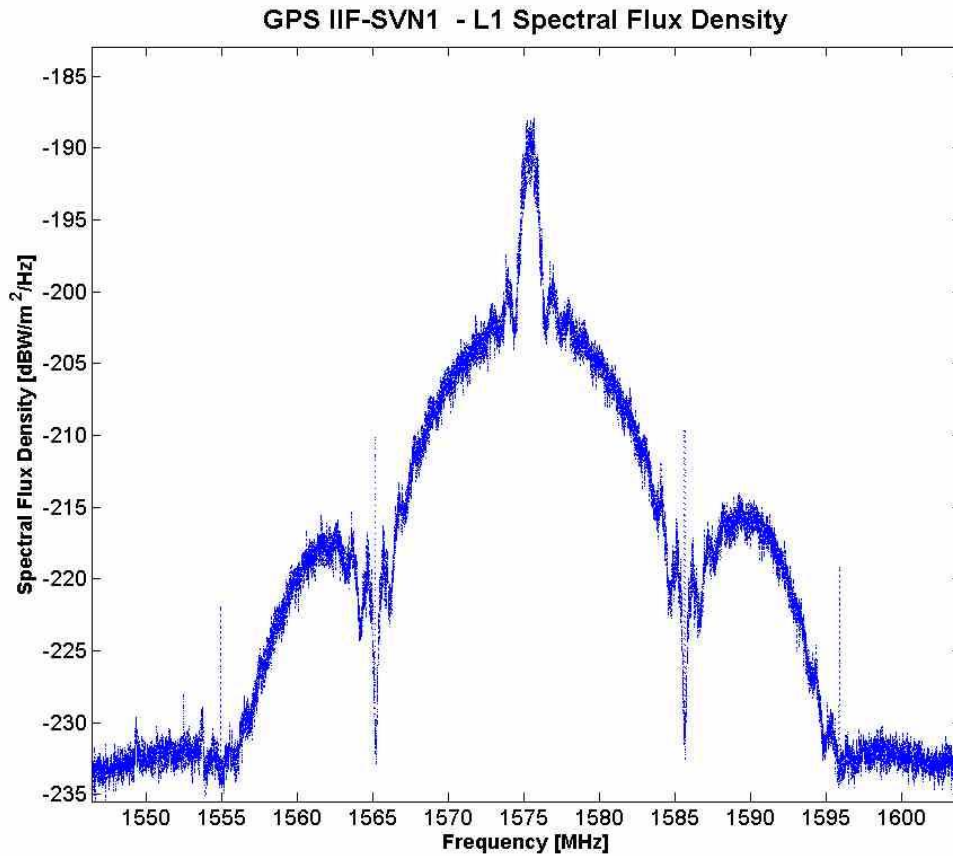
Figure 2-4: L1-Frequency GPS Satellite Signal Spectrum [38]

As observed in Figure 2-4, the L1-frequency spectrum has a center frequency of 1575.42 MHz. The civil spread spectrum code, which has a chip rate of 1.023 Mchips/sec, results in a narrow 2 MHz (± 1 MHz) main lobe around the center frequency. A wideband 20 MHz (± 10 MHz) main lobe around the center frequency is also observable, due to the military spread spectrum code which has a chip rate of 10.23 Mchips/ sec
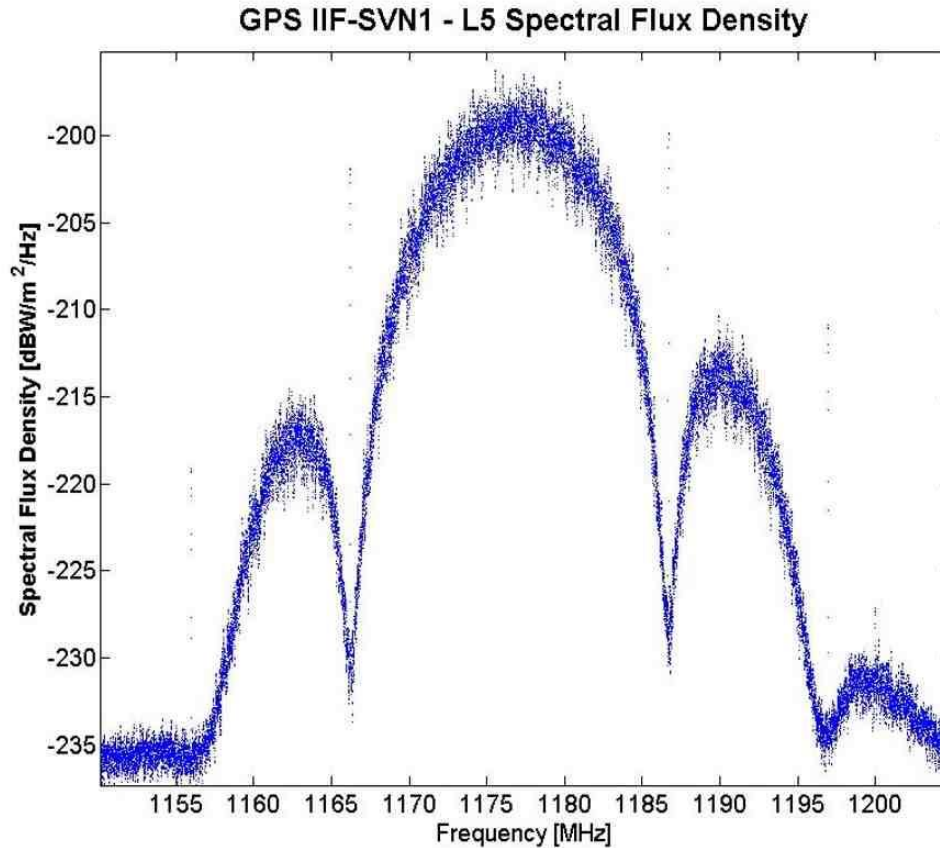
Figure 2-5: L5-Frequency GPS Satellite Signal Spectrum [39]

As seen in Figure 2-5, the L5-frequency spectrum has a center frequency of 1176.45 MHz. It contains a single wideband 20 MHz (± 10 MHz) main lobe, due to the civil spread spectrum code which has a chipping rate of 10.23 Mchips/sec, or a rate 10 times higher than that of the L1 civil spread spectrum code (1.023 Mchips/sec). Interestingly, despite the factor of 10 increase in chip-rate, this signal only gives a factor of 3 improvement in navigational performance; the reasons are dicussed in Appendix F.

2.3   Receiver Basics

This section introduces the basic operations within a GPS receiver (Figure 2-6).
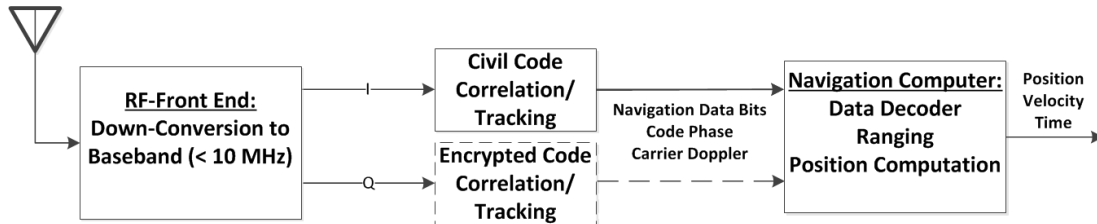
Figure 2-6: Overview of Functional Operations of GPS Receiver

When the GPS receiver receives the L-band signal, it downconverts the signal to baseband and samples it. Next it removes the spread-spectrum modulation by generating a local replica of the spread-spectrum code, to correlate with / match-filter the incoming signal. The receiver continues to track the phase of the received spread spectrum code, and decodes the navigation data bits to recover the navigation message. Using this information, the receiver is able to obtain time of transmission, satellite position, and range, which it uses to compute the user position and user clock bias.

2.3.1 Antennas and Filters for Downcoversion
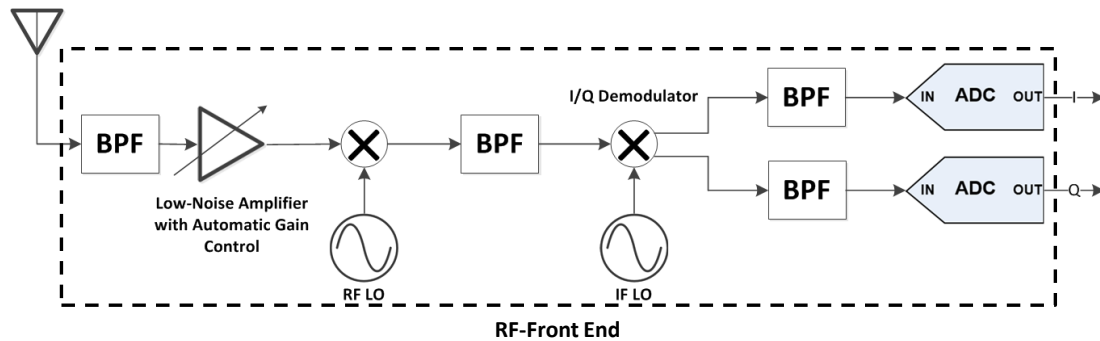
Figure 2-7: GPS Receiver RF-Front End

(Adapted from [30])

The GPS Receiver RF-Front End module downconverts the received signal from L-band to baseband, then digitally samples the baseband signal for further processing (Figure 2-7). These operations are broken down as follows:

- Filtering the signal to remove out-of-band noise

- Using a low-noise amplifier (typically Noise Figure < 2 dB) with automatic gain control, to amplify the weak received signal without reaching saturation

- 1st Downconversion stage: A local oscillator and mixer are used to mix the signal from L-band down to an intermediate frequency (typically < 100-200 MHz), followed by a bandpass filter to reject out-of-band spectra

- 2nd and subsequent Downconversion stages again use local oscillator(s) and mixer(s) to mix the signal from intermediate frequency to baseband (typically ≤ 20 MHz). Additional baseband filters are used to reject out-of-band noise and interference.

- Analog-to-Digital Converter to sample baseband in-phase and quadrature signal to produce digital in-phase and quadrature samples.

2.3.2   Code Correlation

As shown in Figure 2-7, to recover the data message from the digital in-phase samples and perform ranging (Section 2.3.4), the receiver needs to remove the spread spectrum code modulation (Section 2.3.3), which in turn requires an estimate of the code phase of the incoming signal.
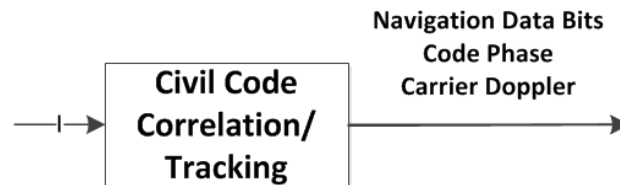
Figure 2-8: Correlation and Tracking within Receiver to Determine the Code Phase

and Recover Navigation Data Message

To estimate the incoming signal's code phase, the receiver generates a (known) copy of the incoming signal's code waveform, which is a matched filter corresponding to the incoming received code waveform. The receiver then correlates/convolves the local copy with the incoming signal (Figure 2-9).
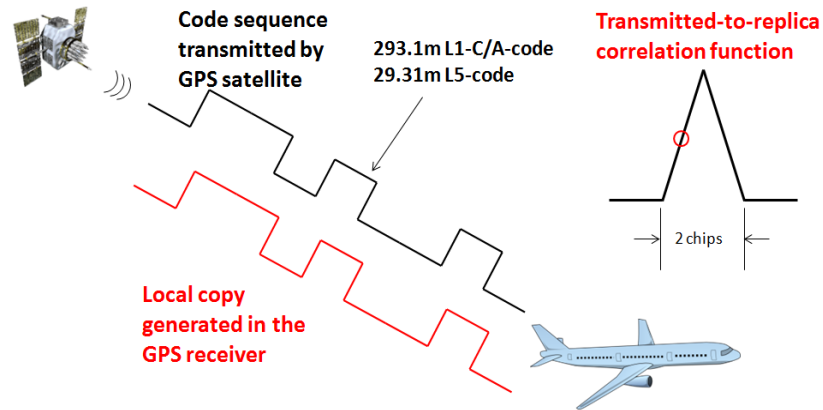
Figure 2-9: Determining the code phase of received GPS signal using correlation

When the code phases between the incoming signal and the replica signal are exactly matched, the correlation output will be maximized. This output starts to decrease approximately linearly as the relative code phases diverge for offsets of up to 1 chip (Figure 2-10). When the relative code phase offset is 1 chip or more, the correlation output is negligible.

Figure 2-10a: Phase of received GPS signal is **advanced (Early) by 0.5 chips** relative to local copy.	
Figure 2-10b: Phase of received GPS signal is **advanced (Early) by 0.25 chips** relative to local copy.	
Figure 2-10c: Phase of receiver's local copy **exactly matched** with received GPS signal.	
Figure 2-10d: Phase of received GPS signal is **delayed (Late) by 0.25 chips** relative to local copy.	
Figure 2-10e: Phase of received GPS signal is **delayed (Late) by 0.5 chips** relative to local copy.	

Figure 2-10: Correlation outputs for different relative phases between received GPS

code signal and receiver local copy

In practical GPS receiver implementations, the receiver uses at least two replicas to determine the phase of the incoming signal. One replica is at a slight advance, and the other replica at a slight delay. These are commonly referred to as "Early" and "Late" correlators. The time delay between them is referred to as the **correlator spacing**,

which is typically specified in terms of L1 or L5 chips, depending on the incoming signal.

For the L1 signal, this correlator spacing may be as short, or "narrow," as 0.05 L1 chips, (corresponding to a time delay of 48.9 µsec between the Early and Late correlators, or 14.65 m), or as long, or "wide," as 1 L1 chip (corresponding to 977.5 µsec or 293.05 m) (Figure 2-11). Other typical correlator spacings are 0.1 L1 chips (29.31 m or 97.8 µsec) and 0.2 L1 chips (58.61 m or 195.5 µsec).
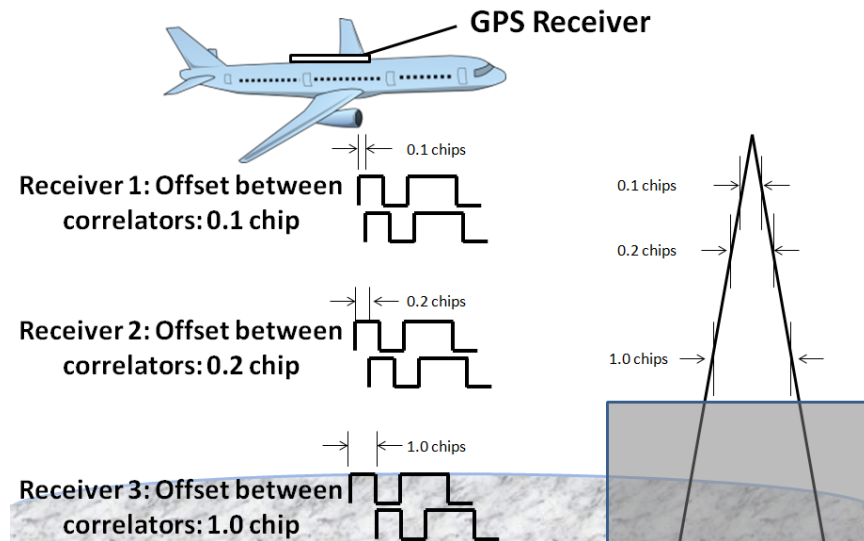
Figure 2-11: Typical L1 signal correlator spacings in user receivers

The L5 signal has a 10x narrower waveform in time (Figure 2-12), resulting in a correlation waveform that is correspondingly 10x narrower. Consequently, for L5 signal tracking, the correlator spacing, or time delay between the Early and Late correlators, is typically 1.0 L5 chips (corresponding to 97.8 µsec or 29.31 m) (Figure 2-13).
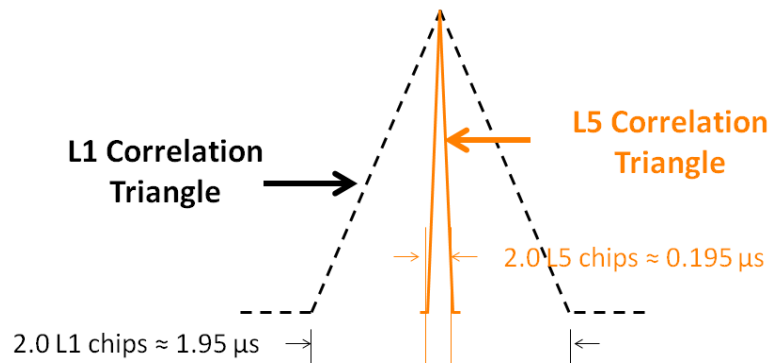
Figure 2-12: Correlation characteristics of GPS signals at L1 and L5 frequencies
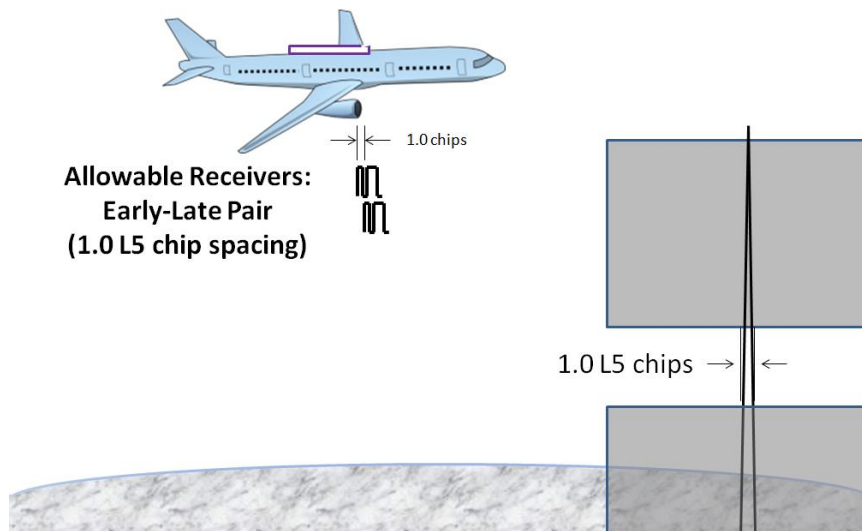
Figure 2-13: L5 signal correlator spacings in user receivers

2.3.3   Code Tracking and Removal of Spread Spectrum Modulation

In the Code Tracking Loop (Figure 2-14), the receiver uses the outputs from the pair of Early and Late correlators to "track" the phase of the incoming signal. Both

correlator outputs are inputs to an "Early-Minus-Late" discriminator. The resulting discriminator output is filtered and in turn adjusts the code phase in the numerically controlled oscillator, which is input to the code-generator used to generate the Early and Late correlators.
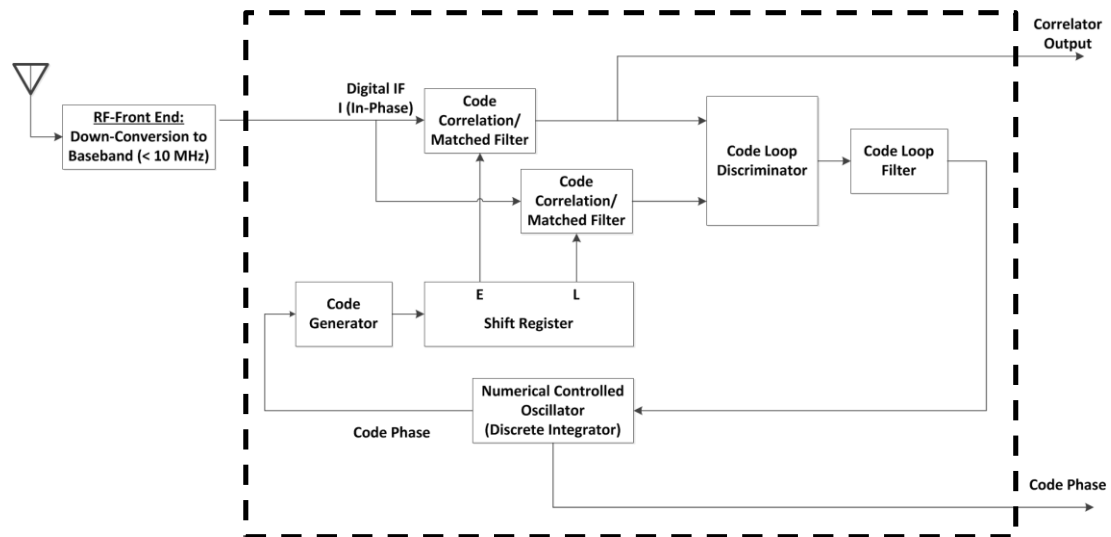
Figure 2-14: Code Tracking Loop

The code tracking feedback loop continually adjusts the code phase until the Early and Late correlator outputs are identical. This is the "code-tracking" process that occurs continuously, enabling the receiver to estimate the code phase of the incoming signal: the midpoint between the receiver's Early and Late replica code phases. This allows the receiver to remove the spread-spectrum modulation to recover the transmitted navigation message. The tracked "code-phase" is used for ranging and position computation (Section 2.3.4).

2.3.4 Time, Ranging and Satellite Positions

Upon successful tracking of the incoming signal, the receiver is able to decode the navigation data bits. These data bits contain the orbital parameters for the transmitting satellite, as well as the coarse times of transmission, in increments of 1.5 seconds.

With additional processing, and using the code phase available from the code tracking loop, the receiver obtains the **time of transmission** of the *ith* received satellite signal, $t_{tr}^{(i)}$, for all received satellite signals, to sub-µs precision.

Using the orbital parameters together with the time of transmission, the receiver is able to compute the **satellite positions** at their times of transmission, $\underline{x}_{sv}^{(i)}(t_{tr}^{(i)})$ (Figure 2-15)

$$
\begin{bmatrix}
\underline{x}_{sv}^{(1)}(t_{tr}^{(1)}) \\
\underline{x}_{sv}^{(2)}(t_{tr}^{(2)}) \\
\ldots \\
\underline{x}_{sv}^{(i)}(t_{tr}^{(i)}) \\
\ldots \\
\underline{x}_{sv}^{(N)}(t_{tr}^{(N)})
\end{bmatrix}
$$
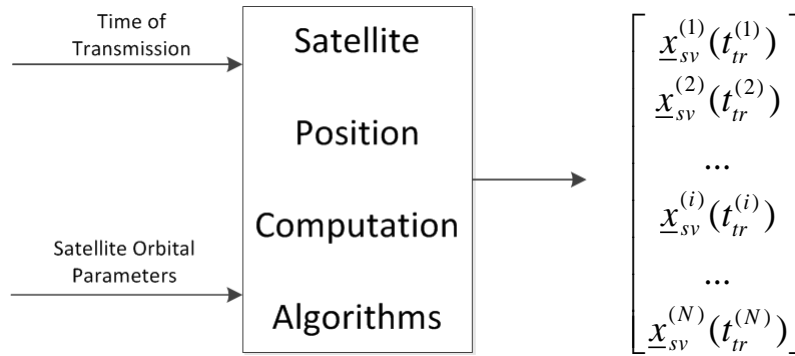
Figure 2-15: Computation of Satellite Positions at the different Times of Transmission

for all satellites in View

Where

$t_{tr}^{(i)}$:   Time of transmission for satellite i

$\underline{x}_{sv}^{(i)}(t_{tr}^{(i)})$:   Satellite position vector in Earth-Centered Earth Fixed (ECEF) at time

                 of transmission, $t_{tr}^{(i)}$, for satellite i

N :   Number of satellites in view at the user receiver

2.3.5   User Position Computation

This discussion of user position computation largely follows the treatment of Farrell [40]. Assuming the user receiver and the satellites are time-synchronized, subtracting the time of satellite signal transmission from the local time of arrival yields the signal propagation time. In the absence of clock biases and other errors, the true range, which is the distance between the satellite and the user receiver antenna, is the signal propagation time multiplied by the speed of light [Equation (2.4)].

$$\hat{r}^{(i)}(\underline{x}_u(t),t) = r^{(i)}(\underline{x}_u(t),t) = c \times (t - t_{tr}^{(i)}) \tag{2.4}$$

Where

t :   True time of signal reception at user receiver

$\hat{r}^{(i)}(\underline{x}_u(t),t)$:   Range estimate from user location $\underline{x}_u(t)$ to satellite i at time t

$r^{(i)}(\underline{x}_u(t),t)$:   True range from user location $\underline{x}_u$ to satellite i at time t

$t_{tr}^{(i)}$:   Time of transmission for satellite i

The true range can also be expressed as:

$$r^{(i)}(\underline{x}_u(t),t) = \left\| \underline{x}_u(t) - \underline{x}_{sv}^{(i)}(t_{tr}^{(i)}) \right\| = \sqrt{(x_u(t) - x_{sv}^{(i)}(t_{tr}^{(i)}))^2 + (y_u(t) - y_{sv}^{(i)}(t_{tr}^{(i)}))^2 + (z_u(t) - z_{sv}^{(i)}(t_{tr}^{(i)}))^2}$$

$$(2.5)$$

Where

$r^{(i)}(\underline{x}_u(t),t)$:   True range from user location $\underline{x}_u$ to satellite i at time t

$\underline{x}_u(t)$:   User position vector in ECEF (Earth-centered Earth-Fixed) co-

                                      ordinate system, at time of signal reception t

$x_u(t)$: x-coordinates of user's position in ECEF at time t

$y_u(t)$: y-coordinates of user's position in ECEF at time t

$z_u(t)$: z-coordinates of user's position in ECEF at time t

$\underline{x}_{sv}^{(i)}(t_{tr}^{(i)})$:   Satellite position vector at time of transmission, $t_{tr}^{(i)}$, for satellite i

$x_{sv}^{(i)}(t_{tr}^{(i)})$: x-coordinates of satellite i's position in ECEF at time $t_{tr}^{(i)}$

$y_{sv}^{(i)}(t_{tr}^{(i)})$: y-coordinates of satellite i's position in ECEF at time $t_{tr}^{(i)}$

$z_{sv}^{(i)}(t_{tr}^{(i)})$: z-coordinates of satellite i's position in ECEF at time $t_{tr}^{(i)}$

For subsequent computation, the variables' functional dependence on time is implied.
In the presence of measurement errors, the range equations are as follows. These range
equations are similar for L1 and L5 transmission frequencies.

$$\hat{r}^{(i)}(\underline{x}_u) = r^{(i)}(\underline{x}_u) + I^{(i)} + T^{(i)} + MP^{(i)} + SSD \qquad (2.6)$$

$$= r^{(i)}(\underline{x}_u) + v^{(i)} \qquad (2.7)$$

Where

$\hat{r}^{(i)}(\underline{x}_u)$:   Range estimate from user location $\underline{x}_u(t)$ to satellite i

$r^{(i)}(\underline{x}_u)$:   True range from user location $\underline{x}_u(t)$ to satellite i

$I^{(i)}$:   Ionospheric error

$T^{(i)}$:   Tropospheric error

$\varepsilon^{(i)}$:   Radio-Frequency Interference and Receiver White Noise error

$MP^{(i)}$:   Multipath error

$SSD^{(i)}$:   Satellite Signal Deformation range bias

$v^{(i)}$:   Total range measurement error for satellite i

Furthermore, a clock/timing error at the receiver would lead to range biases. If the true time of signal reception is t, and the local (incorrect) time at the receiver is t_u instead of t, the receiver measures a pseudorange, which includes a clock bias, instead of a range estimate.

$$\rho^{(i)}(\underline{x}_u, t_b) = c \times (t_u - t_{tr}^{(i)}) = c \times (t_u - t + t - t_{tr}^{(i)})$$

$$= r^{(i)}(\underline{x}_u) + v^{(i)} + c \times (t_u - t) \qquad (2.8)$$

$$= r^{(i)}(\underline{x}_u) + v^{(i)} + ct_b \qquad (2.9)$$

Where

$\rho^{(i)}(\underline{x}_u, t_b)$:   Pseudorange estimate (includes clock bias)

$r^{(i)}(\underline{x}_u)$:   True range from user location $\underline{x}_u$ to satellite i

$v^{(i)}$:   Total range measurement error for satellite i

t_u :   Local (incorrect) time of signal reception at user receiver

t :   True time of signal reception at user receiver

t_b :   Clock bias at user receiver

Let the unknown to be computed be:

$$\underline{w}_u = \begin{bmatrix} \underline{x}_u \\ c \times t_b \end{bmatrix} = \begin{bmatrix} x_u \\ y_u \\ z_u \\ c \times t_b \end{bmatrix} \tag{2.10}$$

Linearizing about $\underline{w}_0 = \begin{bmatrix} \underline{x}_0 \\ t_{b0} \end{bmatrix}$,

$$\rho^{(i)}(\underline{x}_u, t_b) = \rho^{(i)}(\underline{x}_0, t_{b0}) + \left[\frac{\partial \rho^{(i)}(\underline{x}_u, t_b)}{\partial x} \quad \frac{\partial \rho^{(i)}(\underline{x}_u, t_b)}{\partial y} \quad \frac{\partial \rho^{(i)}(\underline{x}_u, t_b)}{\partial z} \quad \frac{\partial \rho^{(i)}(\underline{x}_u, t_b)}{\partial t_b} \right] \bullet \begin{bmatrix} x_u - x_0 \\ y_u - y_0 \\ z_u - z_0 \\ c \times (t_b - t_{b0}) \end{bmatrix} + v^{(i)} + hot$$

$$\tag{2.11}$$

$$\delta\rho^{(i)} = \rho^{(i)}(\underline{x}_u, t_b) - \rho^{(i)}(\underline{x}_0, t_{b0}) = \underline{g}^{(i)} \delta\underline{w} + v^{(i)} + hot \tag{2.12}$$

Where

$$\delta \underline{w} = \underline{w}_u - \underline{w}_0 = \begin{bmatrix} \underline{x}_u - \underline{x}_0 \\ c \times (t_b - t_{b0}) \end{bmatrix} = \begin{bmatrix} x_u - x_0 \\ y_u - y_0 \\ z_u - z_0 \\ c \times (t_b - t_{b0}) \end{bmatrix} \tag{2.13}$$

$$\underline{g}^{(i)} = \left[\frac{\partial \rho^{(i)}(\underline{x}_u, t_b)}{\partial x_u} \quad \frac{\partial \rho^{(i)}(\underline{x}_u, t_b)}{\partial y_u} \quad \frac{\partial \rho^{(i)}(\underline{x}_u, t_b)}{\partial z_u} \quad \frac{\partial \rho^{(i)}(\underline{x}_u, t_b)}{\partial t_b} \right]_{\underline{x}_0}$$

$$= \left[\frac{\partial \rho^{(i)}(\underline{x}_u, t_b)}{\partial x_u} \quad \frac{\partial \rho^{(i)}(\underline{x}_u, t_b)}{\partial y_u} \quad \frac{\partial \rho^{(i)}(\underline{x}_u, t_b)}{\partial z_u} \quad 1 \right]_{\underline{x}_0} \tag{2.14}$$

where

$$\frac{\partial \rho^{(i)}(\underline{x}_u, t_b)}{\partial x_u} = \frac{x_u - x_{sv}}{\sqrt{(x_u - x_{sv}^{(i)})^2 + (y_u - y_{sv}^{(i)})^2 + z_u - z_{sv}^{(i)})^2}} \tag{2.15}$$

$$\frac{\partial \rho^{(i)}(\underline{y}_u, t_b)}{\partial y_u} = \frac{y_u - y_{sv}}{\sqrt{(x_u - x_{sv}^{(i)})^2 + (y_u - y_{sv}^{(i)})^2 + z_u - z_{sv}^{(i)})^2}} \tag{2.16}$$

$$\frac{\partial \rho^{(i)}(\underline{z}_u, t_b)}{\partial z_u} = \frac{z_u - z_{sv}}{\sqrt{(x_u - x_{sv}^{(i)})^2 + (y_u - y_{sv}^{(i)})^2 + z_u - z_{sv}^{(i)})^2}} \tag{2.17}$$

hot: *Higher-order terms*

For a system of *N* pseudoranges,

$$\delta \underline{\rho} = G \delta \underline{w} + v^{(i)} + hot \approx G \delta \underline{w} \tag{2.18}$$

Where

$$G = \begin{bmatrix} \underline{g}^{(1)} \\ ... \\ \underline{g}^{(i)} \\ ... \\ \underline{g}^{(N)} \end{bmatrix} \tag{2.19}$$

Solving the system of linearized Equations (2.14)-(2.19) for N ranges (where $N \geq 4$),

$$\delta \underline{w} \approx (G^T G)^{-1} G^T \delta \underline{\rho} \tag{2.20}$$

In cases where some (pseudo)ranges are of better quality (lower noise) than others, there may be reason to use a diagonal weighting matrix W. In this case, the solution of linearized equations for N ranges would be as follows:

From Equation (2.18)

$$\delta \underline{\rho} \approx G \delta \underline{w} \tag{2.21}$$

$$G^T W \delta \underline{\rho} \approx (G^T W G) \delta \underline{w} \tag{2.22}$$

$$\delta \underline{w} \approx (G^T W G)^{-1} G^T W \delta \underline{\rho} \tag{2.23}$$

Where

W :   Diagonal Weighting Matrix for the N (pseudo)ranges.

From $\delta \underline{w}$, the user position and the user clock bias are computed as follows:

$$\underline{w}_u = \begin{bmatrix} \underline{x}_u \\ c \times t_b \end{bmatrix} = \begin{bmatrix} x_u \\ y_u \\ z_u \\ c \times t_b \end{bmatrix} = \underline{w}_0 + \delta \underline{w} = \begin{bmatrix} x_0 \\ y_0 \\ z_0 \\ c \times t_{b0} \end{bmatrix} + \delta \underline{w} \tag{2.24}$$

From an initial estimate of position $\underline{x}_0$ and clock bias t_{b0}, the solution converges within four to five iterations of least-squares solution. It can be observed that any errors common across all (pseudo)ranges will result in an erroneous computed receiver clock bias, but not result in any position error.

2.4   GNSS Error Sources and Common Mitigation Approaches

GNSS Error Sources

For ideal error-free and distortion-free signals, the receiver is able to correctly match the code phase of the incoming signal and obtain accurate estimates of the time of transmission of the incoming satellite signal. However, various error sources (Figure 2-16) can negatively impact the correlation process, leading to erroneous code phase estimates, range estimates, and ultimately user position errors.

Signal-in-space Errors
Eg. **Clock, ephemeris**,
Satellite Signal Deformation

Propagation Errors
Eg. **Tropospheric, ionospheric**

Receiver Errors
Eg. **Multipath, Receiver noise**

User airplane
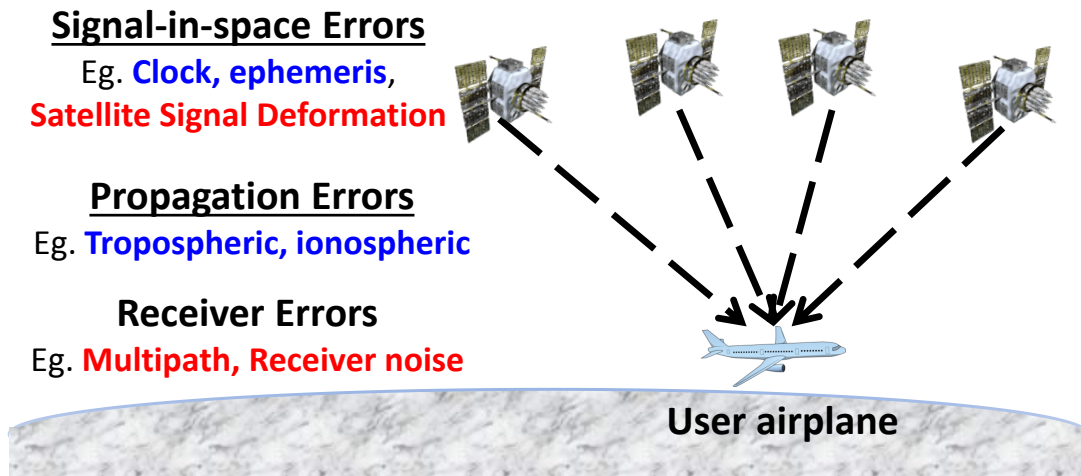
Note:
Receiver-dependent errors: Multipath, Receiver noise, Satellite Signal Deformation
Receiver-independent errors: Clock, Ephemeris, Tropospheric, ionospheric

Figure 2-16: Various GPS Errors

These error sources can be broadly classified into two categories: receiver-dependent errors, which have different effects on user receivers depending on the receiver configuration, and receiver-independent errors, which affect user receivers almost identically regardless of the receiver configuration. Different mitigation techniques are required to be effective for these two categories of errors (Refer to Table 1-1, which was presented in Chapter 1 and is reproduced here).

Category	Error	Mitigation
Receiver-independent	Clock Ephemeris Ionosphere Troposphere	Differential-GPS
Receiver-dependent	Radio Frequency Interference (RFI) Receiver White Noise	Time-Averaging
	Multipath	Time-Averaging Antenna/ Environment
	Measurement Equipment Time-varying errors (Seen mainly in dish antennas)	Calibration Repeated measurements Cross-verification
	Signal Deformation Range Biases (Signal of Interest)	**Specially-Configured Receivers**

Table 1-1: Measurement Errors and Mitigation

Common Mitigation Approaches

Mitigation methods can be divided into two categories: standalone single receiver configuration and differential dual/multi-receiver configuration. In the absence of reference receivers, or if the errors between the reference and user receivers are not

spatially and temporally correlated (such as for multipath and receiver white noise), standalone mitigation methods must be used.

Differential-GPS (or DGPS), a differential dual/multi-receiver configuration, may be employed when one or more reference receivers at pre-surveyed locations are available. The reference receivers compute the errors in the GPS signal which are then transmitted to the user receiver to be used as error corrections. Differential GPS is effective in removing receiver-independent errors, such as space-based clock and ephemeris errors and atmospheric errors, in situations where the reference and user receivers are physically proximate and there is little time lag in applied corrections. DGPS is not effective when the errors are not correlated, as in the case of receiver-dependent errors such as multipath and receiver white noise.

These errors, and how the mitigation methods are applied to reduce their effect, will be described in greater detail in subsequent sections.

2.4.1   Receiver-Dependent Errors

Receiver-dependent errors have different effects on receivers with different configurations of antennas, filters, and correlator spacings. Receiver-dependent errors include multipath, radio-frequency interference, and receiver thermal noise; these originate from the receiver's immediate environment and are ground based or environmental in nature.

Receiver-dependent errors also include satellite signal deformation (SSD) errors, which are space-based: they originate within the satellite's on-board signal generation hardware chain (Section 2.2.1). These space-based errors create waveform distortions on the ground whose effects are dependent on the configuration of the receiver. How these satellite-originated errors cause receiver dependent errors will be explained later in this section.

Figure 2-17 demonstrates these receiver-dependent errors, based on actual data from receivers at the same location but with different correlator spacings. The range differences between the receivers reveal white (Gaussian) receiver noise, slowly varying pseudo-sinusoidal multipath errors, and satellite signal deformation range biases – constant biases between the different satellite signals.
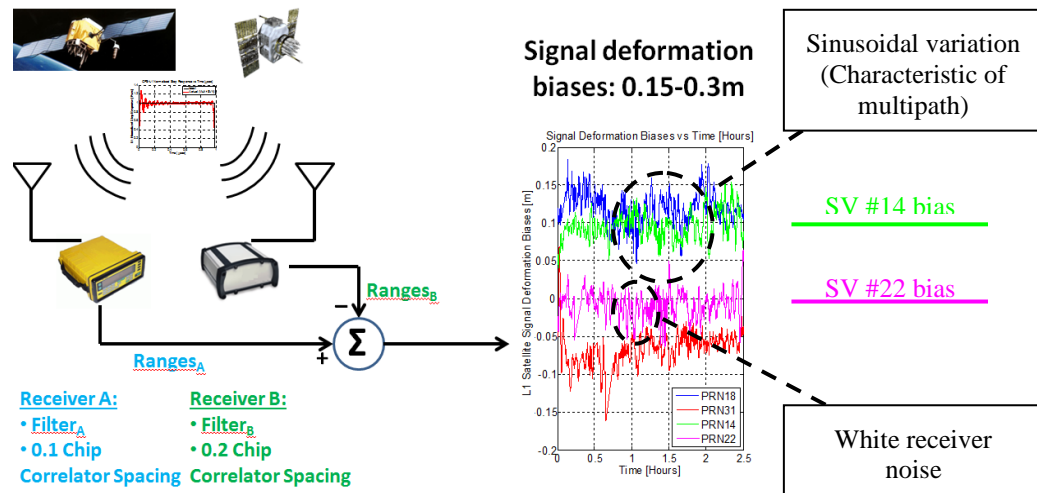
Figure 2-17: Actual receiver results containing white receiver noise, multipath and satellite signal deformation range biases

The main goal of this dissertation is to separate these effects, so as to be able to quantify and mitigate the space-based satellite signal deformation range biases. The ability to do so is limited by the other ground-based or environmental errors. Both sets of errors will be discussed in subsequent sections.

Space-Based Receiver-Dependent Error: Satellite Signal Deformation

Under nominal, everyday operating conditions, the transmitted satellite signals are not ideal square waveforms; instead, they contain deviations from ideal. These deviations are known as nominal satellite signal deformations. They originate within the satellite's signal generation hardware chain and result in range biases at the user receiver (Figure 2-18). (In contrast, abnormal satellite signal deformations occur due to faults in the same satellite hardware. This happened previously and led to much larger errors of up to 8 m vertical errors [6], [20]. It also launched the research field of satellite signal deformation/quality monitoring.)
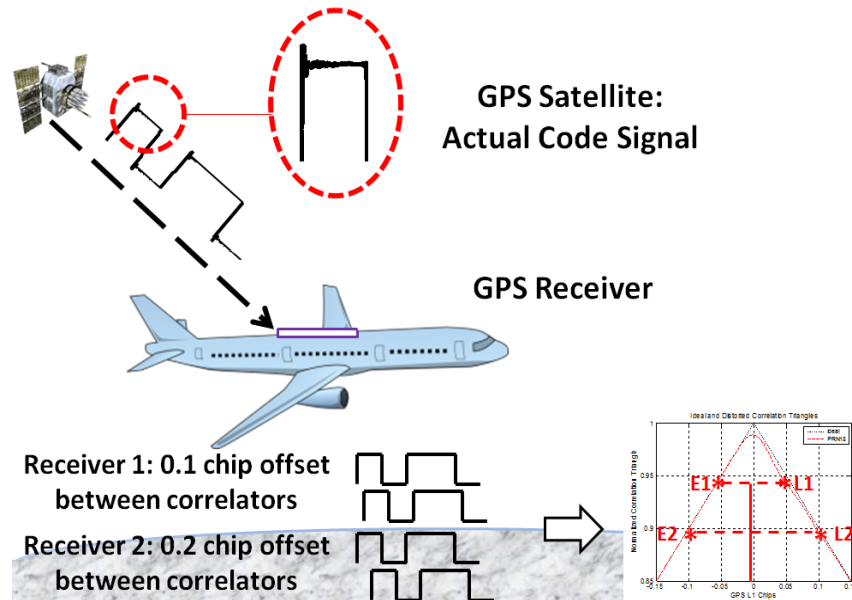
Figure 2-18: Satellite signal deformation in GPS code waveform leads to correlation

waveform distortions, range biases and position errors

For ideal received signals without signal deformations, there would be no resultant

range biases regardless of the correlator spacings used in the receiver tracking loop

(Figure 2-19).
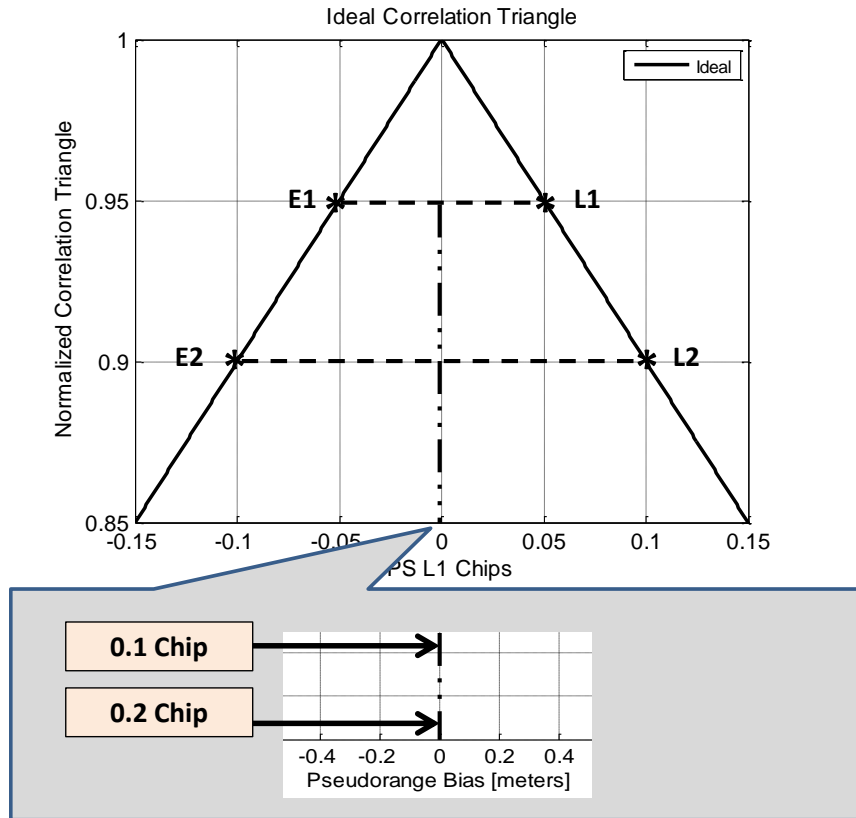
Figure 2-19: Range biases for receivers with different correlator spacings for ideal

waveform.

The resultant range biases are identically zero.

Unfortunately, satellite signal deformations are present. In this situation, the range

biases experienced by the user receiver are non-zero. In addition, these biases depend

on the correlator spacings within the receiver's tracking loop. Figure 2-20 shows the

distorted correlation waveform for satellite ID PRN #12, as well as the resultant biases

for two different correlator spacings in the user receiver tracking loop.
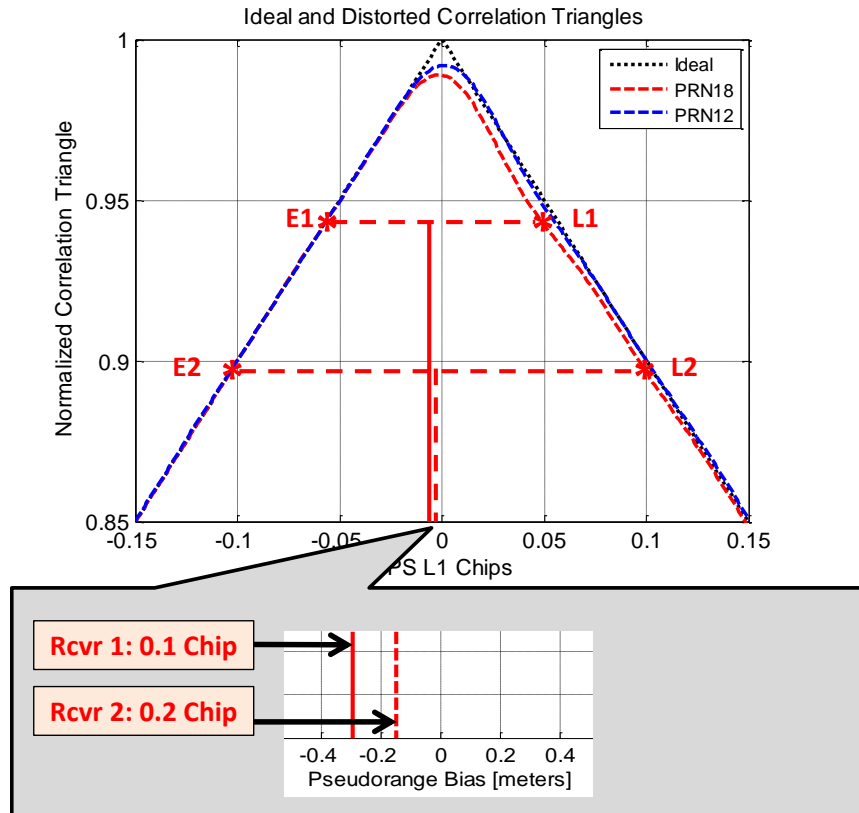
Figure 2-20: Non-zero range biases experienced by receivers with correlator spacings

of 0.1 and 0.2 chips for satellite signal PRN #**12**

Range biases depend on the correlator spacing in the user receiver tracking loop.

Furthermore, the satellite signal deformations are different and unique (Appendix B-5) for each individual satellite. Receivers experience different range biases which are specific to the individual satellites. These resultant range biases are called satellite signal deformation range biases.

Figure 2-21 shows biases at two different correlator spacings for a different satellite, satellite ID PRN# 18. Figure 2-22 compares the biases for the two different satellites for user receivers of two different correlator spacings.
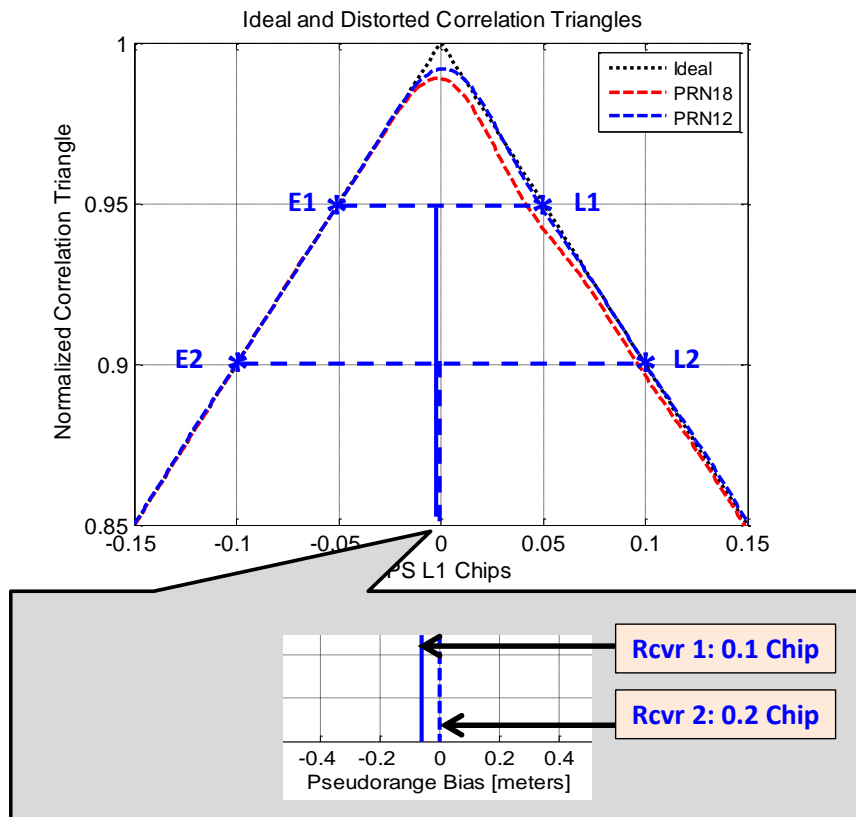
Figure 2-21: Range biases experienced by receivers with correlator spacings of 0.1 and 0.2 chips for a different satellite signal, satellite PRN# **18**.
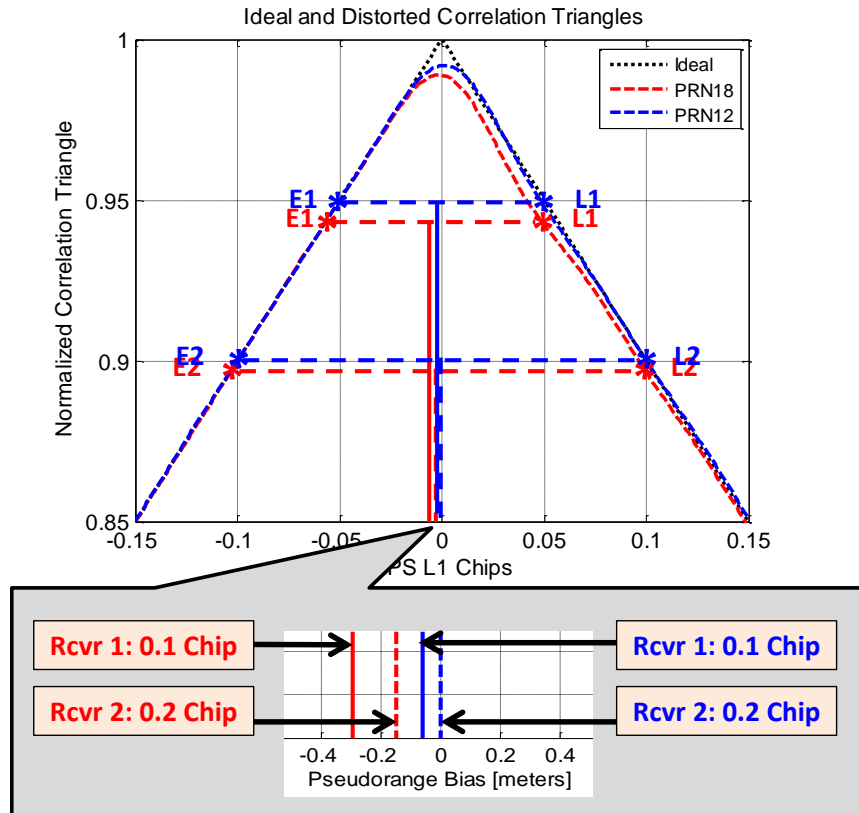
Figure 2-22: Satellite signal deformation range biases experienced by receivers with different correlator spacings of 0.1 and 0.2 chips for satellite signals PRN #**12** and PRN #**18**.

Range biases are different for different satellites and different correlator spacings.

Environmental Receiver-Dependent Error: Multipath & Thermal Noise

Ground-based/environmental receiver-dependent errors include thermal noise and multipath. The received thermal noise power [41] (also known as Johnson–Nyquist noise) is dependent on the antenna and the front end filter implementation and bandwidth.

Multipath is caused by the satellite signal propagating through the environment and reflecting off obstacles close to the receiver. These multiple delayed indirect paths also travel to the receiver, resulting in multiple delayed copies of the signal (Figure 2-23).

In turn, the multipath causes range errors at the output of the code-tracking process. These errors depend on the phase, amplitude, and delay of the multipath, which vary according to the electromagnetic nature of the obstacles, distance of the obstacle to the receiver, and the relative motions of the satellite, the receiver, and the obstacles.
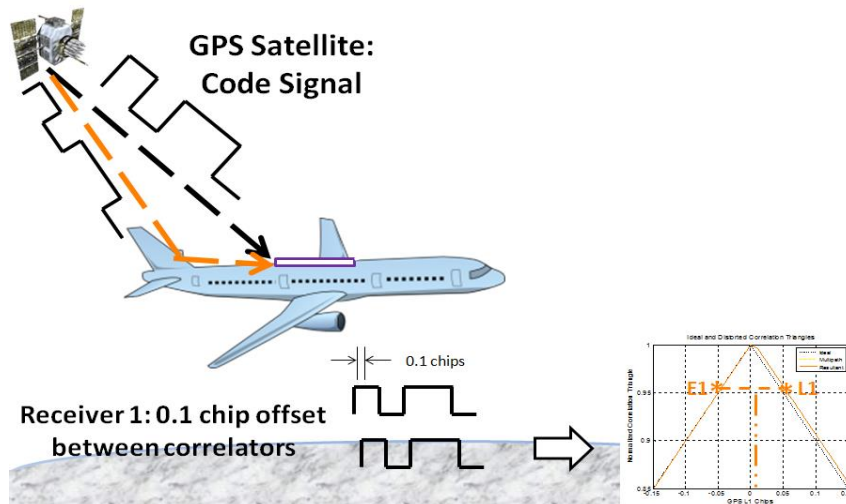
Figure 2-23: Multipath

When the multipath is in phase with the signal, constructive interference occurs; destructive interference occurs when the multipath is in anti-phase with the signal. In both cases, range biases result as shown in the correlation triangles (Refer to Figure 2-24). The magnitude of these biases also depends on the receiver tracking loop's correlator spacings.

As the multipath phase varies continually between in-phase and anti-phase due to relative motion of the satellites and the user, the biases also vary continually in a pseudo-sinusoidal fashion. In fact, GPS satellite orbits approximately repeat in a sidereal day (≈ 23 hrs 56 mins). Thus for a stationary user, multipath effects approximately repeat on a daily basis.
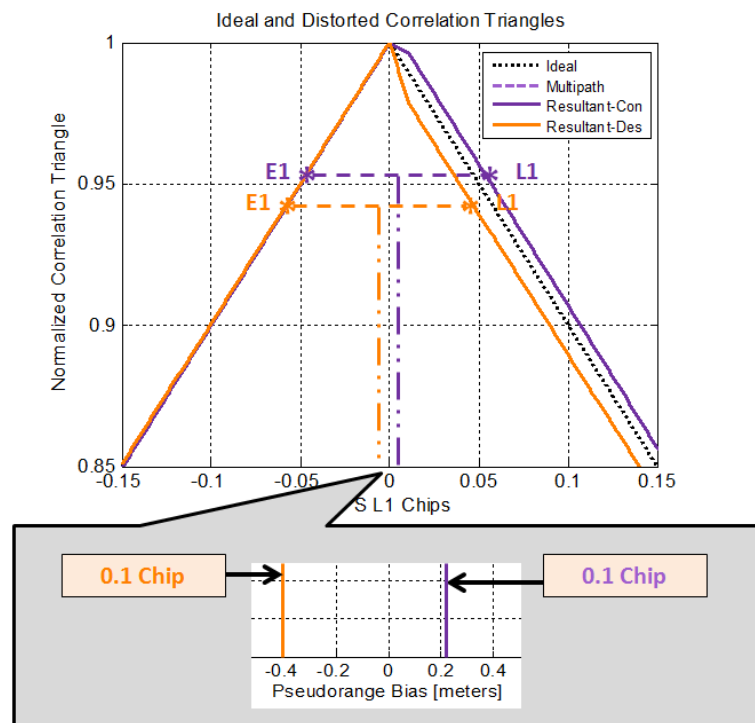
Figure 2-24: Range Biases from Multipath

2.4.2   Mitigation of Receiver-Dependent Errors

Multipath, Radio Frequency Interference and Receiver White Noise Mitigation

Antennas (Section 3.3.1) could effectively limit white noise and multipath. Directional, high-gain dish antennas or helical antennas reduce the effects of multipath and noise. Other multipath-limiting antennas include choke-ring antennas, which have very low gains for signals arriving at elevation angles less than 3-5°; these antennas attenuate multipath which typically arises from signal reflections off the ground or low-lying obstacles. Proper siting of the antennas in clear open environments without nearby obstacles (Section 3.3.2) would also result in reduced multipath.

Suitable receiver designs also reduce the effects of multipath and white noise. Besides the use of higher quality front-end components (Section 2.3.1) with lower noise figures, multicorrelator-based methods are used to reduce multipath and noise. Such methods make use of strategically spaced correlators (Section 2.3.2), weighting, and linearly combining their outputs for multipath and noise minimization. One such effective technique is the narrow correlator receiver implementation [42, 43], where a shorter than typical time delay between the Early and Late correlators is used: 0.1 chips instead of 1.0 L1-chips (hence, the term narrow correlator). The noise components in the early and late correlator outputs are highly correlated, leading to greater cancellation in the Early-minus-Late discriminator. The discriminator also experiences less distortion from multipath when the correlator spacing is small. Other similar multicorrelator-based methods include the strobe correlator [44], [45], double-delta and real-time Tracking Error Compensator (TrEC) [46], [47] techniques.

Other multipath mitigation strategies use probabilitistic techniques, such as maximum likelihood (ML), maximum *a posteriori* (MAP), or minimum mean square multipath errors (MMSE) methods, to estimate the amplitude, phase, and delay of the multipath. The estimated multipath signals are subsequently removed. These methods include the Multipath Estimating Delay Lock Loop (MEDLL) [48] and MMT [49]. Note that these multipath estimation algorithms could actually increase signal deformation effects in the process of multipath estimation and correction.

Time-filtering and carrier-smoothing [50] algorithms also decrease the impact of multipath and white noise. These algorithms are efficacious in mitigating white noise, which typically is zero mean, but may have varied effectiveness in attenuating the impact of multipath, which could have non-zero averages over time.

<u>Mitigation of Satellite Signal Deformation Range Biases</u>

In the absence of mitigation strategies, Vertical Protection Level equations (Section 2.5.2; [51]) could be used to account for the satellite signal deformation range biases. This is known as the "Bound and Exclude" method and is briefly discussed in Section 5.2.2. Effective mitigation techniques are also available, such as the "Measure-and-Correct" strategy to precisely measure and calibrate the biases in user receivers (Sections 5.2.1 and 6.2.2), and the "Restrict-User-Space" method (Section 5.2.3). The "Restrict-User-Space" method is advocated due to its practicality and efficacy, and will be discussed in greater detail later in Sections 5.2.3 and 5.3.

2.4.3   Receiver-Independent Errors

The receiver-independent errors include errors in clock (timing) and ephemeris (satellite location information) originating on board the satellites, as well as errors caused by the propagation of the satellite signals through Earth's atmosphere.

Atmospheric propagation errors are introduced as the GPS signal is transmitted through Earth's atmosphere. They include dispersive ionospheric errors and non-dispersive tropospheric errors. Both introduce delays to signal propagation.

Ionospheric delays are correlated with the density of ions in the ionosphere, which in turn is highly dependent on solar activity. The ionosphere is dispersive; signals of different frequencies experience different delays inversely proportional to the square of the signal frequencies. Ionospheric delays are the largest of the errors: zenith ionospheric delays vary at mid-latitudes from about 1-3 m at night to 5-15 m in the midafternoon. Near the equator at the peak of a solar cycle, zenith delays as large as 36 m were reported; taking into account the obliquity factor, the resultant slant range delays were larger than 100 m [52], [53]. Tropospheric delays depend on air pressure and water content of the air. The troposphere is non-dispersive, that is, tropospheric delays are independent of signal frequency. Zenith tropospheric errors are smaller than tropospheric errors; they could be 2.3-2.6 m at sea level. In addition, the effects of tropospheric and ionospheric delays depend on the elevation angle of the satellite with respect to the user receiver. Signals arriving from lower elevation angles pass through

more of the atmosphere, and suffer greater path delays, than do those arriving from higher elevation angles.

2.4.4 Mitigation of Receiver-Independent Errors

<u>Clock and Ephemeris Errors</u>

Satellite clock and ephemeris errors have characteristics closer in nature to random biases and drifts than white noises. Common error reduction methods used in standalone receivers, such as time-filtering, averaging, and carrier-smoothing, are designed to handle white noise and are ineffective as a result.

Differential-GPS is both practical and effective. Using this technique, the satellite clock and ephemeris errors are easily detected and mitigated.

<u>Atmospheric Errors</u>

Differential-GPS, dual-frequency ranging (for ionospheric errors only), and empirical atmospheric model corrections are commonly used to mitigate these errors.

<u>Differential-GPS</u>

Atmospheric errors tend to be receiver-independent, i.e., have almost identical effects on user receivers of different configurations. Consequently, it is straightforward to correct for them using the differential-GPS approach: When there is a high degree of

spatial correlation between the errors at the reference and user receiver (< 10 km), correction via differential-GPS is very effective.

However, ionospheric errors can quickly become uncorrelated even over short distances and short time periods in extreme rare-normal conditions such as during solar flares or solar storms. For instance, ionospheric delay differences of up to 6 m over a distance of 19 km, or 316 mm/km, were reported in 2001 due to ionospheric anomalies [54]. As a result, differential ionospheric corrections can quickly become ineffective for reference and user receivers spread over larger distances; only dual-frequency ranging would be useful in this case.

Dual-frequency Ranging for Ionospheric Errors

Dual-frequency ranging would be extremely helpful in mitigating large errors during times of extreme conditions, such as during solar flares or solar storms. The dispersive nature of the ionosphere can be exploited to mitigate the ionospheric errors, by using multiple range measurements at different frequencies that are time-synchronized and phase-aligned.

From Section 2.3.5 Equation (2.6),

$$\widehat{r}_{L1} = r + I_{L1} + T + \varepsilon_{L1} + MP_{L1} + SSD_{L1} \tag{2.25}$$

$$\widehat{r}_{L5} = r + I_{L5} + T + \varepsilon_{L5} + MP_{L5} + SSD_{L5} \tag{2.26}$$

Where

$\hat{r}_{Ln}$:   Range estimate at L1-frequency (1.57542) GHz or L5-frequency (1.17645 GHz)

r :   True range

I_{Ln} :   Ionospheric error at L1-frequency (1.57542) GHz or L5-frequency (1.17645 GHz)

T :   Tropospheric error (non-dispersive; independent of frequency)

ε_{Ln} :   Radio-Frequency Interference and Receiver White Noise error at L1-frequency (1.57542) GHz or L5-frequency (1.17645 GHz)

MP_{Ln} :   Multipath error at L1-frequency (1.57542) GHz or L5-frequency (1.17645 GHz)

SSD_{Ln} :   Satellite Signal Deformation range error at L1-frequency (1.57542) GHz or L5-frequency (1.17645 GHz)

$$I_{L1} \approx OF \times \frac{40.3 \times TEC}{f_{L1}^2} \tag{2.27}$$

$$I_{L5} \approx OF \times \frac{40.3 \times TEC}{f_{L5}^2} \tag{2.28}$$

Where

I_{L1} :   Ionospheric error at L1-frequency, 1.57542 GHz

TEC :   Total Electron Content in atmosphere

OF :   Obliquity factor - The increase in path length through the ionosphere that an oblique ray takes relative to a vertical ray [55]

f_{L1} :   L1-frequency, 1.57542 GHz

I_{L5} :   Ionospheric error at L5-frequency, 1.17645 GHz

f_{L5} :   L5-frequency, 1.17645 GHz

Scaling (2.25) and (2.26) appropriately and substituting one into the other,

$$
\begin{aligned}
\widehat{r}_{iono-free} &= \frac{f_{L1}^2}{f_{L1}^2 - f_{L5}^2}\widehat{r}_{L1} - \frac{f_{L5}^2}{f_{L1}^2 - f_{L5}^2}\widehat{r}_{L5} \\[2mm]
&= K_{L1} \times \widehat{r}_{L1} - K_{L5} \times \widehat{r}_{L5} \\[2mm]
&= r + K_{L1} \times (\varepsilon_{L1} + MP_{L1} + SSD_{L1}) - K_{L5} \times (\varepsilon_{L5} + MP_{L5} + SSD_{L5}) \\[2mm]
&= r + (K_{L1} \times (\varepsilon_{L1} + MP_{L1}) - K_{L5} \times (\varepsilon_{L5} + MP_{L5})) \\
&\quad + (K_{L1} \times SSD_{L1} - K_{L5} \times SSD_{L5}) \qquad\qquad\qquad (2.29)
\end{aligned}
$$

$$
K_{L1} = \frac{f_{L1}^2}{f_{L1}^2 - f_{L5}^2} \approx 2.26 \qquad\qquad\qquad\qquad\qquad\qquad (2.30)
$$

$$
K_{L5} = \frac{f_{L5}^2}{f_{L1}^2 - f_{L5}^2} \approx 1.26 \qquad\qquad\qquad\qquad\qquad\qquad (2.31)
$$

Where

$\widehat{r}_{iono-free}$: Ionospheric-free range estimate

ε_{Ln} : Radio-Frequency Interference and Receiver White Noise error at L1-frequency (1.57542) GHz or L5-frequency (1.17645 GHz)

MP_{Ln} : Multipath error at L1-frequency (1.57542) GHz or L5-frequency (1.17645 GHz)

SSD_{Ln} : Satellite Signal Deformation range biases at L1-frequency (1.57542) GHz or L5-frequency (1.17645 GHz)

K_{L1} : Dual-frequency ionosphere-error-removal scale factor for L1-frequency. Also amplification factor for L1-frequency multipath, noise, and satellite signal deformation range biases.

K_{L5} : Dual-frequency ionosphere-error-removal scale factor for L5-frequency. Also amplification factor for L5-frequency multipath, noise, and satellite signal deformation range biases.

The disadvantage of the dual-frequency linear combination is the amplification of L1-frequency multipath, noise, and satellite signal deformation range biases by a factor of $K_{L1} = 2.26$, and L5-frequency multipath, noise, and satellite signal deformation range biases by $K_{L5} = 1.26$.

Assuming uncorrelated multipath, noise, and and satellite signal deformation range biases between the two frequencies, the total amplification is the root-sum-square of the two factors: 2.6 [Equation (2.32)]. Applications requiring highly-precise navigation may be limited in the absence of further mitigation.

$$K_{DUAL-FREQ-IONO} = \sqrt{2.26^2 + 1.26^2}$$

$$= \sqrt{2.26^2 + 1.26^2}$$

$$\approx 2.6 \tag{2.32}$$

Empirical Atmospheric Model Corrections

Where there are no reference receivers, differential GPS is unavailable and empirical atmospheric model corrections would have to be used for mitigation.

For mitigation of ionospheric error, the Kloubuchar ionospheric model estimates the Total Electron Content (TEC) in Equations (2.27) and (2.28), and typically is able to remove 50% of the ionospheric error in mid-latitudes [56], leaving a zenith residual error of 1-10 m, or more [52]. As mentioned previously, this method is only effective when the ionosphere is quiescent and there are no sudden spatial or temporal gradients in the ionosphere.

For mitigation of tropospheric error [56], the delay depends on the refractivity which can be modeled using dry and wet components. The dry component arises from dry air and is responsible for about 90% of the delay; it can be predicted very accurately using temperature and pressure information. The wet component is caused by water vapor and is less predictable. Without meteorological data, the zenith residual error could be 5-10 cm.

2.5   Augmented GNSS for Aviation Users: WAAS

The Wide Area Augmentation System (WAAS) was developed by the Federal Aviation Administration (FAA) for civil aviation users. WAAS aims to meet the accuracy, integrity, and continuity requirements of en route and terminal phases of

flight, and non-precision and near-Category I precision approaches. WAAS is designed to be available all the time, to user receivers at all locations, for all classes of aircraft [1].

To meet the stringent safety requirements, WAAS is required to provide highly accurate position estimates to users (4 m errors at 95% confidence; 35 m at 99.99999% confidence) with high integrity, i.e., to guarantee that users have an extremely small chance (less than 1 in 10,000,000 approaches) of experiencing hazardously large positioning errors. WAAS is also required to provide timely warnings to users (within 6 seconds) when the GPS/WAAS system is unusable due to faults, system errors, or other effects. While meeting these stringent safety requirements, WAAS is also expected to at least maintain 99.9% availability [57].

In summary, the goal of WAAS is to "guarantee bounded-error navigation for safety-critical applications," at high availability. Subsequent sections will discuss the accuracy, integrity, and availability considerations.

2.5.1 Accuracy

To meet the accuracy requirements, WAAS makes use of differential-GPS (Section 2.4 and 2.4.4). 38 WAAS reference stations are situated in North America and Hawaii. These stations estimate the errors caused by satellite clock, ephemeris and atmospheric delays, and broadcast these error corrections to users via geostationary satellites over

CONUS. As a result, WAAS users experience an improved positioning error of 0.9 m (95% horizontal) and 1.3 m (95% vertical) instead of 2.3 m (95% horizontal) and 7.4 m (95% vertical) for unaided GPS users [58].

Presently, WAAS broadcasts only L1-frequency ionospheric error corrections to support current L1-frequency users. As the new L5-frequency signals become available in the future, WAAS will also provide dual-frequency ranging and error corrections for L1/L5 users.

2.5.2   Integrity

Besides the improved accuracy of WAAS, what sets WAAS apart as a safety critical system is in the provision of worst case error bounds (or Protection Levels) to the user, and timely warnings of rare system faults and atmospheric anomalies [59].

WAAS estimates and provides error variances to the user, for satellite clock, ephemeris and ionospheric error components for each individual satellite [60].

For practical implementation reasons, the distributions of these error components are represented using independent Gaussian distributions, even though these assumptions may not be entirely true. Bruce Decleene and Jason Rife demonstrated that independent Gaussian distributions can be found to overbound the actual error distributions, through the use of larger, or "inflated," variances [61], [62].

Using the overbound Gaussian variances for the error components for individual satellites, the user computes a root-sum-square aggregated overall error variance based on the satellite signals used [60]. This process is detailed further in Section 4.2.1 Subsection 2.

Using the aggregated overall error variance, the user is able to generate a worst case error bound or Protection Level (PL) (Section 4.2.1 Subsection 4). The true error must not exceed the Protection Level more than once in 10^7 approaches, as specified in the Minimum Operational Performance Standards (MOPS) for WAAS [63]. That is,

P(True error from worst case nominal and undetected faults > PL) < 1e-7   (2.33)

The user can compare his computed worst-case-error bound with the minimum hazardous position error, or Alert Limit, to determine if WAAS/GPS is safe to use for the desired operation.

$$\{PL \leq AL\} \rightarrow \text{WAAS Safe to Use} \tag{2.34}$$

Where

PL :   Protection Level, an integrity bound for 99.99999% of GPS position errors.

The exact computation is found in Section 4.2.1 Equation (4.5).

AL   :   Alert Limit, the minimum hazardous vertical position error, beyond which

WAAS should be declared unavailable

For Localizer Performance with Vertical Guidance with a decision height of 200 ft, or

LPV200 [63], the Vertical Alert Limit is 35 m. For Localizer Performance with

Vertical Guidance with a decision height of 250 ft, the Vertical Alert Limit is 50 m.

Horizontal Alert Limits are 40 m in both cases.

The challenge for WAAS is to provide error bounds that are sufficiently conservative

to be safe − a bound for 99.99999% of worst case errors, yet also sufficiently tight

such that the Protection Limits are below the Alert Limits most of the time for WAAS

system availability (Section 2.5.3).

The other aspect of WAAS integrity, or trusted navigation, is the monitoring of system

faults and rare normal events (such as ionospheric storms or solar flares). When these

occur (rarely), WAAS users are to be notified in a timely fashion: within 6 secs.

Monitors used include the signal deformation monitor, which detects faulted,

anomalous satellite signal deformation (Section 1.3). Other monitors include Code-

Carrier divergence monitors and the Extreme Storm Detector Monitor [59].

As in the choice of error overbounds, the choice of over-conservative fault detection

thresholds could lead to a loss of availability (Section 2.5.3). Thus fault detection

thresholds are required to be analyzed carefully and chosen judiciously.

2.5.3 Availability

WAAS is required to have availability of at least 99.999%, where availability is the fraction of the time that integrity and continuity requirements are met by WAAS [64].

Recall in Section 2.5.2 that for WAAS, the probability of true errors from worst case nominal and undetected faults exceeding the worst case error bound (Protection Level) is required to be at most 1 in 10,000,000 [Equation (2.33)]. An integrity test is conducted by verifying that the worst case error bound, or Protection Level (PL), does not exceed the Alert Limit (AL), which is the minimum hazardous error. If the integrity test is met for both nominal and faulted conditions, WAAS is safe to use and declared available [Equation (2.34)].

The worst case error bound/ Protection Level is determined by the individual error bounds for components of satellite errors, fault detection thresholds, and even receiver types and user design. The individual error bounds, fault detection thresholds and allowed receiver and user design spaces need to be chosen conservatively so that safety is maintained by sufficiently binding all true errors from worst case nominal and undetected faults [Equation (2.33)]. Yet the Protection Level is also required to be tight and not overly conservative, or availability could be adversely affected [Equation (2.34)].

In this dissertation, the goal is to protect all users, and maximize this protection for the

widest possible range of receiver design spaces and types.

Chapter 3

Measurement of Satellite Signal Deformation Range Biases

3.1   Overview

This chapter articulates the main contribution of this dissertation – rendering nominal satellite signal deformation range biases observable and measurable. To do so, several measurement errors need to be effectively suppressed. The use of differential-GPS removes much of the receiver-independent errors (Section 2.4.4). For effective measurement of the residual receiver-dependent errors, the research community has traditionally used two different techniques: "one-in-view" schemes with high-resolution, high-gain large parabolic dishes, and "all-in-view" schemes with hemispherical low-resolution, low-gain antennas.

Due to the inherent, irremovable errors in both of these techniques, the obtained measurement results are of "measure-and-trust" nature, thus necessitating the development of a novel, "measure-and-verify" hybrid approach. This latter technique uses the "one-in-view" method to measure, and the "all-in-view" method to verify, leveraging the benefits and mitigating the limitations of either individual method. The "measure-and-verify" approach renders satellite signal deformation range biases quantifiable and repeatable, with an order of magnitude improvement compared to either prior technique.

The new method provides high quality nominal satellite signal deformation range bias measurements for both the L1-frequency and L5-frequency signals. These in turn facilitate the accurate determination of the resultant position errors experienced by user receivers under nominal conditions, i.e., without a signal deformation fault.

Section 3.1 introduces the specialized equipment used in this dissertation to measure satellite signal deformation range biases: atomic clock reference and high-rate data logger/modified GPS receiver. Section 3.2 revisits the challenges posed by measurement errors in the accurate quantification of satellite signal deformation range biases. These are overcome through suitable experimental setup and feasible choices of hardware. The different configurations of hardware and experimental setup used in this thesis are summarized in Section 3.3.

Results from the two prior "measure-and-trust" measurement techniques are next presented and discussed. Section 3.4 presents "one-in-view" large parabolic dish measurements of satellite signal deformation range biases, and Section 3.5 presents corresponding measurements using the "all-in-view" hemispherical antennas. The limitations of the measurement methods are also highlighted and discussed.

Section 3.6 introduces the "measure-and-verify" method. This method is used to measure satellite signal deformation range biases for both L1-frequency and L5-frequency signals. Differences in method and results, compared to the two prior methods, are highlighted. Section 3.7 discusses the significance of the results obtained.

Another measurement approach using Controlled Pattern Reception Array (CRPA) was also explored; this is described in Appendix C of the dissertation.

3.2   Equipment to Measure Satellite Signal Deformation Range Biases

Two types of specialized hardware were used in this dissertation to observe and measure satellite signal deformation range biases: a highly stable reference clock source such as a rubidium atomic clock, and high-bandwidth, high-rate data loggers-cum-GPS receiver.

3.2.1   Reference Atomic Clock

Figure 3-1 shows a Rubidium atomic clock used in this dissertation. This clock was used to provide a stable reference for the measurement of satellite signal deformation range biases, to minimize clock biases and drifts especially over long periods of data collection.
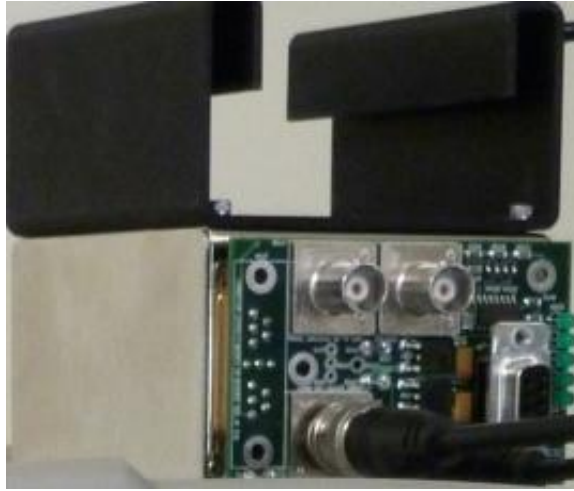
Figure 3-1: Rubidium Atomic Clock

3.2.2   Specialized Data Logger/ Modified GPS Receiver
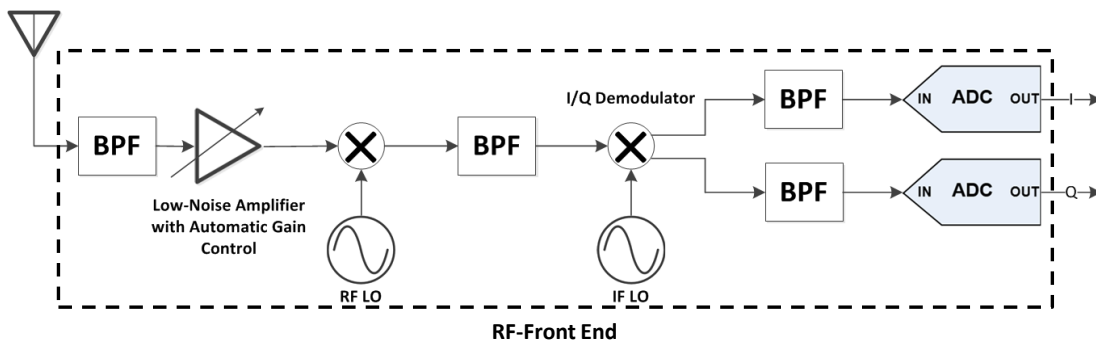
Figure 2-7: GPS Receiver RF-Front End

Figure 2-7 (previously described in Section 2.3.1) shows the signal processing chain. The very weak radio-frequency signal from the GNSS antenna first passes through a Radio-Frequency Front-End (RF-FE), which filters, amplifies and down-converts the GNSS signal from L-band Radio-Frequencies (RF) of larger than 1 GHz to Intermediate Frequencies (IF) lower than 100 MHz. This high-rate, high-bandwidth data is then sampled and either logged using a Vector Spectrum Analyzer for subsequent offline processing, or processed in real-time using a USRP (Universal Software Receiver Protocol) receiver.

High-rate, High-Bandwidth Vector Spectrum Analyzer (VSA)

The Agilent 89600 Vector Spectrum Analyzer (Figure 3-2) was used in the large dish method (Section 3.4). It has a large input bandwidth (36 MHz one-sided), high sampling rate (46.08 MSps), 2-channel complex sampling, and incorporates a Radio Frequency Front End with excellent noise properties. Unfortunately, due to hardware constraints, only 2 seconds of data can be logged at a time for post-processing. Its large input bandwidth, high-sampling rate, and excellent noise properties were useful for determining the raw signal waveforms, waveform distortions, and range biases (Appendix B-5).

Figure 3-2: Agilent 89600 Vector Spectrum Analyzer (VSA), a high-rate, high-

resolution, large bandwidth data logger

Specially Configured USRP GNSS Receiver

In this dissertation, a specially-configured software GNSS receiver based on the

Universal Receiver Software Protocol (USRP) hardware [65] was used for the

hemispherical "all-in-view" "measure-and-trust" technique (Section 3.5) and the

hybrid "measure-and-verify" strategy (Section 3.6). The USRP front-end hardware's

filter bandwidth, center-frequency, and output sampling rate are configurable. It is

connected to a laptop for real-time computation of satellite signal deformation range

biases. The setup is shown in Figure 3-3.
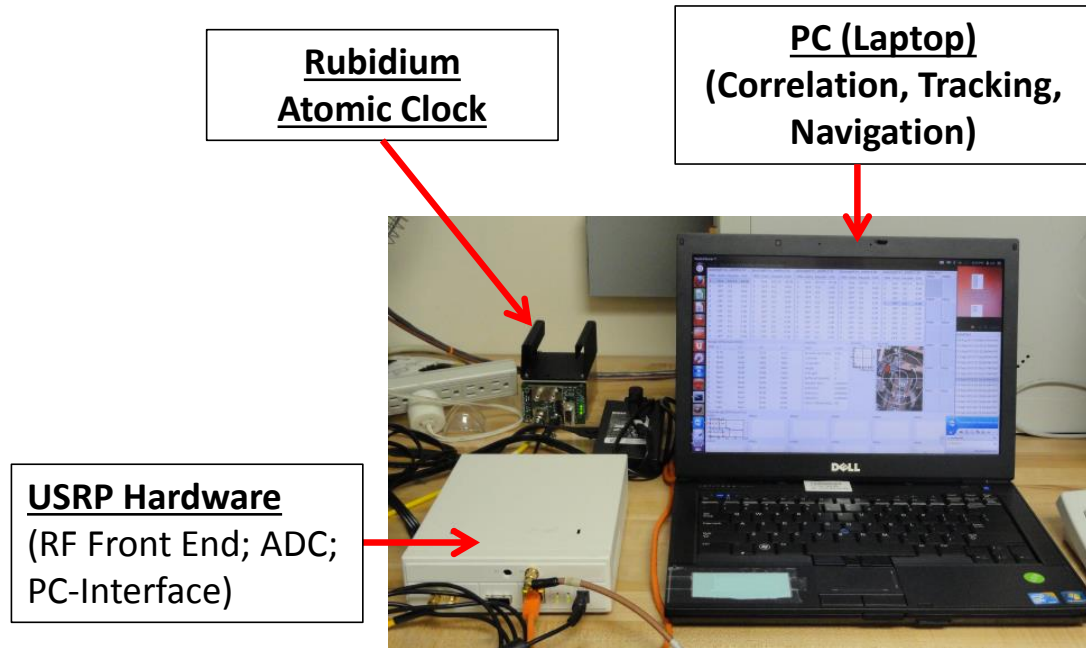
Figure 3-3: USRP GPS Receiver

Using this specially configured GNSS receiver, GNSS ranges all synchronized to the same clock could be computed at different correlator spacings. The GNSS ranges at the other correlator spacings are differenced from the "truth" GNSS range at the reference correlator spacing to yield differential range bias measurements.

3.3   Setup to Mitigate Measurement Errors

The measurement methods for satellite signal deformation range biases contain various measurement errors. These measurement errors need to be attenuated to accurately observe and quantify the biases. In this dissertation, the receiver-independent measurement errors, such as the clock, ephemeris, ionospheric and tropospheric errors, were largely eliminated using a differential-GPS configuration

with two different receivers, each sharing a common receiver clock and common antenna feed. What remained was the satellite signal deformation differential range bias between the two receivers, which is the quantity of interest, as well as residual errors from radio-frequency interference, receiver white noise, multipath, and long-term time-varying errors. Radio-frequency interference and receiver noise are generally "white" and zero-mean and can be effectively mitigated via averaging over longer time periods (e.g., minutes). However, multipath errors and long-term time-varying effects (Section 3.5.2) are the most challenging to remove because they could possibly have non-zero means, limiting the effectiveness of averaging methods.

When "one-in-view" parabolic dish antennas were used (Section 3.4), the high antenna gain and directivity resulted in lower levels of radio-frequency interference, white noise, and multipath. Unfortunately, long-term time-varying drifts were observed and could only be alleviated using intensive calibration processes [66]. This calibration was not practical or feasible for the large SRI dish antenna, but was implemented for the 1.8 m mini-dish on the rooftop of the Stanford GPS Lab (Section 3.6).

For hemispherical antennas (Section 3.5 and 3.6), multipath is generally dominant due to the lower antenna gain and directivity. Three important ways to reduce multipath are to use averaging where multipath amplitudes are small [67], use multipath-limiting antennas, and choose low-multipath environments for measurement collection.

Subsequent sections describe the strategies used in this dissertation to reduce the multipath, the dominant residual error in the hemispherical dish measurements, to render signal deformation range biases observable.
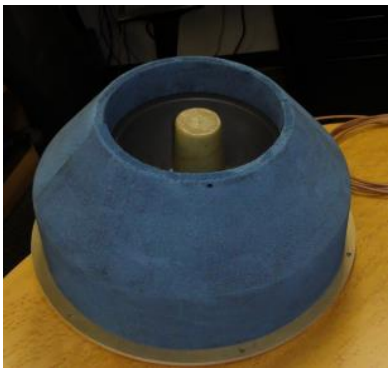
3.3.1   Multipath Limiting Antennas

A variety of different antennas were used for the measurement of satellite signal deformation range biases. Since the measurement locations were land-based, ground multipath was usually dominant, from signal reflections off obstacles on the ground. To combat this multipath, multipath-limiting hemispherical "all-in-view" antennas were used (Section 3.5). These antennas had hemispherical beam patterns with normal gain for satellites above certain elevation cutoff angles (ranging between 3° - 30° depending on antenna); below the cutoff angles, the signal gain rapidly decreased, to reduce the effects of ground multipath.

A more sophisticated Controlled-Pattern Reception Pattern (CRPA) antenna made use of beamforming to focus narrow antenna gain patterns in the direction of several individual satellites simultaneously, further attenuating interfering signals from the ground or in other directions (Appendix C).

In the most extreme case, parabolic dish antennas were used (Sections 3.4 and 3.6). These "one-in-view" antennas focused a single, narrow, and high-gain antenna beam at satellites. These antennas were able to provide the most effective suppression of

multipath errors and radio-frequency noise. However, the narrow beam-widths also limited the antennas' ability to monitoring only a single satellite at a time. The use of these antennas is summarized in Table 3-1.

Antenna	Description	# satellites in view
	Survey-grade geodetic antennas (Hemispherical) (Section 3.5)	
	Choke Ring Multipath Limiting Antenna (Hemispherical) (Section 3.5)	"All-in-view": Multiple satellites simultaneously
	Helibowl* Multipath Limiting Antenna (Hemispherical) (Section 3.5)	
	Controlled Reception-Pattern Array (CRPA) Antenna [4] (Narrow-beam) (Appendix C)	
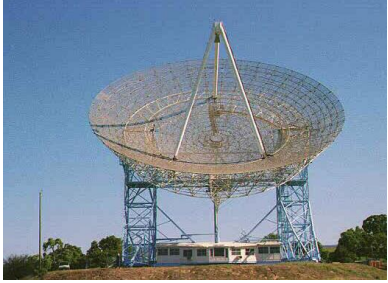
Antenna	Description	# satellites in view
	1.8 m Mini-Dish Antenna on Durand Rooftop (Section 3.6)	"One-in-view": One-satellite-at-a-time
	Large 46 m SRI Dish Antenna (Section 3.4)	

Table 3-1: Different multipath-limiting antennas used for measurement collection

*Helibowl: helical antenna in a metallic bowl limiting measurements from satellites

below 30° in elevation.

3.3.2 Environments for Multipath Reduction

To combat multipath, particularly when hemispherical "all-in-view" antennas were used (Sections 3.5 and 3.6), low-multipath environments were chosen to site the antennas. Ideal low multipath environments were high-altitude, flat, wide open areas with minimal obstructions that could cause signal reflections. The following figures show three examples of low multipath environments used in the measurement process in this dissertation.

Figure 3-4: Durand Rooftop

Figure 3-5a: Roble Field Aerial View	Figure 3-5b: Roble Field Ground View
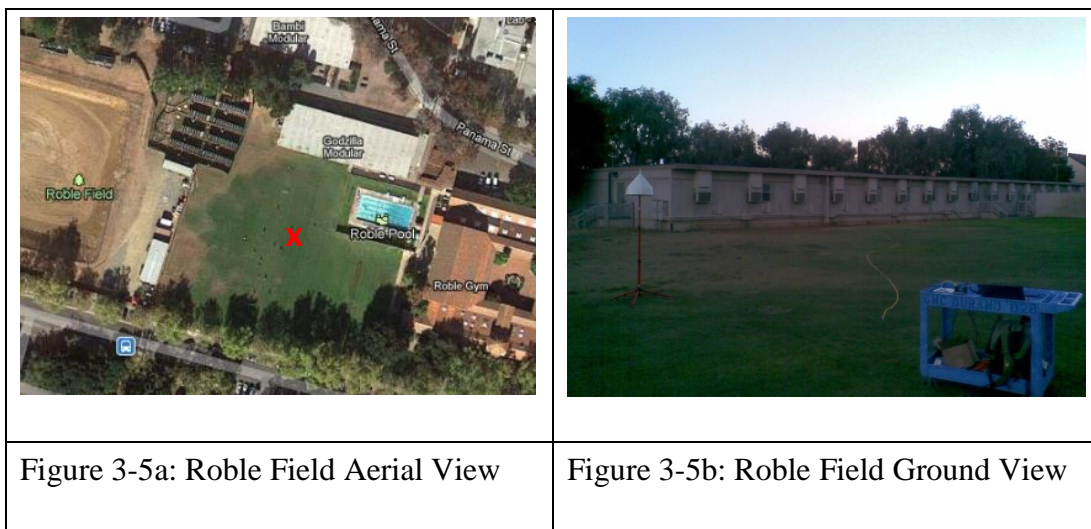
Figure 3-5: Roble Field

Figure 3-6a: Lake Lagunita Aerial View	Figure 3-6a: Lake Lagunita Ground View
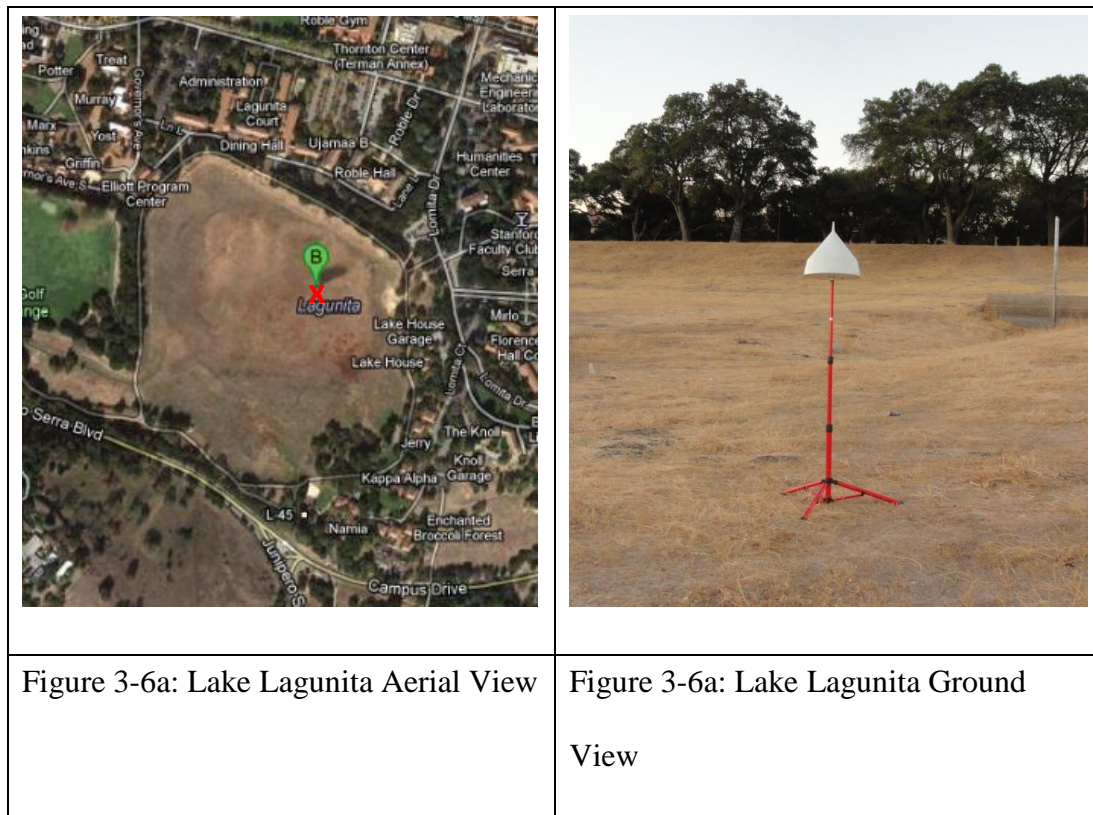
Figure 3-6: Lake Lagunita (Dry lake bed)

3.4   Summary of Measurement Setup Used in This Dissertation

Table 3-2 summarizes the equipment and measurement setup used in this dissertation for the measurement of satellite signal deformation range biases. These are described for the two prior "measure-and-trust" techniques and the hybrid "measure-and-verify" strategy.

The WAAS reference correlator spacing is 0.1 L1-chips for the L1-frequency signal and 1.0 L5-chips for the L5-frequency signal (Section 2.3.2). The measurement

configurations used in this thesis match these specifications. For measurement of L1-frequency range biases (Sections 3.5.1, 3.6.2, and 3.7.3):

- the range at correlator spacing of 0.1 L1-chips was the reference (taken as "truth")

- ranges at other correlator spacings were differenced from the reference to determine the differential range biases.

- The front-end filter bandwidth used was 36 MHz for the VSA and **<u>16</u>** MHz for the USRP-based receiver.

Similarly, for measurement of L5-frequency range biases (Section 3.7.4):

- the range at correlator spacing of 1.0 L5-chips was the reference (taken as "truth")

- ranges at all other correlator spacings were differenced from the reference to determine the differential range biases.

- The front-end filter bandwidth used was 36 MHz for the VSA and **<u>24</u>** MHz.

Section	Antenna	Environment	Hardware	Filter Bandwidth [MHz]	Reference Correlator Spacing (Chips)	Waveform Distortions (Analog and Digital)	Satellite Signal Deformation Range Biases
3.5	Large 46 m SRI Dish *("One-in-view")*	Stanford Foothills	Data Logger (VSA)	36*	0.1 L1-Chips 1.0 L5-Chips	√	√
3.6	Various Hemispherical *("All-in-view")*	Various low-multipath locations (Section 3.2)	Modified GPS Receiver (USRP + Laptop)	16 (L1) 24 (L5)	0.1 L1-Chips 1.0 L5-Chips		√
3.7	Mini 1.8 m Rooftop Dish *("One-in-view")*	Rooftop of Stanford GPS Lab	Modified GPS Receiver (USRP + Laptop)	16 (L1) 24 (L5)	0.1 L1-Chips 1.0 L5-Chips		√ (Measurement)
3.7	Hemispherical Multipath-Limiting *("All-in-view")*	Rooftop of Stanford GPS Lab	Modified GPS Receiver (USRP + Laptop)	16 (L1) 24 (L5)	0.1 L1-Chips 1.0 L5-Chips		√ (Verification)

Table 3-2: Summary of different hardware configurations used in this dissertation

*: For measurement of waveform distortions, it is advisable to have widest possible bandwidth for data-logger: 36 MHz.

3.5   46-meter SRI Dish Antenna Range Bias Measurements

This section presents "one-in-view" dish antenna measurements using a large 46 meter SRI dish antenna. Using this antenna, satellite signal waveforms were logged over a single 24-hour time period. These waveforms were processed to determine the nominal satellite signal deformation range biases for all individual GPS and WAAS-GEO satellite signals. These range biases and the inherent limitations in the dish method are presented and discussed in Sections 3.5.1 and 3.5.2. Section 3.5.3 summarizes the large satellite dish method, results, and implications.

The detailed measurement procedures and processing steps are listed in Appendix B-2 and Appendix B-3. In addition, Appendix B also analyzes the signal waveform distortions for all individual GPS and WAAS-GEO satellite signals at the time of data collection in August 2010. This complete set of analog and digital signal waveform distortions, based on data collected over a single 24-hour period, was published for the first time in open literature. Besides their importance in the analyses of the resultant range biases, these waveform distortion results are significant for the following two reasons. The digital distortions have shown long-term constancy over a period of up to nine years. Also, the distortion results include the first of a new block of GPS satellites, which could be indicative of the distortion characteristics of the entire block. Finally, Appendix B-6 also describes the detailed processing steps to determine the range biases from raw logged waveforms.

3.5.1 Dish-Measured Range Biases

Appendix B-2 and Appendix B-3 describe the meausrements of actual transmitted satellite signal waveforms. The measured waveforms contain both analog distortions (overshoot and ringing) and digital distortions (asymmetry of durations of positive and negative chip waveforms). (These distortions are illustrated for clarity in Appendix B-4.2; digital distortion results are presented in Appendix B-5.3; the analog distortions are presented in Appendix B-5.1 and Appendix B-5.2 and reproduced here for discussion.
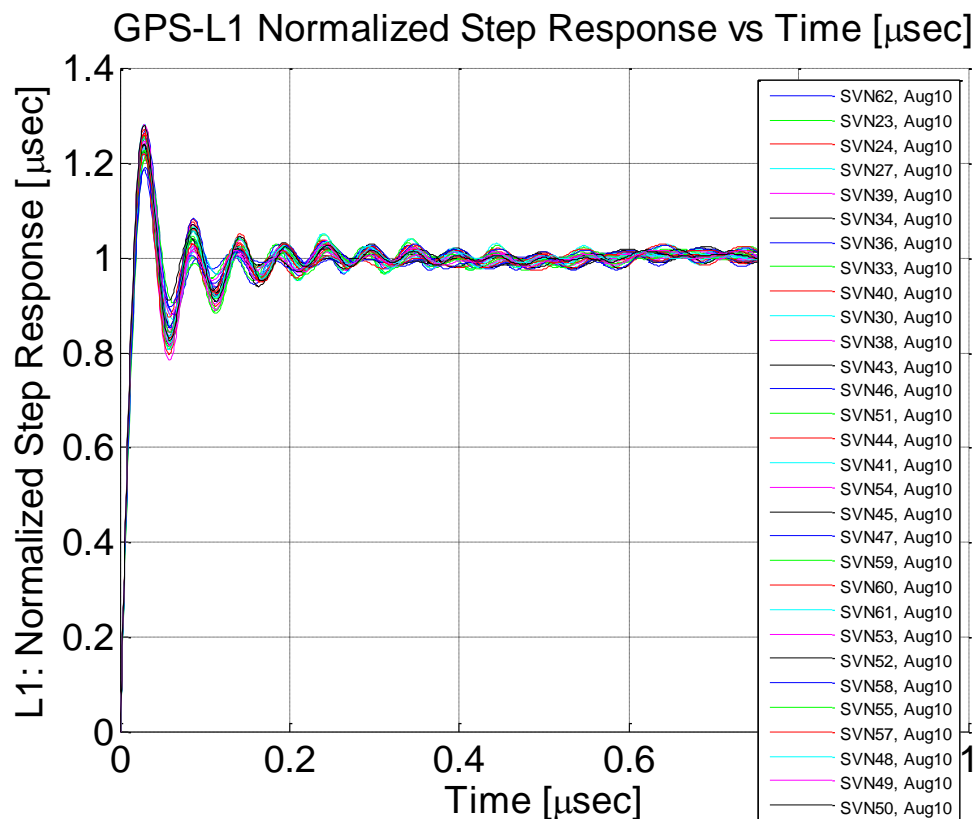
Figure 3-7: Chip-shape waveforms showing analog distortions for GPS satellite signals at L1 frequency based on SRI dish data measurements made in Aug 2010

(Reproduced from Figure B-21

As demonstrated in Appendix B-4.2, analog signal distortions result in distorted, asymmetric correlation triangles with slightly undulating characteristics. Digital signal distortions cause a flattening of the correlation peak. Both these distortions contribute to biases at the output of the Early-Minus-Late discriminator in the code tracking loop, which in turn lead to range biases.

To determine these resultant range biases, the chip-shape waveforms are processed using operations similar to those in actual GPS receivers: correlation (matched filter) with ideal replica chip-shape waveform, discriminator and determination of resultant biases. These processing steps are described in more detail in Appendix B-6 (Resultant Range Biases from Waveform Distortions).

Figure 3-8 shows the range biases for all GPS satellites after correction for time-varying drifts (Section 3.5.2 and Appendix B-6). This figure shows the nominal satellite signal deformation biases experienced by user receivers of different correlator spacings and for all GPS L1 satellite signals, with a reference receiver of 0.1-chip correlator spacing providing the reference truth.
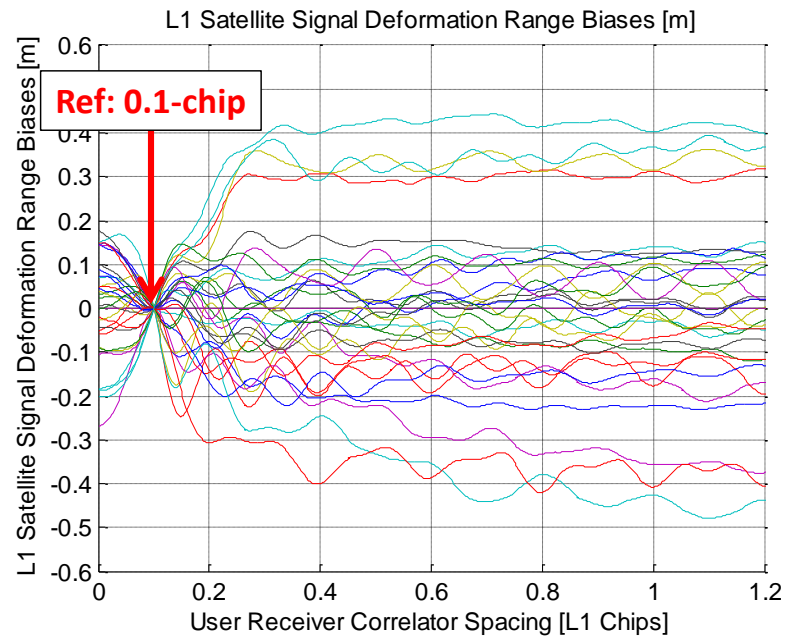
Figure 3-8: L1 Satellite signal deformation range biases for all user receiver correlator

spacings

(Reference: 0.1 L1-chip correlator spacing)

The range biases experienced by the user for specific user receiver correlator spacings of 0.2 chips and 1.0 chips can be determined from the corresponding curves in Figure 3-9.
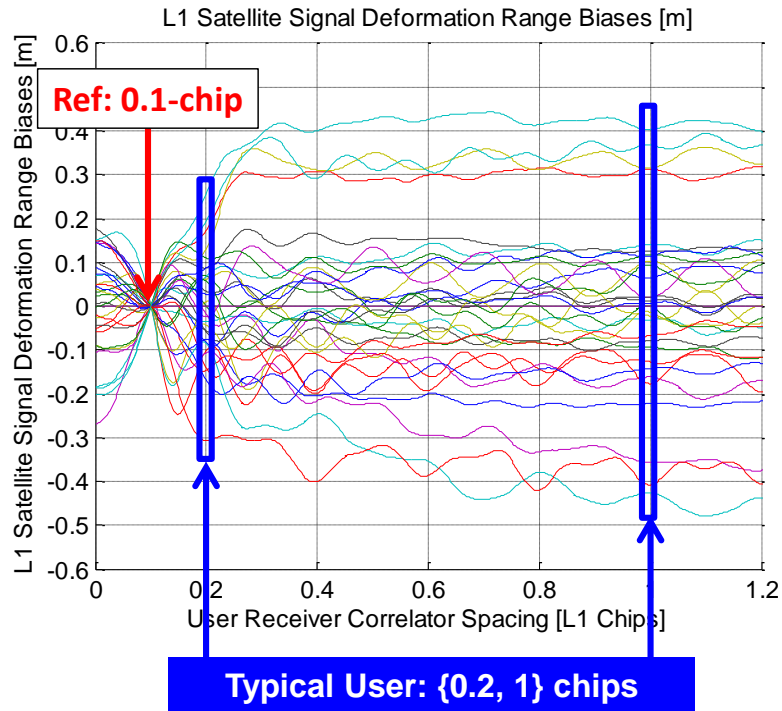
Figure 3-9: Extracting L1 Satellite signal deformation range biases at specific user

receiver correlator spacings

(Reference: 0.1 L1-chip correlator spacing; Typical User: 0.2 or 1.0 L1-chip correlator

spacing)

Figure 3-10a and Figure 3-10b show the range biases experienced by the user for specific user receiver correlator spacings of 0.2 chips and 1.0 chips, respectively, indexed by satellite PRN number. Table 3-3 summarizes the range of possible biases experienced by user receivers.

| Figure 3-10a: Reference: 0.1 L1-chip correlator spacing; User: **0.2** L1-chip correlator spacing | Figure 3-10b: Reference: 0.1 L1-chip correlator spacing; User: **1.0** L1-chip correlator spacing |
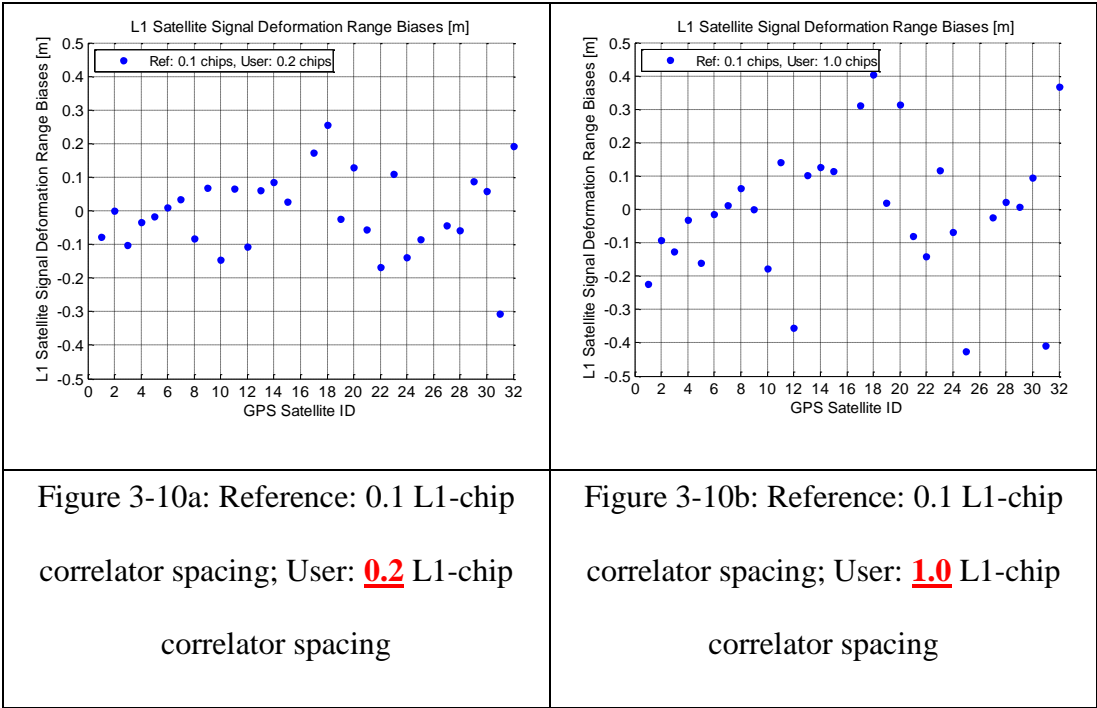
Figure 3-10: L1-frequency satellite signal deformation range biases measured using

the "One-in-View" Large SRI Antenna Dish

(Reference: 0.1 L1-chip correlator spacing; user: 0.2, 1.0 L1-chip correlator spacings)

	User Correlator Spacing [L1 Chips]	
	0.2	1
User Satellite Signal Deformation Range biases [m]	0.1-0.3	0.15-0.5

Table 3-3: L1-frequency satellite signal deformation range biases for user receiver

correlator spacings

(Reference: 0.1 L1-chip correlator spacing; user: 0.2, 1.0 L1-chip correlator spacings)

The satellite dish measurement results in Figure 3-10 and Table 3-3 show that user receivers experience possible differential range biases of up to 0.3 m (reference: 0.1 L1-chip correlator spacing; user: <u>0.2</u> L1-chip correlator spacing) or as large as 0.5 m (reference: 0.1 L1-chip correlator spacing; user: <u>1.0</u> L1-chip correlator spacing). Figure 3-9 shows that these biases diverge as the user receiver correlator spacing moves further away from the reference receiver correlator spacing of 0.1 chips.

3.5.2   Limitations of Satellite Dish Technique

With effective suppression of multipath and radio-frequency noise, the high-gain "one-in-view" satellite dish measurement technique produces high quality measurements of satellite signal deformation range biases and appears attractive. However, this measurement technique contains inherent errors that are difficult to mitigate. Some of these errors are time-varying drifts that vary throughout the day, and short-term errors in measurements taken just minutes apart. Absent of any calibration, it would be impossible to differentiate these errors from the satellite signal deformation range biases of interest, since the dish is capable of observing only one satellite at a time. (If the dish were capable of simultaneous multiple measurements, such time-varying drifts would appear as a common-mode error and be removable.) Both of these errors can be as large as, or in some cases larger than, the nominal satellite signal deformation range biases. Left unaccounted for, these errors can result in a lack of repeatability between measurements and prevent the biases from being quantified accurately.

Daily Time-Varying Drifts

The "one-in-view" satellite dish measurements were susceptible to long-term time-varying drift effects. Different sets of satellite dish measurements collected at different times of the day exhibited markedly different average values, even for the same satellites. Using the set of large satellite dish measurements collected and presented earlier in Section 3.5.1, the presence of these long-term time-varying drifts can be demonstrated.

Four sets of satellite dish measurements were collected, each at a different time: the first data set was collected between 5 pm - 9 pm; the second between 12 am - 3 am; the third between 7 am - 9 am; and the last data set between 2 pm - 4 pm. (All specified times are local times.) These sets of data were processed to yield four sets of satellite signal deformation range bias curves.

Figure 3-11 presents these four sets of range bias curves for a reference receiver correlator spacing of 0.1 L1-chips. Satellite signal deformation range biases for the entire day are in green, while satellite signal deformation range biases for the time period of interest are highlighted in red. Compared to time period 1 (Figure 3-11a), satellite signal deformation range biases for time periods 2 and 3 (Figure 3-11b and Figure 3-11c) appeared to show positive biases for user correlator spacings larger than 0.2 L1-chips, while time period 4 (Figure 3-11d) seemed to exhibit negative biases at those same user correlator spacings.

Figure 3-11a: Time period 1 highlighted.

Figure 3-11b: Time period 2 highlighted.

Figure 3-11c: Time period 3 highlighted.

Figure 3-11d: Time period 4 highlighted.

Figure 3-11: Satellite signal deformation range biases for data collected at different times of day.
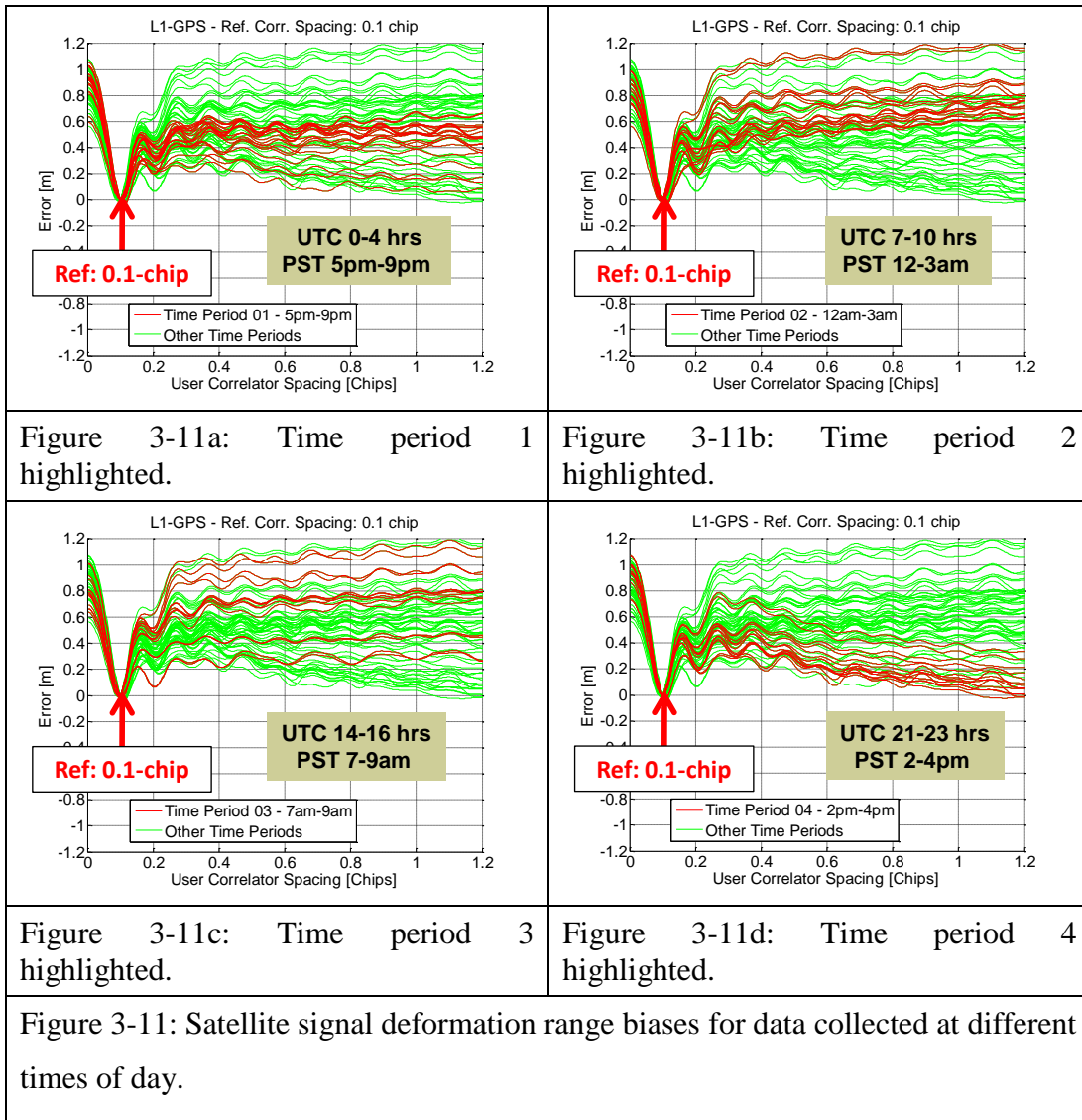
The signal waveforms from the three WAAS-GEO reference satellites, also collected in the same time periods, confirmed the presence of these time-varying drifts. (Figure 3-12). Figure 3-12 shows that the estimates of these time-varying drifts differed by up to ±0.2 m between the different WAAS-GEO satellites.

Figure 3-12a: GPS signals

Figure 3-12b: WAAS-GEO PRN133 signals

Figure 3-12c: WAAS-GEO PRN135 signals

Figure 3-12d: WAAS-GEO PRN138 signals

Figure 3-12: Differences between satellite signal deformation range biases in different time periods and the average over all time periods.

These differences are for GPS and individual WAAS-GEO satellite signals.
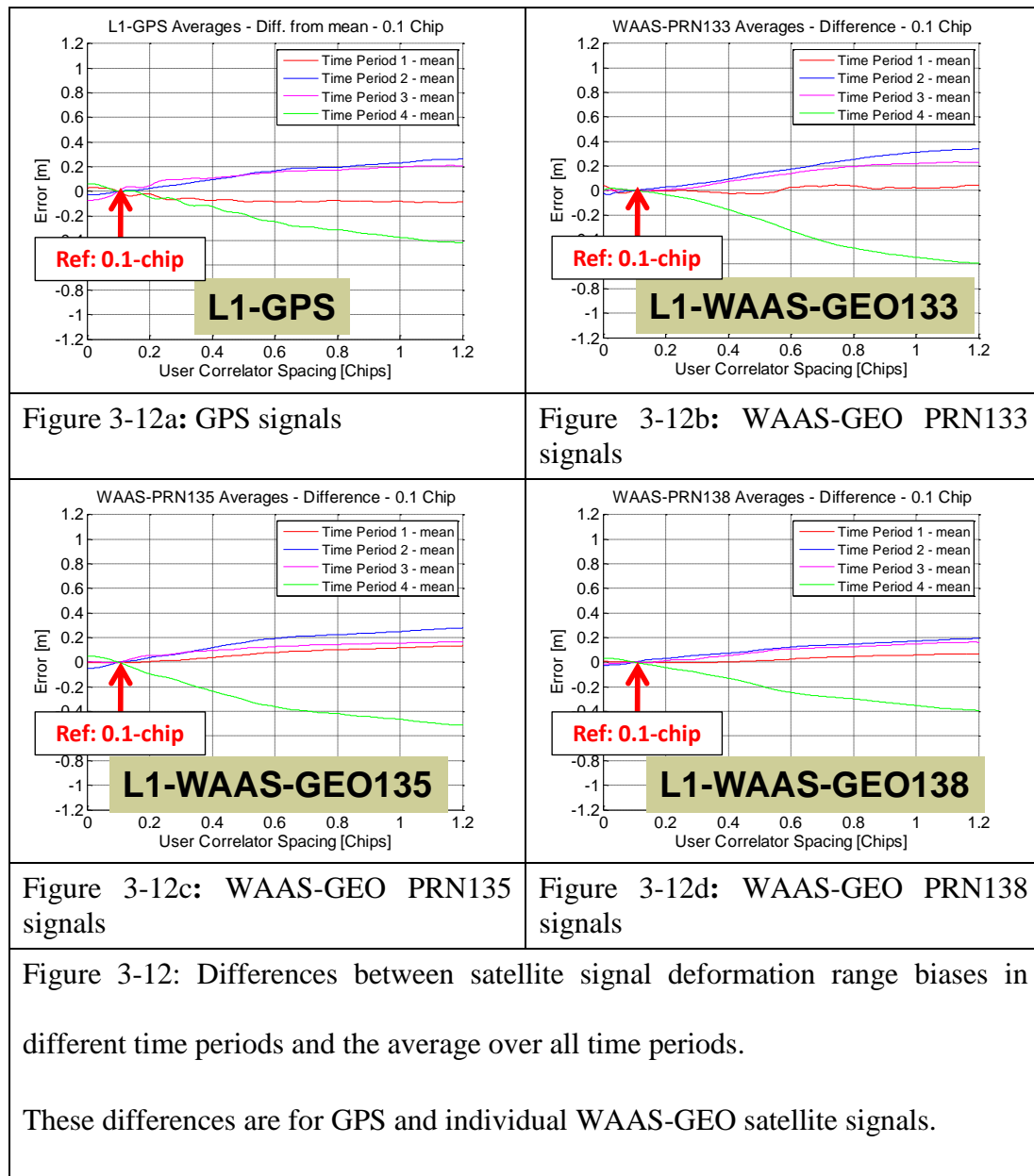
Such biases were not observed in measurements from "all-in-view" hemispherical antennas (discussed in Section 3.6.2). These time-varying drifts present in the large dish measurements could possibly have been due to time-varying thermal effects on the satellite dish, signal feedhorn, and filter, even over a short duration of minutes.

Calibration of the full satellite dish properties would remove most of these biases, but could possibly be uneconomical, requiring continuous dish access over many days and months.

An alternative, more practical calibration process was used in this dissertation, as described in Appendix B-6. Large SRI dish WAAS-GEO range bias measurements collected in the same time period provided an estimate of the time-varying drifts present in the GPS range bias measurements. The estimated time-varying drifts were then subtracted and removed from the GPS range bias measurements

Table 3-4 shows the worst case and root-mean-square (RMS) error for the entire set of GPS signals, before and after applying the corrections for time-varying drifts. Both the worst case and RMS errors are reduced from before.

	RMS [m]	Worst Case Error [m]
Before WAAS-GEO correction	0.24	1.15
After WAAS-GEO correction	0.17	0.97

Table 3-4. Worst case error [m] and root-mean-square (RMS) error [m] for the GPS

signals

While the calibration process based on reference WAAS-GEO signals did remove a significant portion of the time-varying drifts, the overall effectiveness depended on the

quality of the WAAS-GEO range bias measurements. These reference measurements were susceptible to short-term noises (described in Section 3.5.2) and introduced residual errors with magnitudes as large as 0.2 m, which were on the same order of magnitude as the satellite signal deformation range biases of interest.

Short-Term Noise

Besides the longer-term time-varying drifts over a day described in the previous section, the GPS and WAAS-GEO satellite signals also contain short term noise, which are instantaneous random errors contained in measurements taken minutes apart in time. The magnitude of these errors and how they are estimated are discussed in this section.

For each satellite signal, a pair of measurements is collected a short time (2-3 minutes) apart and processed to obtain satellite signal deformation range biases, to estimate the instantaneous random errors in the measurement process. The worst-case difference and root-mean-square (RMS) difference between these tracking error curves give an estimate of the short-term errors in the measurement process. Figure 3-13 and Figure 3-14 show the differences for GPS and WAAS-GEO satellite signals, respectively. The results are summarized in Table 3-5.
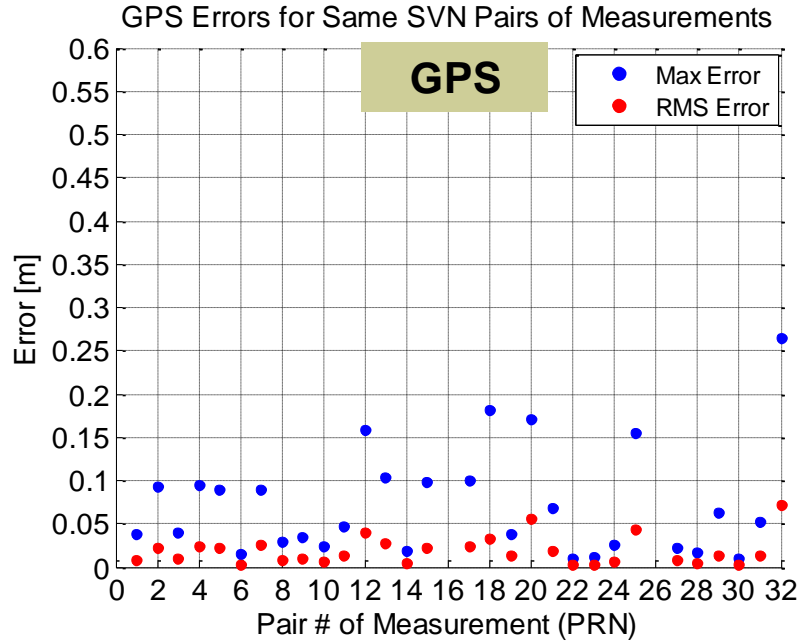
Figure 3-13: Worst-case and RMS differences between each pair of GPS

measurements
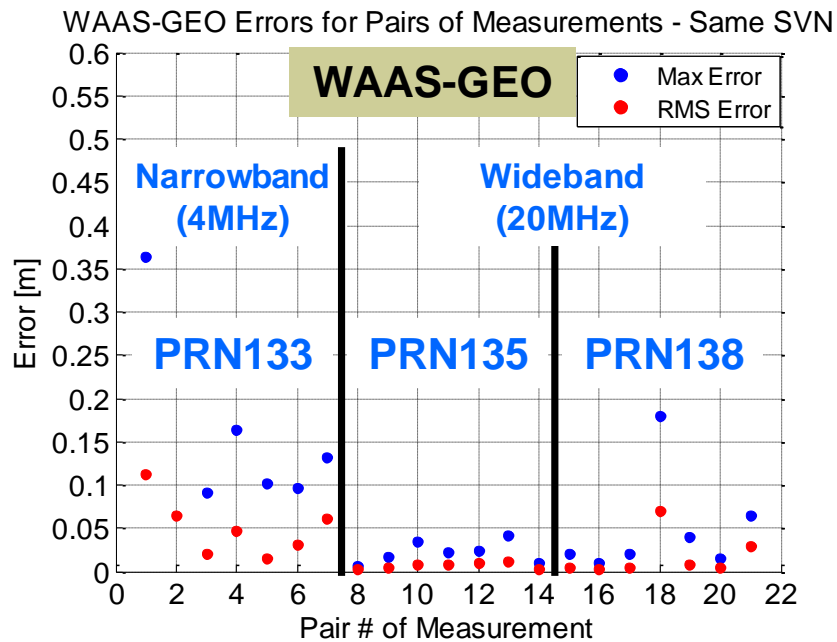
Figure 3-14: Worst-case and RMS differences between each pair of WAAS-GEO

measurements

	RMS Difference [m]	Worst Case Difference [m]
GPS	0.02	0.26
WAAS-GEO #133 (narrowband)	0.05	0.36
WAAS-GEO #135 (wideband)	0.01	0.04
WAAS-GEO #138 (wideband)	0.02	0.18

Table 3-5: Root-mean-square (RMS) and worst-case differences [m] for the pairs of

GPS and WAAS-GEO measurements.

As seen from the table, pairs of measurements taken minutes apart contain worst case errors that are as large as or larger than the nominal satellite signal deformation range biases.

Consequently, when the reference WAAS-GEO satellite signal measurements are used to calibrate and remove long-term time-varying drifts present in the GPS satellite signal measurements, additional short-term noise is introduced. This in turn affects the quality of the measurements from the "one-in-view" satellite dish technique.

3.5.3   Discussion of Large Satellite Dish Method and Results

Using the large "one-in-view" dish antenna, satellite signal deformation range biases as large as ±0.3 m (reference: 0.1 L1-chip correlator spacing; user: 0.2 L1-chip correlator spacing) or even ±0.5 m (reference: 0.1 L1-chip correlator spacing; user: 1.0 L1-chip correlator spacing) were observed.

One of the main disadvantages of the high-gain dish antenna method is the ability to observe only one satellite at a time. Absent of calibration, the short-term and long-term errors in this measurement process cannot be distinguished from the satellite signal deformation range biases. These errors can be as large as, or in some cases larger than, the nominal satellite signal deformation range biases.

Thus calibration of the SRI dish antenna seems necessary and could improve the accuracy of the satellite signal deformation range bias measurements. However, calibration [66] is an involved, time-consuming process. Also, access to the SRI dish is expensive, rendering SRI large dish calibration impractical.

Driven by these constraints, alternative techniques to measure the satellite signal deformation range biases were explored. These techniques are discussed in subsequent sections.

3.6 Hemispherical Antennas Direct Range Bias Measurements

The previous section described the use of "one-in-vew" antennas to obtain high resolution, high-rate raw data, and subsequently to derive satellite signal waveform distortions and range biases. The measurements contained inherent long-term time-varying drifts and short-term noises on the order of the satellite signal deformation range biases. Therefore, by collecting measurements one at a time, it would not be possible to distinguish the long-term time-varying drifts and short-term noises from the satellite signal deformation range biases of interest.

This section describes the use of an alternative measurement technique for measurement of satellite signal deformation range biases: "all-in-view" hemispherical antennas. This method was previously used in the monitoring of faulted satellite signal distortions [8], [23] and showed:

- Satellite "natural biases" (a.k.a., satellite signal deformation range biases) of up to ±0.3 m between satellites [23].

- Residual multipath standard deviations of 0.05 m – 0.1 m for narrow correlator, and up to 0.2 m for wide correlator spacing in the receiver error, even for satellites at high evelation angles (which would have reduced multipath) [8], [22].

This dissertation focuses specifically on measuring nominal satellite signal distortion range biases, which requires mitigating the measurement errors associated with the particular user equipment and environmental setup.

Due to their wider beamwidths, these antennas are able to collect measurements from multiple satellites simultaneously. As a result, any long-term time-varying drifts (described in Section 3.3) would be observable, common-mode, and removable from the simultaneous multiple satellite measurements.

However, the wider-beamwidths of these hemispherical "all-in-view" antennas result in lower-gain and higher susceptibility to radio-frequency interference and multipath. To effectively attenuate the increased measurement noise and errors, it would be imperative to choose suitably designed multipath-reducing antennas and environments as well as hardware which would facilitate longer-term averaging over hours.

To meet these requirements, a specially configured GPS receiver connected to an "all-in-view" hemispherical multipath-limiting antenna is used for measurement of satellite signal deformation range biases. Different multipath-limiting antennas and low-multipath environments are evaluated and the results are presented.

The results demonstrate that the magnitude of residual multipath is at least as large as the average satellite signal deformation range bias magnitude. This renders the "all-in-view" hemispherical antenna technique a "measure-and-trust" approach, and unsuitable as a standalone method for measurement of satellite signal deformation range biases.

Sections 3.3.1 and 3.3.2 described the specific multipath limiting antennas and environments evaluated. Section 3.6.1 presents the results and Section 3.6.2 discusses the limitations of this technique.

3.6.1   Measurement Setup: Hardware, Environment, Antenna

Raw IF-frequency data loggers used previously in the "one-in-view" technique (described in Section 3.5) have high output data rates with large storage requirements. As a result, they are not practical for hemispherical antenna measurements that require long averaging times over hours.

Instead, specially configured GPS receivers (Section 3.2.2), which provide direct range outputs at a much lower data rate, are required and utilized. A hybrid data-logger/GPS receiver Universal Receiver Software Protocol (USRP) hardware is used to record and process raw data in real time to yield range biases for the different GPS and WAAS-GEO satellites.

This GPS receiver provides range outputs at correlator spacings of 0.1, 0.2, 0.3, 0.4, and 1.0 L1-chips. Differencing the range output at 0.1 L1-chip from those at 0.2, 0.3, 0.4, and 1.0 L1-chips removes the receiver independent errors (Sections 2.4.3 and 2.4.4), leaving the residual multipath and differential satellite signal deformation range biases (reference: 0.1 L1-chip correlator spacing; user: 0.2, 0.3, 0.4 and 1.0 L1-chip correlator spacings).

Measurements were collected from three different types of antennas (described in Section 3.3.1): survey-grade geodetic antennas, multipath-limiting choke-ring antennas, and helibowl antennas. In addition, these measurements were collected in three low-multipath environments (described in Section 3.3.2) – Durand rooftop, Roble Field, and Lake Lagunita (dry lake bed) – and compared.

3.6.2   Results and Discussion for L1-frequency Satellite Signal

Figure 3-15 shows the L1-frequency satellite signal biases over 4 hours for GPS satellite ID PRN #11 on two consecutive days (reference: 0.1 L1-chip correlator spacing; user: 0.2 L1-chip correlator spacing). These results were obtained with a multipath-limiting choke-ring antenna located on the Durand rooftop. The blue trace shows the raw, un-averaged 1-sec bias data; the red trace shows the same data averaged over 100 sec, and the green trace shows the same data averaged over 900 sec. As can be seen, white noise errors are effectively attenuated by averaging, and a clear constant non-zero bias slowly becomes visible.

However, the averaged signals still contain an undulating time-varying component that repeats from one day to the next. Signals of such signatures have previously been observed [68] and attributed to multipath induced by the GPS satellite orbit, which has a repeating ground track and an (almost) 24-hour orbit period.

As seen in the figure, the multipath is on the same order of magnitude as the constant biases even after 900 sec of averaging. Since multipath errors may have non-zero means, this data does not permit a clear differentiation between biases from satellite signal deformation and those from multipath.

Figure 3-15a: Satellite ID PRN #11 (SVN 46). Data on 09 Mar 2013 (Day 01).	Figure 3-15b: Satellite ID PRN #11 (SVN 46). Data on 10 Mar 2013 (Day 02).
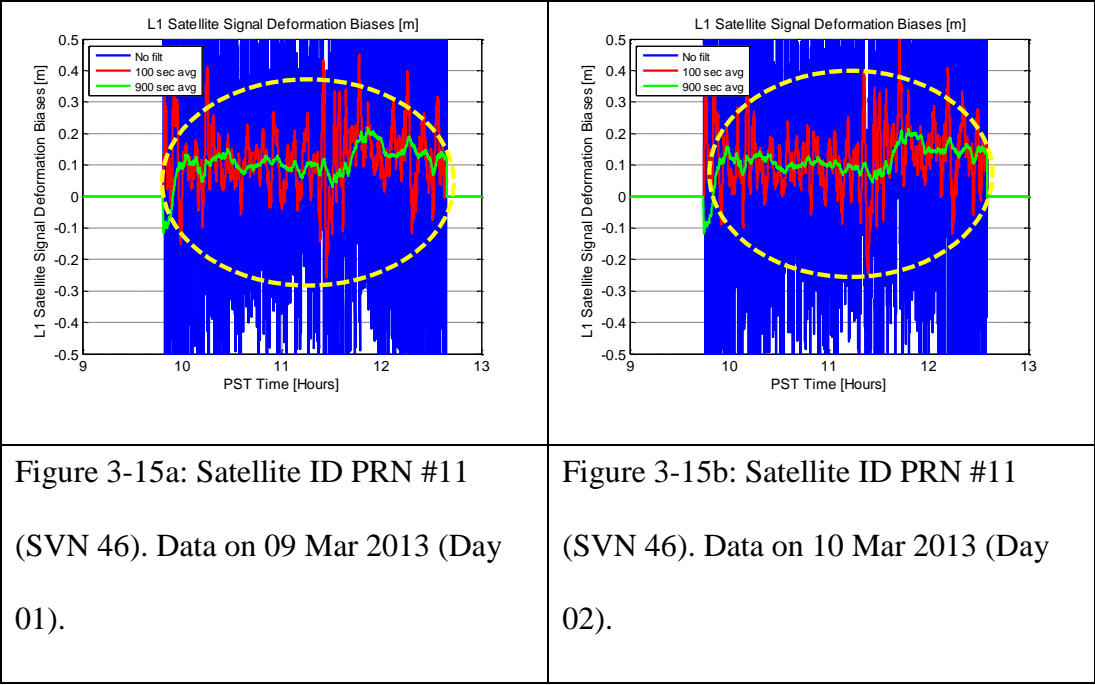
Figure 3-15: Large repeated residual multipath for choke-ring hemispherical "all-in-view" antenna measurements

(Reference: 0.1 L1-chip correlator spacing; user: 0.2 L1-chip correlator spacing)

Table 3-6 summarizes the effectiveness (as indicated by standard deviation) of the different multipath limiting antennas and low-multipath environments (reference: 0.1 L1-chip correlator spacing; user: 0.2, 0.3, 0.4, and 1.0 L1-chip correlator spacings). Just as for the large dish antenna measurements, errors increase as the user correlator

spacing diverges from the reference, leading to increased standard deviations for all antenna and environment types.

The average standard deviations in Table 3-6 are indicative of measurement uncertainty due to measurement errors such as multipath. This could be a concern since some of these errors, especially multipath, could have non-zero means and affect range bias measurements. If the average standard deviation is greater than a large percentage of the biases, this is an indication that the measurement method contains too much measurement uncertainty to be an effective means of measurement.

Configuration			User Correlator Spacing (Chips) (Ref: 0.1 L1-Chips)			
			0.2	0.3	0.4	1.0
Environment	*Antenna*	*# satellites in view*	*Average Standard Deviation (m)*			
Rooftop	Geodetic Survey-Grade	Multiple ("All-in-view")	0.11	0.2	0.26	0.39
Rooftop	Choke-Ring/ Helibowl	Multiple ("All-in-view")	0.08	0.13	0.18	0.31
Roble Field/ Lake Lagunita	Helibowl	Multiple ("All-in-view")	0.04	0.08	0.11	0.18

Table 3-6: Summary of Results for Hemispherical Antennas

Table 3-7 compares previous range bias measurements using the large dish antenna (Section 3.5.1 Figure 3-10) with the average standard deviations, by showing the

percentage of biases for which the measurement uncertainty is greater, for the different measurement setups and user receiver correlator spacings [Reference receiver correlator spacing: 0.1 L1-chips].

Measurement Configuration			User Correlator Spacing (Chips) (Ref: 0.1 L1-Chips)			
			0.2	0.3	0.4	1.0
Environment	*Antenna*	*# satellites in view*	*Percentage of Large Dish biases Smaller Than Average Standard Deviation [%]*			
Rooftop	Geodetic Survey-Grade	Multiple	71.6%	82.1%	85.1%	89.6%
Rooftop	Choke-Ring/ Helibowl	Multiple	52.2%	64.2%	71.6%	85.1%
Roble Field/ Lake Lagunita	Helibowl	Multiple	22.4%	47.8%	53.7%	70.1%

Table 3-7: Percentage of Measured Large Antenna Dish biases Larger Than Average

Standard Deviation [%]

(Reference: 0.1 L1-chip correlator spacing)

Table 3-7 shows that for the geodetic survey grade antenna on the rooftop, the measurement uncertainty of the hemispherical "all-in-view" antenna measurements is greater than 72% of the large dish range bias measurements (reference: 0.1 L1-chip correlator spacing; user: 0.2 L1-chip correlator spacing). As the user correlator spacing increasingly diverges from the reference receiver's correlator spacing of 0.1 L1-chips,

the measurement uncertainty is now greater for an increased percentage of the large dish measured biases.

For the multipath-limiting choke ring and helibowl antennas on the rooftop, the measurement uncertainty is greater than 52.2% of the large dish biases (reference: 0.1 L1-chip correlator spacing; user: 0.2 L1-chip correlator spacing). This is an improvement from before, but still not ideal − the measurement uncertainty is still larger than half of the biases measured by the large dish. As before, as the user correlator spacing increasingly diverges from the reference receiver's correlator spacing of 0.1 L1-chips, the measurement uncertainty is greater than an increased percentage of the large dish biases.

For the multipath-limiting choke ring and helibowl antennas in Roble field and on the dry lake bed of Lake Lagunita, the measurement uncertainty is greater than only 22.4% of the biases. This is a vast improvement from before; unfortunately, this method is impractical for long-term data collection as it involves transporting cumbersome lab equipment to remote locations with inadequate power and security.

Consequently, these results show that the hemispherical "all-in-view" antenna technique would not be suitable as a standalone technique to directly measure the satellite signal deformation range biases.

3.7   Hybrid "Measure-and-Verify" Technique

The previous two sections (Sections 3.5 and 3.6) described two prior techniques for measurement of satellite signal deformation range biases: "one-in-view" parabolic dish methods and "all-in-view" hemispherical antenna methods. The "one-in-view" measurements had repeatability issues due to inherent long-term, time-varying hardware/antenna drifts and short-term noise, while the "all-in-view" measurements contained significant multipath and residual noise. As a result, these standalone techniques were "measure-and-trust" in nature.

This section articulates the primary contribution of this dissertation: the development of a novel hybrid technique in response to the limitations of the prior methods. Low multipath measurements are obtained using a calibrated, "one-in-view" 1.8 m parabolic satellite dish antenna over days and months. These are verified using measurements from hemispherical "all-in-view" antennas. As will be demonstrated, this combined "measure-and-verify" method produces consistent measurements, demonstrating the presence of the satellite signal deformation range biases, quantifying their magnitudes with an order of magnitude reduction in uncertainty, and thus rendering the range biases observable and measurable.

Section 3.7.1 describes the hardware, environment and antenna setup for this "measure-and-verify" hybrid approach. Section 3.7.2 presents the calibration procedure for the mini-dish antenna. Measured satellite signal deformation range bias

results for single L1-frequency, single L5-frequency and dual frequency L1/L5 combination are presented in Sections 3.7.3, 3.7.4, and 3.7.5, respectively.

3.7.1   Measurement Setup: Hardware, Environment, Antenna

Similar to the measurement of satellite signal deformation range biases using hemispherical antennas (Section 3.6), a hybrid data-logger/GPS receiver Universal Receiver Software Protocol (USRP) hardware (described in Section 3.2.2) is used to log and process raw data in real time to yield range biases for the different GPS and WAAS-GEO satellites.

As previously described (Section 3.6.1), the specially configured GPS receiver provides range outputs at correlator spacings of 0.1, 0.2, 0.3, 0.4, and 1.0 L1-chips. Differencing the range output at 0.1 L1-chip from those at 0.2, 0.3, 0.4, and 1.0 L1-chips removes the receiver independent errors (Section 2.4.3), leaving the residual multipath and differential satellite signal deformation range biases (reference: 0.1 L1-chip correlator spacing; user: 0.2, 0.3, 0.4 and 1.0 L1-chip correlator spacings).

Instead of the large 46 m SRI dish antenna, or one of the three different types of hemispherical multipath limiting antennas (described in Section 3.3.1), a different antenna is used for primary data collection – a rooftop 1.8 m mini-dish. This mini-dish antenna is more accessible and more easily calibrated than a large dish antenna, yet provides much better multipath attenuation than the hemispherical multipath-limiting

antennas. Satellite signal deformation bias data is logged, one satellite at a time, for as long as the satellite is in view of the ground station, typically a total time of approximately 3-6 hours.

To verify that the mini-dish measurements contain insignificant amounts of time-varying drifts, separate measurements from a rooftop-mounted, choke-ring multipath-limiting hemispherical antenna connected to the specially configured GPS receiver are used.

3.7.2   Temperature Calibration

The large 46 m SRI dish antenna exhibited time-varying drifts which were dependent on the time of day (Section 3.5.2). To determine if there was a similar phenomenon for the 1.8 m mini-dish antenna, the antenna was used to collect data from a geostationary WAAS-GEO satellite PRN 138, which was one of the satellite signals used in the calibration and correction of the big-dish time-varying drifts (Appendix B-6 Subsections 4 and 6). As was the case for the SRI Dish, the advantage of this satellite is its geostationary orbit. It is constantly at an approximately fixed azimuth and elevation relative to the antenna throughout the day so its signal properties should be relatively stable.

Figure 3-16 shows the variations of the satellite signal deformation biases for WAAS-GEO PRN138 over time. The temperature variation over time at a local weather

station is also plotted for reference. From the figure, a clear correlation between the bias variations and the time of day and/or temperature can be seen. It can also be seen that the measurements between 6 pm-10 am local time were relatively constant and not subject to significant time-varying drifts. Accordingly, to minimize temperature/ time-of-day related variations, all subsequent mini-dish bias measurements were collected between 10 pm-6 am local time.
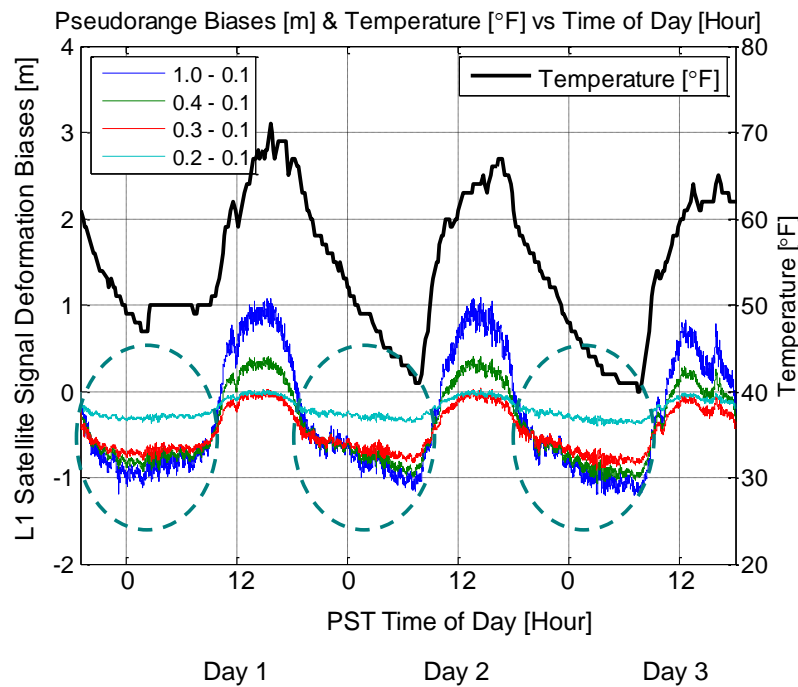
Figure 3-16: Variation of satellite signal deformation biases with temperature for different correlator spacing differences.

Note that the time-varying drifts are approximately constant in the time period 1800 hrs − 1000 hrs (PST local time).

3.7.3   Results for L1

Figure 3-17 compares the satellite signal deformation range biases measured by the hemispherical antenna and those measured by the mini-dish antenna (both antennas are situated on the rooftop). The mini-dish measurements were collected between 0200 hrs - 0600 hrs (within the constant time-varying drifts period of 1800 hrs – 1000 hrs).

The two plots show a similar constant average bias; however, the mini-dish measurements contain significantly smaller variations from multipath and residual noise. Thus the biases shown result more from satellite signal deformation range biases than that of biased multipath. The plots demonstrate that the satellite signal deformation range biases are now observable and measurable using the mini-dish antenna.

Figure 3-17a: Satellite ID PRN #11 (SVN 46). Data on 09 Mar 2013 (Day 01). Hemispherical "all-in-view" antenna	Figure 3-17b: Satellite ID PRN #11 (SVN 46). Data on 10 Mar 2013 (Day 02). 2 m "One-in-view" Mini-Dish Antenna Time of Measurement: 0200-0600 hrs (between 6 pm – 10 am: constant time-varying drifts)
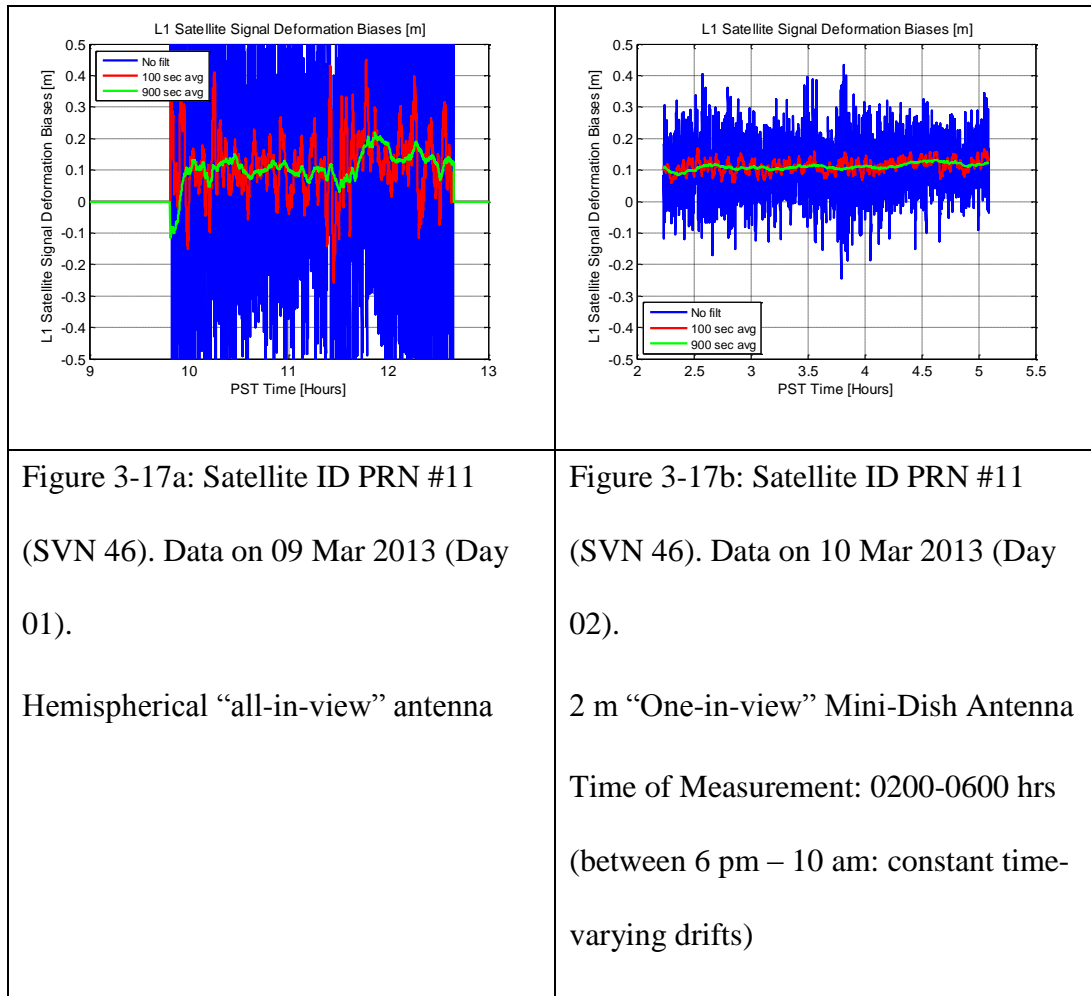
Figure 3-17: Highly reduced residual multipath using the mini-dish approach

The mini-dish was used to measure signal deformation range biases for all satellites, one at a time, over a period of 9 months (reference: 0.1 L1-chip correlator spacing; user: 0.2 L1-chip correlator spacing). All measurements were made within the time period of 1800 hrs – 1000 hrs, when the time-varying drifts were constant.

Table 3-8 compares the results from the mini-dish with those from the previous hemispherical antennas. As seen in the plots of range biases over time in Figure 3-17,

the measurement uncertainty is now improved by at least a factor of two compared

with the previous hemispherical antenna measurement methods.

Configuration			User Correlator Spacing (Chips) (Ref: 0.1)			
			0.2	0.3	0.4	1.0
Environment	*Antenna*	*# satellites in view*	*Average Standard Deviation (m)*			
Rooftop	Geodetic Survey-Grade	Multiple ("All-in-view")	0.11	0.2	0.26	0.39
Rooftop	Choke-Ring/ Helibowl	Multiple ("All-in-view")	0.08	0.13	0.18	0.31
*Roble Field/ Lake Lagunita	Helibowl	Multiple ("All-in-view")	0.04	0.08	0.11	0.18
Rooftop	1.8 m Mini-Antenna Dish	Single ("One-in-view")	0.02	0.04	0.05	0.09

Table 3-8: Summary of Results for All Antennas

Table 3-9 shows the percentage of large dish biases for which the measurement

uncertainty is greater. The table includes the measurement uncertainties from the 1.8

m, "one-in-view" mini-antenna dish on the rooftop. For these measurements, the

measurement uncertainty is now only greater than 13% of the range biases measured

using the large dish (reference: 0.1 L1-chip correlator spacing; user: 0.2 L1-chip

correlator spacing). This is a significant improvement even over the Helibowl situated

in low multipath environment, the most multipath-limiting previous configuration.

Measurement Configuration			User Correlator Spacing (Chips) (Ref: 0.1 L1-Chips)			
			0.2	0.3	0.4	1.0
Environment	*Antenna*	*# satellites in view*	*Percentage of Large Dish biases Within Average Standard Deviation [%]*			
Rooftop	Geodetic Survey-Grade	Multiple	71.6%	82.1%	85.1%	89.6%
Rooftop	Choke-Ring/ Helibowl	Multiple	52.2%	64.2%	71.6%	85.1%
Roble Field/ Lake Lagunita	Helibowl	Multiple	22.4%	47.8%	53.7%	70.1%
Rooftop	1.8 m Mini-Antenna Dish	One-at-a-time	13.4%	22.4%	29.9%	43.3%

Table 3-9: Percentage of Measured Large Antenna Dish biases Larger Than Average

Standard Deviation [%]

(Reference: 0.1 L1-chip correlator spacing)

As the user receiver correlation spacing increases to 1.0 L1-chips, due to additional noise, the measurement uncertainty increases and is now greater than 43.3% (almost half) of the large dish bias measurements. This shows that at larger user receiver correlator spacings (user correlator spacing: 1.0 L1-chips), even the mini-dish on the rooftop may not be an ideal measurement method, due to the amount of measurement uncertainty relative to the satellite signal deformation range bias magnitudes.

Figure 3-18 shows the mini-dish measurement results for the satellite signal deformation range biases for all GPS satellites, for the single-frequency L1-only signal.
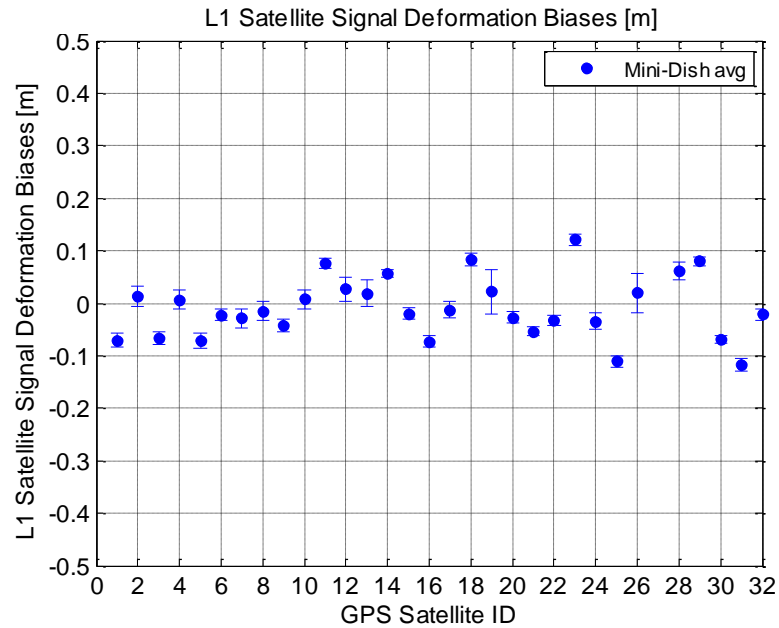
Figure 3-18: Satellite Signal Deformation Range Biases Measured by Mini-Dish

(Reference: 0.1 L1-chip correlator spacing; user: 0.2 L1-chip correlator spacing)

To verify that the mini-dish measurements were not largely corrupted by time-varying drifts, a cross-check was performed with measurements taken using the same hardware, but with a different antenna (multipath-limiting, choke-ring hemispherical antenna). These results are shown in Figure 3-19. While most of the bias magnitudes were between 0.00 m - 0.05 m, some were as large as 0.12 m, (reference: 0.1 L1-chip correlator spacing; user: 0.2 L1-chip correlator spacing).
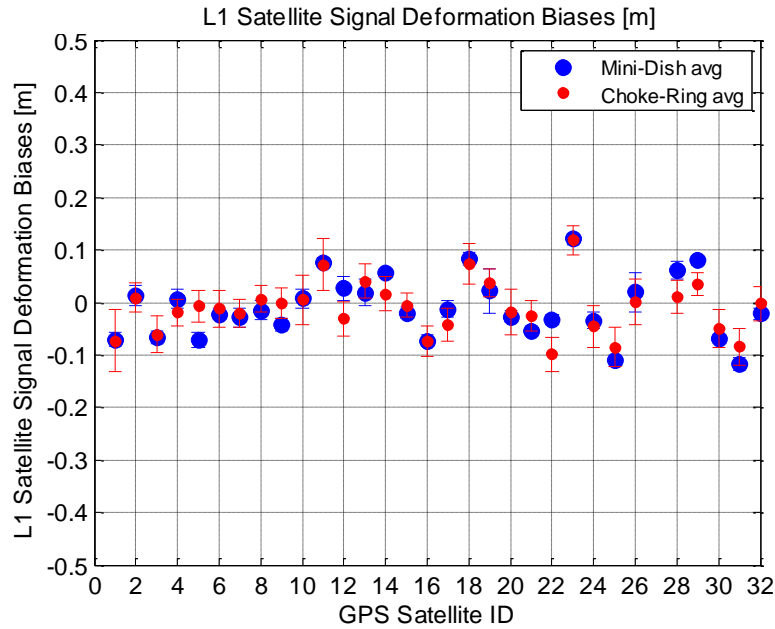
Figure 3-19: Satellite Signal Deformation Range Biases Measured by both Mini-Dish

and Hemispherical Antenna

(Reference: 0.1 L1-chip correlator spacing; user: **0.2** L1-chip correlator spacing)

There is a high degree of consistency between the two sets of measurements. Of the differences between the 31 pairs of satellite measurements, 15 are within the mini-dish antenna measurement standard deviation (agreement of 15/31 = 48.4%), and 24 are within the choke ring antenna measurement standard deviation (agreement of 24/ 31 = 77.4%). The computed χ^2 test statistic using the combined variance is 24.26, which corresponds to a confidence level of approximately 79% and is consistent with this result. The larger measurement differences could be due to measurement error outliers.

The high degree of consistency between the two sets of measurements strongly demonstrates that the observed biases are due to satellite signal deformation and not to measurement errors. The mini-dish antenna measurements made over a period of 9 months, one satellite at a time (each measurement was made in the zone of constant time-varying drift), contain mostly time-varying drifts and little multipath; the choke ring hemispherical antenna measurements, made for multiple satellites simultaneously on separate days 6 months apart, contain largely multipath. It is extremely unlikely that these separate sets of measurement errors are correlated.

Figure 3-20 shows the results for a wider user receiver correlator spacing (reference: 0.1 L1-chip correlator spacing; user: **1.0** L1-chip correlator spacing). As the large-dish results showed previously, the biases have increased. The largest biases have magnitudes are large as 0.25 m, and average magnitudes of 0.11 m, approximately twice as large as before. However, there is noticeably less consistency between the mini-dish and the hemispherical choke-ring antenna results. This is due to the increased but differing amounts of multipath in the two sets of measurements.
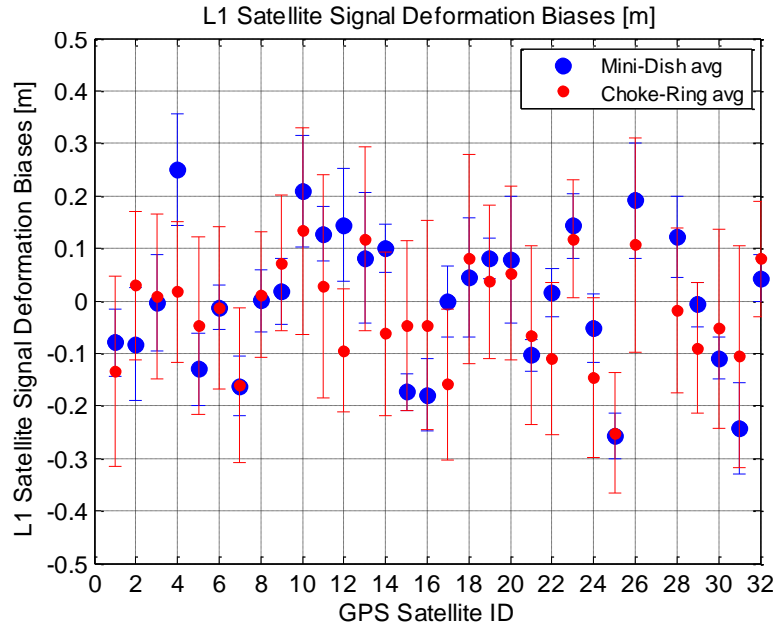
Figure 3-20: Satellite Signal Deformation Range Biases measured by Mini-Dish

(Reference: 0.1 L1-chip correlator spacing; user: **1.0** L1-chip correlator spacing)

3.7.4   Results for L5

The mini-dish approach was also applied to measure the satellite signal deformation range biases for the signal at the L5 frequency. At the time of writing, there were three GPS satellites transmitting this new signal.

Figure 3-21 shows the measurement results over a single day for the three GPS satellites that contain signals at the new L5 frequency (reference: 1.0 L5-chip correlator spacing; user: 1.4 L5-chip correlator spacing). As can be seen, the biases remain largely constant over the course of 24 hours. Time-varying, temperature-related drifts, which were observed for L1-frequency signals collected with the mini-

dish, were absent for the L5-frequency signals over the course of an entire day. As a

result, calibration of our measurement setup was not necessary for these signals.
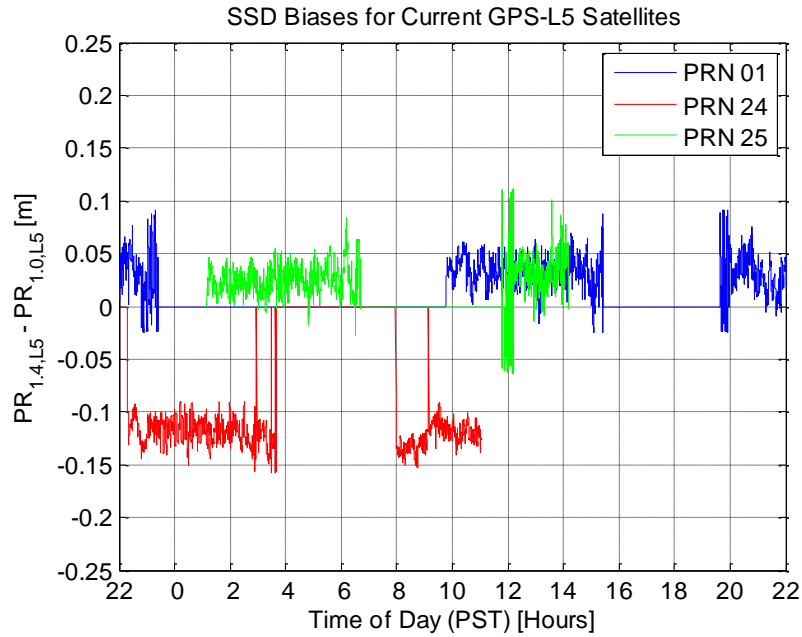
Figure 3-21: Time traces of mini-dish L5 satellite signal deformation range biases over

a day

Figure 3-22 shows the satellite signal deformation range bias measurements for the

three GPS satellites with L5-frequency signals (reference: 1.0 L5-chip correlator

spacing; user: 1.4 L5-chip correlator spacing). These biases have a maximum

magnitude as large as 0.11 m and mean magnitudes of 0.06 m.
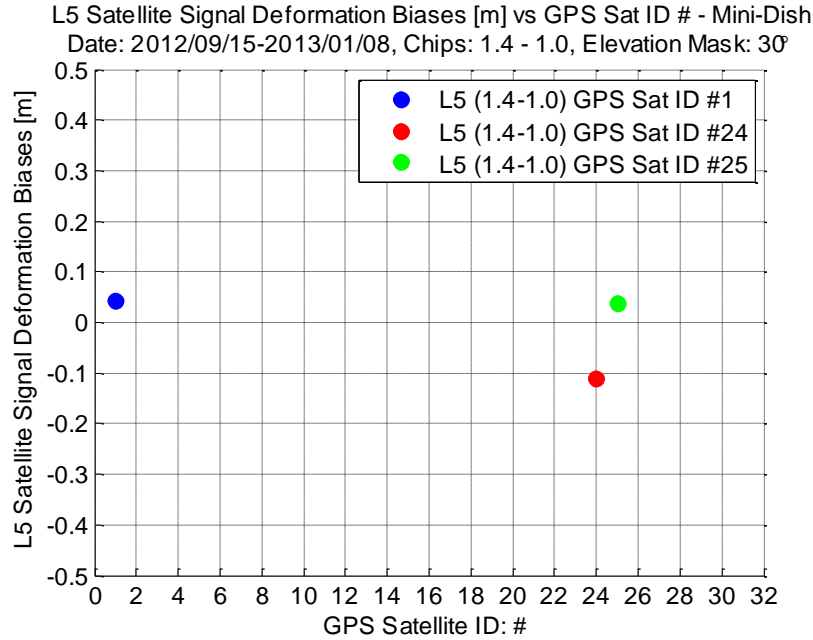
Figure 3-22: Satellite Signal Deformation Range Biases for L5 (as measured by Mini-

Dish)

3.7.5 Results for Dual-Freqency L1-L5

One of the main concerns with satellite signal deformation biases is their potential

amplification when signals of both frequencies are used together to eliminate the

ionospheric error [Refer to Section 2.4.4, Equations (2.29) and (2.32)]. The

amplification factors for L1-frequency and L5-frequency signals, K_{L1} and K_{L5}

respectively, would be worst in the case when the biases are negatively correlated

[Refer to Section 2.4.4, Equation (2.29)]. Figure 3-23 compares these biases for the

three current satellites with both L1- and L5-frequency signals. For these satellites, the

biases in the two frequencies do not appear to show much correlation.

Figure 3-23a: Satellite signal deformation biases for L1- and L5-frequency signals. L1-Frequency: Reference: 0.1 L1-chip correlator spacing; user: **<u>0.2</u>** L1-chip correlator spacing L5-Frequency: Reference: 1.0 L5-chip correlator spacing; user: 1.4 L5-chip correlator spacing.	Figure 3-23b: Satellite signal deformation biases for L1- and L5-frequency signals. L1-Frequency: Reference: 0.1 L1-chip correlator spacing; user: **<u>1.0</u>** L1-chip correlator spacing L5-Frequency: Reference: 1.0 L5-chip correlator spacing; user: 1.4 L5-chip correlator spacing.

Figure 3-23: Satellite Signal Deformation Biases for L1 and L5 Frequencies

(L1-Frequency: Reference: 0.1 L1-chip correlator spacing; user: **<u>0.2</u>**, **<u>1.0</u>** L1-chip

correlator spacing.

L5-Frequency: Reference: 1.0 L5-chip correlator spacing; user: 1.4 L5-chip correlator

spacing)

The equation for dual-frequency ionosphere error removal [Section 2.4.4, Equation (2.29)] is applied for the three satellite signals with both L1- frequency and L5-

frequency components, to find the worst case dual-frequency combination of biases. These dual-frequency biases are computed for the following configurations.

1. L1-Frequency: Reference: 0.1 L1-chip correlator spacing; user: **0.2**, **1.0** L1-chip correlator spacing.

2. L5-Frequency: Reference: 1.0 L5-chip correlator spacing; user: **0.6**, **1.4** L5-chip correlator spacing.

The unmitigated biases before dual-frequency combination are shown in Table 3-10.

GPS Satellite ID	L1-Frequency Biases (m) *User correlator spacing (L1 Chips)*		L5-Frequency Biases (m) *User correlator spacing (L5 Chips)*	
	0.2	**1.0**	**0.6**	**1.4**
1	-0.07	-0.08	-0.04	0.04
24	-0.03	-0.05	0.07	-0.11
25	-0.11	-0.26	-0.04	0.04
Others (min)	-0.12	-0.24	-	-
Others (max)	0.12	0.25	-	-

Table 3-10: Unmitigated Single-Frequency Satellite Signal Deformation Biases for Satellites with Signals at both L1 and L5 Frequencies

(L1-Frequency: Reference: 0.1 L1-chip correlator spacing; user: **0.2**, **1.0** L1-chip correlator spacing.

L5-Frequency: Reference: 1.0 L5-chip correlator spacing; user: **0.6**, **1.4** L5-chip correlator spacing)

Table 3-11 shows the unmitigated biases after application of the equation for dual-frequency linear combination to remove ionosphere errors (Refer to Section 2.4.4 Equation (2.29)). As shown in the table, GPS Satellite ID PRN #25 exhibits the worst case dual-frequency biases. These biases have magnitudes as large as:

1. 0.30 m (L1-Frequency: Reference: 0.1 L1-chip correlator spacing; user: **0.2** L1-chip correlator spacing. L5-Frequency: Reference: 1.0 L5-chip correlator spacing; user: **0.6**, **1.4** L5-chip correlator spacing); or

2. 0.63 m (L1-Frequency: Reference: 0.1 L1-chip correlator spacing; user: **1.0** L1-chip correlator spacing. L5-Frequency: Reference: 1.0 L5-chip correlator spacing; user: **0.6**, **1.4** L5-chip correlator spacing)

GPS Satellite ID	L1-Frequency		L5-Frequency		Dual-Frequency L1/L5 Bias: K_{L1} * Bias_L1 - K_{L5} * Bias_L5
	User correlator spacing:	Single-Frequency Bias	User correlator spacing:	Single-Frequency Bias	
1	0.2	-0.07	0.6	-0.04	-0.11
24	0.2	-0.03	0.6	0.07	-0.16
25	0.2	-0.11	0.6	-0.04	-0.20
1	0.2	-0.07	1.4	0.04	-0.21
24	0.2	-0.03	1.4	-0.11	0.06
25	0.2	-0.11	1.4	0.04	-0.30
1	1.0	-0.08	0.6	-0.04	-0.13
24	1.0	-0.05	0.6	0.07	-0.20
25	1.0	-0.26	0.6	-0.04	-0.53
1	1.0	-0.08	1.4	0.04	-0.23
24	1.0	-0.05	1.4	-0.11	0.02
25	1.0	-0.26	1.4	0.04	-0.63

Table 3-11: Unmitigated Satellite Signal Deformation Biases - Dual Frequency

Combination

(Note: K_{L1} = 2.26 and K_{L5} = 1.26. Refer to Section 2.4.4 Equations (2.30) and (2.31))

From Table 3-11, the worst case single-frequency (L1) bias magnitudes for the other satellites are comparable to that for GPS Satellite ID PRN #25. Thus it is reasonable to assume that dual-frequency combinations for other satellite signals could also yield bias magnitudes at least as large as that of GPS Satellite ID PRN #25: 0.30-0.63 m.

3.8 Summary of Satellite Signal Deformation Range Bias Measurement

This chapter described the main contribution of the dissertation: to render satellite signal deformation range biases observable and measurable. Three methods were explored. The first two legacy techniques contained inherent errors: the "one-in-view" parabolic dish method contained long-term biases and short-term noise and the "all-in-view" hemispherical dish method had multipath magnitudes on the order of the biases. These errors were impractical to isolate and remove. Consequently, as standalone individual methods, these "measure-and-trust" techniques produced results that were difficult to verify.

The third method, a novel hybrid technique, proved to be effective in leveraging the strengths and weaknesses of the two legacy methods. The "one-in-view" parabolic dish technique produced low-multipath measurements, and the "all-in-view" hemispherical antenna verified that the long-term-biases previously present had been largely removed by the employed simple calibration process. As a consequence, consistent measurements were produced from this new measurement method.

The hybrid "measure-and-verify" technique was used to measure satellite signal deformation range biases for GPS single frequency L1-only, single frequency L5-only, and dual-frequency L1/L5 GPS satellite signals.

It was found that biases for single-frequency L1-only signals could be as large as:

- ±0.12 m (reference: 0.1 L1-chip correlator spacing; user: 0.2 L1-chip correlator spacing); or

- ±0.25 m (reference: 0.1 L1-chip correlator spacing; user: 1.0 L1-chip correlator spacing).

Single-frequency L5-only signals could be as large as:

- ±0.07 m (reference: 1.0 L1-chip correlator spacing; user: 0.6 L1-chip correlator spacing); or

- ±0.11 m (reference: 1.0 L1-chip correlator spacing; user: 1.4 L1-chip correlator spacing)

For dual-frequency L1/L5 combination, these biases could be as large as:

- 0.30 m (reference: 0.1 L1-chip, 1.0 L5-chip correlator spacings; user 0.2 L1-chip correlator spacing, 1.4 L5-chip correlator spacings), or

- 0.65 m (reference: 0.1 L1-chip, 1.0 L5-chip correlator spacings; user: 1.0 L1-chip correlator spacing, 1.4 L5-chip correlator spacings).

These biases increased as the user receiver correlator spacing was increasingly different from that of the reference receiver.

Note that this analysis was based on range bias measurements from reference and user receivers with different correlator spacings but with identical front-end filters. Filter differences, such as different bandwidths and different filter implementations, could lead to increased range biases. These differences are beyond the scope of the analysis in this chapter and are briefly discussed in Section 6.3: Future Research.

Comparing the results from the hybrid "measure-and-verify" method with the earlier range error contributions (Figure 3-24), it is observed that:

- there is a close match in the average and maximum magnitudes of range biases

- The multipath errors on the "measure-and-verify" technique were not as pronounced due to use of the multipath-limiting mini 1.8 m dish antenna.
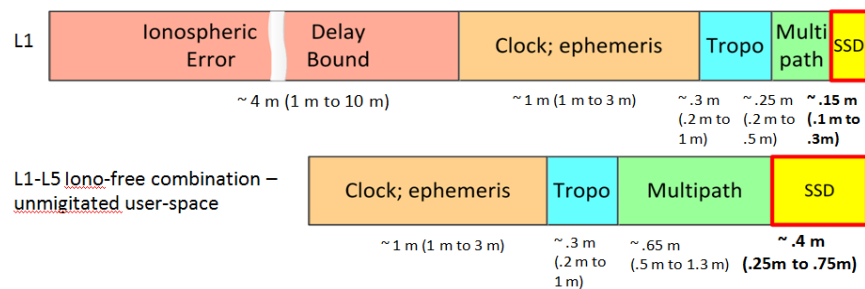
Figure 3-24: Contribution of Satellite Signal Deformation Range Biases to Overall Range Error

With the satellite signal deformation biases quantified, it becomes possible to analyze the impact on user aviation receivers. This is the subject of Chapter 4.

Chapter 4

Impact of Unmitigated Satellite Signal Deformation Range Biases on Aviation Applications

4.1 Overview

This chapter analyzes the impact of **nominal** satellite signal deformation range biases on the availability, accuracy, and worst-case position errors for WAAS-augmented GPS aviation users. (Section 1.3 discusses the distinction between faulted and nominal satellite signal deformation; [16] gives an excellent analysis on the impact of faulted satellite signal deformation on range biases). The analysis includes both single frequency L1-only and dual-frequency L1/L5 users. The impact is determined for

different cases where the set of GPS satellites is not completely available, from the full constellation up to five unhealthy or inaccessible satellites (all possible combinatorial cases). This analysis uses the validated Stanford-developed Matlab Algorithm Availability Simulation Tool (MAAST).

MAAST is introduced in Section 4.2. Section 4.3 describes the performance of single-frequency L1-only and dual-frequency L1/L5 WAAS in the absence of satellite signal deformation range biases. Section 4.4 shows the impact of unmitigated satellite signal deformation range biases on expected 95% vertical position errors for both single-frequency L1-only and dual-frequency L1/L5 WAAS users. Section 4.5 shows the impact of these same unmitigated biases on worst case vertical position errors for single-frequency and dual-frequency WAAS users. Section 4.6 gives a summary and comparison of the impact for various WAAS users.

4.2   Analysis of Availability and Vertical Position Errors using MAAST

As introduced earlier in Section 2.5, the availability, expected position accuracy, and position errors of Satellite-Based Augmentation Systems such as WAAS are determined from confidence estimates of the various residual errors after differential corrections have been applied. These confidence estimates are expressed as scaled variances of the different residual errors. Thus, given estimates of the variances of residual errors, as well as satellite and user positions and satellite-user geometries, the availability, expected accuracy, and position errors can be accurately predicted.

Matlab Algorithm Availability Simulation Tool (MAAST) is a simple and effective tool for such analyses and predictions. It is comprised of a set of fast, accurate, highly customizable, and user-friendly MATLAB functions developed for such analyses [69]. MAAST has been verified to closely match actual WAAS system performance given the same input error variances. Subsequent analyses and predictions in this dissertation rely extensively on MAAST.

MAAST inputs for the analyses in this dissertation were satellite almanacs (orbital parameters) from July 29, 2012 and user positions distributed over the entire conterminous US (CONUS). Other MAAST inputs were overbound error variances and actual error variances, and satellite signal range biases. From these inputs, MAAST first computed the satellite positions and satellite-user geometry matrices for all user positions, and from these, the desired outputs: availability, expected 95% vertical position accuracy in the absence of satellite signal deformation range biases, and expected 95% and worst case vertical position errors in the presence of satellite signal deformation range biases and other GPS range errors. The user position equations [Refer to Section 2.3.5, Equations (2.14)-(2.19), (2.23)-(2.24)] and the WAAS protection level equations [Refer to Section 2.5.2, Equations (2.33) and (2.34)] were used in this process. The detailed MAAST equations and parameters are described in the next section, Section 4.2.1.
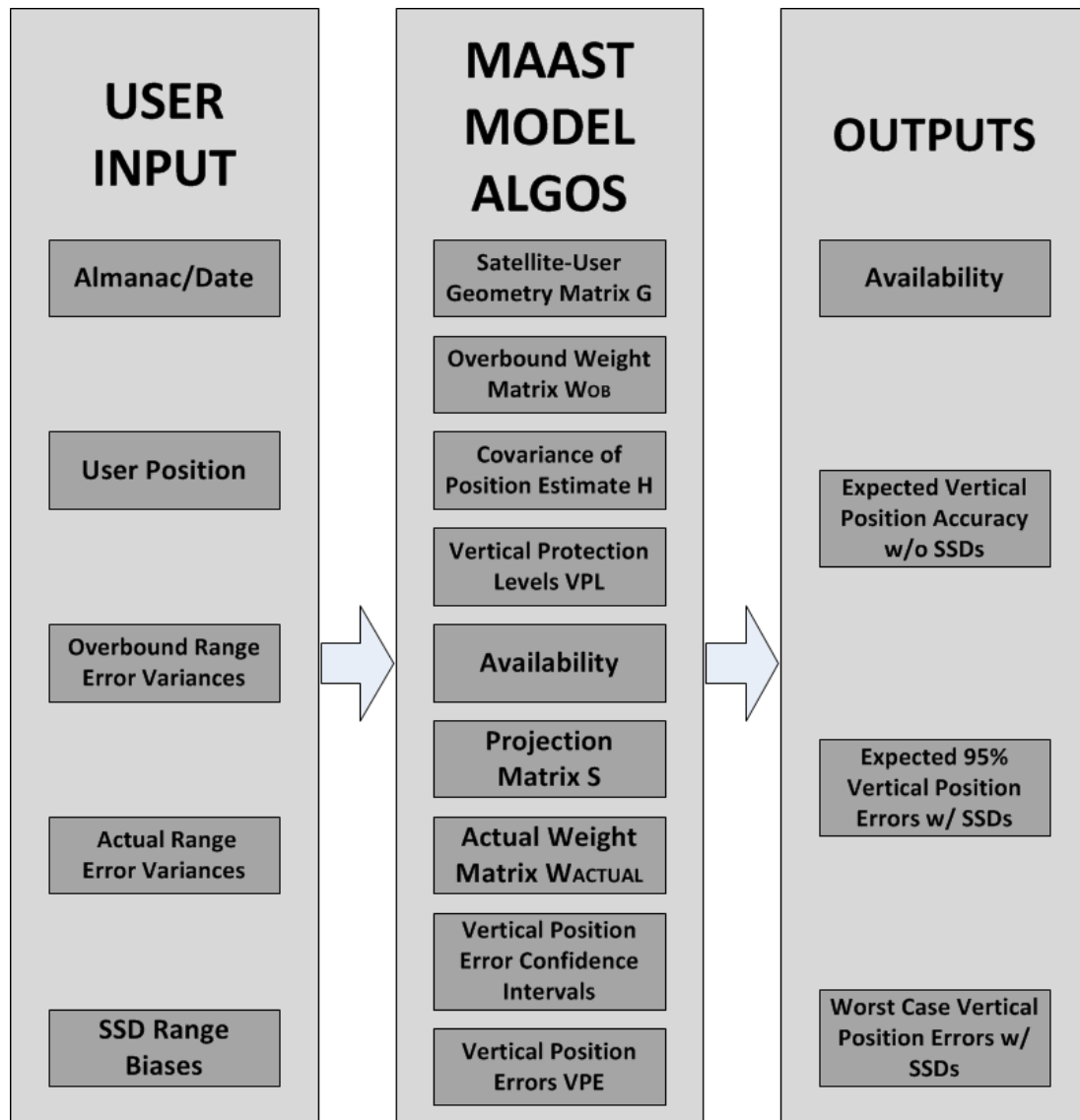
Figure 4-1: Process of using MAAST to determine desired outputs

4.2.1 MAAST Detailed Equations

This section details some of the more involved processes in the MAAST analysis.

1. Satellite-user geometry matrix G

Based on the almanac (satellite orbital parameters) for July 29, 2012, the satellite positions are computed for an entire day. Next, for each user position spaced 1° latitude and longitude apart in CONUS, satellite-user geometry matrices G are computed [Section 2.3.5, Equations (2.14)-(2.19)]. Note that for these analyses, the geometry matrix G is computed in East-North-Up local coordinates referenced to the user positions.

From the satellite and user positions, the satellite elevation angles are also computed to determine visibility of satellite at the user positions.

2. Diagonal overbound weight matrix W_{OB} using overbounded error variances

For each user location, W_{OB} is a diagonal weighting matrix containing the overall **overbounded** confidence (estimated by inverse of variance overbound) associated with the range measurement of each visible satellite:

$$W_{OB} = \begin{bmatrix} 1/\sigma_{OB,1}^2 & 0 & \cdots & 0 & \cdots & 0 \\ 0 & 1/\sigma_{OB,2}^2 & \cdots & 0 & \cdots & 0 \\ & & \ddots & & & \\ \vdots & \vdots & & 1/\sigma_{OB,i}^2 & & \vdots \\ & & & & \ddots & \\ 0 & 0 & \cdots & 0 & \cdots & 1/\sigma_{OB,N}^2 \end{bmatrix} \qquad (4.1)$$

where

W_{OB} : Diagonal overbound weighting matrix containing the inverse of the overall **<u>overbounded</u>** variance associated with the range measurement of each visible satellite

$\sigma^2_{OB,i}$: Overall variance overbound associated with the range measurement of ith visible satellite.

The overbound variances, $\sigma^2_{OB,i}$, are key parameters used in computing the availability, expected vertical position accuracy, and the predicted vertical position errors from the satellite signal deformation range biases. For each satellite range measurement, this overall variance overbound $\sigma^2_{OB,i}$ is computed based on the variance (confidence) overbounds of the following various error components:

For single frequency L1-only,

$$\sigma^2_{OB,L1-ONLY,i} = \sigma^2_{OB,UDRE,i} + \sigma^2_{OB,UIVE,i} * OF^2 + \sigma^2_{OB,CNMP,i} + \sigma^2_{OB,TROP,i} \tag{4.2}$$

where

$\sigma^2_{OB,L1-ONLY,i}$: Overall variance overbound for the various errors in the single-frequency L1-only range measurements from the ith visible satellite

$\sigma^2_{OB,UDRE,i}$: Variance overbound for User Differential Range Errors (UDREs) – satellite clock and ephemeris errors in the range measurements from the ith visible satellite

$\sigma^2_{OB,UIVE,i}$: Variance overbound for User Ionospheric Vertical Errors (UIVEs) at each of his ionospheric pierce point locations, in the range measurements from the ith visible satellite.

OF   : Obliquity Factor - The increase in path length through the ionosphere that an oblique ray takes relative to a vertical ray [55]

$\sigma^2_{OB,CNMP,i}$: Variance overbound for the receiver Code Noise and Multipath (CNMP) errors in the range measurements from the ith visible satellite

$\sigma^2_{OB,TROP,i}$: Variance overbound for tropospheric delay errors in the range measurements from the ith visible satellite

The values used for the overbound standard deviations of the individual error terms are listed in Table 4-1. For simplicity of analysis, identical constant values over all CONUS are used for overbounded standard deviations for satellite clock and ephemeris errors, $\sigma_{OB,UDRE}$, and overbounded standard deviation for ionospheric delay errors, $\sigma_{OB,UIVE}$. The overbounded standard deviation for airborne receiver and multipath errors, $\sigma_{OB,CNMP}$, and overbounded standard deviation for tropospheric delay errors, $\sigma_{OB,TROP}$, are as computed from standard algorithms [70], [71].

Error Term in Equation	Description of Error	Overbound Standard Deviation [m]
$\sigma_{OB,UDRE}$	Overbounded standard deviation for satellite clock and ephemeris errors. For simplicity, fixed values were used.	0.84 (Corresponding to 3.29σ value of 3.0)
$\sigma_{OB,UIVE}$	Overbounded standard deviation for ionospheric delay errors. For simplicity, fixed values were used.	1.88 (Corresponding to 3.29σ value of 4.5)
$\sigma_{OB,CNMP}$	Overbounded standard deviation for airborne receiver and multipath errors	Nominal overbounded values as calculated by MAAST algorithms
$\sigma_{OB,TROP}$	Overbounded standard deviation for tropospheric delay errors	Nominal overbounded values as calculated by MAAST algorithms = 0.12 x Mapping Function

Table 4-1: Quantites used in the computation of overall variance overbound, using

Equations (4.1) and (4.2).

These quantities are representative of nominal WAAS system parameters apart from coastal areas where the actual ionospheric error uncertainty is larger (larger σ_{UIVE}) due to the lack of WAAS monitoring stations in these areas. For simplicity, in these analyses the same nominal ionospheric error uncertainty, σ_{UIVE}, is used throughout all satellite positions in the conterminous United States (CONUS). The results of these analyses are indicative of actual system performance especially in areas toward the interior of CONUS.

For dual-frequency L1/L5,

$$\sigma^2_{OB,L1/L5,i} = \sigma^2_{OB,UDRE,i} + \sigma^2_{OB,CNMP,i} * K^2_{DUAL-FREQ-IONO} + \sigma^2_{OB,TROP,i} \qquad (4.3)$$

where

$\sigma^2_{OB,L1/L5,i}$: Overall variance overbound for various errors components in the dual frequency L1/L5 range measurements from the ith visible satellite

$K_{DUAL-FREQ-IONO}$: Dual-frequency ionosphere-error-removal scale factor. Assuming uncorrelated noise and multipath on L1 and L5, this factor is 2.6 [Refer to Section 2.4.4 Equation (2.32)].

and $\sigma^2_{OB,UDRE,i}$, $\sigma^2_{OB,CNMP,i}$, and $\sigma^2_{OB,TROP,i}$ are the same quantities as in Equation (4.2).

Note that in the dual frequency case, the ionospheric error bound, $\sigma_{OB,UIVE}$, is not required as the ionospheric error is removed by the dual-frequency linear combination for ionosphere error removal. Unfortunately, this linear combination of the dual-frequency measurements has the effect of amplifying the multipath errors. Correspondingly, the code-noise and multipath error (CNMP) overbound, $\sigma_{OB,CNMP}$, is also amplified [Refer to Section 2.4.4 Equation (2.29)]. The removed ionospheric error bound is typically much larger than the amplified multipath, thus the combined effect of both these factors results in a lower dual-frequency overall variance overbound. This in turn results in a lower dual-frequency Vertical Protection Level (discussed in Section 4.2.1 Subsection 4, Equation (4.5).

The overall standard deviation overbound, square root of the overall variance overbound, is illustrated in Figure 4-2 for single frequency L1-only and dual frequency L1/L5 range errors for a single satellite in view. Note the inverse relationship between the overall overbound standard deviation and elevation angle. This is because the overall overbound standard deviation is dependent on tropospheric errors, ionospheric errors (in the case of single-frequency L1-only WAAS users), and multipath. The former two errors are larger at lower elevation angles due to obliquity and a longer path through the atmosphere, while the signals from low-elevation satellites are more adversely affected by ground reflections resulting in greater multipath distortions.
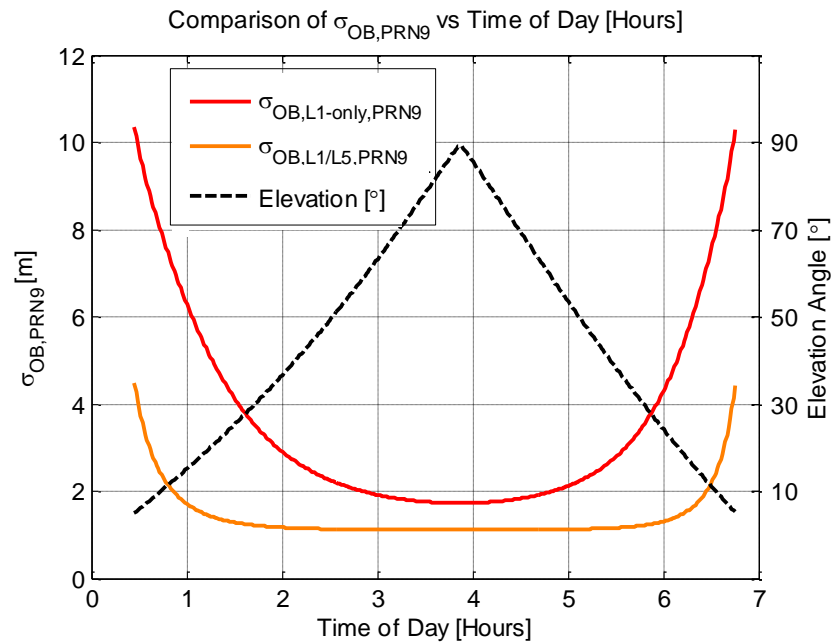
Figure 4-2: Overall overbound standard deviation for Single Frequency L1-only and

Dual Frequency L1/L5 range errors, for a single satellite (PRN 9)

Note that these are range error overbounds for range measurements from a single satellite in view. The error overbounds in the vertical or horizontal dimensions for WAAS users are computed by scaling these overbounds for all satellites in view using the satellite-user geometry matrice G. This is discussed further in Section 4.2.1 Subsections 3 and 4 (Equations (4.4) and (4.5)).

3. Covariance Matrix of Position Estimate H

H, the covariance matrix of the position estimate, is computed as follows:

$$H = (G^T \cdot W_{OB} \cdot G)^{-1} \tag{4.4}$$

where

H : Covariance matrix of the position estimate

G : Computed Satellite-user geometry matrices G [Refer to Section 2.3.5,

                   Equations (2.14)-(2.19), (2.23)-(2.24)].

and W_{OB} is as defined in Equations (4.1)-(4.3).

The focus is on the third element along the diagonal of H. This element represents the estimated overbound of the vertical error variance, which is used in the computation of the vertical protection level (VPL).

4. Vertical Protection Level (VPL)

Section 2.5.2 computed the Protection Level, the worst case error bound for the true errors from worst-case nominal and undetected faults [Equation (2.33)]. Since the concern is over the more critical vertical errors (discussed in Subsection 5 in this section), only the Vertical Protection Level (VPL) is evaluated. This is computed from the overbound estimate of the vertical error variance, the third element along the diagonal of H:

$$VPL = 5.33\sqrt{\left[(G^T \cdot W_{OB} \cdot G)^{-1}\right]_{3,3}}$$
$$= 5.33\sqrt{\left[H\right]_{3,3}} \tag{4.5}$$

where

VPL : Vertical protection level, an integrity bound for 99.99999% of GPS vertical position errors

and G and W_{OB} are as previously described in Equations (4.1)-(4.3).

The Vertical Protection Level (VPL) is set to the Gaussian tail value of 5.33σ and is a bound for 99.99999% of the vertical position errors. This bound is computed in the absence of satellite signal deformation range biases. To compute the single-frequency L1-only and dual-frequency L1/L5 vertical protection levels (VPLs), the corresponding W_{OB} for single-frequency and dual-frequency are used, respectively. The single-frequency and dual-frequency VPLs are shown in Figure 4-3, for the case of two unhealthy satellites over a day and over all CONUS.

VPLs over a day, single location, combos of 2 Unhealthy SVs [m]
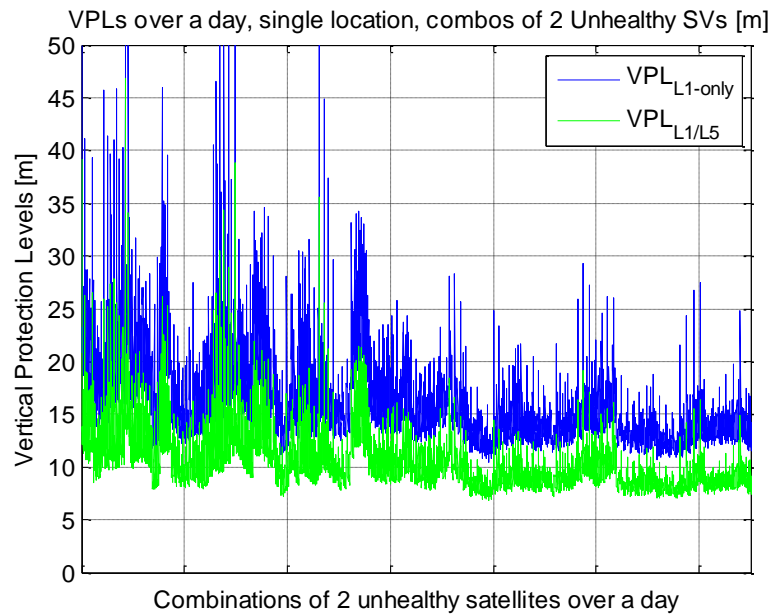
Figure 4-3: Vertical Protection Levels for Single Frequency L1-only and Dual Frequency L1/L5 WAAS Users; two unhealthy satellites, at a single user location

As shown in Figure 4-3, the dual-frequency Vertical Protection Level is smaller in magnitude than the single-frequency Vertical Protection Level. This is because the dual-frequency L1/L5 range overbounds for the individual satellites in view are smaller in magnitude than the corresponding single-frequency L1-only range overbounds, as discussed previously in Section 4.2.1 Subsection 2. This results in a lower overall uncertainty in the vertical dimension, and a lower Vertical Protection Level, for dual-frequency L1/L5 WAAS users. On a separate note, the corresponding Vertical Protection Levels in Figure 4-3 are amplified compared to the range error overbounds in Figure 4-2, due to multiplication by the geometry matrix *G*. This amplification factor increases as the user-satellite geometry deteriorates, as in the case when satellites are unhealthy or unavailable.

The vertical protection levels determine the availability of the WAAS system, which is discussed in the next subsection.

5. Availability

Recall in Section 2.5.3 that availability is the percentage of time the WAAS system is available for aviation users. WAAS is declared available only when the computed 99.99999% bounds for the horizontal and vertical position errors, the Horizontal Position Level (HPL) and the Vertical Position Level (VPL), respectively, lie within specified horizontal and vertical safety limits, the Horizontal Alert Limit (HAL) and Vertical Alert Limit (VAL), respectively. Otherwise, WAAS is declared unavailable, protecting the aviation user.

Recall in Section 2.5.2 Equations (2.33) and (2.34) that WAAS is available if

$$VPL \leq VAL \tag{4.6}$$

And

$$HPL \leq HAL \tag{4.7}$$

where

VPL   :   Vertical Protection Level, an integrity bound for 99.99999% of GPS vertical

                position errors, as previously defined in Equation (4.5).

VAL   :   Vertical Alert Limit, the minimum hazardous vertical position error, beyond

which WAAS should be declared unavailable

HPL   :   Horizontal Protection Level, an integrity bound for 99.99999% of GPS

horizontal position errors

HAL   :   Horizontal Alert Limit, the minimum hazardous horizontal position error,

beyond which WAAS should be declared unavailable

As stated in Section 2.5.2, for Localizer Performance with Vertical Guidance at the

200-foot level, or LPV200, the Vertical Alert Limit, or VAL, is set at 35 m, and the

Horizontal Alert Limit, or HAL, is set at 40 m.

In general, the vertical safety requirement, Equation (4.6), dominates over the

horizontal safety requirement, Equation (4.7). Thus, for this analysis, availability was

determined solely from the vertical requirement. The results are not expected to be

significantly different than if both requirements had been considered.

Figure 4-3 presented the Vertical Protection Levels (VPLs) for Single-Frequency L1-

only and Dual-Frequency L1/L5 WAAS users, for the case of two unhealthy satellites

at a single user location over a day. In Figure 4-4, the same Vertical Protection Levels

are shown in comparison with the Vertical Alert Limit (VAL) of 35 m (LPV-200). The

red and blue rectangular outlines indicate when WAAS is unavailable and available,

respectively.
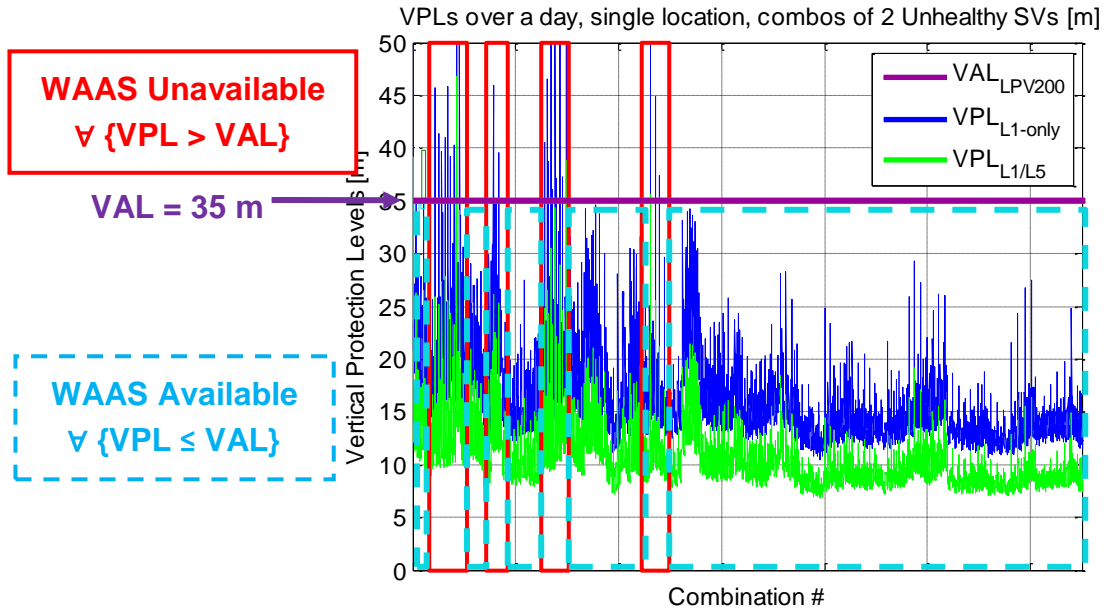
Figure 4-4: Availability of WAAS, based on Vertical Protection Levels (VPLs) and

Vertical Alert Limit (VAL) for Single Frequency L1-only and Dual Frequency L1/L5

WAAS Users; two unhealthy satellites, at a single user location

WAAS is unavailable when Vertical Protection Levels (VPLs) exceed the Vertical

Alert Limit (VAL) of 35 m for LPV-200.

6. Projection Matrix S

The projection matrix S is used to compute the position errors from satellite signal deformation range biases, and the expected position accuracy from all GPS errors in the absence and presence of these biases. S is computed from the geometry matrix G, the covariance matrix of position estimate H, and weight matrix W_{OB} :

$$S = H \cdot G^T \cdot W_{OB} \tag{4.8}$$

where

S : Projection matrix which determines the amount of satellite range errors that are projected into the position and time domain.

and G and W_{OB} are as previously described in Equations (2.14)-(2.19) and Equations (4.1)-(4.3), respectively.

In particular, S_{3i}, the third row of S, expresses how errors in the satellite range measurements impact the vertical position error. S_{3i} is used in the computation of the vertical position errors from satellite signal deformation range biases and expected vertical position accuracy (Section 4.1.1, Subsection 10 and Subsections 8 and 11, respectively).

7. Diagonal weight matrix W_{ACTUAL} using actual WAAS error variances

Similar to W_{OB} discussed in Subsection 2 earlier in this section, W_{ACTUAL} is also a diagonal matrix made up of error variances (confidence) associated with the range measurement of each visible satellite in view. Unlike W_{OB}, which consists of overall variance overbounds for range errors at the 99.99999% confidence level, W_{ACTUAL} is computed from the overall actual variances of range errors, σ^2_{ACTUAL}. σ^2_{ACTUAL} is in turn estimated from the variances of the different error components in the WAAS

range measurements, based on 1.7 billion points of data collected over 3 years from 20

WAAS receivers over the entire CONUS [72], [73], [74].

For each visible satellite i to N, W_{ACTUAL} is given by:

$$W_{ACTUAL} = \begin{bmatrix} 1/\sigma^2_{ACTUAL,1} & 0 & \cdots & 0 & \cdots & 0 \\ 0 & 1/\sigma^2_{ACTUAL,2} & \cdots & 0 & \cdots & 0 \\ & & \ddots & & & \\ \vdots & \vdots & & 1/\sigma^2_{ACTUAL,i} & & \vdots \\ & & & & \ddots & \\ 0 & 0 & \cdots & 0 & \cdots & 1/\sigma^2_{ACTUAL,N} \end{bmatrix} \quad (4.9)$$

where

W_{ACTUAL} :   Diagonal weighting matrix containing the inverse of the overall actual

variances of the range errors from each satellite in view

$\sigma^2_{ACTUAL,i}$:   Overall actual variance of range errors from the ith visible satellite.

For single frequency L1-only WAAS users,

$$\sigma^2_{ACTUAL,L1-ONLY,i} = \sigma^2_{ACTUAL,UDRE,i} + \sigma^2_{ACTUAL,UIVE,i} * OF^2$$
$$+ \sigma^2_{ACTUAL,CNMP,i} + \sigma^2_{ACTUAL,TROP,i} \quad (4.10)$$

where

$\sigma^2_{ACTUAL,L1-ONLY,i}$:   Single-frequency L1-only overall actual variance of range errors

from the ith visible satellite

$\sigma^2_{ACTUAL,UDRE,i}$: Variance of actual satellite clock and ephemeris errors in the range measurements from the ith visible satellite

$\sigma^2_{ACTUAL,UIVE,i}$: Actual variance for ionospheric delay errors in the range measurements from the ith visible satellite

OF : Obliquity factor - The increase in path length through the ionosphere that an oblique ray takes relative to a vertical ray [55]

$\sigma^2_{ACTUAL,CNMP,i}$: Actual variance for airborne receiver and multipath errors in the range measurements from the ith visible satellite

$\sigma^2_{ACTUAL,TROP,i}$: Actual variance for tropospheric delay errors in the range measurements from the ith visible satellite

Figure 4-5 illustrates the single-frequency L1-only overall actual standard deviation of range errors, square root of ooverall actual variance of range errors, from the ith visible satellite, at a single WAAS user location. For comparison, the corresponding single-frequency L1-only overall standard deviation overbound (Figure 4-2) is also shown. The actual error standard deviation, representing nominal errors, is an order of magnitude smaller than the overall overbound standard deviation, which bounds errors with 99.99999% probability.
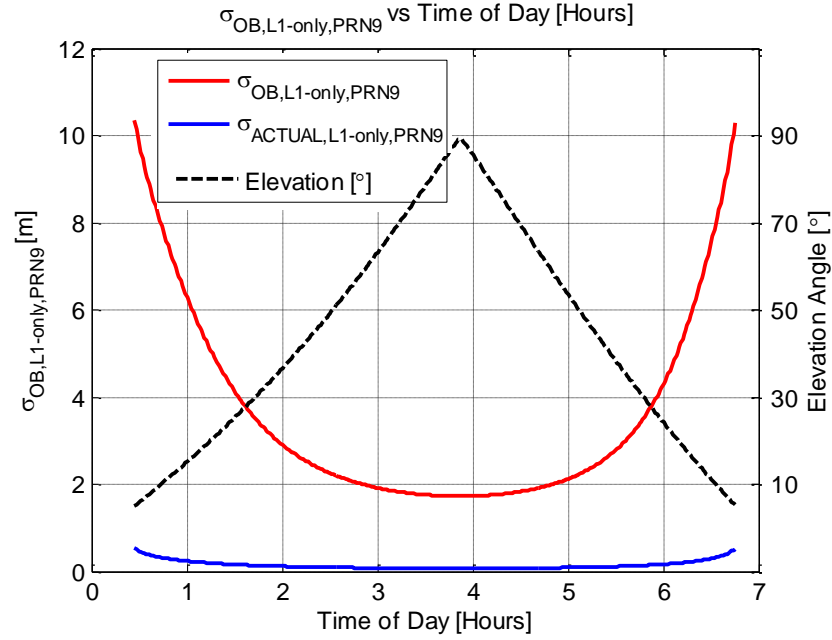
Figure 4-5: Overall actual standard deviation of range errors for single-frequency L1-only WAAS users, for a single satellite in view at a single user location

The corresponding overall standard deviation overbound, previously shown in Figure 4-2, is illustrated for comparison.

Similarly for dual-frequency L1/L5,

$$\sigma^2_{ACTUAL,L1/L5,i} = \sigma^2_{ACTUAL,UDRE,i} + \sigma^2_{ACTUAL,CNMP,i} * K^2_{DUAL-FREQ-IONO} + \sigma^2_{ACTUAL,TROP,i} \qquad (4.11)$$

where

$K_{DUAL\text{-}FREQ\text{-}IONO}$: Dual-frequency ionosphere-error-removal scale factor of 2.6 [Refer to Section 2.4.4 Equation (2.32)].

and $\sigma^2_{ACTUAL,i}$, $\sigma^2_{ACTUAL,UDRE,i}$, $\sigma^2_{ACTUAL,CNMP,i}$, and $\sigma^2_{ACTUAL,TROP,i}$ are the same quantities as in Equation (4.10).

Similar to Figure 4-5, Figure 4-6 illustrates the dual-frequency L1/L5 overall actual standard deviation of range errors from the ith visible satellite, at a single WAAS user location. For comparison, the corresponding dual-frequency L1/L5 overall standard deviation overbound (Figure 4-2) is also shown. As in the single-frequency L1-only case, the actual error standard deviation, representing nominal errors, is smaller than the overbound error standard deviation, but not by as much as in the single-frequency case due to the smaller range error overbound for the dual-frequency L1/L5 ranges.
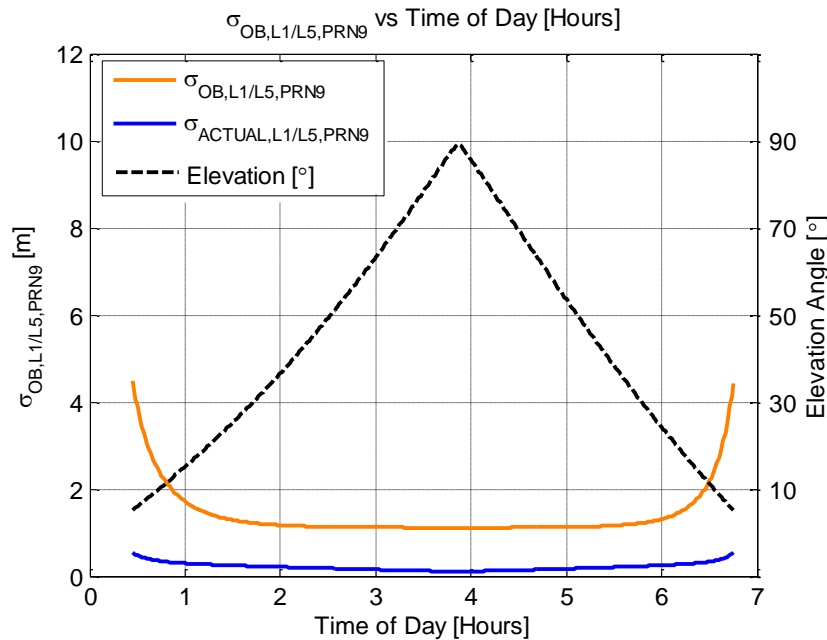
Figure 4-6: Overall actual standard deviation of range errors for dual-frequency L1/L5 only WAAS users, for a single satellite in view at a single user location.

The corresponding overall standard deviation overbound, previously shown in Figure 4-2, is illustrated for comparison.

8. Expected Vertical Position Accuracy in the Absence of Satellite Signal Deformation Range Biases

This subsection shows the computation of Expected Vertical Position Accuracy, $\overline{VPA}_{No\_SSD}$, from the overall actual range error variances computed in Subsection 7. The expected vertical position accuracy, or 95% confidence level, was previously verified and found to closely match the 95% vertical position errors from actual data [70]. It is used as a reference baseline to evaluate the impact of unmitigated and mitigated signal deformation on vertical position errors (VPE) (discussed in Sections 4.4, 4.5, and 5.3), for all cases where WAAS is available. This computation broadly follows the method outlined in [70].

The overall actual range error variance was previously calculated from its constitutent range error components, in the absence of signal deformation, for each satellite in view. From these actual measured range error variances, the instantaneous actual vertical position error variances and standard deviations are computed from the user-satellite geometry, at different times and different WAAS user locations. Using the projection matrix S:

$$\sigma^2_{WAAS-VERT} = \left[(S^T \cdot W_{ACTUAL} \cdot S)^{-1} \right]_{3,3} \tag{4.12}$$

$$\sigma_{WAAS-VERT} = \sqrt{\sigma^2_{WAAS-VERT}} = \sqrt{\left[(S^T \cdot W_{ACTUAL} \cdot S)^{-1} \right]_{3,3}} \tag{4.13}$$

where

$\sigma^2_{WAAS-VERT}$: Actual vertical position error variance for WAAS user due to nominal GPS errors, in the absence of satellite signal deformation range biases.

$\sigma_{WAAS-VERT}$: Actual vertical position error standard deviation for WAAS user due to nominal GPS errors, in the absence of satellite signal deformation range biases.

and S and W_{ACTUAL} are as previously defined in Equations (4.8) and (4.9), respectively. Similar to Equation (4.5), the third element along the diagonal represents the standard deviation in the vertical dimension, but of the actual measured errors rather than overbounded errors.

Assuming Gaussian distribution for the errors, twice the actual vertical position error standard deviation would be an instantaneous estimate for vertical position errors at the 95% confidence level, or estimated Vertical Position Accuracy (VPA). This estimate is for a WAAS user at a single location and single time instant. Averaging the instantaneous VPA over an entire day results in the Expected Vertical Position Accuracy in the absence of signal deformation, or $\overline{VPA}_{No\_SSD}$.

Expected vertical position accuracy in the absence of signal deformation, $\overline{VPA}_{No\_SSD}$

$\approx$ 95% Confidence Interval of GPS Vertical Position Errors, Averaged over Day

$$\approx 2 \times \mathrm{E}[\sigma_{WAAS-VERT}] \tag{4.14}$$

$$\approx 2 \times \overline{\sigma}_{WAAS-VERT} \tag{4.15}$$

where

$\overline{VPA}_{No\_SSD}$: Expected vertical position accuracy in the absence of satellite signal deformation range biases. This is a 95% confidence level estimate for 95% GPS Vertical Position Errors, averaged over a day.

$\sigma_{WAAS-VERT}$: Instantaneous standard deviation of vertical position errors for WAAS user due to nominal GPS errors, in the absence of signal deformation. Previously computed in Equation (4.13), from standard deviations of actual WAAS vertical position errors.

$\overline{\sigma}_{WAAS-VERT}$: Average over a day of instantaneous standard deviation of vertical position errors for WAAS user due to nominal GPS errors, in the absence of signal deformation, $\sigma_{WAAS-VERT}$.

To obtain the expected vertical position accuracy for single-frequency L1-only and dual-frequency L1/L5 WAAS, the appropriate single-frequency or dual-frequency

standard deviations, $\sigma_{ACTUAL,i}$ [Equation (4.10) or (4.11)], and Weight Matrix, $\mathbf{W_{ACTUAL}}$ [Equation (4.9)], are used in Equations (4.13) and (4.14).

Figure 4-7 and Figure 4-8 present the Expected Position Accuracy ($\overline{VPA}_{No\_SSD}$) for single-frequency L1-only and dual-frequency L1/L5 WAAS users, respectively, in the absence of satellite signal deformation range biases. The results are for a single-frequency L1-only WAAS user at a single location over a day.
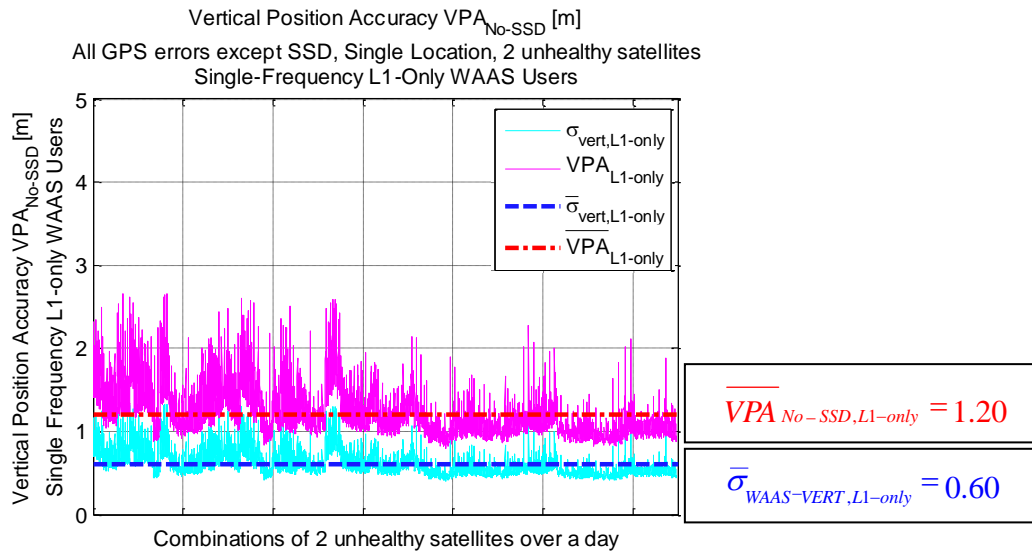
Figure 4-7: Instantaneous Vertical Position Accuracy, $VPA_{No\_SSD,L1-only}$, and average over a day, $\overline{VPA}_{No\_SSD,L1-only}$ for single-frequency L1-only WAAS users at a single user location

(Two unhealthy/inaccessible satellites, Reference: 0.1 L1-chip correlator spacing; User: 0.2 L1-chip correlator spacing)
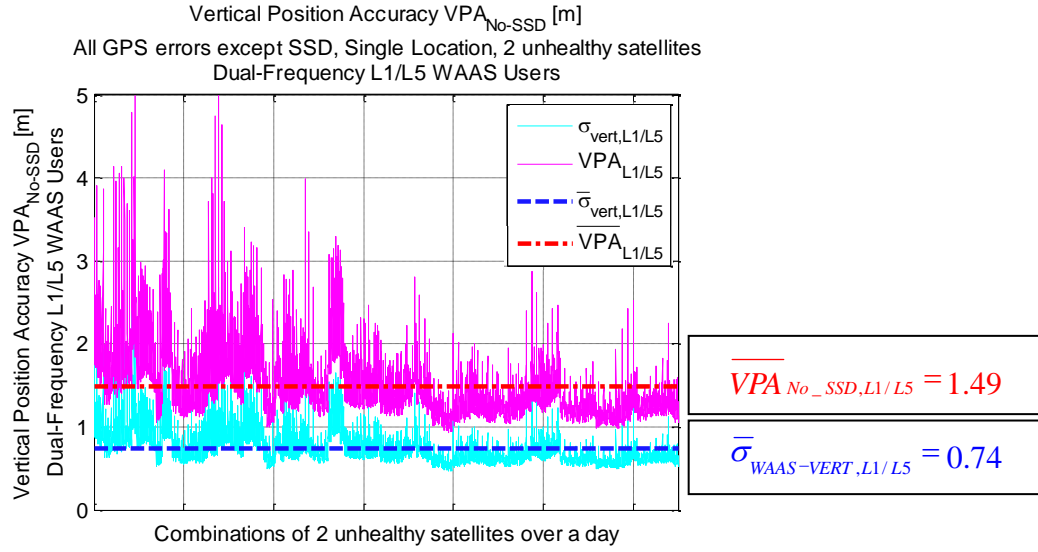
Figure 4-8: Instantaneous Vertical Position Accuracy, $VPA_{No\_SSD,L1/L5}$, and average

over a day, $\overline{VPA}_{No\_SSD,L1/L5}$ for dual-frequency L1/L5 WAAS users at a single user

location

(Two unhealthy/inaccessible satellites, Reference: 0.1 L1-chip correlator spacing;

User: 0.2 L1-chip correlator spacing)

9. Projection of Dual-Frequency L1/L5 Biases from Single-Frequency L1-only

Biases for Computation of Dual-Frequency Vertical Position Errors

The resultant vertical position errors are computed from the measured satellite signal

range biases. As discussed in Section 3.7.4, all 31 GPS satellites transmit the L1-

frequency signals, but only 3 (at time of writing) transmit both the L1-frequency and

L5-frequency signals. (New dual-frequency L1/L5 satellites will replace the older

single-frequency L1-only satellites, launched at the rate of one to two per year.)

The vertical position errors for single-frequency L1-only WAAS users can be computed solely from the L1-frequency biases; unfortunately, computation of vertical position errors for dual-frequency L1/L5 WAAS users requires both L1-frequency biases and L5-frequency biases. Since the L5-frequency measured biases are not fully available, the dual-frequency L1/L5 biases for this analysis were projected from the L1-frequency measured biases:

$$b_{SSD,i,L1/L5} = K_{DUAL-FREQ-IONO} * b_{SSD,i,L1-only} \qquad (4.16)$$

where

$b_{SSD,i,L1/L5}$: Dual-frequency L1/L5 satellite signal deformation range bias

$b_{SSD,I,L1-only}$: Single-frequency L1-only satellite signal deformation range biases

$K_{DUAL-FREQ-IONO}$: Dual-frequency ionosphere-error-removal scale factor of 2.6 [Refer to Section 2.4.4 Equation (2.32)]. Identical to scale factor for L1-frequency airborne receiver noise and multipath standard deviation to obtain the corresponding dual-frequency L1/L5 standard deviation.

This projection assumes that the L1-frequency biases and L5-frequency biases are uncorrelated . The results in Section 3.7.5 show this assumption to be reasonable. Recent ionospheric research has also shown that strong scintillation is less correlated between the different transmission frequencies [75], [76].

10. Vertical Position Errors from Satellite Signal Deformation Range Biases Only

The vertical position errors entirely from satellite signal deformation range biases, in the absence of other GPS range errors, are computed from S_{3i}, elements of the third row of the projection matrix S (computed in Subsection 6) and $b_{SSD,i}$, elements of the vector of satellite signal deformation range biases:

$$VPE_{SSD} = \sum_{i=1}^{N} S_{3,i} b_{SSD,i} \tag{4.17}$$

Where:

VPE_{SSD} : Vertical Position Error due to satellite signal deformation only

$S_{3,i}$: Elements of third row of the projection matrix S

$b_{SSD,i}$: Satellite signal deformation range biases (obtained in the previous chapter) corresponding to visible satellites

N : Total number of satellites visible at user

Figure 4-9 and Figure 4-10 illustrate the vertical position errors entirely from satellite signal deformation range biases, in the absence of other GPS errors, for single-frequency L1-only and dual-frequency L1/L5 WAAS users, respectively, at a single user location in CONUS. The **reference receiver**'s correlator spacing is **0.1 L1-chips** and the **user receiver**'s correlator spacing is **0.2 L1-chips**. The results in the figures are as expected: the dual-frequency L1/L5 errors are approximately a factor of 2.6

larger than the single frequency L1-only errors. This factor corresponds to the dual-frequency ionosphere-error-removal scale factor – Refer to Equations (2.29)-(2.32).
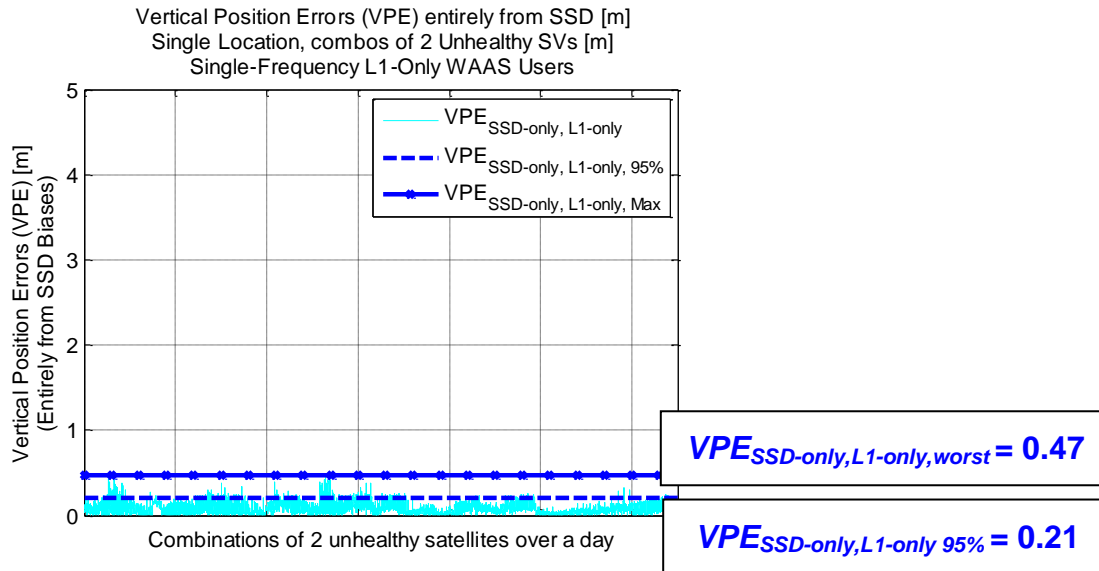
Figure 4-9: Vertical Position Errors (VPE) [m] entirely from Satellite Signal

Deformation only, in the absence of other GPS errors; for single-frequency L1-only

WAAS users at a single user location

(Two unhealthy/inaccessible satellites, Reference: 0.1 L1-chip correlator spacing;

User: 0.2 L1-chip correlator spacing)
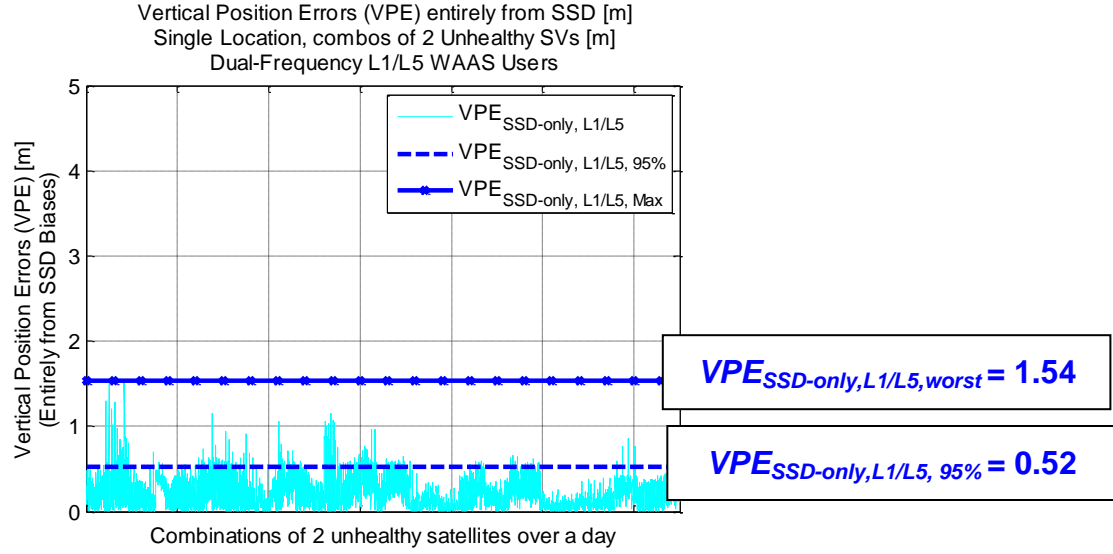
Figure 4-10: Vertical Position Errors (VPE) [m] entirely from Satellite Signal

Deformation, in the absence of other GPS errors; for dual-frequency L1/L5 WAAS

users at a single user location

(Two unhealthy/inaccessible satellites, Reference: 0.1 L1-chip correlator spacing;

User: 0.2 L1-chip correlator spacing)

11. Combined Vertical Position Errors from Satellite Signal Deformation Range
    Biases and other Nominal GPS Errors

In the presence of satellite signal deformation range biases together with other GPS range errors, the **Expected 95% Vertical Position Error (VPE)** experienced by WAAS users is computed as:

$$VPE_{Expected\,95\%} = [VPE_{SSD}]_{95\%} + \overline{VPA}_{No\_SSD} \tag{4.18}$$

Where:

$VPE_{Expected95\%}$: Expected 95% Vertical Position Error (VPE) experienced by WAAS users over an entire day due to satellite signal deformation range biases, in addition to nominal GPS errors

$[VPE_{SSD}]_{95\%}$: 95th-percentile Vertical Position Error (VPE) experienced by WAAS users over an entire day, due to satellite signal deformation only

and $\overline{VPA}_{No\_SSD}$ is as defined in Equation (4.14).

Similarly, in the presence of satellite signal deformation range biases, the **Worst Case Vertical Position Error** experienced by WAAS users is computed as:

$$VPE_{WorstCase} = [VPE_{SSD}]_{WorstCase} + \overline{VPA}_{No\_SSD} \qquad (4.19)$$

Where:

$VPE_{WorstCase}$: Worst case vertical position error experienced by WAAS users over an entire day, due to satellite signal deformation range biases, in addition to nominal GPS errors

$[VPE_{SSD}]_{WorstCase}$: Worst case vertical position error experienced by WAAS users over an entire day, due to satellite signal deformation only

and $\overline{VPA}_{No\_SSD}$ is as defined in Equation (4.14).

The Expected 95% Vertical Position Error and Worst Case Vertical Position Error are illustrated in Figure 4-11 and Figure 4-12 for single-frequency L1-only WAAS users at a single user location. Figure 4-11 shows the vertical position errors in the absence and presence of satellite sgnal deformation, and Figure 4-12 shows the same errors with daily averages, daily 95% errors, and daily worst case errors superimposed for comparison. Figure 4-13 and Figure 4-14 show the corresponding curves for dual-frequency L1/L5 WAAS users. These daily results are presented graphically for all WAAS user locations in CONUS in Sections 4.3, 4.4, 4.5, and 5.3.2. These daily results are further averaged over all user locations to form the summary tables presented in Sections 4.4.3, 4.5.3, and 5.3.2.3.
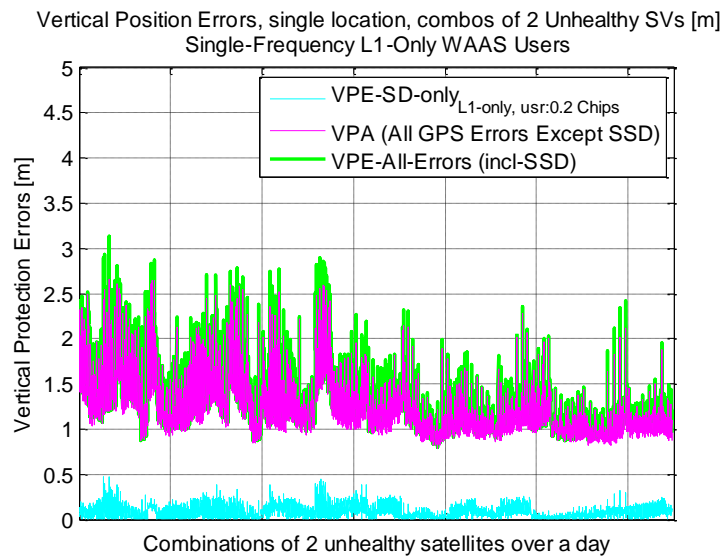
Figure 4-11: Vertical Position Errors (VPE) [m] from sum of GPS errors and Satellite Signal Deformation; for single-frequency L1-only WAAS users, at a single user location

(Two unhealthy/inaccessible satellites, Reference: 0.1 L1-chip correlator spacing; User: 0.2 L1-chip correlator spacing)
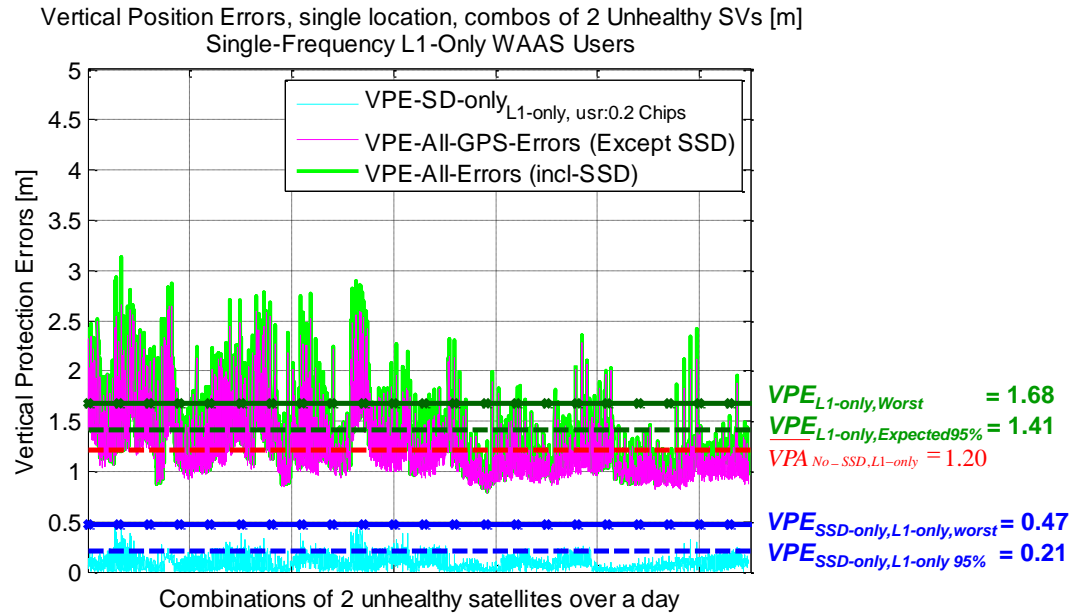
Figure 4-12: Vertical Position Errors (VPE) [m] from sum of GPS errors and Satellite

Signal Deformation; for single-frequency L1-only WAAS users, at a single user

location (including daily averages, daily 95% errors and daily worst case errors)

(Two unhealthy/inaccessible satellites, Reference: 0.1 L1-chip correlator spacing;

User: 0.2 L1-chip correlator spacing)

Vertical Position Errors, single location, combos of 2 Unhealthy SVs [m]
Dual-Frequency L1/L5 WAAS Users

Figure 4-13: Vertical Position Errors (VPE) [m] from sum of GPS errors and Satellite

Signal Deformation; for dual-frequency L1/L5 WAAS users, at a single user location

(Two unhealthy/inaccessible satellites, Reference: 0.1 L1-chip correlator spacing;

User: 0.2 L1-chip correlator spacing)

Figure 4-14: Vertical Position Errors (VPE) [m] from sum of GPS errors and Satellite

Signal Deformation; for dual-frequency L1/L5 WAAS users, at a single user location

(including daily averages, daily 95% errors and daily worst case errors)

(Two unhealthy/inaccessible satellites, Reference: 0.1 L1-chip correlator spacing;

User: 0.2 L1-chip correlator spacing)

The impact of satellite signal deformation range biases on WAAS users is quantified

by comparing the **Expected 95% Vertical Position Error,** $VPE_{Expected95\%}$, [Equation

(4.18)] and **Worst Case Vertical Position Error,** $VPE_{WorstCase}$, [Equation (4.19)] with

the baseline expected vertical position accuracy, $\overline{VPA}_{No\_SSD}$ [Equation (4.14)]. Section

4.4 discusses these comparisons for the expected 95% vertical position errors, and

Section 4.5 discusses these comparisons for the worst case vertical position errors, in

the case of unmitigated satellite signal deformation. Sections 5.3.2 and 5.3.3 discuss the corresponding comparisons in the case of mitigated satellite signal deformation.

12. Effect of Inaccessible or Unhealthy Satellites

The Availability, Expected Vertical Position Accuracy in the absence of satellite signal deformation range biases, Expected 95% Vertical Position Error, and Worst Case Vertical Position Error were previously computed for a fully healthy set of GPS satellites. To determine the impact of satellite signal deformation range biases on weak geometries due to unhealthy or inaccessible satellites, these quantities are now computed for all combinations of unhealthy satellites, from fully healthy up to five unhealthy satellites. The procedures for fully healthy satellites have already been described; they are outlined in this subsection for the case of M unhealthy satellites, where M ranges from one to five. The results are then tabulated according to the number of unhealthy satellites.

- To compute the availability for the case of M unhealthy satellites, the individual constituent quantities are first derived for each combination containing M unhealthy satellites, then averaged across all such combinations.

For each combination containing M unhealthy satellites, the covariance matrix of the position estimate is computed as follows:

$$H_M = (G_M^T \cdot W_{OB,M} \cdot G_M)^{-1} \tag{4.20}$$

where

$W_{OB,M}$: Diagonal overbound weighting matrix as in fully healthy case (refer to Equation (4.1)-(4.3)), but omitting the overall overbounded variances for the M unhealthy satellites.

H_M : Covariance matrix of the position estimate (refer to Equation (4.4)), omitting the contribution from the M unhealthy satellites.

G_M : Computed Satellite-user geometry matrices [Refer to Section 2.3.5, Equations (2.14)-(2.19), (2.23)-(2.24), and also Equation (4.4)], omitting the contribution from the M unhealthy satellites.

The Vertical Protection Level for the same combination containing M unhealthy satellites:

$$VPL_M = 5.33\sqrt{\left[(G_M^T \cdot W_{OB,M} \cdot G_M)^{-1}\right]_{3,3}}$$
$$= 5.33\sqrt{\left[H_M\right]_{3,3}} \qquad\qquad (4.21)$$

where

VPL_M :   Vertical Protection Level (refer to Equation (4.6)), omitting the contribution from the M unhealthy satellites.

and G_M, $W_{OB,M}$, and H_M are as previously described in Equation (4.20).

Availability for this particular combination containing M unhealthy satellites:

$$VPL_M \leq VAL \tag{4.22}$$

where

VPL_M : Vertical protection level for this combination of M unhealthy satellites, as previously defined in Equations (4.5) and (4.21).

VAL : Vertical Alert Limit, the minimum hazardous vertical position error, beyond which WAAS should be declared unavailable. For Localizer Performance with Vertical Guidance at 200-foot level, or LPV200, the Vertical Alert Limit, or VAL, is set at 35 m.

Similar to Subsection 5,

$$\text{Overall availability for } M \text{ unhealthy satellites} = \frac{T_{N,M,AVAIL}}{T_{N,M}} \tag{4.23}$$

where

$T_{N,M,AVAIL}$: Number of combinations containing M unhealthy satellites, throughout the entire day, satisfying the availability test (refer to Equation (4.22))

$T_{N,M}$: Total number of combinations of M unhealthy satellites throughout the day

- Similarly, to compute the Expected Vertical Position Accuracy in the absence of signal deformation for the case of M unhealthy satellites, the individual constituent

quantities are first derived for each combination of M unhealthy satellites, then averaged across all such combinations.

For each combination containing M unhealthy satellites satisfying the availability criterion (Equation (4.22)), the Projection Matrix S is computed as follows:

$$S_M = H_M \cdot G_M^T \cdot W_{OB,M} \tag{4.24}$$

where

S_M : Projection matrix as previously defined in Equation (4.8), omitting the contribution of the M unhealthy satellites.

and H_M, G_M, and $W_{OB,M}$ are as previously described in Equation (4.20).

The instantaneous actual vertical position error variance and standard deviation for the same combination containing M unhealthy satellites:

$$\sigma^2_{WAAS-VERT,M} = \left[(S_M^T \cdot W_{ACTUAL,M} \cdot S_M)^{-1} \right]_{3,3} \tag{4.25}$$

$$\sigma_{WAAS-VERT,M} = \sqrt{\sigma^2_{WAAS-VERT,M}} = \sqrt{\left[(S_M^T \cdot W_{ACTUAL,M} \cdot S_M)^{-1} \right]_{3,3}} \tag{4.26}$$

where

$W_{ACTUAL,M}$: Diagonal weighting matrix containing the inverse of the overall actual variances of the range errors from each satellite in view (refer to Equation (4.9)), omitting the contribution from the **M** unhealthy satellites.

$\sigma^2_{WAAS-VERT,M}$: Instantaneous actual vertical position error variance in the absence of satellite signal deformation range biases (refer to Equation (4.12)), omitting the contribution from the **M** unhealthy satellites

$\sigma_{WAAS-VERT,M}$: Instantaneous actual vertical position error standard deviation in the absence of satellite signal deformation range biases (refer to Equation (4.13)), omitting the contribution from the **M** unhealthy satellites

and S_M was previously defined in Equation (4.24).

Expected vertical position accuracy for *M* unhealthy satellites, in the absence of signal deformation, $\overline{VPA}_{No\_SSD,M}$

$$\approx \begin{cases} \bullet \ \ \text{95\% Confidence Interval of GPS Vertical Position Errors in the case of } \textit{M} \text{ unhealthy satellites} \\ \bullet \ \ \text{Averaged over a Day} \\ \bullet \ \ \text{Averaged over all possible combinations containing } \textit{M} \text{ unhealthy satellites which satisfy safety requirement Equation (4.22) ie } VPL_M \leq VAL \end{cases}$$

$$\approx 2 \times \mathrm{E}[\sigma_{WAAS-VERT,M}] \tag{4.27}$$

$$\approx 2 \times \overline{\sigma}_{WAAS-VERT,M} \tag{4.28}$$

where

M   : Number of satellites designated as unhealthy, from one to five

$\overline{VPA}_{No\_SSD,M}$: Similar to $\overline{VPA}_{No\_SSD}$ in Equation (4.15), this is the estimated 95% confidence level for GPS Vertical Position Errors in the absence of signal deformation, averaged over a day and over all possible combinations of *M* unhealthy satellites meeting the availability requirement [Equation (4.6)], ie *VPL < VAL*

$\overline{\sigma}_{WAAS-VERT,M}$: Average of $\sigma_{WAAS-VERT}$, instantaneous standard deviation of vertical position errors for WAAS user due to nominal GPS errors, in the absence of signal deformation, over a day and over all possible combinations of *M* unhealthy satellites meeting the availability requirement [Equation (4.6)], ie *VPL < VAL*

and $\sigma_{WAAS-VERT,M}$ is as previously defined in Equation (4.26).

- The Expected 95% Vertical Position Error [Refer to Section 4.2.1 Subsection 11, Equation (4.18)] was computed as follows:

$$VPE_{Expected95\%,M} = [VPE_{SSD}]_{95\%,M} + \overline{VPA}_{No\_SSD,M} \qquad (4.29)$$

where:

M : Number of satellites designated as unhealthy, from one to five.

$VPE_{Expected95\%,M}$: Expected 95% Vertical Position Error (VPE) experienced by WAAS users over an entire day, due to satellite signal deformation range biases and nominal GPS errors, for the case of M unhealthy satellites.

$[VPE_{SSD}]_{95\%,M}$: 95th-percentile Vertical Position Error (VPE) experienced by WAAS users due to satellite signal deformation only, over an entire day and over all possible combinations of M unhealthy satellites meeting the availability requirement [Refer to Equation (4.6), i.e., *VPL* < *VAL*]

and $\overline{VPA}_{No\_SSD,M}$ is as defined in Equation (4.28).

- Similarly, the Worst Case Vertical Position Error [Refer Section 4.2.1 Subsection 11, Equation (4.19)] was computed as follows:

$$VPE_{WorstCase,M} = [VPE_{SSD}]_{WorstCase,M} + \overline{VPA}_{No\_SSD,M} \qquad (4.30)$$

Where:

M : Number of satellites designated as unhealthy, from one to five.

$VPE_{WorstCase,M}$: Worst Case Vertical Position Error (VPE) experienced by WAAS users over an entire day, due to satellite signal deformation range biases and nominal GPS errors, for the case of M unhealthy satellites.

$[VPE_{SSD}]_{WorstCase,M}$: Worst Case Vertical Position Error (VPE) experienced by WAAS users due to satellite signal deformation only, over an entire day and over all possible combinations of M unhealthy satellites meeting the availability requirement [Refer Equation (4.6), ie $VPL < VAL$].

and $\overline{VPA}_{No\_SSD,M}$ is as defined in Equation (4.28).

In the subsequent sections, results for the case of two unhealthy or inaccessible satellites will be presented, to highlight key conclusions. Complete results can be found in Appendix D for the cases of full constellation and from one to five unhealthy or inaccessible satellites.

4.3 Availability and Accuracy of Single-Frequency and Dual-Frequency WAAS without Satellite Signal Deformation Range Biases

MAAST was used to analyze the availability and accuracy of single-frequency L1-only and dual-frequency L1/L5 WAAS, in the absence of satellite signal deformation range biases. These results were derived from recorded GPS ranges that included all range errors except satellite signal deformation. Graphical results are presented for two unhealthy satellites; they are later summarized in tabular form for up to five unhealthy or inaccessible satellites. These results highlight the key benefit of dual-frequency WAAS – increased availability, especially when fewer satellites are available and during periods of heightened ionospheric activity. This dual-frequency benefit comes at a cost of slightly poorer accuracy.

Section 4.3.1 presents the availability results and comparison between single-frequency L1-only WAAS and dual-frequency L1/L5 WAAS. Section 4.3.2 presents the corresponding accuracy results for single-frequency and dual-frequency WAAS. These results are used as reference baselines in later sections (Sections 4.5 and 5.3.2) when the impact of satellite signal deformation range biases is examined.

4.3.1   Availability for Single- and Dual-Frequency WAAS Users in the Absence of Satellite Signal Deformation

Figure 4-15 and Figure 4-16 show the availability experienced respectively by single-frequency L1-only and dual-frequency L1/L5 WAAS users in the absence of satellite signal deformation, when two satellites are unavailable. Single-frequency L1-only WAAS is unable to meet the user availability specification of 99.9% over most of CONUS, while dual-frequency L1/L5 WAAS meets this specification over some parts of CONUS, and is close to meeting it (99.5%) over most of CONUS.
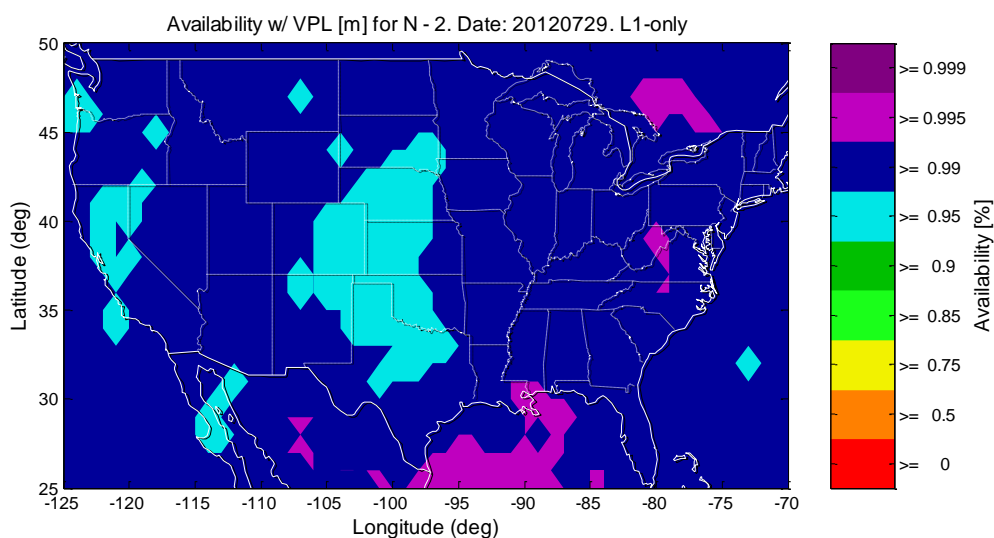
Figure 4-15: Availability for case of two unhealthy/inaccessible satellites for Single Frequency L1-only WAAS Users, in the Absence of Satellite Signal Deformation
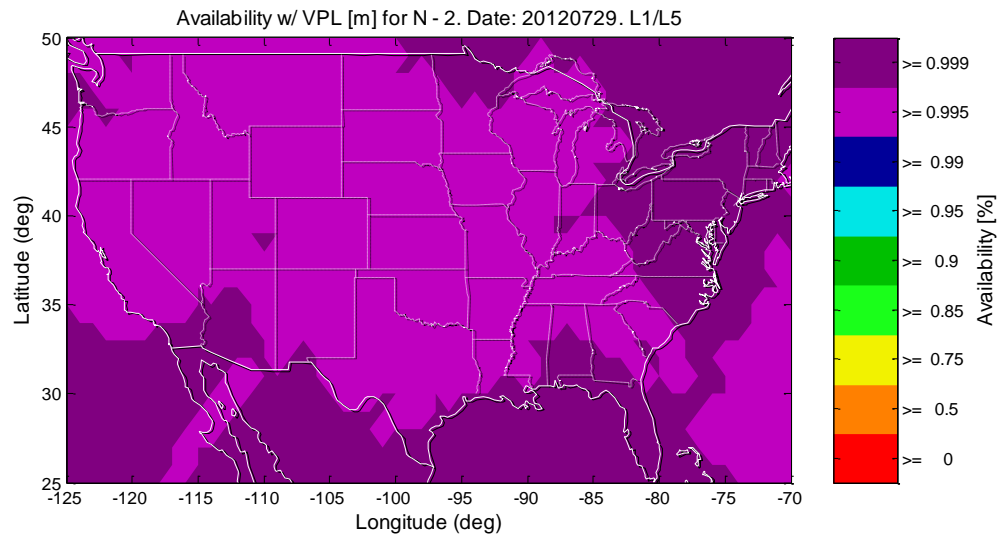
Figure 4-16: Availability for case of two unhealthy/inaccessible satellites for Dual

Frequency L1/L5 WAAS Users, in the Absence of Satellite Signal Deformation

The average availability over all locations is summarized in Table 4-2.

Satellite Status	Average Availability [%]	
	Frequency: L1-Only	Frequency: L1/L5
N - 0	100.00%	100.00%
N - 1	99.91%	99.99%
N - 2	99.26%	99.88%
N - 3	97.01%	99.31%
N - 4	91.32%	97.15%
N - 5	80.46%	91.44%

Table 4-2: Average Availability for Single Frequency L1-only and Dual Frequency

L1/L5 WAAS Users, in the Absence of Satellite Signal Deformation

Under nominal ionospheric conditions, dual-frequency L1/L5 WAAS users (Figure 4-16) experience greater availability compared to single-frequency L1 WAAS users (Figure 4-15), especially in the cases where there are fewer satellites than in a full

constellation (Table 4-2). This benefit is even more pronounced in severe ionospheric conditions, when single-frequency WAAS users operate under increased ionospheric error bounds and thus lower availability. This is a key motivation for the use of dual-frequency WAAS.

Table 4-2 also shows that the dual-frequency WAAS system is very close to meeting the system performance specification (99.9% availability) when up to two satellites are unavailable, while single-frequency WAAS would only meet the specifications when at most one satellite is unhealthy or otherwise inaccessible. The availability gap between single-frequency and dual-frequency widens as there are fewer healthy and accessible satellites.

4.3.2   Expected Accuracy for Single-Frequency and Dual-Frequency WAAS Users in the Absence of Satellite Signal Deformation

Figure 4-17 and Figure 4-18 show the Expected Vertical Position Accuracy experienced respectively by single-frequency L1-only and dual-frequency L1/L5 WAAS users, in the absence of satellite signal deformation range biases, when two satellites are unavailable.

Expected Accuracy Vertical Position Errors - No SSD [m] for N - 2. Date: 20120729. L1-only
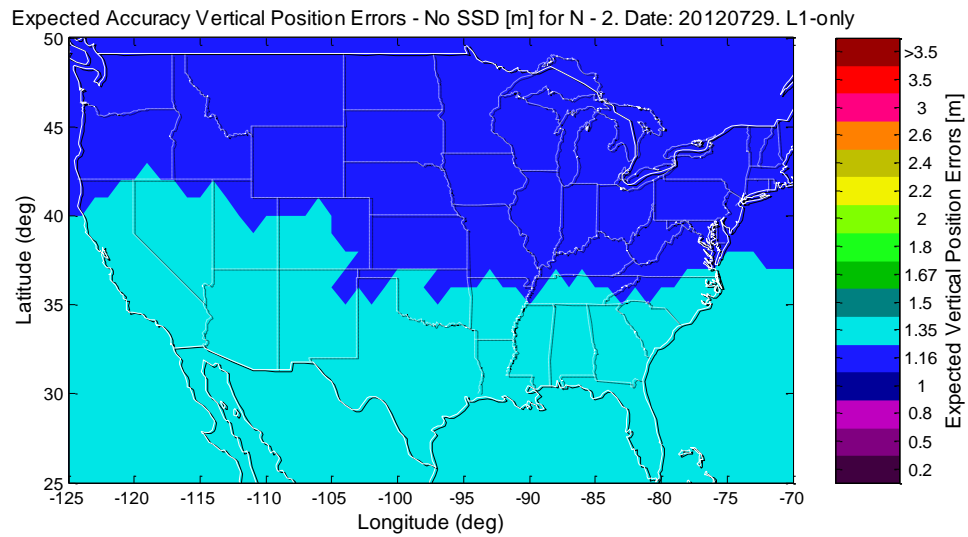
Figure 4-17: Nominal Accuracy (95% 2σ) for case of two unhealthy/inaccessible

satellites for Single Frequency L1-only WAAS Users, in the Absence of Satellite

Signal Deformation

Expected Accuracy Vertical Position Errors - No SSD [m] for N - 2. Date: 20120729. L1/L5
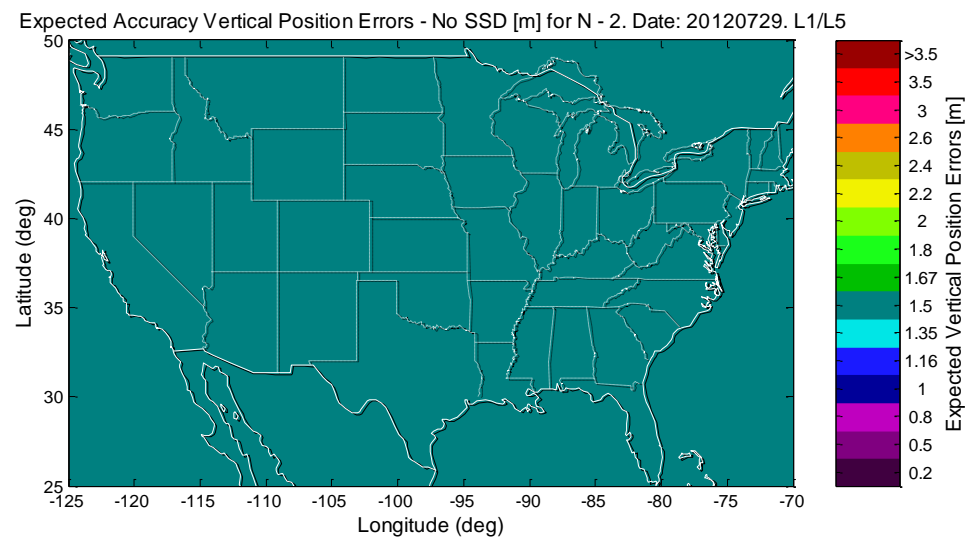
Figure 4-18: Nominal Accuracy (95% 2σ) for case of two unhealthy/inaccessible

satellites for Dual Frequency L1/L5 WAAS Users, in the Absence of Satellite Signal

Deformation

The average nominal accuracy over all locations is summarized in Table 4-3.

Satellite Status	Average Nominal Accuracy [m]	
	Frequency: L1-Only	Frequency: L1/L5
N - 0	0.99	1.21
N - 1	1.07	1.31
N - 2	1.16	1.43
N - 3	1.27	1.61
N - 4	1.39	1.82
N - 5	1.50	2.06

Table 4-3: Average Nominal Accuracy for Single L1- and Dual L1/L5 Frequency

WAAS Users, in the Absence of Satellite Signal Deformation

Figure 4-17, Figure 4-18, and Table 4-3 present possibly counter-intuitive results: nominal accuracy for dual-frequency WAAS users is actually slightly worse than for single frequency users.

The reason for this is that most of the time, the ionospheric conditions are nominal and ionospheric errors are small. However, in the dual-frequency system, the amplification of multipath range errors by the dual-frequency ionosphere-error-removal scale factor outweighs the benefits of ionosphere error removal, leading to increased position errors. As a result, while all cases easily meet the LPV-200 4 m requirement, the increased availability of dual-frequency WAAS positioning comes at the cost of slightly poorer nominal position accuracy.

4.4 Impact of Unmitigated Satellite Signal Deformation Range Biases on Expected 95% Vertical Position Errors

This section analyzes and presents the impact of unmitigated satellite signal deformation range biases on Expected 95% Vertical Position Errors in the presence of satellite signal deformation range biases, as defined in Section 4.2.1 Subsection 8 and Subsections 10-12.

The impact on single-frequency L1-only WAAS users is first discussed for two common reference receiver and user receiver configurations, followed by the impact on dual-frequency L1/L5 users for the same pairs of reference receiver-user receiver configurations. These results are summarized in tabular form for both single and dual frequency users, and for up to five unhealthy or inaccessible satellites.

4.4.1 Impact on Expected 95% Vertical Position Errors for Single-Frequency L1-only WAAS users

Figure 4-19 and Figure 4-20 show the impact of unmitigated satellite signal deformation range biases on expected 95% vertical position errors for single-frequency L1-only WAAS users, for the case when two satellites are unavailable. The **reference receiver**'s correlator spacing is **0.1 L1-chips** for both figures. Figure 4-19 shows the results for user receiver correlator spacing of **0.2 L1-chips** and Figure 4-20 shows the results for user receiver correlator spacing of **1.0 L1-chips**.

Expected Accuracy Vertical Position Errors - Incl. SSD(95%) [m] for N - 2. 0.2 chips. Date: 20120729. L1-only

Figure 4-19: Nominal Accuracy Including Expected 95% Vertical Position Errors

from Unmitigated Satellite Signal Deformation Range Biases [m] for Single

Frequency L1-only WAAS Users

(Two unhealthy/inaccessible satellites, Reference: 0.1 L1-chip correlator spacing;
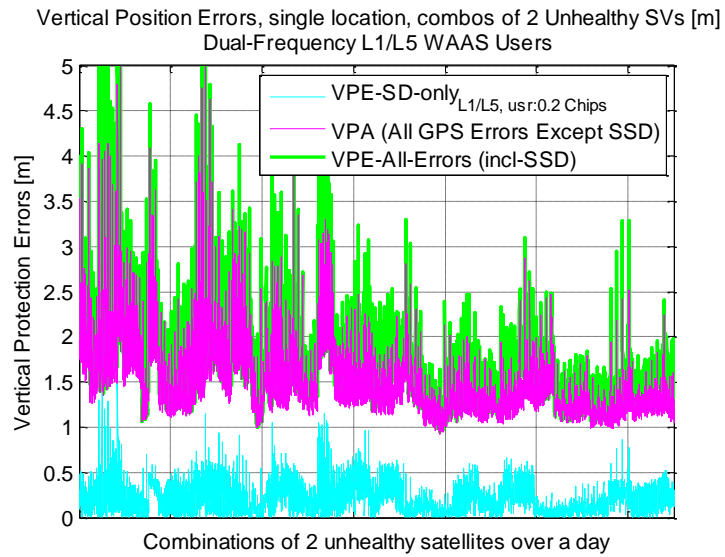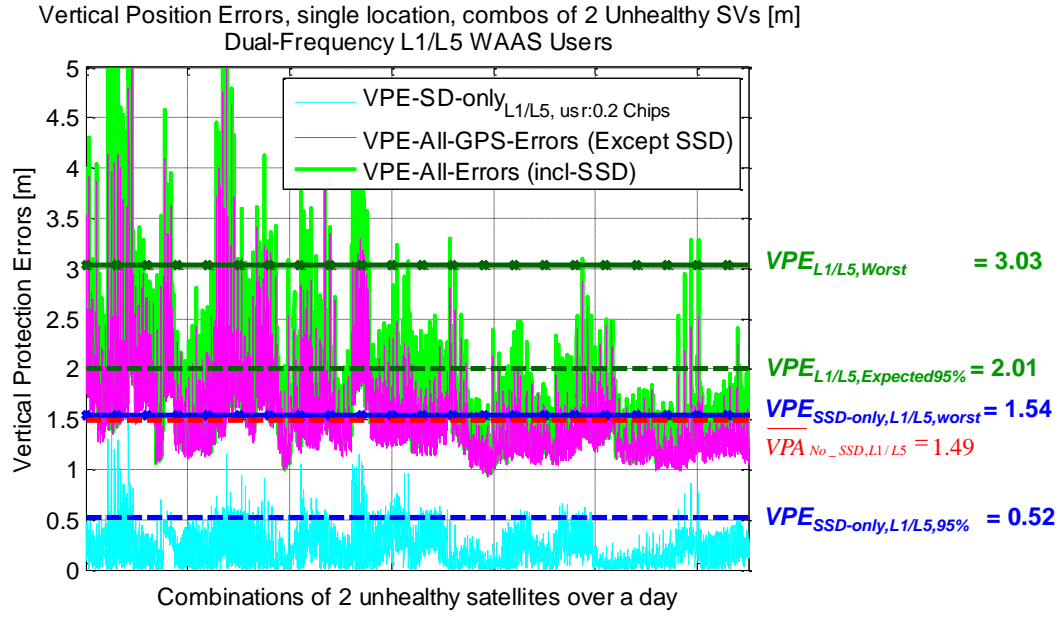
User: 0.2 L1-chip correlator spacing)

Figure 4-20: Nominal Accuracy Including Expected 95% Vertical Position Errors

from Unmitigated Satellite Signal Deformation Range Biases [m] for Single

Frequency L1-only WAAS Users

(Two unhealthy/inaccessible satellites, Reference: 0.1 L1-chip correlator spacing;

User: **1.0** L1-chip correlator spacing)

Figure 4-19 shows that single-frequency users with correlator spacings of **0.2** L1-chips will experience expected 95% vertical position errors over CONUS of between 1.35-1.5 m. These errors increase to 1.67 m over most of CONUS for single-frequency users with correlator spacings of **1.0** L1-chips, as seen in Figure 4-20.

These results will be further discussed in Section 4.4.2 together with the dual-frequency cases, for all unhealthy or inaccessible satellites from zero to five.

4.4.2   Impact on Expected 95% Vertical Position Errors for Dual-Frequency L1/L5 WAAS users

Figure 4-21 and Figure 4-22 show the impact of satellite signal deformation range biases on expected 95% vertical position errors for dual-frequency L1/L5 WAAS users, for the case when two satellites are unavailable. The **reference receiver**'s correlator spacing is **0.1 L1-chips** for both figures. Figure 4-21 shows the results for user receiver correlator spacing of **0.2 L1-chips** and Figure 4-22 shows the results for user receiver correlator spacing of **1.0 L1-chips.**

(Note: The equivalent L5-only biases, projected from L1-only biases, are for user correlator spacings of **0.6-1.4** L5-chips for the L5-frequency signal).

Expected Accuracy Vertical Position Errors - Incl. SSD(95%) [m] for N - 2. 0.2 chips. Date: 20120729. L1/L5

Figure 4-21: Nominal Accuracy Including Expected 95% Vertical Position Errors

from Unmitigated Satellite Signal Deformation Range Biases [m] for Dual Frequency

L1/L5 WAAS Users

(Two unhealthy/inaccessible satellites, Reference: 0.1 L1-chip correlator spacing;

User: **0.2** L1-chip correlator spacing)

Expected Accuracy Vertical Position Errors - Incl. SSD(95%) [m] for N - 2. 1.0 chips. Date: 20120729. L1/L5

Figure 4-22: Nominal Accuracy Including Expected Vertical Position Errors from

Unmitigated Satellite Signal Deformation Range Biases [m] for Dual Frequency

L1/L5 WAAS Users

(Two unhealthy/inaccessible satellites, Reference: 0.1 L1-chip correlator spacing;

User: **1.0** L1-chip correlator spacing)

Figure 4-21 shows that dual-frequency users with correlator spacings of **0.2** L1-chips will experience expected 95% vertical position errors over CONUS of around 2 m. These errors increase to between 2.4-2.6 m over CONUS for dual-frequency users with correlator spacings of **1.0** L1-chips, as seen in Figure 4-22. These errors are larger than the errors of 1.35-1.5 m and 1.67 m for the corresponding single-frequency configurations.

These results will be further discussed in the next section, together with the single-frequency cases, for all number of unhealthy or inaccessible satellites from zero to five.

4.4.3 Summary Table of Impact of Unmitigated Satellite Signal Deformation Range Biases on Expected 95% Vertical Position Errors for WAAS Users

Table 4-4 summarizes the impact of unmitigated satellite signal deformation range biases on the average expected 95% vertical position errors for single-frequency L1-only and dual-frequency L1/L5 WAAS users, for the cases of zero to five unhealthy satellites, averaged for user locations distributed over CONUS.

The reference results are listed in the first column, under the "0.1 L1-chips/ No SSD" heading. These are the average expected 95% vertical position errors due to all other GPS errors apart from satellite signal deformation range biases. These results are from user receivers identical to the reference receiver, with the same correlator spacing of 0.1 L1-chips. For these user receivers, the signal deformation would be almost entirely removed via differential corrections, leaving only the position errors from other GPS error sources.

The average expected 95% vertical position errors, including the effects of signal deformation, are shown in subsequent columns. These results are from user receivers with different correlator spacing configurations (user receiver correlator spacing of 0.2 L1-chips and 1.0 L1-chips) from the reference receivers. Such receivers experienced non-zero signal deformation, with increasing signal deformation effects as the user correlator spacing diverged from the reference correlator spacing of 0.1 L1-chips.

For each entry, the first row shows the average expected 95% vertical position errors in the presence of satellite signal deformation range biases. The second and third rows show the absolute and percentage increases in average expected 95% vertical position errors, as compared to the reference results in the absence of satellite signal deformation range biases.

Satellite Status	Nominal Accuracy Including Average **Expected 95% Vertical Position Errors** from Unmitigated Satellite Signal Deformation Range Biases [m]						
	Single Frequency: L1-Only				Dual Frequency: L1/L5		
	User Correlator Spacing [L1-chips]				User Correlator Spacing [L1-chips]		
	0.10	**0.20**	**1.00**		**0.10**	**0.20**	**1.00**
	No SSD*	Unmitigated SSD			No SSD*	Unmitigated SSD	
N – 0	0.99	1.15 (+0.16) (+16.2%)	1.29 (+0.30) (+30.3%)		1.21	1.59 (+0.38) (+31.4%)	1.98 (+0.77) (+63.6%)
N – 1	1.07	1.24 (+0.17) (+15.9%)	1.41 (+0.34) (+31.8%)		1.31	1.74 (+0.43) (+32.8%)	2.18 (+0.87) (+66.4%)
N – 2	1.16	1.36 (+0.20) (+17.2%)	1.55 (+0.39) (+33.6%)		1.43	1.93 (+0.50) (+35.0%)	2.43 (+1.00) (+69.9%)
N – 3	1.27	1.49 (+0.22) (+17.3%)	1.71 (+0.44) (+34.6%)		1.61	2.17 (+0.56) (+34.8%)	2.78 (+1.17) (+72.7%)
N – 4	1.39	1.63 (+0.24) (+17.3%)	1.87 (+0.48) (+34.5%)		1.82	2.48 (+0.66) (+36.3%)	3.20 (+1.38) (+75.8%)
N – 5	1.50	1.76 (+0.26) (+17.3%)	2.02 (+0.52) (+34.7%)		2.06	2.81 (+0.75) (+36.4%)	3.62 (+1.56) (+75.7%)

Table 4-4: Nominal Accuracy Including Average Expected 95% Vertical Position

Errors from Unmitigated Satellite Signal Deformation Range Biases [m] for Single

L1- and Dual L1/L5 Frequency WAAS Users

Notes on table:

1. *No SSD: The user receiver is identical to the reference receiver. Thus signal

   deformation is entirely removed via differential corrections.

2. Dual-frequency satellite signal deformation range biases projected from single-

   frequency L1-only satellite signal deformation range biases.

3. Figures in parentheses are absolute and percentage increases from the reference No Satellite Signal Deformation (No SSD) results.

Under conditions of two inaccessible or unhealthy satellites (highlighted in Table 4-4), for user receiver correlator spacing of 0.20 L1-chips, single-frequency L1-only WAAS users experience an additional 0.2 m error over the reference. The error increases to 0.39 m over the reference for user correlator spacing of 1.0 L1-chips. Dual-frequency L1/L5 WAAS users experience an additional 0.5 m error over the reference for user receiver correlator spacing of 0.20 L1-chips, and 1.0 m for user correlator spacing of 1.0 L1-chips. The dual-frequency L1/L5 vertical position errors are 2.4-3 times as large as the corresponding single-frequency L1-only vertical position errors, similar to the dual-frequency ionosphere-error-removal scale factor of 2.6.

For other numbers of inaccessible or unhealthy satellites, Table 4-4 shows that the absolute additional errors due to satellite signal deformation range biases (second row of entries) are 2.4 to 3 times as large for dual frequency WAAS as for single-frequency WAAS. This factor increases as fewer satellites are available. As a ratio of the reference results (third row of entries), additional errors due to satellite signal deformation range biases are as large as 1/6 for the single-frequency user with correlator spacing of 0.2 L1-chips, increasing to 1/3 for the dual-frequency user with the same correlator spacing. For users with correlator spacings of 1.0 L1-chips, these ratios approximately double to 1/3 and 3/4 for single-frequency and dual-frequency users, respectively. The ratios also increase as fewer satellites are available.

These errors as a result of satellite signal deformation range biases highlight that without effective mitigation, WAAS would not be able to meet the required performance specifications (Section 2.5).

4.5   Impact of Unmitigated Satellite Signal Deformation Range Biases on Worst Case Vertical Position Errors

The previous section examined the impact of unmitigated satellite signal deformation range biases on expected 95% vertical position errors over an entire day. This section analyzes the unmitigated impact of satellite signal deformation range biases on the worst case vertical position errors at each modeled user location over the same day, as defined in Section 4.2.1 Subsections 8 and Subsections 10-12. As in the previous section, the impact on single-frequency L1-only WAAS users is first discussed for two common reference receiver and user receiver configurations, followed by the impact on dual-frequency L1/L5 users for the same pairs of reference receiver-user receiver configurations. These results are summarized in tabular form for both single and dual frequency users, and for up to five unhealthy or inaccessible satellites.

4.5.1   Impact on Worst Case Vertical Position Errors for Single-Frequency L1-only WAAS Users

Figure 4-23 and Figure 4-24 show the impact of unmitigated satellite signal deformation range biases on worst case vertical position errors for single-frequency

L1-only WAAS users, when two satellites are unavailable. The **reference receiver**'s correlator spacing is **0.1 L1-chips** for both figures. Figure 4-23 shows the results for user receiver correlator spacing of **0.2 L1-chips** and Figure 4-24 shows the results for user receiver correlator spacing of **1.0 L1-chips**.
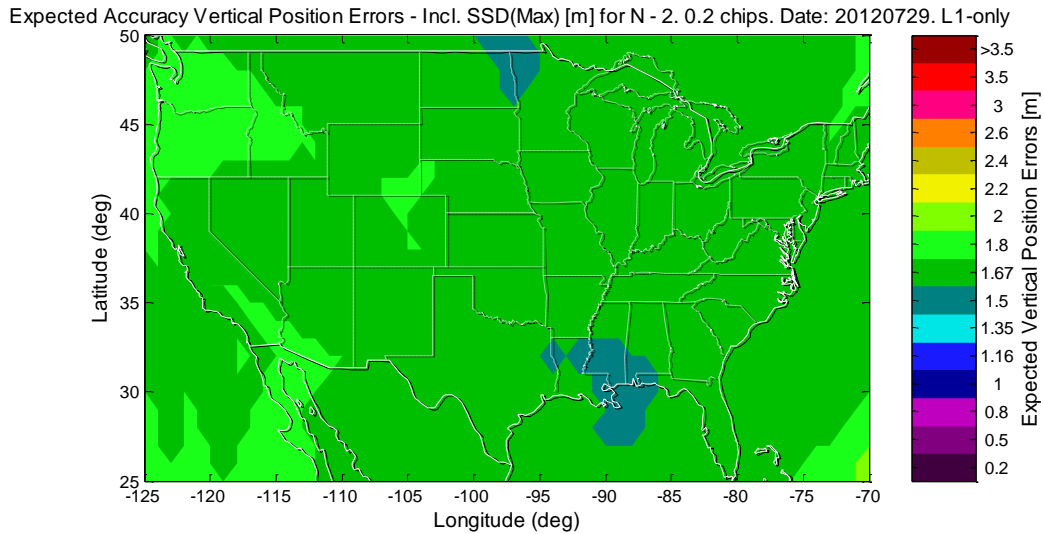
Figure 4-23: Nominal Accuracy Including Worst Case Vertical Position Errors from Unmitigated Satellite Signal Deformation Range Biases [m] for Single Frequency L1-only WAAS Users

(Two unhealthy/inaccessible satellites, Reference: 0.1 L1-chip correlator spacing;

User: **0.2** L1-chip correlator spacing)
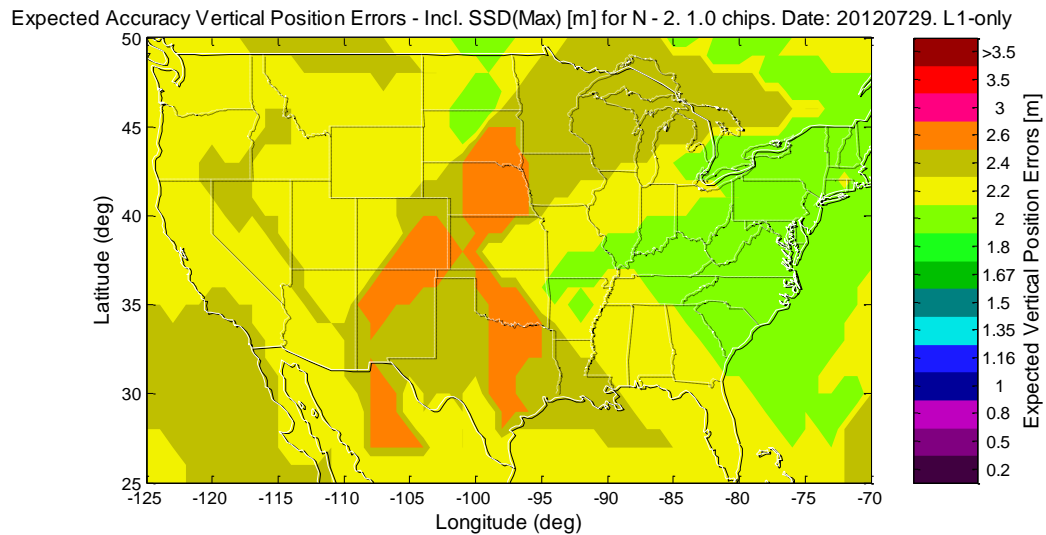
Figure 4-24: Nominal Accuracy Including Worst Case Vertical Position Errors from

Unmitigated Satellite Signal Deformation Range Biases [m] for Single Frequency L1-

only WAAS Users

(Two unhealthy/inaccessible satellites, Reference: 0.1 L1-chip correlator spacing;

User: **1.0** L1-chip correlator spacing)

Figure 4-23 shows that single-frequency users with correlator spacings of **0.2** L1-chips will experience an error of 1.67 m over most CONUS. For single-frequency users with correlator spacings of **1.0** L1-chips, the error rises to 2.2 m over most of CONUS, with errors as large as 2.6 m in some parts of CONUS (Figure 4-24).

These results will be further discussed in Section 4.5.2 together with the dual-frequency cases, for all unhealthy or inaccessible satellites from zero to five.

4.5.2   Impact on Worst Case Vertical Position Errors for Dual-Frequency L1/L5 WAAS Users

Figure 4-25 and Figure 4-26 show the impact of unmitigated satellite signal deformation range biases on worst case vertical position errors for dual-frequency L1/L5 WAAS users, for the case when two satellites are unavailable. The **<u>reference receiver</u>**'s correlator spacing is **<u>0.1 L1-chips</u>** for both figures. Figure 4-25 shows the results for user receiver correlator spacing of **<u>0.2 L1-chips</u>** and Figure 4-26 shows the results for user receiver correlator spacing of **<u>1.0 L1-chips</u>**.
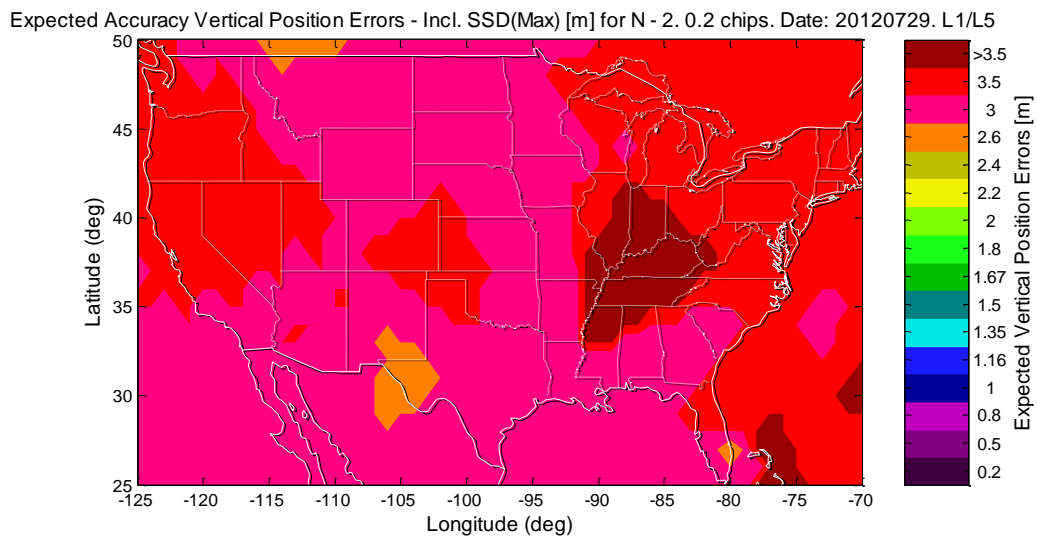
Figure 4-25: Nominal Accuracy Including Worst Case Vertical Position Errors from Unmitigated Satellite Signal Deformation Range Biases [m] for Dual Frequency L1/L5 WAAS Users

(Two unhealthy/inaccessible satellites, Reference: 0.1 L1-chip correlator spacing;

User: **<u>0.2</u>** L1-chip correlator spacing)
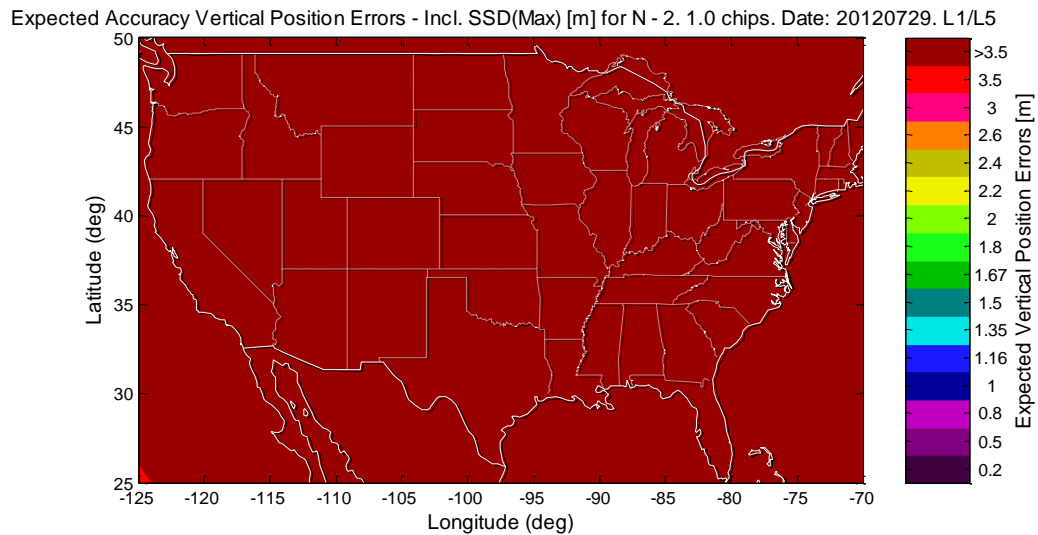
Figure 4-26: Nominal Accuracy Including Worst Case Vertical Position Errors from

Unmitigated Satellite Signal Deformation Range Biases [m] for Dual Frequency

L1/L5 WAAS Users

(Two unhealthy/inaccessible satellites, Reference: 0.1 L1-chip correlator spacing;

User: **1.0** L1-chip correlator spacing)

Figure 4-25 shows that dual-frequency users with correlator spacings of **0.2** L1-chips will experience worst case errors over most of CONUS of around 3.0 m, rising to 3.5 m or more in some parts of CONUS. For dual-frequency users with correlator spacings of **1.0** L1-chips, the worst case errors are larger than 3.5 m over all of CONUS, as seen in Figure 4-26.

These results will be further discussed in the next section together with the single-frequency cases, for all unhealthy or inaccessible satellites from zero to five.

4.5.3   Summary of Impact of Unmitigated Satellite Signal Deformation Range Biases on Worst Case Vertical Position Errors for WAAS Users

Table 4-5 summarizes the impact of unmitigated satellite signal deformation range biases on the worst case vertical position errors over 24 hours, for single-frequency L1-only and dual-frequency L1/L5 WAAS users, for the cases of zero to five unhealthy or inaccessible satellites, averaged for user locations distributed over CONUS.

Similar to Table 4-4 in Section 4.4.3, the reference results are listed in the first column, under the "0.1 L1-chips/ No SSD" heading. These are the worst case vertical position errors over 24 hours due to all other GPS errors apart from satellite signal deformation range biases. These results are from user receivers identical to the reference receiver, with the same correlator spacing of 0.1 L1-chips. For these user receivers, the signal deformation would be almost entirely removed via differential corrections, leaving only the position errors from other GPS error sources.

The worst case vertical position errors, including the effects of signal deformation, are shown in subsequent columns. These results are from user receivers with different correlator spacing configurations (user receiver correlator spacing of 0.2 L1-chips and 1.0 L1-chips) from the reference receivers. Such receivers experienced non-zero signal deformation, with increasing signal deformation effects as the user correlator spacing diverged from the reference correlator spacing of 0.1 L1-chips.

For each entry, the first row shows the worst case vertical position errors in the presence of satellite signal deformation range biases. The second and third rows show the absolute and percentage increases in worst case vertical position errors, as compared to the reference results in the absence of satellite signal deformation range biases.

Satellite Status	Nominal Accuracy Including **Worst Case** Vertical Position Errors from Unmitigated Satellite Signal Deformation Range Biases [m]						
	Single Frequency: L1-Only				Dual Frequency: L1/L5		
	User Correlator Spacing [L1-chips]				User Correlator Spacing [L1-chips]		
	0.10	**0.20**	**1.00**		**0.10**	**0.20**	**1.00**
	No SSD*	Unmitigated SSD			No SSD*	Unmitigated SSD	
N – 0	0.99	1.20 (+0.21) (+21.2%)	1.41 (+0.42) (+42.4%)		1.21	1.74 (+0.53) (+43.8%)	2.25 (+1.04) (+86.0%)
N – 1	1.07	1.39 (+0.32) (+29.9%)	1.78 (+0.71) (+66.4%)		1.31	2.24 (+0.93) (+71.0%)	3.25 (+1.94) (+148.1%)
N – 2	1.16	1.62 (+0.46) (+39.7%)	2.18 (+1.02) (+87.9%)		1.43	3.04 (+1.61) (+112.6%)	5.06 (+3.63) (+253.8%)
N – 3	1.27	1.81 (+0.54) (+42.5%)	2.43 (+1.16) (+91.3%)		1.61	3.8 (+2.19) (+136.0%)	5.86 (+4.25) (+264.0%)
N – 4	1.39	1.96 (+0.57) (+41.0%)	2.59 (+1.20) (+86.3%)		1.82	4.22 (+2.40) (+131.9%)	6.40 (+4.58) (+251.6%)
N – 5	1.50	2.10 (+0.60) (+40.0%)	2.72 (+1.22) (+81.3%)		2.06	4.48 (+2.42) (+117.5%)	6.77 (+4.71) (+228.6%)

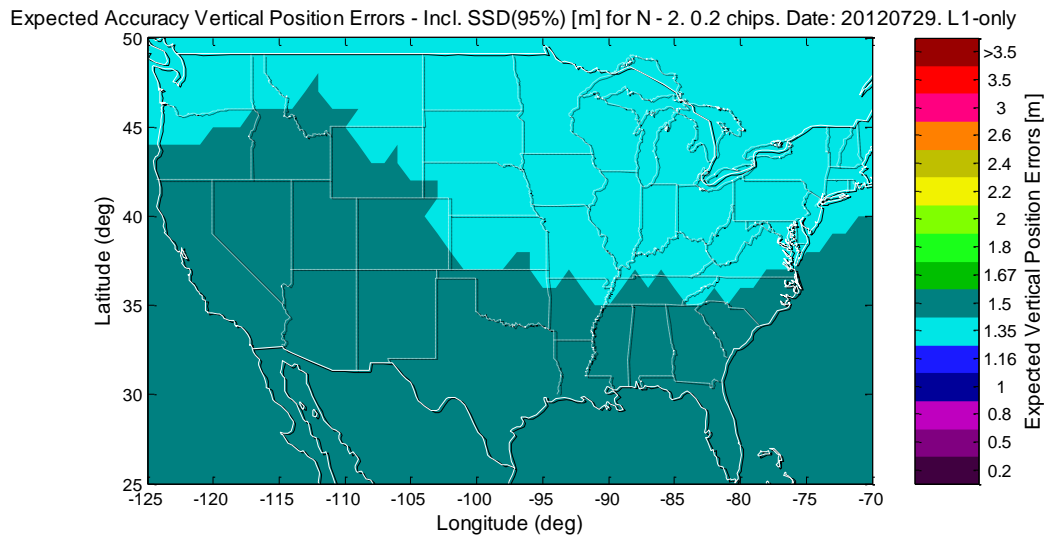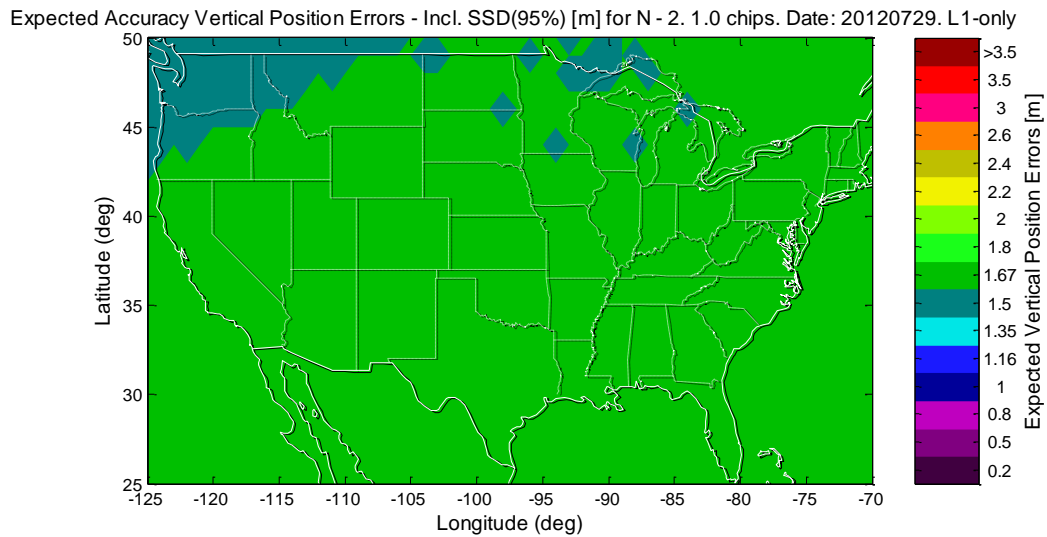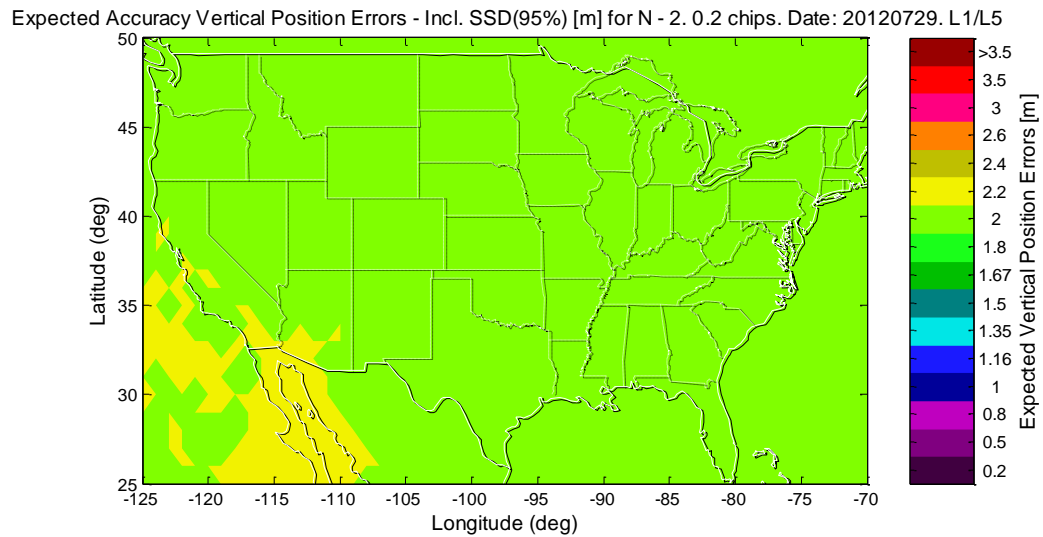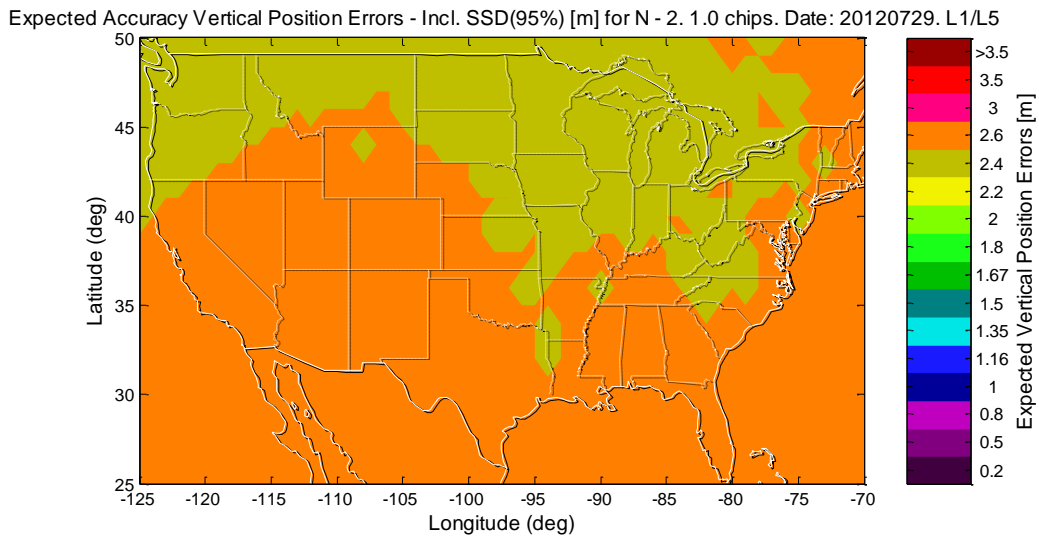Table 4-5: Nominal Accuracy Including Worst Case Vertical Position Errors from Unmitigated Satellite Signal Deformation Range Biases [m] for Single L1- and Dual L1/L5 Frequency WAAS Users

Notes on Table 4-5:

1. *No SSD: The user receiver is identical to the reference receiver. Thus signal deformation is entirely removed via differential corrections.

2. Dual-frequency satellite signal deformation range biases projected from single-frequency L1-only satellite signal deformation range biases.

3. Figures in parentheses are absolute and percentage increases from the reference No Satellite Signal Deformation (No SSD) results.

Under conditions of two inaccessible or unhealthy satellites (highlighted in Table 4-5), for user receiver correlator spacing of 0.20 L1-chips, single-frequency L1-only WAAS users experience an additional **0.5 m** error over the reference, due to unmitigated satellite signal deformation range biases. The error increases to **1.0 m** over the reference for user correlator spacing of 1.0 L1-chips. Dual-frequency L1/L5 WAAS users experience an additional **1.6 m** error over the reference for user receiver correlator spacing of 0.20 L1-chips, and **3.6 m** for user correlator spacing of 1.0 L1-chips. These dual-frequency errors are approximately a factor of 3.6 times larger than the corresponding single-frequency worst case vertical position errors of 0.5 m and 1.0 m, respectively, significantly larger than the dual-frequency ionosphere-error-removal scale factor of 2.6. The errors increase as fewer satellites are available.

For other numbers of inaccessible or unhealthy satellites, Table 4-5 shows that the absolute additional errors for dual-frequency WAAS due to satellite signal deformation range biases (second row of entries) are 2.5 to 4 times that of single-

frequency WAAS. This factor increases as fewer satellites are healthy and accessible.

Unlike the 95% vertical position errors, this factor is significantly larger than the dual-frequency ionosphere-error-removal scale factor of 2.6. This is because at certain times during the day, poor geometries combined with the satellite signal deformation range biases result in large worst case position errors. These poor geometries are admissible under dual-frequency WAAS but are not admissible for single-frequency WAAS [51]. These poor geometry conditions do not happen often throughout the day and thus have a limited impact on the 95% vertical position errors. However, these worst case conditions do occur with certainty and highlight the need for mitigation.

As a ratio of the reference results (third row of entries), the worst case errors due to satellite signal deformation range biases are as large as 40% for single-frequency user receivers with correlator spacing of 0.2 L1-chips, and as large as 90% for single-frequency user receivers with correlator spacing of 1.0 L1-chips. For dual-frequency users, the ratios more than double, to 140% and 260%, for user receivers with correlator spacings of 0.2 L1-chips and 1.0 L1-chips, respectively. As with the absolute errors, the ratios increase as fewer satellites are available. Both the absolute errors and ratios highlight that without effective mitigation, WAAS would not be able to meet the required performance specifications (Section 2.5).

4.6   Summary of Unmitigated Impact of Satellite Signal Deformation Range Biases on WAAS Users

In this chapter, MAAST was used to analyze the impact of unmitigated satellite signal deformation range biases on the availability, accuracy, and worst-case position errors for single-frequency and dual-frequency WAAS-augmented GPS aviation users. The analysis was carried out for all cases when zero to five satellites were unavailable.

In the absence of satellite signal deformation range biases, dual-frequency WAAS users experience greater availability, at the cost of slightly worse accuracy, than single-frequency WAAS users. The benefits and costs are more pronounced as fewer satellites are healthy and accessible.

In the presence of unmitigated satellite signal deformation range biases, the expected 95% vertical position errors increase by 0.16-0.5 m for single-frequency users. For dual-frequency users, these errors increase by 0.38-1.56 m. These errors constitute between 16.2%-34.7% of the other errors for single-frequency WAAS users, and between 31.4%-75.8% of the other errors for dual-frequency WAAS users.

Unmitigated satellite signal deformation range biases have an even greater impact on worst case WAAS vertical position errors. The worst case vertical position errors increase by 0.20-1.22 m for single-frequency users, and 0.53-4.71 m for dual-frequency users. These errors are between 21.2%-81% of the other errors for single-

frequency WAAS users, and between 43.8%-228.6% of the other errors for dual-frequency WAAS users.

The impact of unmitigated satellite signal deformation range biases on vertical position errors is fairly representative of that experienced by the general WAAS user. The effects of different bandwidths and different filter implementations are beyond the scope of the analysis in this chapter (they are discussed in Section 6.3 under Future Research). If included, these factors may increase the satellite signal deformation range biases leading to greater vertical position errors. The need for effective mitigation is clearly evident and is the subject of the following chapter.

Chapter 5

Mitigation of Satellite Signal Deformation Biases

5.1 Overview

The adverse impact of satellite signal deformation range biases on vertical position errors for WAAS users highlights the need for effective mitigation. Mitigation strategies are required to account for the wide variation in the antennas and filters used in user receivers and the inaccessibility of user receivers once installed on the aircraft. Fortunately, an effective, practical mitigation method is available which is able to substantially reduce the negative effect of these biases while meeting user requirements.

Section 5.2 discusses the various mitigation approaches and their relative benefits and disadvantages with regard to aviation user requirements. One particular mitigation method is both effective and practical – narrowing the user receiver correlator space. Analysis of this method and verification results are presented in Section 5.3.

5.2   Aviation Requirements and Bias Mitigation Methods

Aviation applications place unique requirements on receivers. The receivers are designed and qualified as part of an overall navigation system. Once installed, tested, and qualified, the receivers are not intended for easy accessibility, change, and re-configuration, unlike many modern consumer devices. Often, installed aviation GPS receivers remain untouched for years or possibly even decades. These long equipment lifetimes strongly constrain the choice of a preferred mitigation method for satellite signal deformation range biases.

There are three methods for mitigating the impact of satellite signal deformation range biases on user vertical position errors. These are the "Measure and Correct," "Bound and Exclude," and "Restrict User Space" methods. All of these methods require careful measurement of satellite signal deformation range biases. However, they differ in the fidelity and accuracy required of the measurement method, as well as in the ways these biases are reduced, corrected, or otherwise protected against.

In the following sections, these different mitigation methods are discussed. Section 5.2.1 discusses the "Measure and Correct" method – the measurement and correction of satellite signal deformation biases for individual user receivers. Section 5.2.2 presents the "Bound and Exclude" method – the use of Modified Vertical Protection Level Equations on bounded satellite signal deformation range biases. Section 5.2.3 presents the preferred "Restrict User Space" method – the specification of tighter bounds on the allowed user receiver correlator spacing.

5.2.1   "Measure-and-Correct" Method

For this strategy, the current allowed user receiver correlator spacings would remain unchanged. To mitigate the problem of large satellite signal deformation range biases (Chapter 2), these user GPS receiver biases are accurately measured, stored in the avionics system and then applied appropriately as corrections to user receivers. Table 5-1 shows a possible look-up-and-correction table stored in the user avionics. (The measured biases from Chapter 2 were used as a reference).

User Receiver		User Correlator Spacing (L1-chips)	Satellite Signal Deformation Range Biases [m]				
			Satellite ID				
Make	Model		1	2	…	31	32
USRP	N210	0.2	-0.07	0.01		-0.12	-0.02
USRP	N210	1.0	-0.08	-0.08		-0.24	0.04

Table 5-1: Example of Bias Correction Table Stored in Avionics Systems

(Reference Receiver: USRP N210. Correlator Spacing: 0.1 L1-Chips.

(Based on results from Section 3.7)

There are disadvantages with this approach. Accurate measurements are important – the application of erroneous bias corrections could exacerbate the resultant position errors. For such required accuracy, specialized measurement equipment and setup is necessitated.

Under regular manufacturing tolerances, there would be component-to-component variations between user receivers, possibly leading to different bias characteristics. Thermal variations over the short-term, and aging over the long-term, could possibly lead to further bias variations in receivers. In addition, repairs and replacements of user or reference receivers, additional signals due to new GPS satellite launches, or signal changes due to faulty on-board satellite hardware, could all result in changes in bias characteristics.

These bias variations require regular and frequent measurements of user receiver biases and updates of the bias tables within avionics systems, which are challenging tasks since GPS receivers and avionics systems are not designed for regular access and update upon installation. For this reason, this strategy is considered infeasible for GPS avionics.

5.2.2 "Bound-and-Exclude" Method

To avoid the frequent and regular bias measurements, corrections, and avionics updates of the previous technique, this next scheme specifies reasonable bounds on the maximum allowed biases in user receivers. These bounds would take into account variations such as filter differences, component-to-component disparities, and changes induced by thermal and aging effects, as well as system level requirements for maximum allowed vertical position error from satellite signal deformation range biases.

This scheme was previously analyzed in [51] and a brief summary is provided here. With a slight modification to Section 4.2.1, Subsection 10, Equation (4.17), a suitable bound can be obtained for exclusion and protection of large resultant vertical position errors from satellite signal deformation range biases:

$$
VPE_{SSD} = \sum_{i=1}^{N} S_{3,i} b_{SSD,i} \tag{4.17}
$$

$$
\leq \left| \sum_{i=1}^{N} S_{3,i} b_{SSD,i} \right|
$$

$$
\leq \sum_{i=1}^{N} \left| S_{3,i} b_{SSD,i} \right|
$$

$$
\leq \sum_{i=1}^{N} \left| S_{3,i} \right| \left\| b_{SSD,i} \right|
$$

$$
\leq \max_{i} \left(\left| b_{SSD,i} \right| \right) \times \sum_{i=1}^{N} \left| S_{3,i} \right|
$$

$$\leq b_{SSD,BOUND} \times \sum_{i=1}^{N} \left| S_{3,i} \right| \tag{5.1}$$

$$= VPE_{SSD,BOUND} \tag{5.2}$$

Where:

VPE_{SSD} : Vertical Position Error due to satellite signal deformation only

$S_{3,i}$: Elements of third row of the projection matrix S [Refer to Section 4.2.1, Subsection 6, Equation (4.8)]

$b_{SSD,i}$: Satellite signal deformation range biases corresponding to visible satellites (Refer to Sections 3.7.3 and 3.7.4)

N : Total number of satellites visible at user

$b_{SSD,BOUND}$: Bound on satellite signal deformation range biases

$VPE_{SSD,BOUND}$: Bound on Vertical Position Error from satellite signal deformation range biases

Reasonable quantities for $b_{SSD,BOUND}$ and $VPE_{SSD,BOUND}$ are chosen to fulfill system level requirements for maximum allowed vertical position error from satellite signal deformation range biases:

$$VPE_{SSD,BOUND} = b_{SSD,BOUND} \times \sum_{i=1}^{N} \left| S_{3,i} \right| \leq VPE_{SSD,MAX} \tag{5.3}$$

Where:

$VPE_{SSD,MAX}$　　:　Maximum allowed vertical position error from satellite signal

deformation range biases only

One straightforward choice for $b_{SSD,BOUND}$ is $\max_i \left(\left| b_{SSD,i} \right| \right)$, the maximum magnitude of

satellite signal deformation range biases across all satellites. At any time, if the

computed bound, $VPE_{SSD,BOUND}$, exceeds the specified requirement for maximum

vertical position errors, the system is declared unavailable. This would be a simple

way to protect against large position errors from satellite signal deformation range

biases.

The main disadvantage of this method is the reduction of availability. With two

unhealthy or inaccessible satellites, the dual-frequency availability over many parts of

CONUS is already 99.88%, slightly lower than the specified requirement of 99.9%

(Refer to Section 4.3.1, Table 4-2: Average Availability for Single Frequency L1-only

and Dual Frequency L1/L5 WAAS Users). Imposing an additional restriction using

Equation (5.3), to achieve smaller position errors, would only further reduce

availability.

More complicated "Bound-and-Exclude" algorithms are possible to achieve tighter

bounds and thus achieve better availability performance, at the cost of more

complexity in measurement and implementation. However, short of accurately

measuring and regularly updating all the satellite biases, it is difficult to completely

avoid any availability penalty. For this reason, this method is not preferred.

5.2.3 "Restrict User Space" Method for User Receiver Correlator Spacings

To reduce the current large spread of satellite signal deformation range biases and

resultant position errors, this proposed method restricts the allowed set of user receiver

correlator spacings, to more closely match the correlator spacing of the WAAS

reference receiver.

For the L1-frequency, the WAAS reference receiver's correlator spacing is 0.1 L1-

chips. The new permitted set of user receiver correlator spacings is between 0.08 and

0.12 L1-chips; other previously permitted user receiver correlator spacings such as 0.2

L1-chips or 1.0 L1-chips would now be excluded. This is illustrated in Figure 5-1.
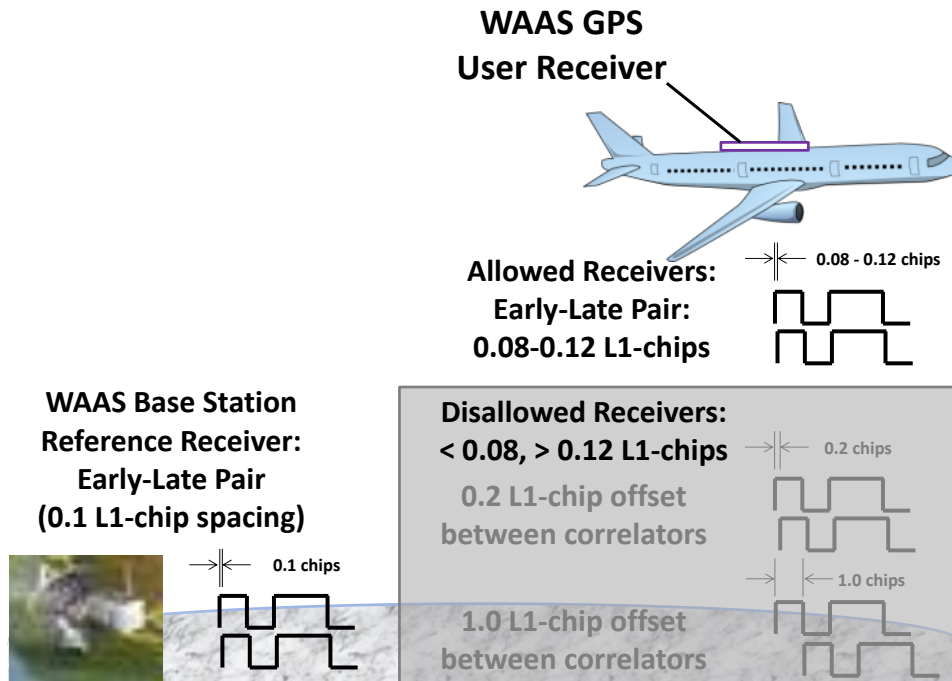
Figure 5-1: Tighter range of Permitted User Receiver Correlator Spacings for L1-

frequency signal

Similarly, for L5-frequency satellite signals, tighter restrictions are also specified on

the permitted user receiver correlator spacings, to more closely match the correlator

spacing of the reference receiver of 1.0 L5-chips. The allowed L5-frequency user

receiver correlator spacings are now a much smaller set: 0.8-1.2 L5-chips. Other

previously permitted user receiver correlator spacings such as 0.6 L5-chips or 1.4 L5-

chips are now excluded. This is illustrated in Figure 5-2.
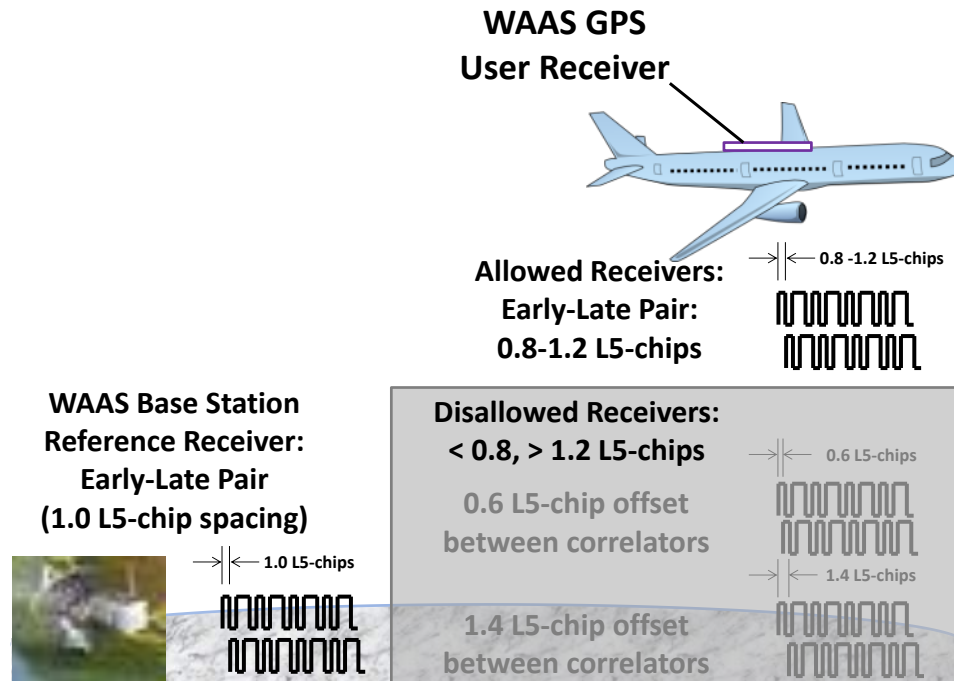
Figure 5-2: Tighter range of allowed User Receiver Correlator Spacings for L5-

frequency signal

Note that the requirement on the L5-frequency biases can be less stringent than on the

L1-frequency biases. This is because L5-frequency biases have approximately half the

impact of L1-frequency biases due to a smaller multiplicative factor (1.26 instead of

2.26) in the dual-frequency linear combination.

Besides being effective in reducing satellite signal deformation biases, as will be

shown in subsequent sections, implementation of this method is straightforward and

practical.

The correlator spacings between reference and user receivers are more closely matched. As a consequence, any changes to the biases at the user receivers from filter effects, component-to-component variations, thermal effects, and aging will be small.

For this process, long term maintenance is simple. Careful measurements with specialized equipment are required for new receivers and whenever there are new satellite signals, to verify that the satellite signal deformation biases are not anomalous but remain within the current range.

Besides this straightforward requirement, there is no further need for previously onerous requirements such as regular measurements, access to avionics systems, and updates of bias correction tables. The availability penalties of "Bound-and-Exclude" strategies can also be avoided. For these reasons, this method is preferred over the two methods presented earlier.

Tightening the bounds on the allowed user receiver correlator spacing significantly reduced the satellite signal deformation range biases. This was explored by re-measuring the single-frequency L1-only and single-frequency L5-only bias measurements using the narrower allowed span of correlator spacings. The subsequent sections will discuss the results for single frequency L1-only signals, single frequency L5-only signals, and dual frequency L1/L5 signals.

5.2.3.1 "Restrict User Space" Method – Effectiveness for Single Frequency L1-Only Signal

For single-frequency L1-only signals, measurements of mitigated satellite signal deformation range biases had maximum magnitudes at the boundaries of the allowed span: user receiver correlator spacings (either **0.08** L1-chips or **0.12** L1-chips) for the L1-frequency signal. At these boundary points, the mitigated satellite signal deformation range biases for L1-frequency were up to an order of magnitude smaller than the unmitigated biases. The results are summarized in Figure 5-3 and in Table 5-2.
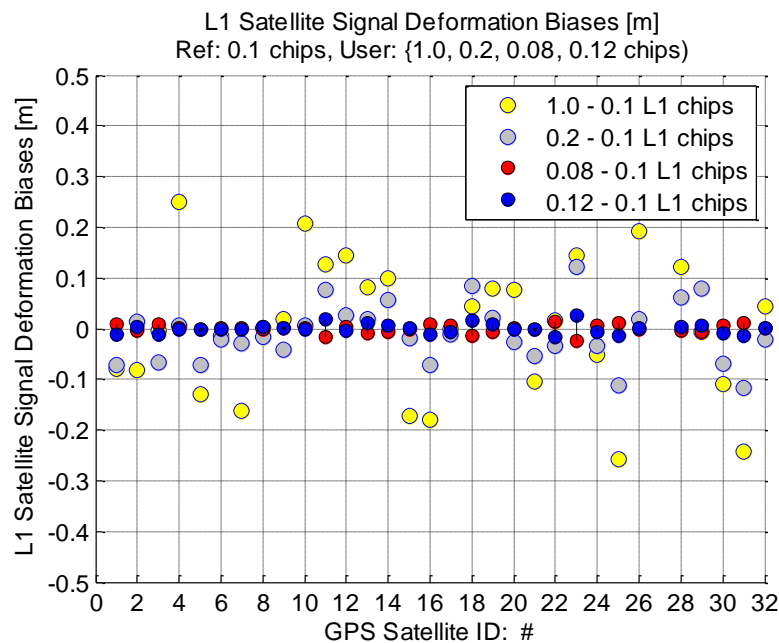
Figure 5-3: Measured Mitigated Satellite Signal Deformation Range Biases for **L1-frequency**

Signal Frequency	Correlator Spacing (L1-chips)		Measured Satellite Signal Deformation Range Biases [m]		
	Reference Receiver	User Receiver	Min	Max	Average magnitude
L1	0.1	1.0	-0.26	0.25	0.11
L1	0.1	0.2	-0.11	0.12	0.05
L1	0.1	0.08-0.12	-0.02	0.03	0.01

Table 5-2: Summary of Mitigated Satellite Signal Deformation Biases for L1-

frequency

As the results in Figure 5-3 and Table 5-2 show, the "Restrict User Space" method is effective in reducing the maximum, minimum, and average magnitudes of single-frequency L1-only satellite signal deformation range biases.

5.2.3.2   "Restrict User Space" Method – Effectiveness for Single Frequency L5-Only Signal (3 Current Satellites)

Figure 5-4 and Table 5-3 show the unmitigated and mitigated L5-frequency satellite signal deformation range biases for the three satellites currently transmitting signals in L5-frequencies. As with the L1-frequency biases, it was found that the measured mitigated L5-frequency satellite signal deformation range biases had maximum magnitudes at the boundaries of the allowed span: user receiver correlator spacings at either **0.8** L5-chips or **1.2** L5-chips. As can be seen, the mitigated L5-frequency satellite signal deformation range biases are smaller than the unmitigated L5-

frequency biases, but the reduction factor is comparatively not as large as in the L1-

frequency case.
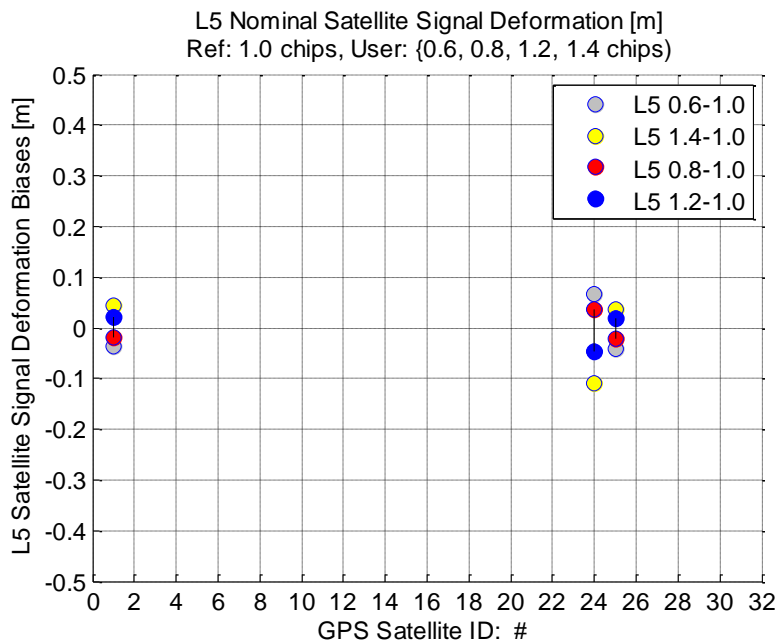
Figure 5-4: Measured Mitigated Satellite Signal Deformation Range Biases for **L5-**

frequency

(Based on three currently available dual-frequency satellites)

Signal Frequency	Correlator Spacing (L5-chips)		Measured Satellite Signal Deformation Range Biases [m]		
	Reference Receiver	User Receiver	Min	Max	Average magnitude
L5	1.0	0.6-1.4	-0.11	0.07	0.07
L5	1.0	0.8-1.2	-0.05	0.04	0.03

Table 5-3: Summary of Measured Mitigated Satellite Signal Deformation Biases for

L5-frequency

(Based on three currently available dual-frequency satellites)

As the results in Figure 5-4 and Table 5-3 show, the "Restrict User Space" method is effective in reducing the maximum, minimum, and average magnitudes of single-frequency L5-only satellite signal deformation range biases, for the three satellites currently transmitting L5-frequency signals.

5.2.3.3   **"Restrict User Space" Method – Effectiveness for Dual Frequency L1/L5 Signals (3 Current Satellites)**

To find the worst case dual-frequency combination of mitigated biases, the equation for dual-frequency linear combination to remove ionosphere errors [Equation (2.29)] is applied to the three satellite signals in both the L1- and L5-frequencies. These dual-frequency biases are computed for two mitigated configurations. First, for the L1-frequency signal, a reference receiver correlator spacing of 0.1 L1 chips and user receiver correlator spacings of 0.08 and 0.12 L1-chips are used. Second, for the L5-frequency signal, a reference receiver correlator spacing of 1.0 L5 chips and user receiver correlator spacings of 0.8 and 1.2 L5-chips are used. (As mentioned previously, the maximum bias magnitudes would occur at these boundaries of allowed user receiver correlator spacings.) The unmitigated and mitigated single-frequency biases before dual-frequency combination are shown in Table 5-4.

GPS Satellite ID PRN#	L1-Frequency Biases (m)				L5-Frequency Biases (m)			
	User correlator spacing (L1 Chips)				*User correlator spacing (L5 Chips)*			
	Unmitigated		Mitigated		Unmitigated		Mitigated	
	0.2	1.0	0.08	0.12	0.6	1.4	0.8	1.2
1	-0.07	-0.08	0.01	-0.01	-0.04	0.04	-0.02	0.02
24	-0.03	-0.05	0.01	-0.01	0.07	-0.11	0.04	-0.05
25	-0.11	-0.26	0.01	-0.01	-0.04	0.04	-0.02	0.02
Others (min)	-0.12	-0.24	-0.02	-0.02	-	-	-	-
Others (max)	0.12	0.25	-0.01	0.03	-	-	-	-

Table 5-4: Unmitigated and Mitigated Single-Frequency Satellite Signal Deformation

Biases for Satellites with Signals at both L1 and L5 Frequencies

(Reference Receiver Correlator Spacings: 0.1 L1-Chips, 1.0 L5-Chips)

Table 5-5 shows the resultant mitigated dual-frequency L1/L5 satellite signal deformation range biases. GPS Satellite ID PRN# 24 exhibits the worst case dual-frequency biases. As seen, these worst case bias magnitudes do not exceed **0.07m**.

(Recall that the largest unmitigated dual-frequency bias was **-0.3 m** for GPS Satellite ID PRN #25 for user correlator spacing of 0.2 L1-Chips and 1.4 L5-Chips. For user correlator spacing of 1.0 L1-Chips and 1.4 L5-Chips, the largest unmitigated bias was **-0.63 m**, also for GPS Satellite ID PRN # 25).

GPS Satellite ID	L1-Frequency		L5-Frequency		Dual-Frequency L1/L5 Bias: $2.26*Bias_{L1} - 1.26*Bias_{L5}$
	User correlator spacing:	Single-Frequency Bias	User correlator spacing:	Single-Frequency Bias	
1	0.08	0.01	0.8	-0.02	0.04
24	0.08	0.01	0.8	0.04	-0.03
25	0.08	0.01	0.8	-0.02	0.05
1	0.08	0.01	1.2	0.02	-0.01
24	0.08	0.01	1.2	-0.05	0.07
25	0.08	0.01	1.2	0.02	0.00
1	0.12	-0.01	0.8	-0.02	0.00
24	0.12	-0.01	0.8	0.04	-0.06
25	0.12	-0.01	0.8	-0.02	0.00
1	0.12	-0.01	1.2	0.02	-0.05
24	0.12	-0.01	1.2	-0.05	0.05
25	0.12	-0.01	1.2	0.02	-0.05

Table 5-5: Mitigated Satellite Signal Deformation Biases – Dual Frequency

Combination

As the results in Table 5-4 and Table 5-5 show, the "Restrict User Space" method is effective in reducing the maximum, minimum, and average magnitudes of dual-frequency L1/L5 satellite signal deformation range biases, for the three satellites currently transmitting L5-frequency signals.

5.2.3.4 Projection of Dual-Frequency Biases for all Satellites from L1-only Biases

As in the unmitigated case, there are only three satellites which currently broadcast dual-frequency signals. Consequently, the mitigated dual-frequency biases for all satellites are projected from their mitigated L1-only biases by multiplying by the dual-frequency ionosphere-error-removal scale factor.

This projection is reasonable: after scaling, the minimum and maximum projected biases are comparable to the minimum and maximum dual-frequency biases for the three current dual-frequency satellites. This projection would need to be verified as more dual-frequency satellites are launched in the future.

5.3 Mitigated Impact of Satellite Signal Deformation Range Biases on Aviation Users

This section analyzes the mitigated impact of satellite signal deformation range biases on the availability, accuracy, and worst-case position errors for WAAS-augmented GPS aviation users. Similar to the analysis in the previous chapter, this analysis:

- includes both single frequency L1-only users and dual-frequency L1/L5 users;

- is performed for different cases where the set of active GPS satellites is not always complete, from the full constellation up to five unhealthy or inaccessible satellites (all possible combinatorial cases); and,

- uses the validated Stanford-developed Matlab Algorithm Availability Simulation Tool (MAAST).

Section 5.3.1 introduces the change to the MAAST configuration to account for the **__mitigated__** satellite signal deformation range biases. Section 5.3.2.1 shows the impact of **__mitigated__** satellite signal deformation range biases on expected 95% vertical position errors for both single-frequency L1-only and dual-frequency L1/L5 WAAS users. Section 5.3.2.2 shows the impact of these same mitigated biases on worst case vertical position errors for single-frequency and dual-frequency WAAS users. Section 5.3.2.3 gives a summary and comparison of the unmitigated and mitigated impact on the various different WAAS users.

5.3.1   MAAST Configuration for Impact Analysis of Mitigated Satellite Signal Deformation Range Biases

As in the previous chapter, MAAST was used for the impact analysis of mitigated satellite signal deformation range biases on vertical position errors. The MAAST configuration is identical to the process listed previously (Section 4.2.1) with one important difference. The vertical position errors are now computed from the mitigated satellite signal deformation biases for user receiver correlator spacings of **__0.08__** L1-chips and **__0.12__** L1-chips. These are the extreme points of the allowed span of mitigated correlator spacings where the biases are maximum in magnitude. (Previously the vertical position error in Section 4.2.1, Subsection 10, Equation (4.17)

was computed from unmitigated satellite signal deformation biases at user receiver

correlator spacings of **0.2** and **1.0** L1-chips.)

$$VPE_{SSD-M} = \sum_{i=1}^{N} S_{3,i} b_{SSD-M,i} \qquad (5.4)$$

Where:

VPE_{SSD-M} :   Vertical Position Error for **mitigated** satellite signal deformation range biases at user receiver correlator spacing of **0.08** L1-chips or **0.12** L1-chips

$S_{3,i}$:   Elements of third row of the projection matrix S

$b_{SSD-M,i}$:   **Mitigated** satellite signal deformation range biases at user receiver correlator spacing of **0.08** L1-chips or **0.12** L1-chips, corresponding to visible satellites

N :   Total number of satellites visible at user

The **mitigated** dual-frequency L1/L5 biases are projected from the **mitigated** L1-only biases (previously the **unmitigated** dual-frequency L1/L5 biases in Section 4.2.1 Subsection 9, Equation (4.16) were projected from the **unmitigated** L1-only biases).

$$b_{SSD-M,i,L1/L5} = K_{DUAL-FREQ-IONO} * b_{SSD-M,i,L1-only} \qquad (5.5)$$

where

$b_{SSD-M,i,L1/L5}$: Dual-frequency L1/L5 satellite signal deformation range bias

$K_{DUAL\text{-}FREQ\text{-}IONO}$: Dual-frequency ionosphere-error-removal scale factor = 2.6 [Refer Section 2.4.4 Equation (2.32), Section 4.2.1 Subsection 9 Equation (4.16)].

$b_{SSD\text{-}M,I,L1\text{-}only}$: Single-frequency L1-only satellite signal deformation range biases

5.3.2 Impact of Mitigated Satellite Signal Deformation Range Biases on Expected 95% Vertical Position Errors for WAAS Users

This section analyzes and presents the impact of mitigated satellite signal deformation range biases on the expected 95% vertical position errors. The impact on single-frequency L1-only WAAS users is first discussed followed by the impact on dual-frequency L1/L5 users WAAS users. Both sets of results are summarized in tabular form for up to five unhealthy/inaccessible satellites.

The graphic results are only shown for two unhealthy/inaccessible satellites in this section. The graphic results for other numbers of unhealthy/inaccessible satellites are found in Appendix D-6.

In addition, the vertical position errors were larger for mitigated user receiver correlator spacings of **<u>0.12</u>** L1-chips than for **<u>0.08</u>** L1-chips. Accordingly, only the results for 0.12 L1-chips are discussed in this section; the results for 0.08 L1-chips are presented in Appendix D.

5.3.2.1 Impact on Expected 95% Vertical Position Errors for Single-Frequency L1-only WAAS users

Figure 5-5 shows the impact of mitigated satellite signal deformation range biases on expected 95% vertical position errors for single-frequency L1-only WAAS users, for the case when two satellites are unavailable. The reference receiver's correlator spacing is **0.1 L1-chips**; the user receiver's correlator spacing is **0.12 L1-chips**.
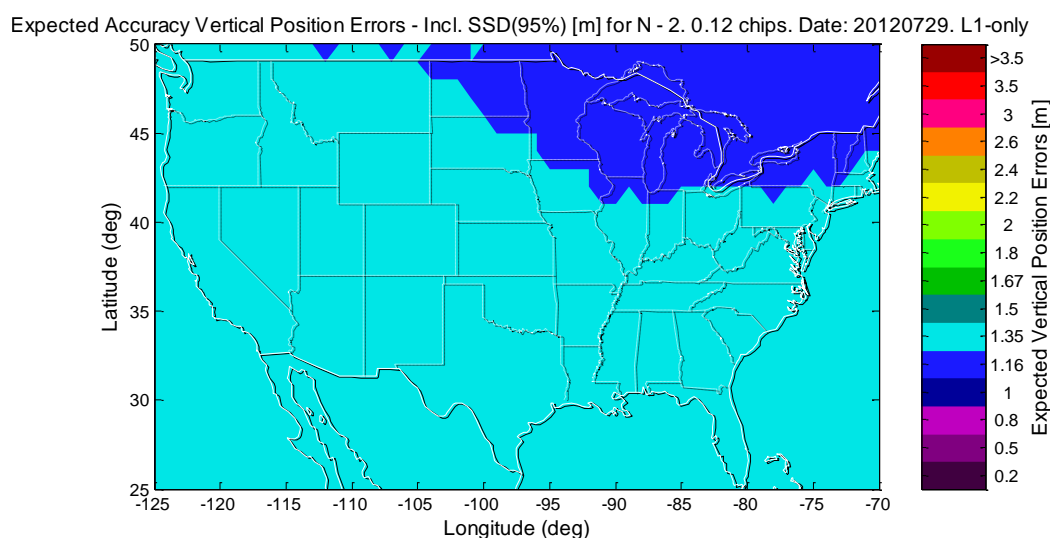
Figure 5-5: Nominal Accuracy Including Expected Vertical Position Errors from Mitigated Satellite Signal Deformation Range Biases [m] for Single Frequency L1-only WAAS Users

(Two unhealthy/inaccessible satellites, Reference: 0.1 L1-chip correlator spacing; User: **0.12** L1-chip correlator spacing)

Figure 5-5 shows that single-frequency users with correlator spacings of **0.12** L1-chips

will experience expected 95% vertical position errors over CONUS of between 1.16 m

and 1.35 m.

These results will be further discussed in Section 5.3.2.2 together with the dual-

frequency cases, for all unhealthy or inaccessible satellites from zero to five.

5.3.2.2   Impact on Expected 95% Vertical Position Errors for Dual-Frequency L1/L5-only WAAS users

Figure 5-6 shows the impact of mitigated satellite signal deformation range biases on

expected 95% vertical position errors for dual-frequency L1/L5 WAAS users, for the

case when two satellites are unavailable. The **reference receiver**'s correlator spacing

is **0.1 L1-chips**; the **user receiver**'s correlator spacing is **0.12 L1-chips.**

(Note: The equivalent L5-only biases, projected from L1-only biases, are for user

correlator spacings of **1.2 L5-chips** for the L5-frequency signal).

Figure 5-6: Nominal Accuracy Including Expected Vertical Position Errors from

Mitigated Satellite Signal Deformation Range Biases [m] for Dual Frequency L1/L5

WAAS Users

(Two unhealthy/inaccessible satellites, Reference: 0.1 L1-chip correlator spacing;

User: **0.12** L1-chip correlator spacing)

Figure 5-6 shows that dual-frequency users with correlator spacings of **0.12** L1-chips

will experience expected 95% vertical position errors over CONUS of around 1.5-1.67

m. These errors are larger than the errors of 1.16-1.35 m for the corresponding single-

frequency configuration.

These results will be further discussed in the next section, together with the single-

frequency cases, for all unhealthy or inaccessible satellites from zero to five.

5.3.2.3   Summary of Mitigated Impact of Satellite Signal Deformation Range Biases on Expected 95% Vertical Position Errors for WAAS Users

Table 5-6 summarizes the impact of unmitigated and mitigated satellite signal deformation range biases on the average expected 95% vertical position errors for single-frequency L1-only and dual-frequency L1/L5 WAAS users, for the cases of zero to five satellites unhealthy or inaccessible, averaged for user locations distributed over CONUS.

Similar to Table 4-4 in Section 4.4.3, the reference results are listed in the first column, under the "0.1 L1-chips/No SSD" heading. These are the average expected 95% vertical position errors due to all other GPS errors apart from satellite signal deformation range biases. These results are from user receivers identical to the reference receiver, with the same correlator spacing of 0.1 L1-chips. For these user receivers, the signal deformation would be almost entirely removed via differential corrections, leaving only the position errors from other GPS error sources.

The average expected 95% vertical position errors, including the effects of signal deformation, are shown in subsequent columns. These results are from user receivers with different correlator spacing configurations from the reference receivers. The earlier results for the unmitigated user receivers (user receiver correlator spacing of 0.2 L1-chips and 1.0 L1-chips) are shown for reference, in columns 2 and 3. Column 4 shows the results for the mitigated user receivers (user receiver correlator spacing of

0.12 L1-chips), which demonstrated significantly reduced average expected 95%

vertical position errors from signal deformation.

As previously shown in Table 4-4 in Section 4.4.3, the first row of each entry shows

the average expected 95% vertical position errors in the presence of satellite signal

deformation range biases. The second and third rows show the absolute and

percentage increases in average expected 95% vertical position errors, as compared to

the reference results in the absence of satellite signal deformation range biases.

Satellite Status	Nominal Accuracy Including Expected 95% Vertical Position Errors from Satellite Signal Deformation Range Biases [m]								
	Single Frequency: L1-Only					Dual Frequency: L1/L5			
	User Correlator Spacing [L1-chips]					User Correlator Spacing [L1-chips]			
	0.10	**0.20**	**1.00**	**0.12**		**0.10**	**0.20**	**1.00**	**0.12**
	No SSD*	Unmitigated		**Mitigated**		No SSD*	Unmitigated		**Mitigated**
N - 0	0.99	1.15 (+0.16) (+16.2%)	1.29 (+0.30) (+30.3%)	1.02 (+0.03) (+3.0%)		1.21	1.59 (+0.38) (+31.4%)	1.98 (+0.77) (+63.6%)	1.27 (+0.06) (+5.0%)
N - 1	1.07	1.24 (+0.17) (+15.9%)	1.41 (+0.34) (+31.8%)	1.10 (+0.03) (+2.8%)		1.31	1.74 (+0.43) (+32.8%)	2.18 (+0.87) (+66.4%)	1.38 (+0.07) (+5.3%)
N - 2	1.16	1.36 (+0.20) (+17.2%)	1.55 (+0.39) (+33.6%)	1.20 (+0.04) (+3.4%)		1.43	1.93 (+0.50) (+35.0%)	2.43 (+1.00) (+69.9%)	1.52 (+0.09) (+6.3%)
N - 3	1.27	1.49 (+0.22) (+17.3%)	1.71 (+0.44) (+34.6%)	1.31 (+0.04) (+3.1%)		1.61	2.17 (+0.56) (+34.8%)	2.78 (+1.17) (+72.7%)	1.70 (+0.09) (+5.6%)
N - 4	1.39	1.63 (+0.24) (+17.3%)	1.87 (+0.48) (+34.5%)	1.43 (+0.04) (+2.9%)		1.82	2.48 (+0.66) (+36.3%)	3.20 (+1.38) (+75.8%)	1.93 (+0.11) (+6.0%)
N - 5	1.50	1.76 (+0.26) (+17.3%)	2.02 (+0.52) (+34.7%)	1.55 (+0.05) (+3.3%)		2.06	2.81 (+0.75) (+36.4%)	3.62 (+1.56) (+75.7%)	2.19 (+0.13) (+6.3%)

Table 5-6: Nominal Accuracy Including Expected 95% Vertical Position Errors from Unmitigated and Mitigated Satellite Signal Deformation Range Biases [m] for Single L1- and Dual L1/L5 Frequency WAAS Users

Notes on table:

1. *No SSD: The user receiver is identical to the reference receiver. Thus signal deformation is entirely removed via differential corrections.

2. Dual-frequency satellite signal deformation range biases projected from single-frequency L1-only satellite signal deformation range biases.

3. Figures in parentheses are absolute and percentage increases from the

   reference No Satellite Signal Deformation (No SSD) results.

Under conditions of two inaccessible or unhealthy satellites (highlighted in Table 5-6), single-frequency L1-only WAAS users with mitigated user receiver correlator spacings of 0.12 L1-chips experience an additional **0.04 m** error over the reference results. For dual-frequency WAAS users, the corresponding errors are **0.09 m**. The amplification factor is similar to the dual-frequency ionosphere-error-removal scale factor of 2.6. As in the unmitigated cases, the errors increase as fewer satellites are available. These errors are much smaller than the errors from unmitigated satellite signal deformation range biases, which were **0.2-0.4 m** for single-frequency L1-only users and **0.5-1.0 m** for dual-frequency L1/L5 users depending on user receiver configuration.

For other numbers of inaccessible or unhealthy satellites, Table 5-6 shows that the absolute additional errors for dual frequency WAAS due to satellite signal deformation range biases (second row of entries) are 2.4 to 3 times that of single-frequency WAAS. This factor generally increases as fewer satellites are available. This was similar to the errors from the unmitigated satellite signal deformation range biases. More importantly, the absolute errors due to mitigated satellite signal deformation range biases are now 8%-20% of the absolute errors from the unmitigated satellite signal deformation range biases, a reduction of approximately 80%-90%.

As a ratio of the reference results (third row of entries), additional errors due to **<u>mitigated</u>** satellite signal deformation range biases are now much smaller than before: 3%-4% of the reference for the single-frequency WAAS user, and 5%-6% of the reference for the dual-frequency WAAS user. These percentages are 1/5-1/10 of the percentages for the **<u>unmitigated</u>** satellite signal deformation range biases.

These results show that the proposed mitigation method is effective in reducing the error contribution of satellite signal deformation range biases to the expected 95% vertical position errors.

5.3.3   Impact of Mitigated Satellite Signal Deformation Range Biases on Worst Case Vertical Position Errors for WAAS Users

The previous section examined the impact of mitigated satellite signal deformation range biases on expected 95% vertical position errors over an entire day for users located throughout CONUS. The impacts of mitigated and unmitigated satellite signal deformation range biases were also compared and the mitigation method was verified to be effective.

This section analyzes the impact of mitigated satellite signal deformation range biases on the worst case vertical position errors at each modeled user location over the same day. As in the previous section, the impact on single-frequency L1-only WAAS users is first discussed, followed by the impact on dual-frequency L1/L5 users. These results

are summarized in tabular form for both single and dual frequency users, for up to five

unhealthy or inaccessible satellites, and for both mitigated and unmitigated cases.

Only the graphic results for two unhealthy/inaccessible satellites are shown in this

section. The graphic results for other numbers of unhealthy/inaccessible satellites are

found in Appendix D.

5.3.3.1 Impact on Worst Case Vertical Position Errors for Single-Frequency L1-only WAAS users

Figure 5-7 shows the impact of mitigated satellite signal deformation range biases on

worst case vertical position errors for single-frequency L1-only WAAS users, for the

case when two satellites are unavailable. The **reference receiver**'s correlator spacing

is **0.1 L1-chips**; the user receiver's correlator spacing is **0.12 L1-chips**.

Expected Accuracy Vertical Position Errors - Incl. SSD(Max) [m] for N - 2. 0.12 chips. Date: 20120729. L1-only
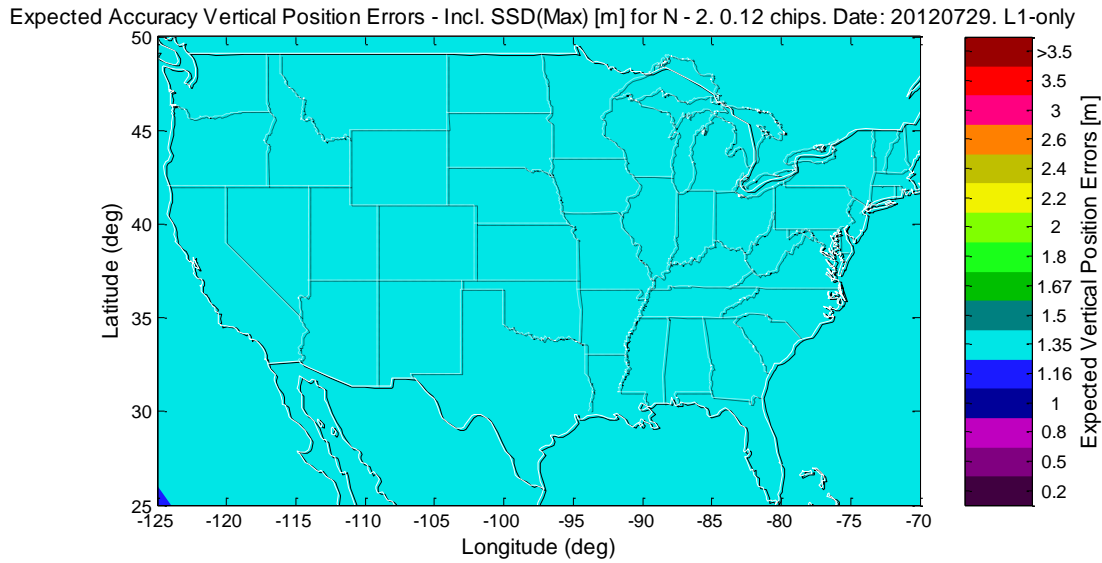
Figure 5-7: Nominal Accuracy Including Worst Case Vertical Position Errors from

Mitigated Satellite Signal Deformation Range Biases [m] for Single Frequency L1-

only WAAS Users

(Two unhealthy/inaccessible satellites, Reference: 0.1 L1-chip correlator spacing;

User: **0.12** L1-chip correlator spacing)

Figure 5-7 shows that single-frequency users with correlator spacings of **0.12** L1-chips will experience worst case vertical position errors over CONUS of 1.35 m. These results will be further discussed in Section 5.3.3.2 together with the dual-frequency cases, for all unhealthy or inaccessible satellites from zero to five.

5.3.3.2 Impact on Worst Case Vertical Position Errors for Dual-Frequency L1/L5-only WAAS users

Figure 5-8 shows the impact of mitigated satellite signal deformation range biases on worst case vertical position errors for dual-frequency L1/L5 WAAS users, for the case when two satellites are unavailable. The **reference receiver**'s correlator spacing is **0.1 L1-chips**; the **user receiver**'s correlator spacing is **0.12 L1- chips**.

(Note: The equivalent L5-only biases, projected from L1-only biases, are for user correlator spacings of **1.2 L5-chips** for the L5-frequency signal.)
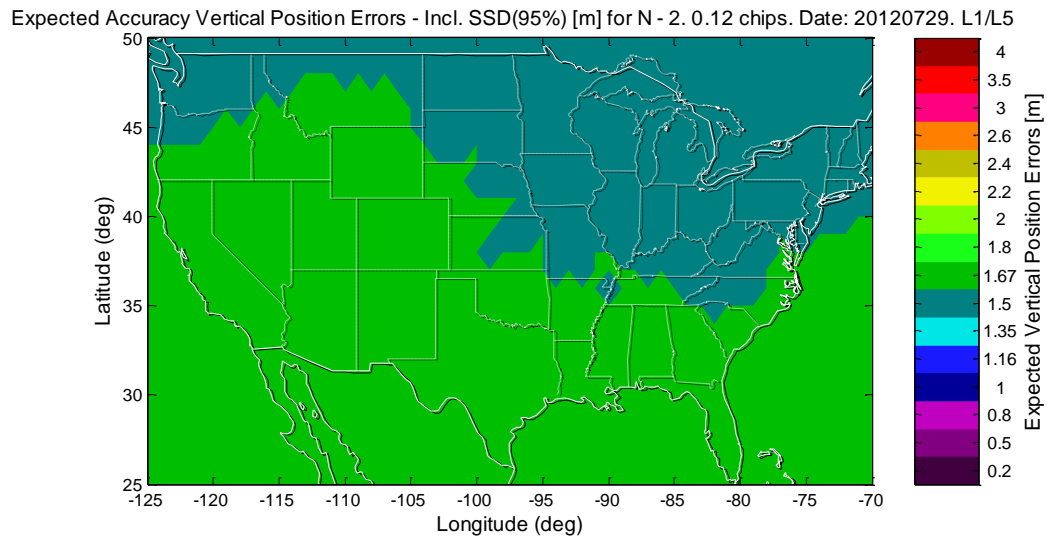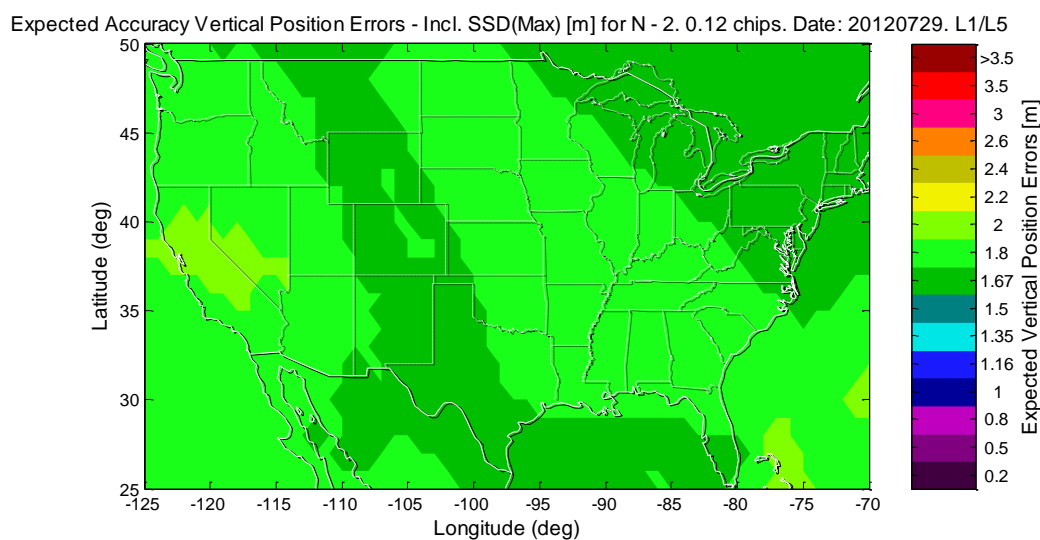

Figure 5-8: Nominal Accuracy Including Worst Case Vertical Position Errors from

Mitigated Satellite Signal Deformation Range Biases [m] for Dual Frequency L1/L5

WAAS Users

(Two unhealthy/inaccessible satellites, Reference: 0.1 L1-chip correlator spacing;

User: **0.12** L1-chip correlator spacing)

Figure 5-8 shows that dual-frequency users with correlator spacings of **0.12** L1-chips

will experience worst case errors over most of CONUS of around 1.67-1.8 m, rising to

2 m over a small portion of CONUS. These errors are larger than the errors of 1.35 m

for the corresponding single-frequency configuration.

These results will be further discussed in the next section, together with the single-

frequency cases, for all unhealthy or inaccessible satellites from zero to five, and

compared with the results for unmitigated satellite signal deformation range biases.

5.3.3.3   Summary of Mitigated Impact of Satellite Signal Deformation Range Biases on Worst Case Vertical Position Errors

Table 5-7 summarizes the impact of unmitigated and mitigated satellite signal

deformation range biases on the worst case vertical position errors over 24 hours, for

single-frequency L1-only and dual-frequency L1/L5 WAAS users, for the cases of

zero to five satellites unhealthy or inaccessible, averaged for user locations distributed

over CONUS.

Similar to Table 4-5 in Section 4.5.3, the reference results are listed in the first

column, under the "0.1 L1-chips/ No SSD" heading. These are the worst case vertical

position errors over 24 hours, due to all other GPS errors apart from satellite signal

deformation range biases. These results are from user receivers identical to the

reference receiver, with the same correlator spacing of 0.1 L1-chips. For these user receivers, the signal deformation would be almost entirely removed via differential corrections, leaving only the position errors from other GPS error sources.

The worst case vertical position errors, including the effects of signal deformation, are shown in subsequent columns. These results are from user receivers with different correlator spacing configurations from the reference receivers. The earlier results for the unmitigated user receivers (user receiver correlator spacing of 0.2 L1-chips and 1.0 L1-chips) are shown for reference, in columns 2 and 3. Column 4 shows the results for the mitigated user receivers (user receiver correlator spacing of 0.12 L1-chips), which demonstrated significantly reduced worst case vertical position errors from signal deformation.

As previously shown in Table 4-5 in Section 4.5.3, the first row of each entry shows the wost case vertical position errors in the presence of satellite signal deformation range biases. The second and third rows show the absolute and percentage increases in worst case vertical position errors, as compared to the reference results in the absence of satellite signal deformation range biases.

Satellite Status	Nominal Accuracy Including Worst Case Vertical Position Errors from Satellite Signal Deformation Range Biases [m]								
	Single Frequency: L1-Only					Dual Frequency: L1/L5			
	User Correlator Spacing [L1-chips]					User Correlator Spacing [L1-chips]			
	0.10	**0.20**	**1.00**	**0.12**		**0.10**	**0.20**	**1.00**	**0.12**
	No SSD*	Unmitigated		**Mitigated**		No SSD*	Unmitigated		**Mitigated**
N - 0	0.99	1.20 (+0.21) (+21.2%)	1.41 (+0.42) (42.4%)	1.03 (+0.04) (+4.0%)		1.21	1.74 (+0.53) (+43.8%)	2.25 (+1.04) (+86.0%)	1.30 (+0.09) (+7.4%)
N – 1	1.07	1.39 (+0.32) (+29.9%)	1.78 (+0.71) (66.4%)	1.13 (+0.06) (+5.6%)		1.31	2.24 (+0.93) (+71.0%)	3.25 (+1.94) (+148.1%)	1.47 (+0.16) (+12.2%)
N - 2	1.16	1.62 (+0.46) (+39.7%)	2.18 (+1.02) (87.9%)	1.24 (+0.08) (+6.9%)		1.43	3.04 (+1.61) (+112.6%)	5.06 (+3.63) (+253.8%)	1.70 (+0.27) (+18.9%)
N - 3	1.27	1.81 (+0.54) (+42.5%)	2.43 (+1.16) (91.3%)	1.37 (+0.10) (+7.9%)		1.61	3.8 (+2.19) (+136.0%)	5.86 (+4.25) (+264.0%)	1.97 (+0.36) (+22.4%)
N - 4	1.39	1.96 (+0.57) (+41.0%)	2.59 (+1.20) (86.3%)	1.49 (+0.10) (+7.2%)		1.82	4.22 (+2.40) (+131.9%)	6.40 (+4.58) (+251.6%)	2.22 (+0.40) (+22.0%)
N - 5	1.50	2.10 (+0.60) (+40.0%)	2.72 (+1.22) (81.3%)	1.61 (+0.11) (+7.3%)		2.06	4.48 (+2.42) (+117.5%)	6.77 (+4.71) (+228.6%)	2.46 (+0.40) (+19.4%)

Table 5-7: Expected Nominal Accuracy Including **Worst Case** Vertical Position Errors from Satellite Signal Deformation Range Biases [m] for Single L1- and Dual L1/L5 Frequency WAAS Users

Notes on table:

1. *No SSD: The user receiver is identical to the reference receiver. Thus signal deformation is entirely removed via differential corrections.

2. Dual-frequency satellite signal deformation range biases projected from single-frequency L1-only satellite signal deformation range biases.

3. Figures in parentheses are absolute and percentage increases from the reference No Satellite Signal Deformation (No SSD) results.

Under conditions of two inaccessible or unhealthy satellites (highlighted in Table 5-7), single-frequency L1-only WAAS users with **<u>mitigated</u>** user receiver correlator spacings of 0.12 L1-chips experience an additional **<u>0.08 m</u>** worst case vertical position error compared to the reference results. For dual-frequency L1/L5 WAAS users, the corresponding error is **<u>0.27 m</u>**, an amplification of more than the dual-frequency ionosphere-error-removal scale factor of 2.6. (The explanation for the larger-than-expected amplification is discussed in Section 4.5.2.) These errors are much smaller than the worst case vertical position errors from **<u>unmitigated</u>** satellite signal deformation range biases, which were **<u>0.46-1.02 m</u>** for single-frequency L1-only users and **<u>1.61-3.63 m</u>** for dual-frequency L1/L5 users depending on user receiver configuration.

For other numbers of inaccessible or unhealthy satellites, Table 5-7 shows that the absolute additional worst case vertical position errors for dual frequency WAAS due to satellite signal deformation range biases (second row of entries) are 2 to 4 times that of single-frequency WAAS. This factor generally increases as fewer satellites are available. This was similar to the errors from the unmitigated satellite signal deformation range biases. More importantly, the absolute errors due to mitigated satellite signal deformation range biases are now 8%-20% of the absolute errors from

the unmitigated satellite signal deformation range biases, a reduction of approximately 80%-90%.

As a ratio of the reference results (third row of entries), additional errors due to **mitigated** satellite signal deformation range biases are now much smaller than before: 4%-8% of the reference for the single-frequency WAAS user, and 7%-23% of the reference for the dual-frequency WAAS user. These percentages are 1/5-1/10 of the percentages for the **unmitigated** satellite signal deformation range biases.

These results show that the proposed mitigation method is effective in reducing the error contribution of satellite signal deformation range biases to the worst case vertical position errors.

5.4 Summary of Mitigation of Satellite Signal Deformation Range Biases

This chapter discussed various mitigation methods for satellite signal deformation range biases. One practical mitigation method was proposed – restriction of user receiver correlator spacing. For the L1-frequency, the proposed allowed span of user receiver correlator spacings was **0.08** L1-chips to **0.12** L1-chips; for the L5-frequency, the proposed allowed span of user receiver correlator spacings was **0.8** L5-chips to **1.2** L5-chips. MAAST was used to analyze the impact of this mitigation method on single-frequency and dual-frequency WAAS users.

With the proposed correlator spacing restrictions, single-frequency WAAS users will experience average expected 95% vertical position errors of 0.03-0.05 m (2.8%-3.4% of other WAAS errors) compared to 0.16-0.5 m (15.9%-34.7% of other WAAS errors) without them. More importantly, for dual-frequency WAAS users, this mitigation is equally effective: average expected 95% vertical position errors of 0.06-0.13 m (5.0%-6.3% of other WAAS errors) compared to 0.38-1.56 m (31.4%-75.8% of other WAAS errors) without mitigation.

In addition, this mitigation proposal can significantly reduce worst case vertical position errors. Single-frequency WAAS users now experience worst case vertical position errors of 0.04-0.11 m (4.0%-7.9% of other WAAS errors) compared to 0.21-1.22 m (21.2%-91.3% of other WAAS errors) without mitigation. Dual-frequency WAAS users experience worst case vertical position errors of 0.09-0.40 m (7.4%-22.4% of other WAAS errors) compared to 0.53-4.71 m (43.8%-264.0% of other WAAS errors) without mitigation.

The results show that the mitigation method effectively reduces the impact of satellite signal deformation range biases on expected 95% vertical position accuracy and worst case vertical position errors for single-frequency and dual-frequency WAAS users. Dual-frequency users especially are able to benefit from increased availability while bearing a significantly reduced penalty from the amplification of satellite signal range biases by the dual-frequency ionosphere-error-removal scale factor.

Again, the effects of different user receiver bandwidths and filter implementations are

beyond the scope of the analysis in this chapter. These effects are discussed in the next

chapter under Future Research.

Chapter 6

Conclusion and Future Work

6.1   Overview

In single-frequency L1-only WAAS-GPS positioning for aviation, the ionospheric errors are one of the largest error sources. In comparison, the nominal satellite signal deformation (SSD) range biases are small and insignificant (Figure 6-1).

L1	Ionospheric Error	Delay Bound	Clock; ephemeris	Tropo	Multi path	SSD
	~ 4 m (1 m to 10 m)		~ 1 m (1 m to 3 m)	~ .3 m (.2 m to 1 m)	~ .25 m (.2 m to .5 m)	**~ .15 m (.1 m to .3m)**
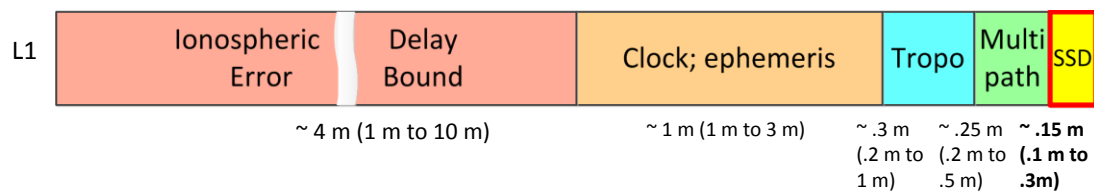
Figure 6-1: Range Error Contributions for single frequency L1-only GPS signal

The use of dual-frequency ranging, to be available in the near future, virtually eliminates the ionospheric errors, but also amplifies the nominal satellite signal

deformation range biases (Figure 6-2). These biases are no longer insignificant; to avoid limiting the future performance of WAAS, they now need to be measured and mitigated.
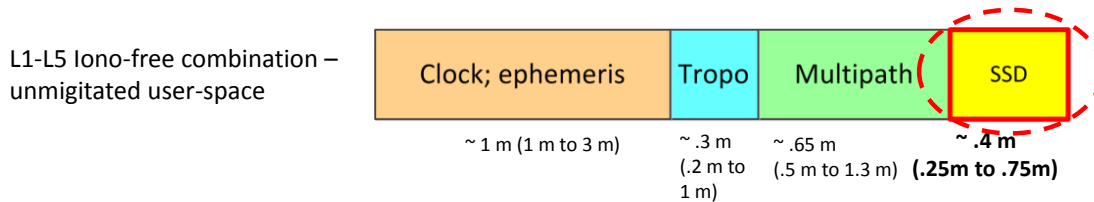
Figure 6-2: Range Error Contributions for unmitigated dual frequency L1/L5 GPS

Legacy measurement methods were limited in their attenuation of multipath and/or time-varying drifts. Consequently, the resultant measurements contained residual measurement noises with similar or larger magnitudes than the range biases. To overcome these limitations, a hybrid "measure-and-verify" measurement technique was developed, providing excellent multipath attenuation while minimizing time-varying drifts.

Using the newly-developed measurement technique, high-quality satellite signal deformation range bias measurements were obtained, enabling an accurate analysis of their impact on user position errors. This technique was also applied to demonstrate the efficacy of different mitigation solutions, the most effective of which was the "Restrict User Space" method. This latter method significantly reduced the contribution from satellite signal deformation (Figure 6-3), while attempting to preserve the largest user receiver design space for legacy aviation receivers.

L1-L5 Iono-free combination –
mitigated user-space

Clock; ephemeris	Tropo	Multipath	SSD
~ 1 m (1 m to 3 m)	~ .3 m (.2 m to 1 m)	~ .65 m (.5 m to 1.3 m)	< .15 m
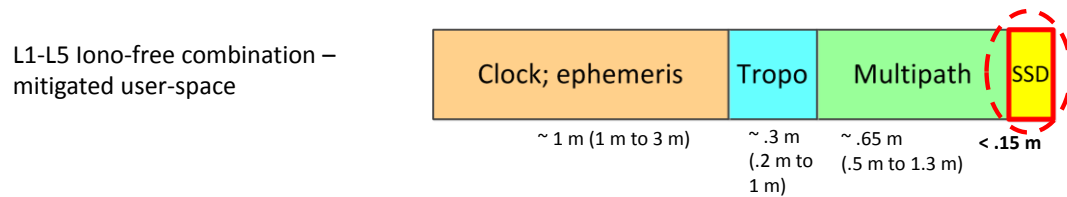
Figure 6-3: Range Error Contributions for mitigated dual frequency L1/L5 GPS

Section 6.2 discusses the research contributions in further detail and Section 6.3 presents other considerations and possible future research in this field.

6.2   Contributions

This section discusses and summarizes the research contributions contained in this dissertation, toward the measurement and mitigation of satellite signal deformation range biases.

- Rendered nominal satellite signal deformation measurable

The main goal of this research was to render nominal satellite signal deformation range biases measurable. The following contributions were made:

o   <u>Determined the nature of the measurement errors inherent in the two legacy</u>
    <u>"measure-and-trust" measurement methods.</u>

Updated measurement results were obtained using the "one-in-vew" SRI 46 m large
dish and the "all-in-view" hemispherical dish (Sections 3.5 and 3.6, respectively).
Their inherent errors, which limited the measurement of satellite signal deformation
range biases, were also explored (Sections 3.5.2 and 3.6.2, respectively).

The large dish-antenna measurements contained worst case time-varying drifts of
magnitudes between ±0.1 m to ±0.3 m over a day (Figure 3-12a). The waveforms used
in the correction of these time-varying drifts contained short-term noise with
magnitudes: 0.01-0.05 m (RMS) and 0.04-0.36 m (Worst Case) (Table 3-5).
Multipath-limiting hemispherical dish antennas located on the rooftop experienced
residual multipath errors of magnitude: 0.08-0.31 m (RMS) (Table 3-6). These
measurement errors are as large as, or in some cases larger than, the actual satellite
signal deformation range biases. Consequently, these legacy measurement methods
were constrained in their ability to measure the biases effectively.

o   <u>Developed a hybrid "Measure-and-Verify" method to mitigate these</u>
    <u>measurement errors.</u>

This was accomplished by careful measurement and calibration (Section 3.7.2) of a
smaller, more readily available 1.8 m rooftop dish. This "one-in-view" dish antenna
provided low-multipath measurements, and the "all-in-view" hemispherical dish

antenna verified that the time-varying drifts associated with "one-in-view" dishes was not significantly present.

This hybrid "measure-and-verify" technique provided significant improvement compared to either standalone legacy measurement method. Multipath attenuation was reduced from 0.08-0.31 m to 0.02-0.09 m (Table 3-8). Previously visible time-varying drifts as large as 0.1-0.3 m (Figure 3-12a) were no longer observed. Furthermore, the measurement results demonstrated repeatability over almost a year.

The new method was used to obtain low-noise range bias measurements, for single-frequency L1-only, single-frequency L5-only, and dual-frequency L1/L5 GPS signals (Sections 3.7.3, 3.7.4, and 3.7.5, respectively), for subsequent quantification of their impact on aviation.

- Quantified Unmitigated Impact on Aviation

The accurate measurements of satellite signal deformation range bias could now be used to analyze the unmitigated impact of nominal satellite signal deformation on aviation users. The availability, average (95%) vertical position accuracy, and worst case vertical position accuracy were evaluated for single-frequency L1-only and dual-frequency L1/L5 users (Sections 4.3.1, 4.3.2, 4.4.1, 4.4.2, 4.5.1, and 4.5.2).

For the case of two unavailable satellites, average (95%) vertical errors were found to increase by 0.2 m - 0.39 m for single-frequency L1-only users, and 0.5 m - 1.0 m for dual-frequency L1/L5 users (Section 4.4 Table 4-4). There was a greater impact on worst case errors (Section 4.5 Table 4-5): these increased by 0.46 m - 1.02 m for single-frequency L1-only users, rising to 1.61 m – 3.63 m for dual-frequency L1/L5 users. (For comparison, these errors from unmitigated signal deformation are listed in Table 6-1 and Table 6-2 later in this section, together with the corresponding position errors from mitigated signal deformation.) These results highlighted the need for effective mitigation of the errors caused by satellite signal deformation range biases.

- Demonstrated an effective mitigation strategy

The hybrid "Measure-and-Verify" measurement technique was successful in facilitating the evaluation and demonstration of an effective mitigation strategy. By imposing restrictions on the user receiver correlator spacings, the errors from satellite signal deformation range biases were mitigated effectively.

For the case of two unavailable satellites, average (95%) vertical errors decreased from 0.2 m - 0.39 m to 0.04 m for single-frequency L1-only users, and from 0.5 m - 1.0 m to 0.09 m for dual-frequency L1/L5 users (Section 5.3.2, Table 5-6; Table 6-1). There was a greater impact on worst case errors: these decreased from 0.46 m - 1.02 m to 0.08 m for single-frequency L1-only users, and from 1.61 m – 3.63 m to 0.27 m for dual-frequency L1/L5 users (Section 5.3.3 Table 5-7; Table 6-2). The results for

unmitigated and mitigated satellite signal deformation are summarized in Table 6-1

and Table 6-2, and demonstrate the effectiveness of the proposed mitigation strategy.

Satellite Status	Nominal Accuracy Including Expected 95% Vertical Position Errors from Satellite Signal Deformation Range Biases [m]							
	Single Frequency: L1-Only				Dual Frequency: L1/L5			
	User Correlator Spacing [L1-chips]				User Correlator Spacing [L1-chips]			
	0.10	0.20	1.00	0.12	0.10	0.20	1.00	0.12
	No SSD*	Unmitigated		**Mitigated**	No SSD*	Unmitigated		**Mitigated**
N - 0	0.99	1.15 (+0.16) (+16.2%)	1.29 (+0.30) (+30.3%)	1.02 (+0.03) (+3.0%)	1.21	1.59 (+0.38) (+31.4%)	1.98 (+0.77) (+63.6%)	1.27 (+0.06) (+5.0%)
N - 1	1.07	1.24 (+0.17) (+15.9%)	1.41 (+0.34) (+31.8%)	1.10 (+0.03) (+2.8%)	1.31	1.74 (+0.43) (+32.8%)	2.18 (+0.87) (+66.4%)	1.38 (+0.07) (+5.3%)
N - 2	1.16	1.36 (+0.20) (+17.2%)	1.55 (+0.39) (+33.6%)	1.20 (+0.04) (+3.4%)	1.43	1.93 (+0.50) (+35.0%)	2.43 (+1.00) (+69.9%)	1.52 (+0.09) (+6.3%)
N - 3	1.27	1.49 (+0.22) (+17.3%)	1.71 (+0.44) (+34.6%)	1.31 (+0.04) (+3.1%)	1.61	2.17 (+0.56) (+34.8%)	2.78 (+1.17) (+72.7%)	1.70 (+0.09) (+5.6%)
N - 4	1.39	1.63 (+0.24) (+17.3%)	1.87 (+0.48) (+34.5%)	1.43 (+0.04) (+2.9%)	1.82	2.48 (+0.66) (+36.3%)	3.20 (+1.38) (+75.8%)	1.93 (+0.11) (+6.0%)
N - 5	1.50	1.76 (+0.26) (+17.3%)	2.02 (+0.52) (+34.7%)	1.55 (+0.05) (+3.3%)	2.06	2.81 (+0.75) (+36.4%)	3.62 (+1.56) (+75.7%)	2.19 (+0.13) (+6.3%)

Table 6-1: Nominal Accuracy Including Expected 95% Vertical Position Errors from

Unmitigated and Mitigated Satellite Signal Deformation Range Biases [m] for Single

L1- and Dual L1/L5 Frequency WAAS Users

(Reproduced from Table 5-6)

Satellite Status	Nominal Accuracy Including Worst Case Vertical Position Errors from Satellite Signal Deformation Range Biases [m]							
	Single Frequency: L1-Only				Dual Frequency: L1/L5			
	User Correlator Spacing [L1-chips]				User Correlator Spacing [L1-chips]			
	0.10	0.20	1.00	0.12	0.10	0.20	1.00	0.12
	No SSD*	Unmitigated		Mitigated	No SSD*	Unmitigated		Mitigated
N - 0	0.99	1.20 (+0.21) (+21.2%)	1.41 (+0.42) (42.4%)	1.03 (+0.04) (+4.0%)	1.21	1.74 (+0.53) (+43.8%)	2.25 (+1.04) (+86.0%)	1.30 (+0.09) (+7.4%)
N – 1	1.07	1.39 (+0.32) (+29.9%)	1.78 (+0.71) (66.4%)	1.13 (+0.06) (+5.6%)	1.31	2.24 (+0.93) (+71.0%)	3.25 (+1.94) (+148.1%)	1.47 (+0.16) (+12.2%)
N - 2	1.16	1.62 (+0.46) (+39.7%)	2.18 (+1.02) (87.9%)	1.24 (+0.08) (+6.9%)	1.43	3.04 (+1.61) (+112.6%)	5.06 (+3.63) (+253.8%)	1.70 (+0.27) (+18.9%)
N - 3	1.27	1.81 (+0.54) (+42.5%)	2.43 (+1.16) (91.3%)	1.37 (+0.10) (+7.9%)	1.61	3.8 (+2.19) (+136.0%)	5.86 (+4.25) (+264.0%)	1.97 (+0.36) (+22.4%)
N - 4	1.39	1.96 (+0.57) (+41.0%)	2.59 (+1.20) (86.3%)	1.49 (+0.10) (+7.2%)	1.82	4.22 (+2.40) (+131.9%)	6.40 (+4.58) (+251.6%)	2.22 (+0.40) (+22.0%)
N - 5	1.50	2.10 (+0.60) (+40.0%)	2.72 (+1.22) (81.3%)	1.61 (+0.11) (+7.3%)	2.06	4.48 (+2.42) (+117.5%)	6.77 (+4.71) (+228.6%)	2.46 (+0.40) (+19.4%)

Table 6-2: Expected Nominal Accuracy Including **Worst Case** Vertical Position Errors from Satellite Signal Deformation Range Biases [m] for Single L1- and Dual L1/L5 Frequency WAAS Users (Reproduced from Table 5-7)

The hybrid measurement technique and mitigation strategies are further extendible to signals from multi-frequency, multi-GNSS configurations. This would be useful given the ubiquity and proliferation of such signals in the near future.

6.3 Future Research

This section presents some of the outstanding issues as well as promising areas of continued research. These include further research on the impact of measurement equipment, alternative mitigation strategies, and signal deformation on waveforms from other constellations.

6.3.1 Impact of Measurement Equipment on Bias Measurements

In the course of this research, it was found that the noise from measurement equipment could be significant relative to the range biases. Possible sources of noise originated from the one-in-view satellite dish antennas and the use of different sets of receiver hardware. Further investigation into these sources of measurement variations would enable more accurate measurements of satellite signal deformation range biases, which would in turn result in more effective mitigation strategies.

Temporal Variation in Large Satellite Dish Antenna Measurements

Significant temporal variations were observed for measurements from both "one-in-view" satellite dishes. Preliminary investigations showed that the time-varying drifts were strongly correlated with time-of-day and temperature (Sections 3.5.2 and 3.7.2).

Further experiments demonstrated that different front-end low-noise amplifiers exhibited different measurement and noise characteristics depending on ambient

temperature. The cavity filter was not subject to detailed investigation, but could also be another additional source of temperature-dependent drifts.

Future work would involve additional experiments to isolate and minimize the time-dependence and/or temperature-dependence of the individual pieces of measurement equipment, leading to more accurate measurements of satellite signal deformation range biases.

User Receiver Characteristics

The relationship between satellite signal deformation range biases and correlator spacing differences between the reference and user receivers was explored in this dissertation.

In addition, other receiver differences could contribute additional variations in range bias measurements. Such differences include: the use of receivers from different manufacturers, front-end filters of different filter bandwidths, filter orders and group delays.

Characterization of the relationship between the filter attributes and the range bias measurements would not only provide more accurate measurements of range biases, it could potentially also provide more effective mitigation strategies (see Section 6.3.2).

6.3.2 "Measure-and-Correct" Mitigation Method for Satellite Signal Deformation

The "Measure-and-Correct" technique was discussed in Section 5.2.1 and found to be infeasible for avionics. However, it could be feasible in other application areas where it is practical to regularly measure and update the satellite signal deformation range biases, for instance in consumer electronics.

The basic idea involves characterizing the signal deformation range bias characteristics of the reference and user receivers. Range bias corrections would be computed and applied using both sets of characteristic parameters, either at a central node or at the user receiver. This could potentially substantially mitigate the signal deformation range biases.

The main challenges of this scheme are twofold. The first challenge is to characterize each receiver's bias characteristics with a minimal set of parameters, accounting for different filter orders, bandwidth, group delays, correlator spacings, and possibly filter changes due to component aging. This set of parameters should be chosen to facilitate computation of range bias corrections for each individual satellite signal. The second challenge pertains to integrity-related applications: the need to determine variance overbounds of the applied corrections, which is not straightforward given the immense variety of user receivers. However, this latter challenge could be less of a concern for primarily accuracy-driven applications such as consumer electronics and cellphones.

6.3.3   Signal deformation on Waveforms from New Constellations

New satellites from existing constellations and new satellite navigation constellations continue to be launched today, such as from Glonass (Russia), Galileo (Europe), and Beidou-2 or Compass (China). Whereas GPS traditionally used BPSK (Binary Phase-Shift Keying) code modulation, many of the newer constellations incorporate Binary Offset Carrier (BOC) code modulation [77]. Given the potential of multi-frequency, multi-constellation ranging and positioning, it is thus important to determine their signal deformation characteristics. Some preliminary characterization of these signals has previously been carried out for modernized BOC code modulations [78] and constellations [79]; this continues to be an active area of current research.

Furthermore, these constellations continue to use truncated square wave modulation instead of the more spectrally efficient pulse-shape modulation and transmission. (Appendix E discusses the reasons in greater detail.) If pulse-shape modulation is chosen instead in the future, it would be of research interest to determine the signal deformation characteristics associated with this new form of modulation.

Appendix A

Acronyms/ Glossary

2OS	2nd order threat model for faulted signal deformation. 3 parameters are included: f_D, σ and Δ (Appendix B-4.2)
ADC	Analog-to-Digital-Converter (Section 2.3.1)
AL	Alert Limit (Section 2.5.2)
ARNS	Aeronautical Radio Navigation Service (Section 2.1; [27], [28])
Beidou	Chinese Global Navigation Satellite System. Current version: Beidou-2; also known as Compass (Section 2.1)
BPF	Bandpass Filter (Section 2.3.1)
bps	Bit-per-second (Section 2.2.1)
BPSK	Binary Phase Shift Keying (Section 2.2)

C/A   Coarse-Acquisition. Non-encrypted transmitted code for open use.

CNMP   Code Noise and Multipath Error (Section 4.2.1)

Compass   Chinese Global Navigation Satellite System. Current version. Also

                 known as Beidou-2 (Section 2.1)

CONUS   Conterminous United States (Section 2.5.1)

CRPA   Controlled Pattern Reception Array (Appendix C)

Δ   Digital Distortion Paramater (Appendix B-4.2)

DGPS   Differential GPS (Section 2.4; Section 2.4.4)

DSSS   Direct Sequence Spread Spectrum (Section 2.2)

ECEF   Earth-centered Earth-Fixed coordinate system to describe position

                 (Section 2.3.4)

EML   Early-Minus-Late (Discriminator) in the Receiver's Code Tracking

                 Loop (Section 2.3.3)

FAA   Federal Aviation Administration (Section 2.5)

Galileo   European Global Navigation Satellite System (Section 2.1)

GNSS   Global Navigation Satellite System (Section 2.1)

Gold Code   Pseudorandom Noise (Code) generated using David Gold's

                 Algorithm, for Direct Sequence Spread Spectrum (DSSS). Has

                 bounded maximum autocorrelation and cross-correlation between

                 the different code sequences (Section 2.2.1)

GPS   Global Positioning System (Section 2.1)

HAL   Horizontal Alert Limit (Section 2.5.2)

Helibowl	A helical antenna combined with a metal bowl at the base. The metal bowl effectively attenuates all signals below 30°. Used for effective multipath suppression of ground multipath (Section 3.3.1)
HPL	Horizontal Protection Level (Section 2.5.2)
I5	L5-Frequency In-Phase Signal (Section 2.2.1)
IF	Intermediate Frequency; typically 2-40 MHz in GPS receivers but could be as high as up to 100 MHz (Section 2.3.3)
L1-C/A	Coarse-Acquisition code; rate 1.023 Mchips/ sec. Non-encrypted for open use, transmitted on L1-frequency signal (Section 2.2.2).
L1-Frequency	1575.42 MHz, in the L-Frequency (1-2 GHz) Tranmission band (Section 2.2.3)
L1-P	Unencrypted precise GPS code at rate 10.23 Mchips/ sec transmitted at L1-frequency. A W encryption code is needed to convert the unenrypted P code into encrypted Y code, or vice versa (Appendix F)
L1-P(Y)	Encrypted precise GPS code transmitted at L1 frequency. Currently transmitted available for military use but not available to the civilian user community.
L2C	Non-encrypted GPS signal at L2 frequency, for civilian users. Currently transmitted and available on 12 of the 32 GPS satellites.
L2-frequency	1227.6 MHz, in the L-Frequency (1-2 GHz) Tranmission band (Section 2.2.3)

L2-P(Y)	Encrypted military GPS code transmitted at L2 frequency. Currently transmitted but not available to the civilian user community. (Section 2.2.2)
L5-Frequency	1176.45 MHz, in the L-Frequency (1-2 GHz) Tranmission band (Section 2.2.3)
LFSR	Linear-Feedback Shift Register, a way to generate the PRNs for transmission (Section 2.2.2)
LNA	Low-noise Amplifier (Section 2.3.1)
LPF	Lowpass Filter
LPV	Localizer Performance with Vertical Guidance with a decision height of 250 ft (Section 2.5.2)
LPV200	Localizer Performance with Vertical Guidance with a decision height of 200 ft (Section 2.5.2)
MAAST	Stanford's Matlab Algorithm Availability Simulation Tool (Section 4.2)
MLA	Multipath Limiting Antenna (Section 3.3.1)
MOPS	(WAAS) Minimum Operational Performance Standards (Section 2.5.2)
OF	Obliquity Factor: The increase in path length through the ionosphere that an oblique ray takes relative to a vertical ray [55]
P(Y)	Encrypted military GPS code at rate 10.23 Mchips/ sec.
PC	Personal Computer

PL	Protection Level (Section 2.5.2)
PRN	Pseudorandom Noise (Code). Each individual GPS satellite is assigned a unique PRN code for DSSS and transmission (Section 2.2.2)
PST	Pacific Standard Time
Q5	L5-Frequency Quadrature Signal (Section 2.2.1)
RF	Radio Frequency (Section 2.3.1)
RF-FE	Radio Frequency Front End (Section 2.3.1)
RF-Front End	Radio Frequency Front End (Section 2.3.1)
RFI	Radio Frequency Interference (Appendix F)
RMS	Root Mean Square
SRCT	Square-Root Raised Cosine Technique
SRI	SRI International is a nonprofit, independent research and innovation center. Formerly the Stanford Research Institute. Operators and maintainers of the 46 m Dish Antenna on the Stanford Foothills (Appendix B)
SSD	Satellite Signal Deformation
SVN	SVN: Satellite Vehicle Number, the ID of any particular GPS satellite. Each satellite has a unique SVN.
TrEC	Tracking Error Compensator multipath mitigation technique (Section 0)
TROP	Troposphere Error (Section 4.2.1)

UDRE	User Differential Range Errors (Section 4.2.1)
UIVE	User Ionospheric Vertical Errors (Section 4.2.1)
USRP	Universal Software Receiver Protocol (Section 3.2.2)
UTC	Coordinated Universal Time
VAL	Vertical Alert Limit (Section 2.5.2)
VPA	Instantaneous Vertical Position Accuracy (Section 4.2.1)
VPA_bar	Expected Vertical Position Accuracy, or average of instantaneous Vertical Position Accuracy over a day (Section 4.2.1)
VPE	Vertical Position Errors (Section 4.2.1)
VPL	Vertical Protection Level (Section 2.5.2)
VSA	Vector Spectrum Analyzer (Section 3.2.2)
w/o	Without
WAAS	Wide-Area Augmentation System (Section 2.5)
WAAS-GEO	Geostationary Satellite deployed in WAAS system (Section 3.5)

Appendix B

Large Dish Antenna Measurements of Waveform Distortions and Range Biases

1 Overview

This section describes the use of a large SRI dish antenna to measure nominal satellite signal deformation waveform distortions, and from these, to derive range biases. Such antennas provide high signal gain and effective suppression of multipath errors and radio-frequency noise through the use of narrow beam-widths. However, due to the narrow beam-widths, the antenna is only able to monitor a single satellite at a time.

Using this method, raw data were collected for GPS and WAAS-GEO satellite signals over a single 24-hr time period, and processed to obtain measurements of waveforms and waveform distortions. This was a first in open literature. Some of these distortion results were consistent over years. Further processing of these waveforms enabled predictions of resultant range biases experienced by user receivers. These were found to be as large as ±0.3 m or ±0.5 m, depending on reference receiver and user receiver configurations.

These measured biases were also found to exhibit daily drifts and short-term noises, which past measurements did not account for or mitigate against (Section A-1.2). These errors limit the accuracy of the measured range biases, and are discussed further in Section 3.5.2 of the main dissertation.

Section 2 details the measurement setup and procedures to log raw data measurements from the 46 m large SRI dish. Section 3 describes the processing steps to convert the raw data to measurements of GPS signal waveforms and waveform distortions, adapting the method originally presented in [7]. Section 4 gives a detailed example of the analog and digital distortion for a particular satellite, satellite ID PRN #2, based on actual measured dish data. Section 5 presents the analog and digital distortion results for all of the GPS and WAAS-GEO satellite signals. Section 6 further processes these waveform measurements to determine resultant satellite signal deformation range biases, for a variety of users with different receiver configurations.

2   Measurement Setup and Procedures

To avoid any temporal variations in ground measurement equipment, raw baseband data for the entire GPS and WAAS-GEO satellites was collected over a single 24-hour period. Six people were involved in planning and operations. SRI's 46 m dish high-gain antenna was used (Figure B-1), together with high-rate, high precision, specialized, data collection equipment (Figure B-2). This data collection effort produced pairs of high-bandwidth, high-resolution measurements − 46.08 Msamples/sec, 16 bit/ sample − for all available GPS and WAAS-GEO satellites at the time of data collection in 2010.

The following steps were involved:

1.   Pre-campaign planning was first carried out. Stanford's MAAST software was used for orbit prediction and planning for satellite data collection.

2.   L5-frequency signals were first collected, followed by all L1 frequency signals. This was to avoid making changes to the sampling and center frequencies of the data collection equipment.

3.   Data collection for L1 frequency satellite signals was split over 4 time periods. For each time period, WAAS-GEO L1 signal measurements were logged at the beginning and end, to serve as a reference/calibration for the GPS signals. In between, all other GPS-L1 signal measurements were logged.

4.   For each data collection, the data collection equipment was re-calibrated, to minimize any possible variations of the clock and equipment over time.

5.   The satellite dish was used to point at individual satellites, one at a time, and 2 sec of data was captured and saved to disk. For each signal, two sets of 2 sec data were collected.

6.   Step #5 was repeated for each WAAS-GEO satellite, then for GPS satellites within the time period, then again for the WAAS-GEO satellites.
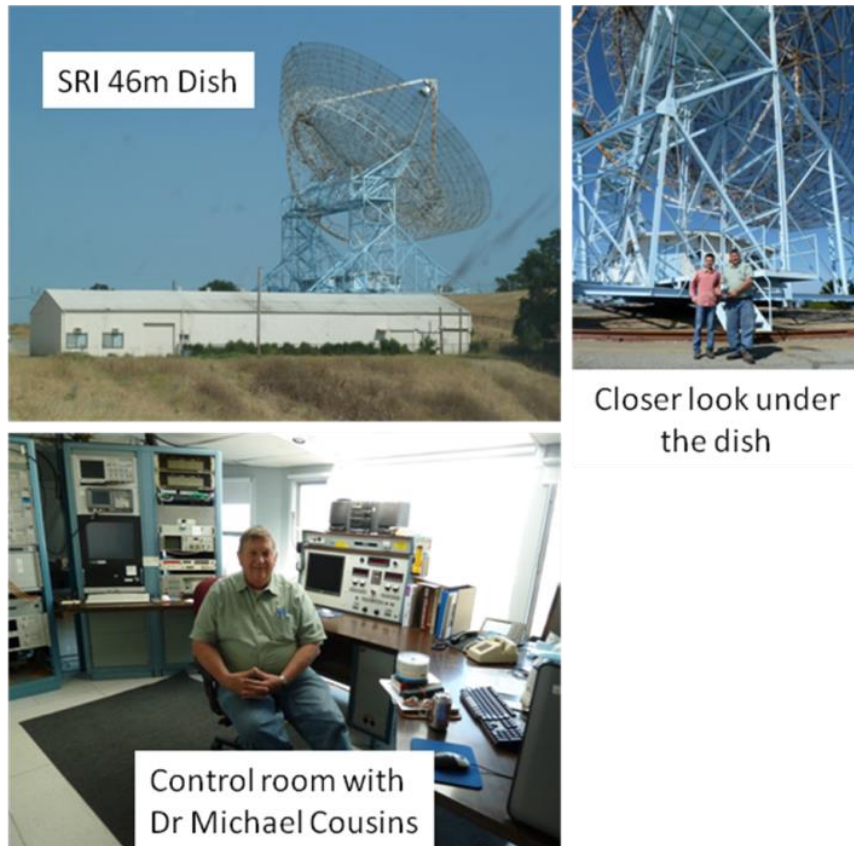
Figure B-1: SRI's Dish Antenna Facility
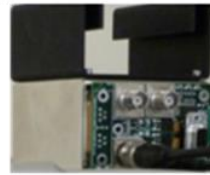
Figure B-2: Specialized data-collection equipment.
Used to collect high-rate, high-precision raw baseband data

3   Processing of Raw Data to Obtain Signal Waveform Distortions

The high-rate, high-precision data collected was processed using signal processing steps which had previously been used for characterization [7]. These are summarized here:

1. Use of high gain antenna

For both terrestrial and airborne applications, the GPS signal is ordinarily below the noise floor at the GPS receiver. To be able to obtain sufficient fidelity for signal deformation measurements using short data sets (less than 10 secs), a high gain antenna to receive the signals is necessary, such as SRI's dish antenna. Subsequent figures show the high-rate, high-precision, raw, baseband signal that was collected during the data collection campaign, for each individual satellite.

The raw baseband signal for the same satellite without the use of a high-gain dish antenna is provided for comparison (Figure B-3). The signal is buried below the noise floor; chips/bits and chip transitions are not visible. With the high-gain dish antenna, the actual C/A code chips/bits and chip transitions are visible (Figure B-4).
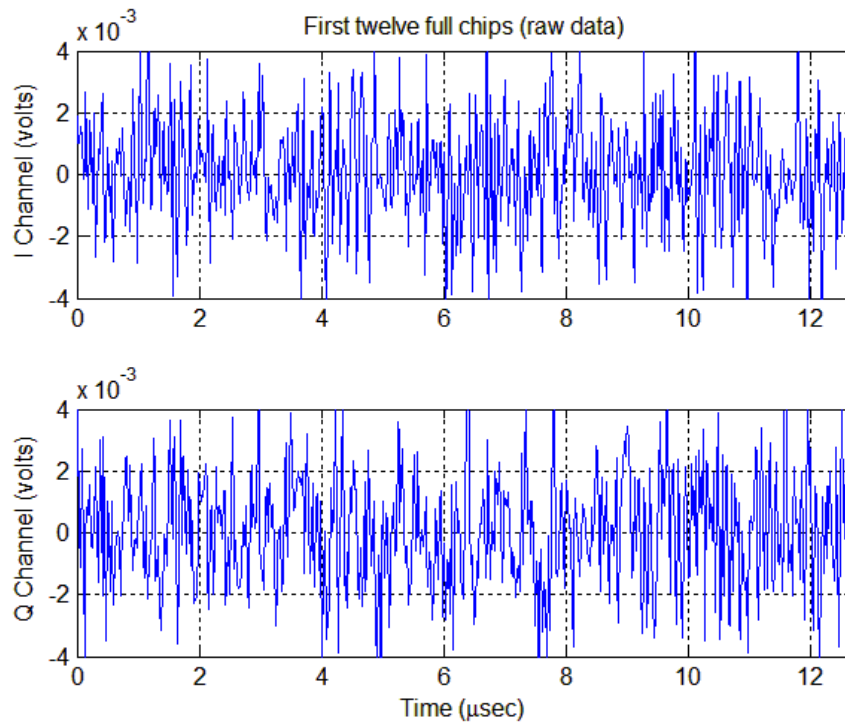
Figure B-3: Raw baseband GPS signal through regular hemispherical antenna
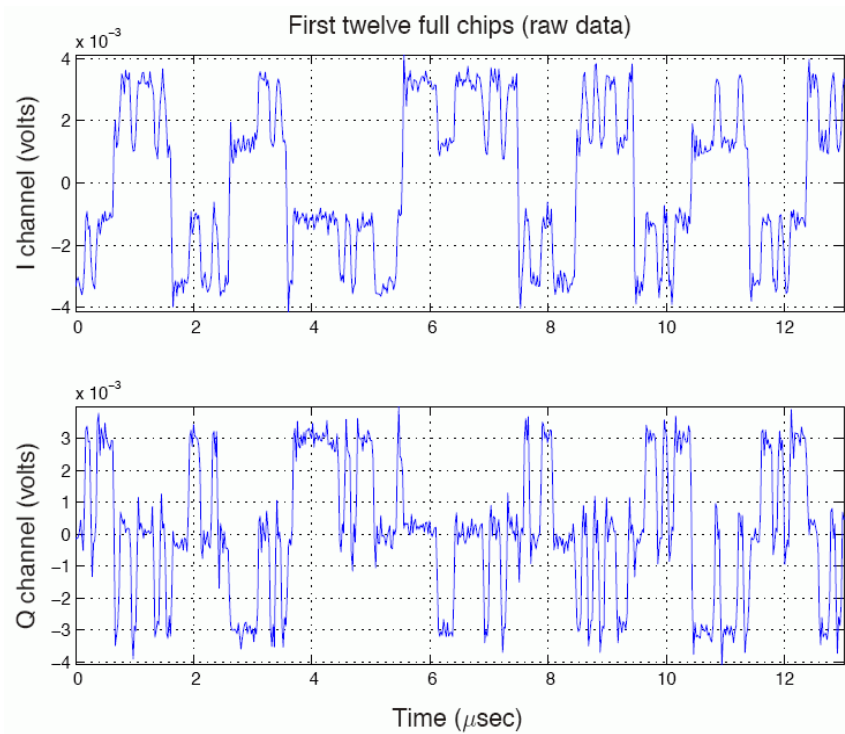
Figure B-4: Raw baseband GPS signal through high-gain dish antenna.

Figure B-4 shows that the L1-C/A code bit/ chip waveforms for civilian users, as well as the L1-P(Y) code bit/ chip waveforms for military users, are present in both the in-phase (I) and quadrature (Q) channels. Signal acquisition and tracking are next used to extract the L1-C/A signal of interest.

2.   Signal acquisition and tracking

In this process, a software GNSS receiver is used for signal acquisition and tracking. This process tracks the carrier and code phases and Doppler frequencies. These are required to extract the L1-C/A code signal of interest into the in-phase channel (Figure B-5).

As a by-product, the L1-P(Y) code signal is extracted into the quadrature channel. The figures show that the L1-C/A and L1-P(Y) code signals are separated into the in-phase and quadrature channels, respectively. In addition, the code phase estimate obtained is used in the new method for multi-period interpolation (discussed later).
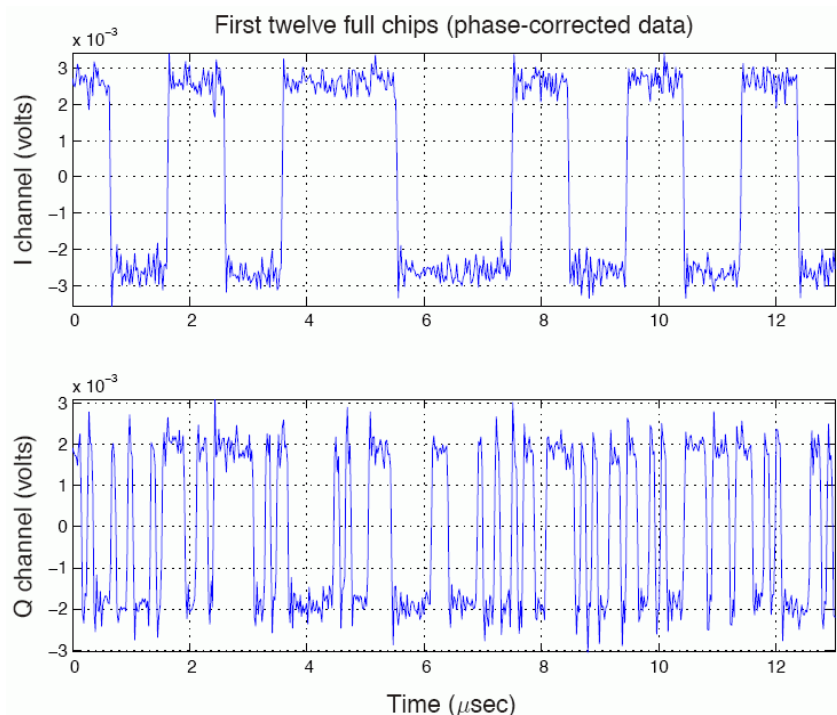
Figure B-5: Baseband signal after signal acquisition and tracking.

3. Multiple C/A code epoch averaging and interpolation

At this stage of processing, the code- and carrier-tracked signal is still very noisy. To distinguish the typically deterministic and repeatable signal deformations from the random noise, multiple epochs of 1 ms of C/A code are averaged and interpolated (Figure B-6 and Figure B-7). After multiple epoch averaging and interpolation of the in-phase tracked signal, the analog waveform deformation features are much more visible.
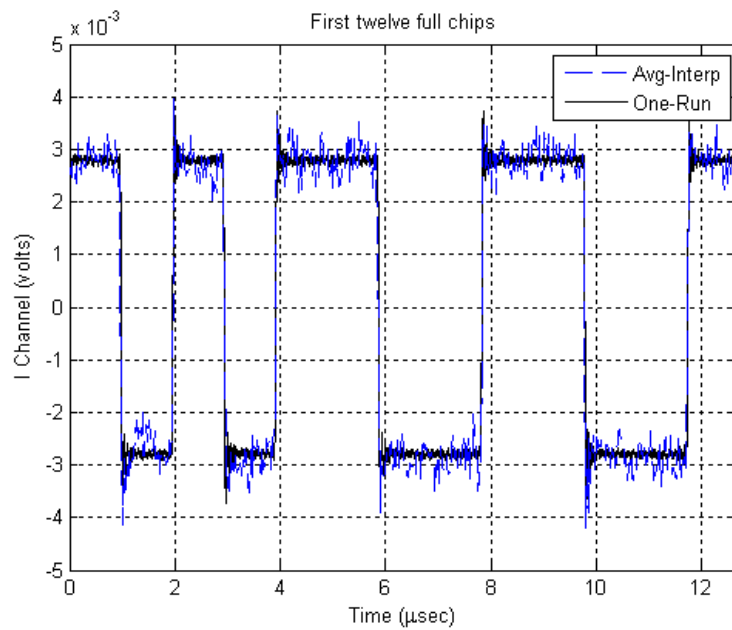
Figure B-6: Multiple epoch averaging and interpolation on in-phase tracked signal
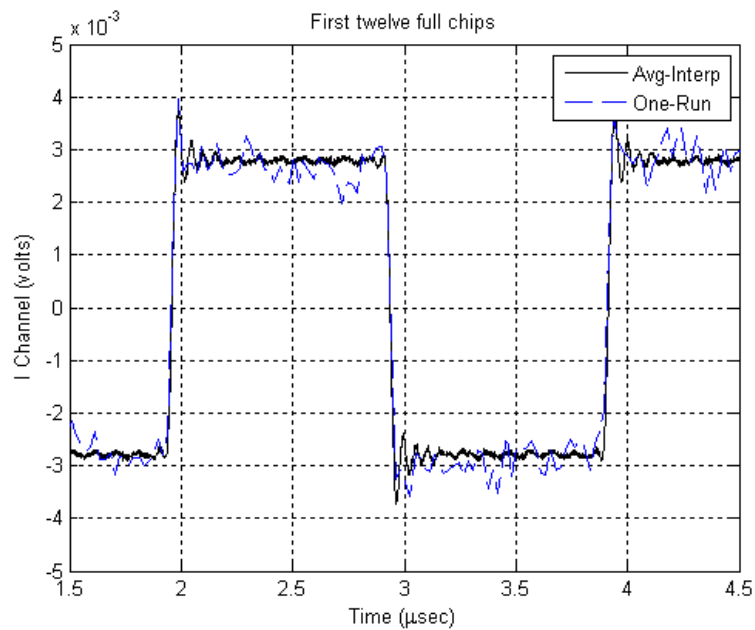
Figure B-7: Multiple epoch averaging and interpolation on in-phase tracked signal

(close-up)

Multiple epoch averaging and interpolation is thus very important to obtaining accurate characterization of the analog and digital signal deformation. An innovative method is used to speed up data collection, and perform averaging and interpolation in a single step [80], [81]. A discussion of previous methods can be found in [7].

4. Additional filtering for either noise reduction and/or interpolation

Suitable filters can be used to perform noise reduction and/or interpolation. These filters should have bandwidths much larger than typical analog signal deformation artefacts (typically 8-17 MHz).

5. Application of zero crossing determination methods

Zero crossings in the signal are extracted. These are used to determine the widths of positive and negative bits/chips, to obtain measurements of the digital signal deformation parameter Δ.

The positions of the zero crossings are also used to perform further averaging of rising- and falling-edge step responses, separately for positive and negative navigation data bits, to obtain less-noisy measurements of the analog signal deformation. At the end of this series of processing steps, measurements of signal waveform distortions are obtained.

4 Example of Refined Dish Observations of Analog and Digital Signal Distortions

This section discusses an example of refined dish measurements of analog and digital distortions and how the distortions result in range biases.

Section 4.1 shows refined dish measurements of the actual received signal waveform for Satellite PRN #2. Section 4.2 examines the waveform in further detail, which reveals the presence of analog and digital distortions (deformations). The resultant distorted correlation triangle for the actual received signal is determined in Section 4.3. The range biases can be accurately modelled and predicted by the differences of appropriately advanced and delayed correlation triangles; the process and the results are demonstrated in Section 4.4. Throughout this example, the ideal signal waveform and its derived results are provided as a reference for comparison.

4.1 Refined Dish Measurements of Satellite Vehicle ID PRN #2

Using the signal processing techniques in Appendix B-3 to process raw measurements from the SRI 46 m dish antenna, the actual GPS nominal signal waveforms are observed with high-precision. Figure B-8 and Figure B-9 show ideal and actual received signal waveforms for a typical satellite, satellite PRN #2. Instead of an ideal square waveform (Figure B-8), the actual signal received from the GPS satellite is clearly non-ideal (Figure B-9). Distortions are clearly visible; these are discussed in the next section.
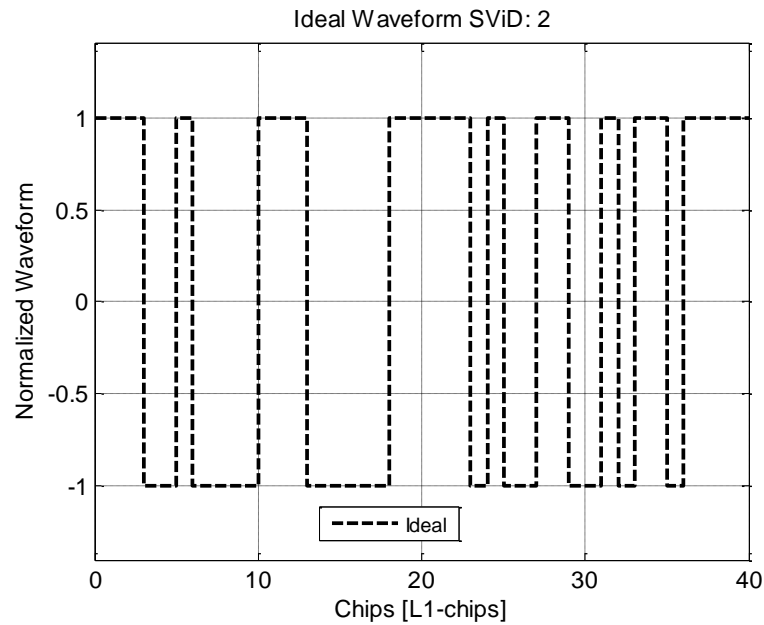
Figure B-8: Ideal Waveform of GPS Signal at L1-frequency (Satellite PRN #: 2)
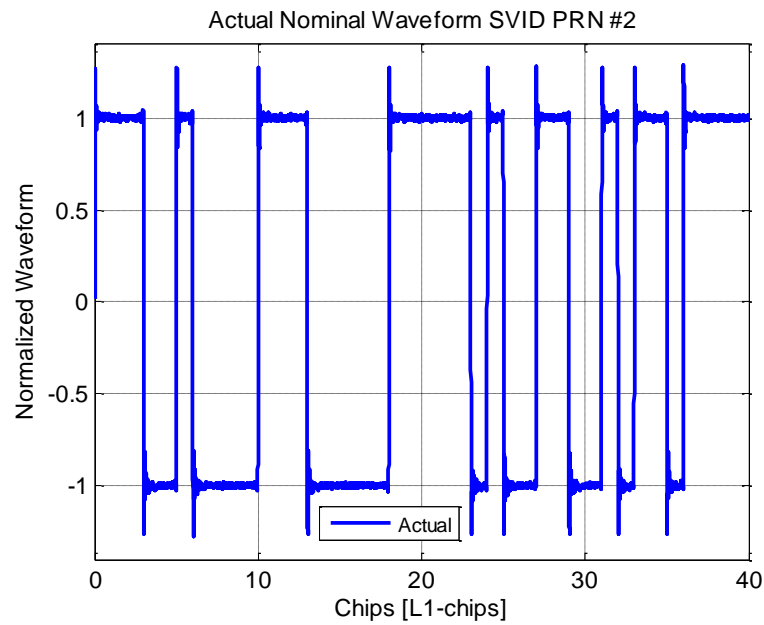
Figure B-9: Actual Nominal Waveform of GPS Satellite Signal at L1 frequency

(Satellite PRN #: 2)

4.2   Analog and Digital Deformations on Signal Waveform

A closer look at the actual signal waveform reveals the presence of two different modes of signal deformations: analog and digital deformations. Visible in Figure B-10 are analog deformations: overshoot and ringing at approximately 8.8 MHz. In Figure B-11, digital deformation is visible: the duration of the positive/HIGH chip is approximately 3 ns (≈ 0.003 chips) longer than the negative/LOW chip.
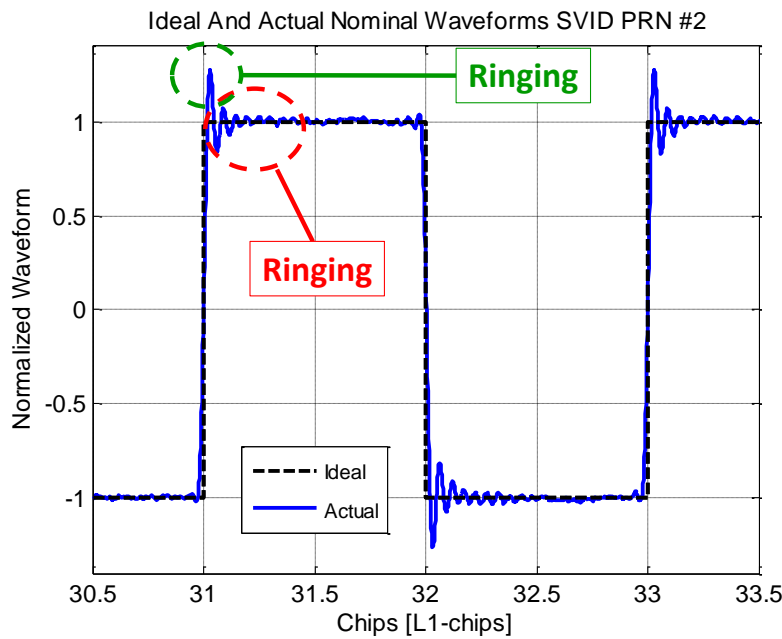
Figure B-10: Close-up view of Ideal and Actual GPS Satellite Signal Waveform at L1 frequency (Satellite PRN #2).

Analog distortions (overshoot and ringing) are clearly visible.

Figure B-11a: Ideal and Actual waveforms' start times are synchronized.	Figure B-11b: Actual waveform for the positive/ HIGH chip ends 3 ns (≈ 0.003 chips) later than ideal waveform.
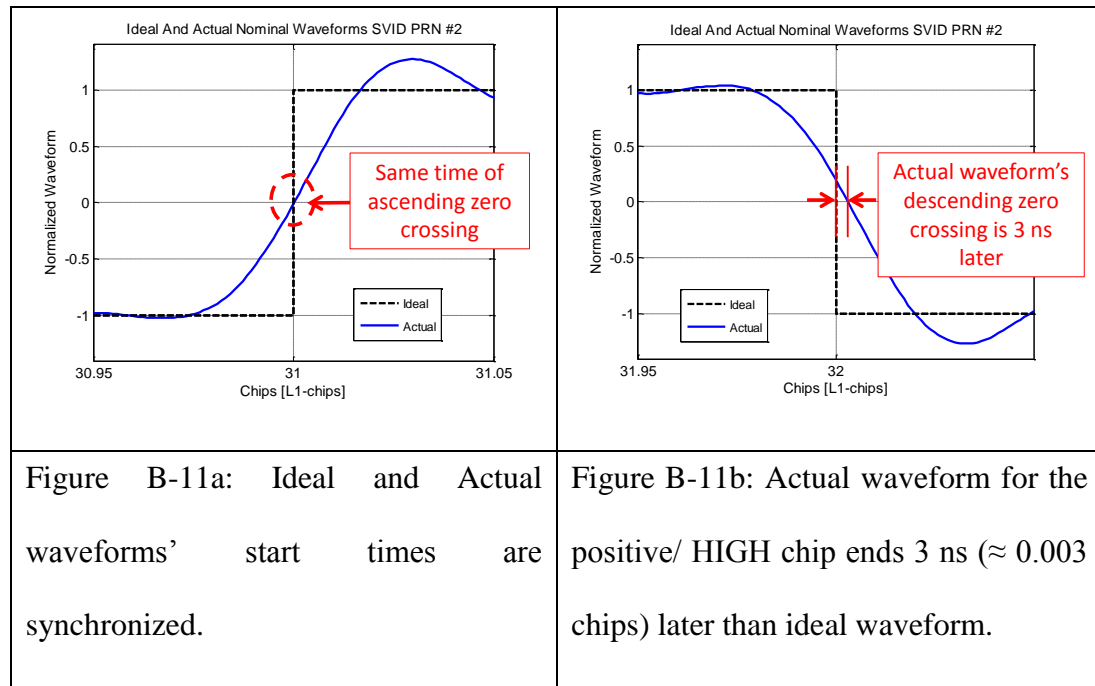
Figure B-11: Waveforms of Ideal Signal and Actual GPS Satellite Signal at L1 frequency – magnified view (Satellite ID PRN# 2).

Digital distortion is clearly visible – the positive/HIGH chip is 3 ns longer in duration than the ideal. The negative/LOW chip is correspondingly shorter in duration by the same amount (not shown in figure).

4.3   Resultant Distorted Correlation Peak from Signal Distortions

When the receiver correlates the actual received satellite signal with its internal ideal replica, the presence of analog and digital deformations results in distorted correlation triangles. Figure B-12, Figure B-13, and Figure B-14 show the correlation triangles at correlator delays of ±1.0 L1-chips, ±0.5 L1-chips, and ±0.1 L1-chips, respectively.

The correlation triangle looks ideal at the scale of ±1.0 L1-chips, but close-up views at finer scales reveal rounding of the peak and additional off-peak distortions. The effects of these correlation peak distortions on range biases are described in the next section.
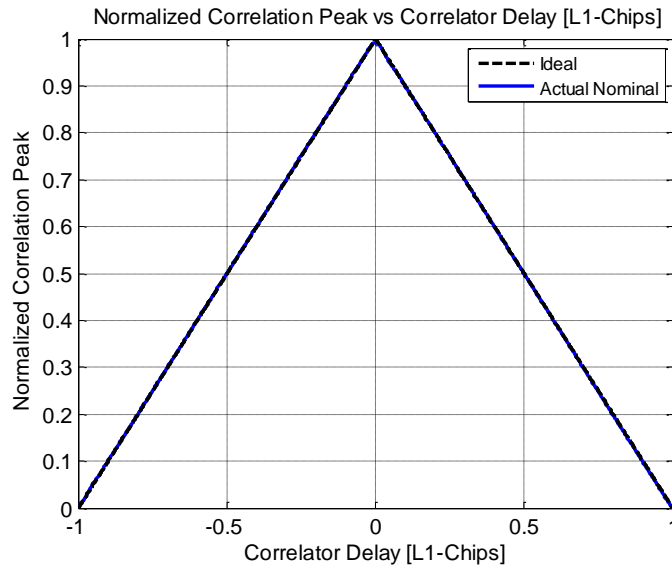
Figure B-12: Resultant Correlation Triangle from Ideal and Actual GPS Satellite

Signals at Correlator Delays of ±1.0 L1-chips (Satellite ID PRN# 2)

(Note that for correlator delays of beyond ±1.0 L1-chips, the correlation output is of

negligible magnitude)
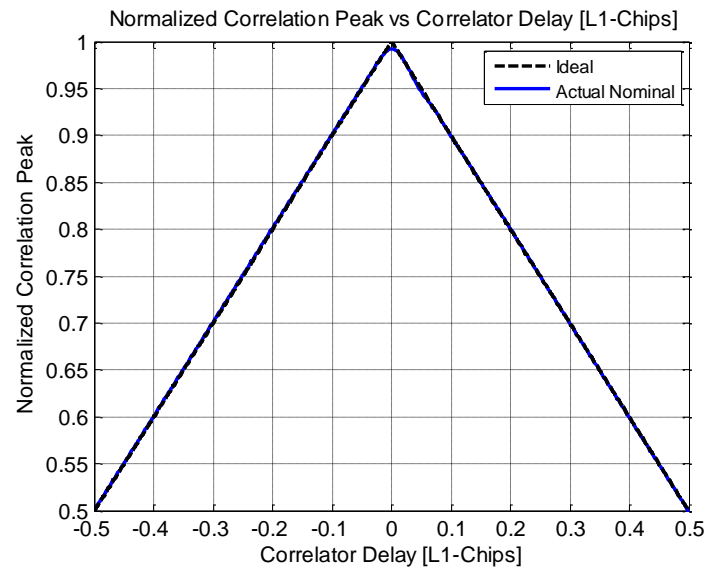
Figure B-13: Resultant Correlation Triangle from Ideal and Actual GPS Satellite

Signals at Correlator Delays of ±0.5 L1-chips (Satellite ID PRN# 2)
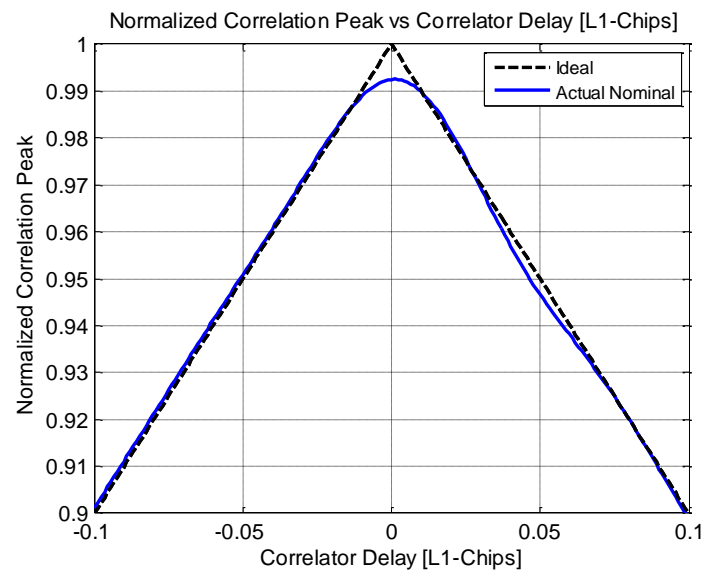
Figure B-14: Resultant Correlation Triangle from Ideal and Actual GPS Satellite

Signals at Correlator Delays of ±0.1 L1-chips (Satellite ID PRN# 2)

The next section describes how the distorted correlation triangles obtained from distorted signal waveforms can be used to predict the resultant range biases.

4.4   Resultant Range Biases in Tracking Loop

Section 2.3.3 described the code tracking process. Recall that any biases at the output of the Early-Minus-Late discriminator will lead to an erroneous estimate of the actual received signal's code phase, and a corresponding error in the estimated time of transmission at the satellite.

For any correlator spacing in the receiver tracking loop, the Early-Minus-Late discriminator output can be accurately predicted using the correlation triangles from the previous section.. For instance, the discriminator output for a correlator spacing of 1.0 L1-chips is determined by differencing the correlator triangle delayed by 0.5 L1-chips from the correlator triangle advanced by 0.5 L1-chips, and finding the zero crossing on the x-axis [82]. (That is, there is a 1.0 L1-chip offset between the Early and Late correlators.) The discriminator output is shown in Figure B-15.

Zero discriminator output should be expected for zero code phase difference, and the close-up figure (Figure B-16) shows this to be the case for the ideal signal. Unfortunately, due to the signal distortions in the actual signal, zero discriminator output instead corresponds to a non-zero chip (and time) delay. The chip bias appears small and the resultant time bias is even smaller. However, when converted to a range

bias via multiplication by the speed of light, the resultant range error is now significant

and no longer negligible: on the order of approximately ±0.2 m.
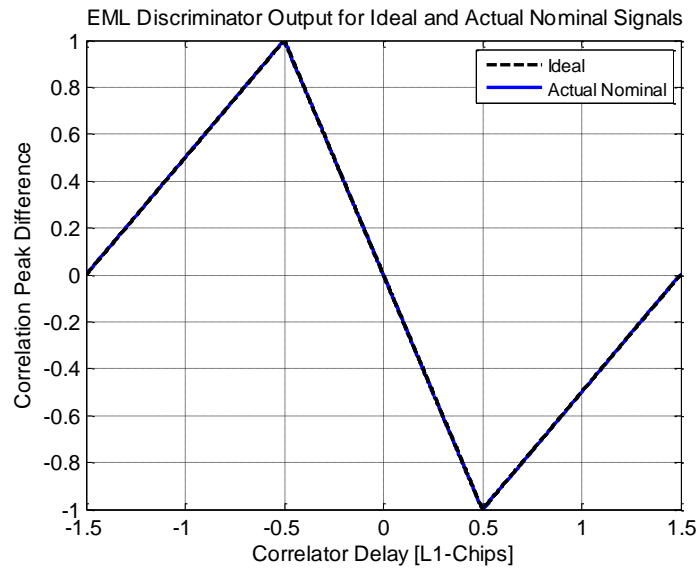
Figure B-15: Early-Minus-Late Discriminator Output for Ideal and Actual Signals at

Correlator Delays of up to ±1.5 L1-chips.

Correlator spacing (offset between Early and Late Correlators) is 1.0 L1-chips.
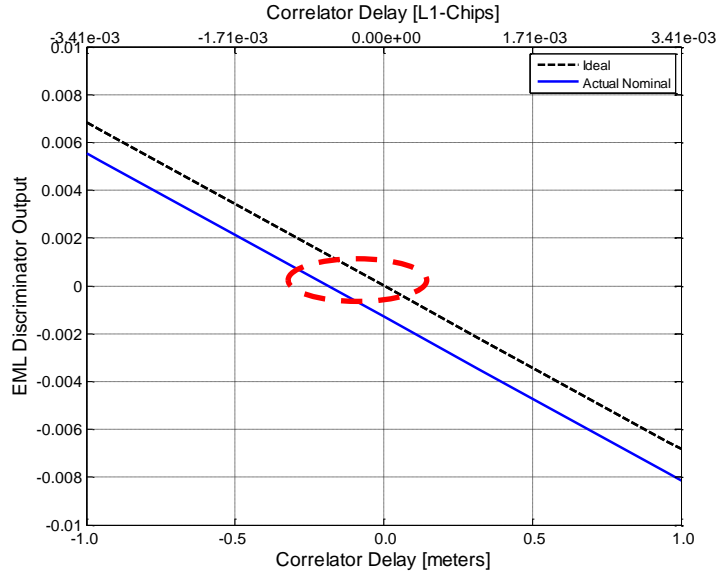
Figure B-16: Early-Minus-Late Discriminator Output for Ideal and Actual Signals –

Close-Up View

Correlator spacing (offset between Early and Late Correlators) is 1.0 L1-chips.

Figure B-17 and Figure B-18 show the predicted Early-Minus-Late discriminator
output for a correlator spacing of 0.2 L1-chips, for both ideal and actual received
signals. (That is, there is a 0.2 L1-chip offset between the Early and Late correlators.)
The predicted discriminator output is computed by differencing the correlator triangle
delayed by 0.1 L1-chips, from the correlator triangle advanced by 0.1 L1-chips.
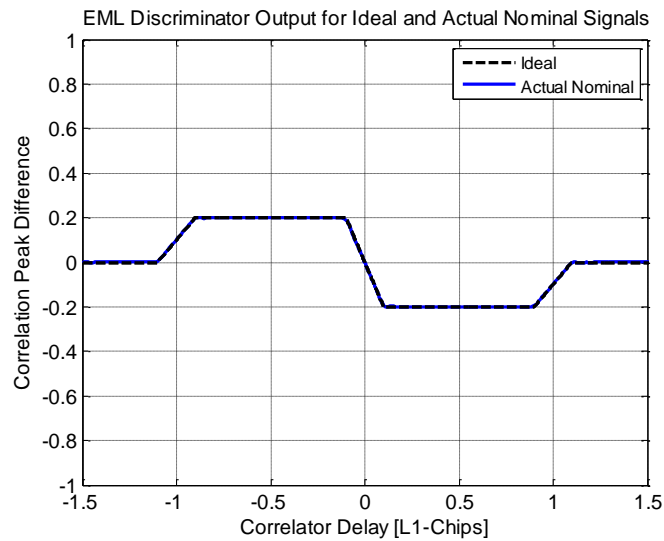
Figure B-17: Early-Minus-Late Discriminator Output for Ideal and Actual Signals at

Correlator Delays of up to ±1.5 L1-chips.

Correlator spacing (offset between Early and Late Correlators) is 0.2 L1-chips.
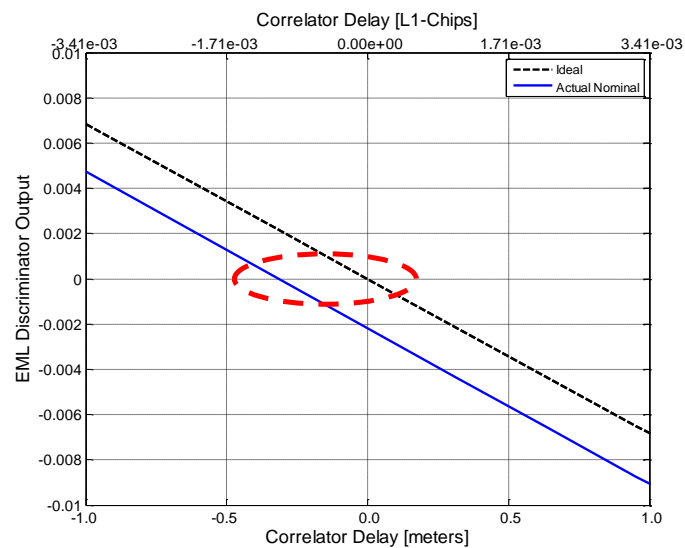
Figure B-18: Early-Minus-Late Discriminator Output for Ideal and Actual Signals –

Close-Up View

Correlator spacing (offset between Early and Late Correlators) is 0.2 L1-chips.

As in the case of Early-Minus-Late discriminator for 1.0 L1-chips correlator spacing, zero discriminator output corresponds to a non-zero chip (and time) delay due to signal waveform distortions in the actual signal. The resultant bias as measured in L1-chips and time appears negligible, but when scaled by the speed of light, the resultant range bias is no longer insignificant: -0.3 m.

The effects of signal waveform distortions on Early-Minus-Late Discriminator biases and resultant range biases are summarized in Table B-1:

Type of Signal	Type of Distortion		Range bias	
			Correlator Spacing	
	Analog	Digital [ns]	0.2 L1-Chips	1.0 L1-Chips
Ideal	-	-	0	0
Nominal	YES	3.0	-0.317 m (-1.08e-3 L1-chips)	-0.189 m (-0.643e-3 L1-chips)

Table B-1: Effects of signal waveform distortions on range biases

As seen in Figure B-16 and Figure B-18, and summarized in Table B-1, the actual induced range biases in GNSS receivers are dependent on the correlator spacings in the receiver tracking loops.

As will be demonstrated in subsequent sections, the signal waveform distortions are also dissimilar between the different satellites, leading to different range biases that

are particular to individual satellites and dependent on correlator spacings. Thus these

distortions and range biases need to be quantified separately to determine their effects

on user position errors.

5   Dish Measurements of Analog and Digital Waveform Distortions

In this section, measurement results for the digital and analog waveform distortions are shown. Figure B-19 shows a summary of these distortions for all satellites.
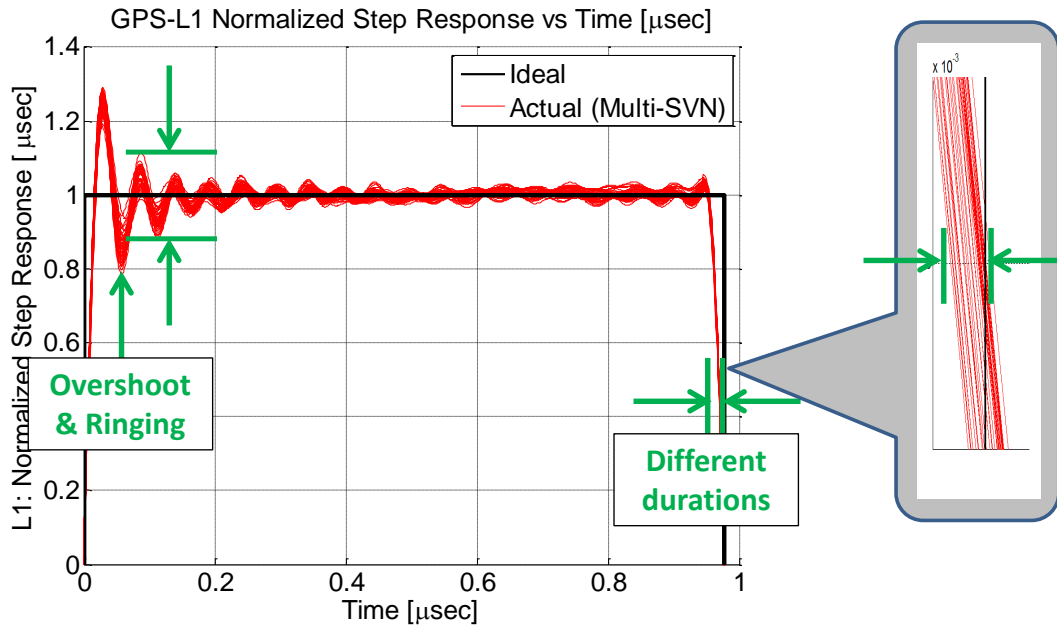
Figure B-19: Satellite signal deformations different for all GPS satellites. Data collected in August 2008, July 2009, and August 2010

Compared to the reference ideal square waveform in black, the actual received signals contain different amounts of overshoot and ringing. The individual satellite waveforms are also of different durations (Appendix B-4.2). Though these differences between the individual waveforms are small, they lead to correlation triangles whose distortions are different for individual satellites (Appendix B-4.3). In turn, these result in differential range biases when the reference receiver configuration differs from that

of the user receiver (Appendix B-6). These analog and digital distortions are discussed in further detail in the subsequent sections.

5.1 Analog Distortion Results

Figure B-20 and Figure B-21 show the chip-shape waveforms of the received signal from the satellites, derived from raw SRI 46 m dish measurements collected in August 2008, July 2009, and August 2010. Analog distortions are visible in the chip-shape waveforms. The chip-shape waveforms and analog distortion measurements in the two figures are very similar for the entire constellation of L1-frequency GPS satellite signals, and show consistency over different time periods of measurement.

Note that these chip-shape waveforms include the effects of ground filtering. These are not expected to be significant given the bandwidth of the ground equipment (36 MHz in the Vector Spectrum Analyzer) in comparison to that of the analog distortion ($\sim$ 8 – 17 MHz).
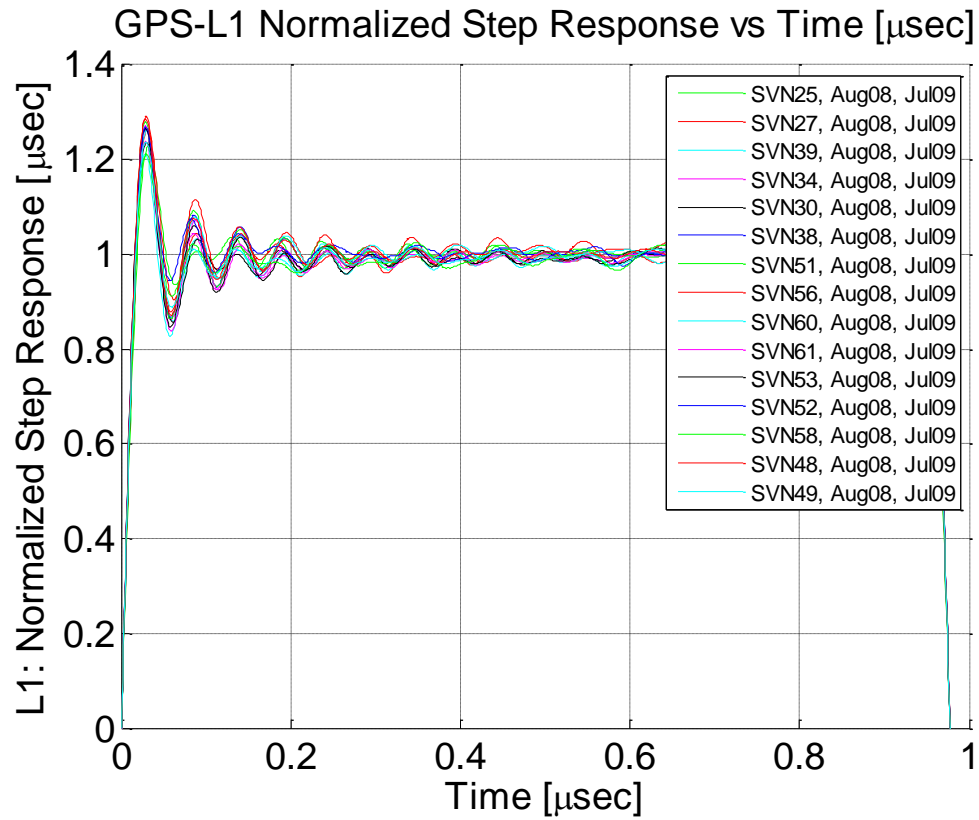
Figure B-20: Chip-shape waveforms showing analog distortions for GPS satellite

signals at L1 frequency based on SRI dish data measurements made in August 2008

and July 2009
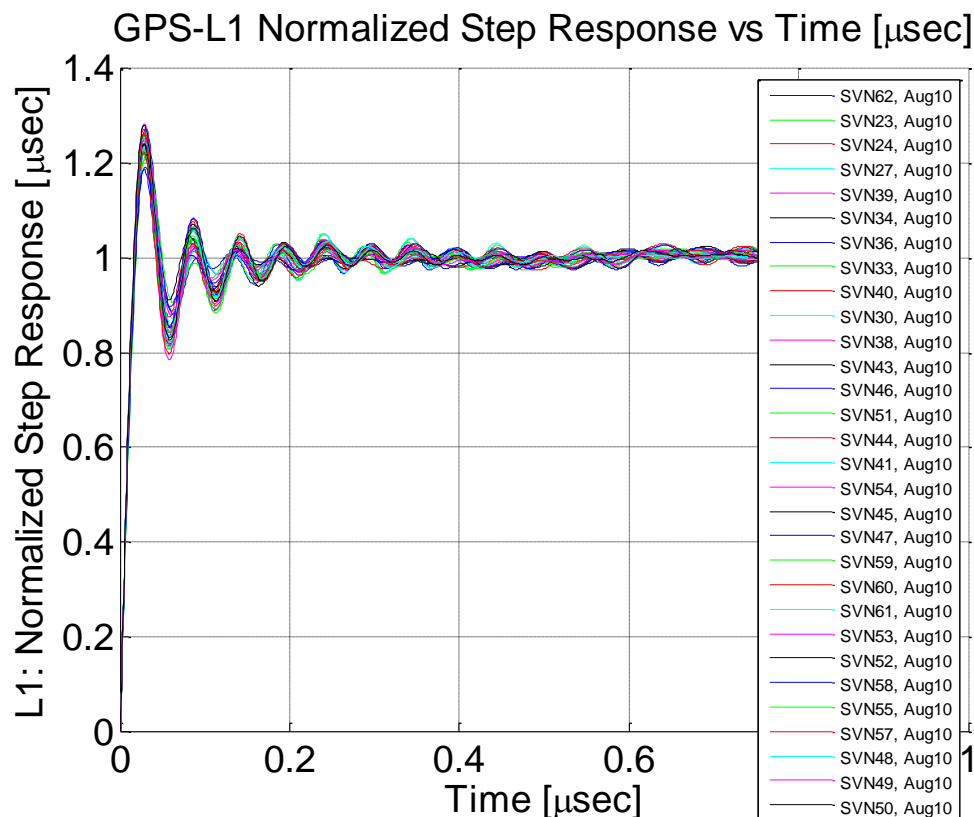
Figure B-21: Chip-shape waveforms showing analog distortions for GPS satellite

signals at L1 frequency based on SRI dish data measurements made in August 2010

Furthermore, the newly launched satellite PRN25/ SVN62, the first of the new set of

satellites with dual frequency (L1/L5) signals, has similar analog distortion

characteristics comparable to the legacy set of L1-only GPS satellite signals. This is

shown in subsequent graphs in the next section.

5.2   Analog Distortion Results for Newly-Launched GPS Satellite PRN25/ SVN62

PRN25/ SVN62, the first of a new block of GPS satellites (Block IIF), was launched in May 2010 and declared operational in August 2010. Unlike past GPS satellites, this satellite transmitted signals at both the legacy L1-frequency (1575.42 MHz) and the new L5-frequency (1176.45 MHz). The waveform distortion measurement technique was applied to signals at both these frequencies to determine if there were any signal anomalies.

The chip shape waveforms in Figure B-22 demonstrate visible analog distortion for the L1-frequency signal of the newly-launched SVN62. This distortion lies within the set of analog distortions for all other satellite signals and does not look anomalous. As before, these waveforms include the effects of ground filtering, which are not expected to be significant given the relative bandwidths of the ground equipment and analog distortions.
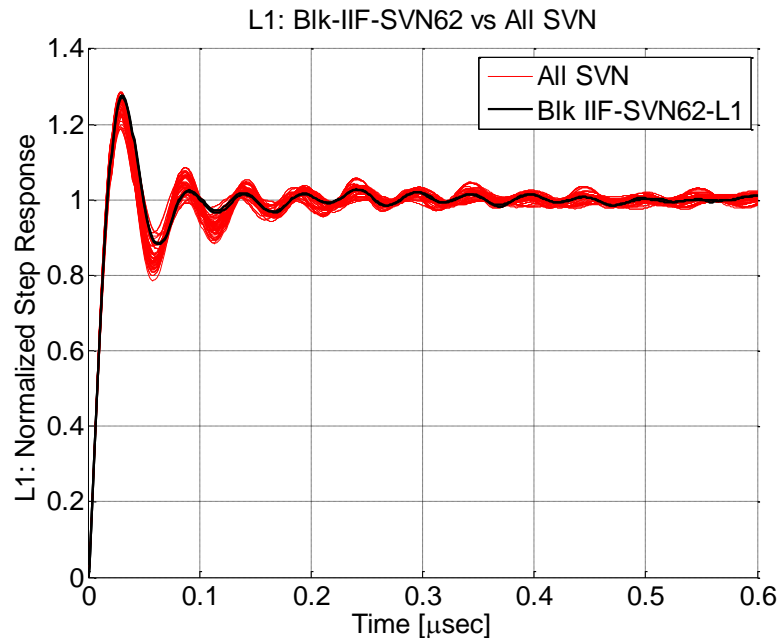
Figure B-22: Chip-shape waveforms showing analog distortion of the SVN62 GPS

satellite signal at L1-frequency, based on SRI dish data measurements made in August

2010.

Shown together with all other GPS satellite signals at L1 frequency.

For both the in-phase and quadrature SVN62-L5 frequency signal, the chip rate is ten

times that of L1, leading to a chip pulse duration 10 times narrower. Thus, for

meaningful comparison, continuous chips of duration 5 L5-chips and above were

averaged to form step response curves. This was done separately for the in-phase and

quadrature signals. The results are shown in Figure B-23. Just as for the L1-frequency

signals, the analog distortions in the SVN62 L5-frequency in-phase and quadrature

signals look very similar to those of the other GPS satellites at L1 frequency. As

before, these waveforms include the effects of ground filtering, which are not expected

to be significant given the relative bandwidths of the ground equipment and analog
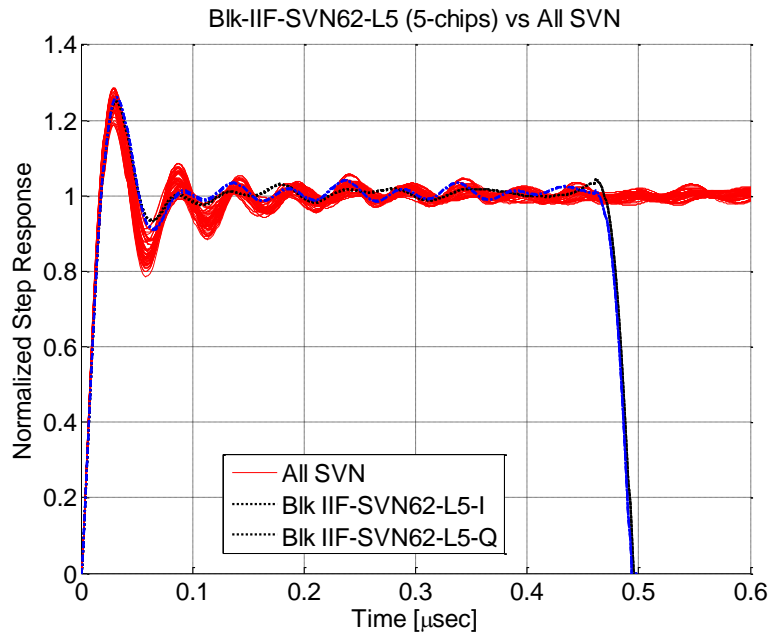
distortion.

Figure B-23: Chip-shape waveforms showing analog distortion in the SVN62 GPS

satellite signal at L5-frequency, based on SRI dish data measurements made in August

2010

Figure B-24 and Figure B-25 show the chip-shape waveforms for SVN62-L5 in-phase

and quadrature signals averaged over 1, 2, 3, 4, 5, and 6 chips separately. As before,

the L5-frequency analog distortions visible in the chip-shape waveforms of different

chip-durations look very similar to those contained in the legacy L1-frequency signals.
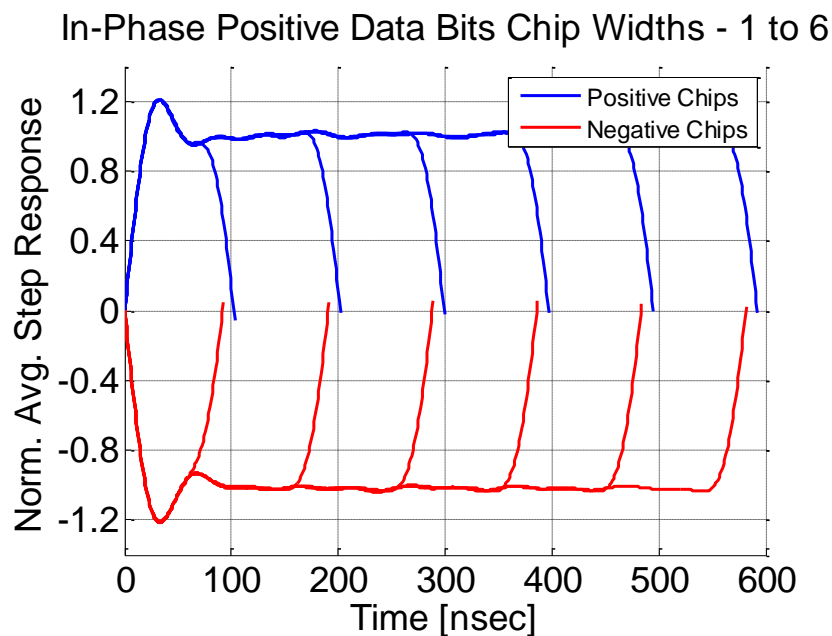
Figure B-24: Chip-shape waveforms showing analog distortions for SVN62 – L5- In-

Phase
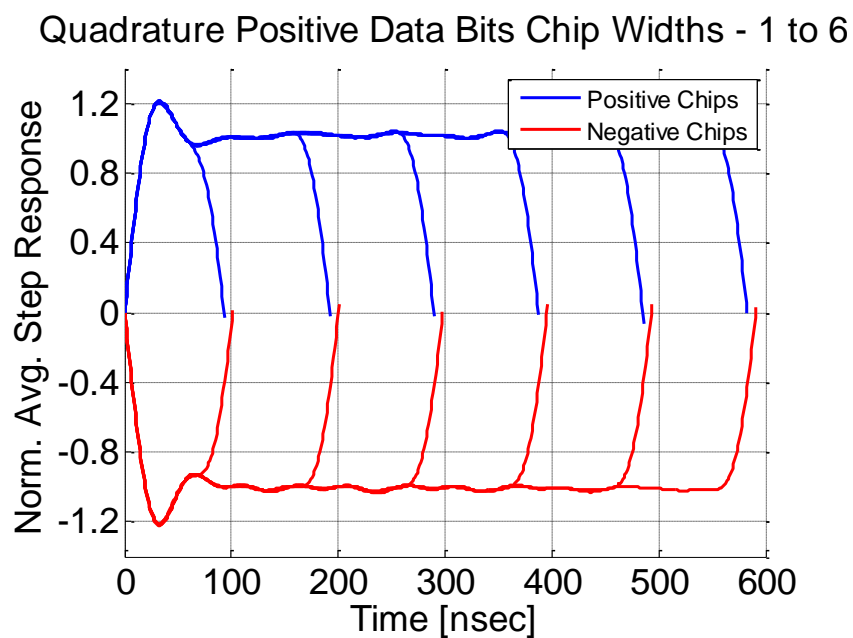
Figure B-25: Chip-shape waveforms showing analog distortions for SVN62 – L5-

Quadrature

5.3   Digital Distortion Results

Previous sections described the analog distortion results for all the L1-frequency GPS signals, and the first L5-frequency signals. This section presents the digital distortion results, which, as seen in Appendix B-4.3 and Appendix B-4.4, also contribute to range biases in user receivers.

Digital distortions seem to change very little even over time periods of years. Figure B-26 shows measurements of the digital distortion parameter, Δ, for past and current GPS satellites which are in common. As can be seen, the digital distortion results for many of the common GPS satellites demonstrate remarkable constancy over time periods as long as nine years apart.
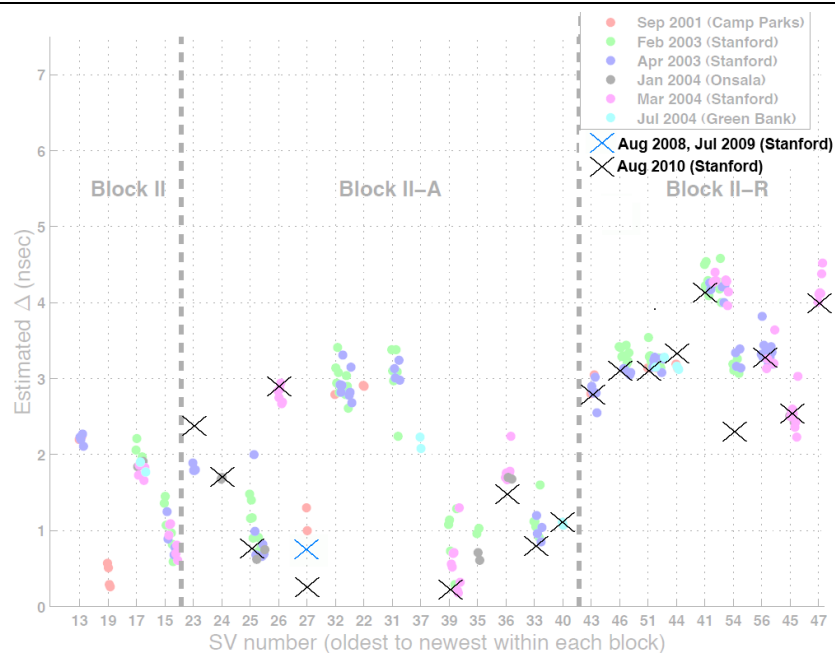
Figure 6.19: Delta estimates by satellite block

Figure B-26: Comparison of digital distortion parameters Δ for past and current

common GPS satellites

Figure B-27 shows a summary of the digital distortion parameter Δ for the entire

current constellation of GPS and WAAS-GEO satellite signals for both L1 and L5

frequencies. At the time of data measurement collection at the SRI Dish in August

2010, most of the satellites only transmitted signals at the L1 frequency; one GPS

satellite (PRN 25) transmitted signals at both the L1 and L5 frequencies.
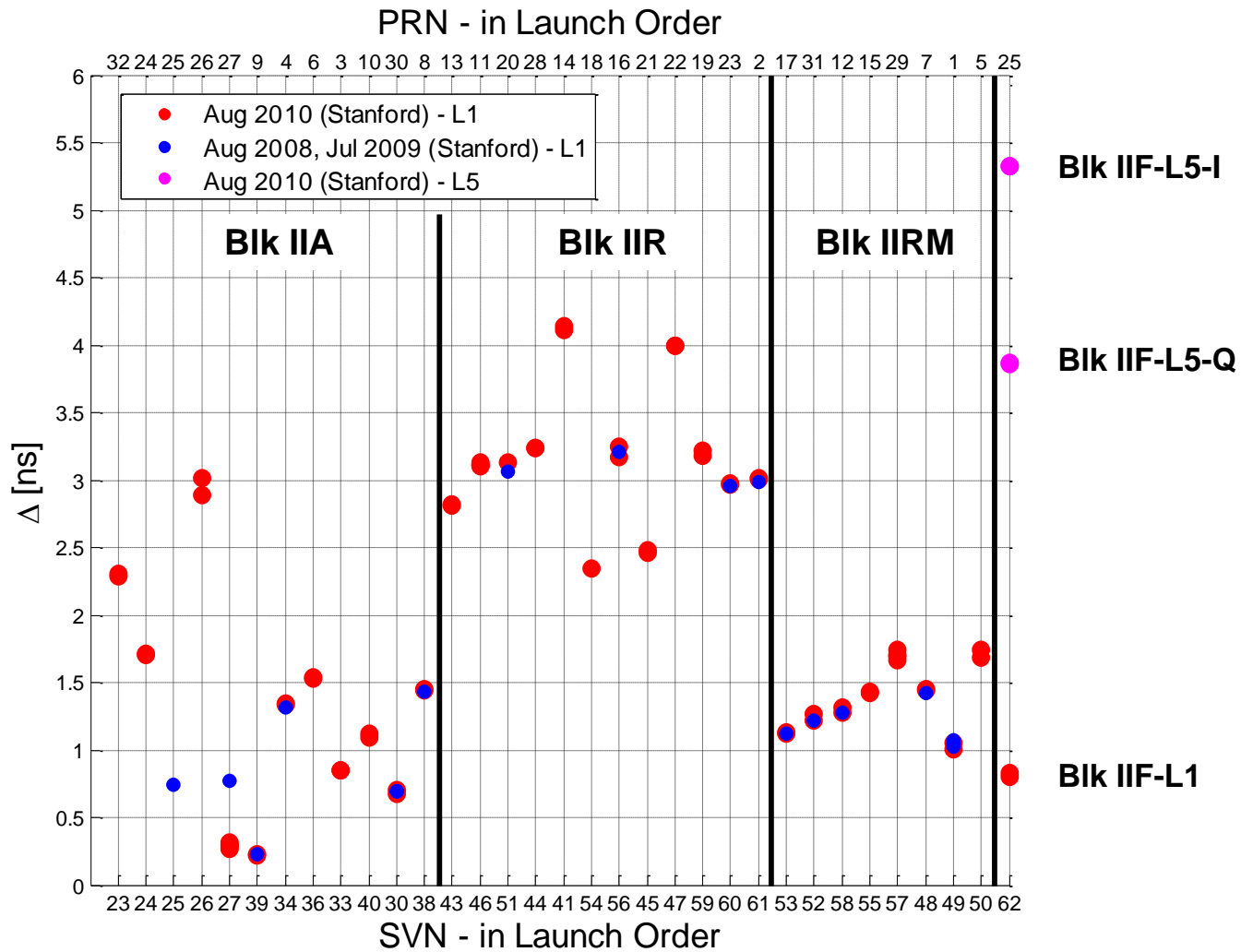
Figure B-27: Digital distortion parameter Δ for GPS satellite signals.

The figure shows the trends in the blocks of satellites. In particular, for GPS, Block IIA and Block IIR-M satellite signals tend to have smaller average digital distortions than Block IIR satellite signals. All the digital distortion parameters are within the nominal specifications (10 ns) [83].

The digital distortion parameters of the entire constellation serve as a useful reference standard to qualify signals for newly launched future satellites. For the L1-frequency, the most recently launched satellite SVN62's digital distortion parameter Δ is comparable to that of other past satellites. The corresponding parameters for L5-In-phase and L5-quadrature signals are higher than that for past satellites, but are still within the nominal specifications of 10 ns [83].

Observation of Digital Distortion in the Chip-Shape Waveforms

Earlier, the chip-shape waveforms for the newly launched satellite, PRN25/SVN62, were displayed for signals transmitted at both the L1-frequency and the L5-frequency. The digital distortions are barely visible in the L1-frequency chip-shape waveforms, because the digital distortions are a very small proportion of the L1-chip duration: less than 5 ns / 977.5 ns = 0.5%.

In contrast, because the L5-frequency chips are 10 times shorter in duration, the digital distortions now occupy a more substantial ratio of the duration of the entire chip waveform. Thus the digital distortions are observable in the L5-frequency chip-shape

waveforms; the digital distortion magnitudes also correspond to the analyzed digital

distortion values. This confirms the intuition of "digital" distortion – distortions that

do not scale linearly with time or chip-duration, but rather remain virtually constant

regardless of chip duration.

In the in-phase chip-shape waveforms in Figure B-28, digital distortions are visible.

The positive chips are on average 5.5 ns longer in duration than nominal, and the

negative chips are on average 5.5 ns shorter than nominal. Note that these distortions

Δ_I are approximately constant regardless of chip durations.
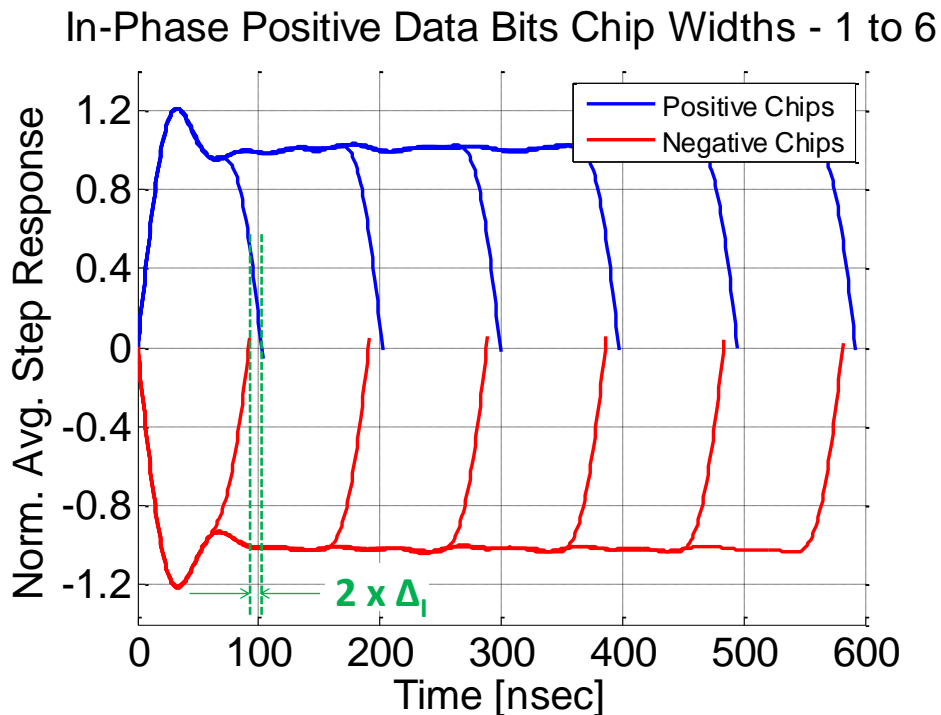
Figure B-28: Chip-shape waveforms showing digital distortion – SVN62 L5-In-phase

Similarly, in the quadrature signal waveforms in Figure B-29, digital distortions are visible. The positive chips are on average 3.9 ns shorter in duration than nominal, and the negative chips are on average 3.9 ns longer than nominal. As before, these distortions Δ_Q are approximately constant regardless of chip durations.
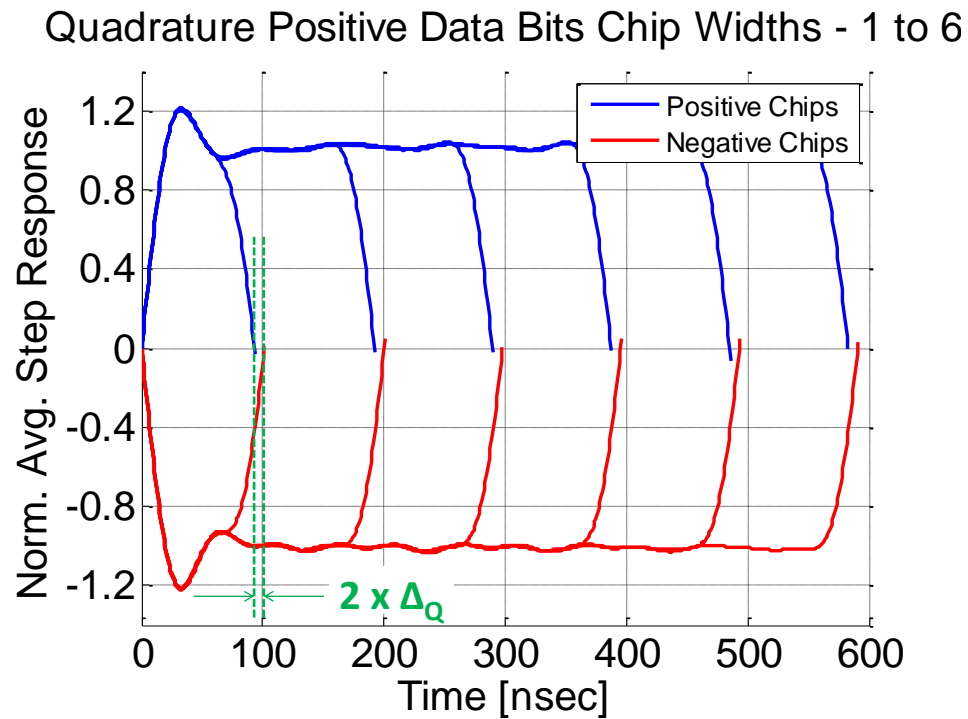
Figure B-29: Chip-shape waveforms showing digital distortion - SVN62 L5-

Quadrature

6   Resultant Range Biases from Waveform Distortions

The resultant range biases for each individual GPS satellite are determined in this section, based on the high resolution waveform measurements from the previous sections. This is accomplished by a series of signal processing steps which mimic the operations in an actual GPS receiver. These steps helped determine the differential range biases experienced by users of various receiver configurations.

The first two processing steps, correlation and discriminator (Steps 1 and 2), are identical to the correlator and discriminator functions in a GPS receiver tracking loop.

The resultant measured range biases contained time-varying drifts which were different in signals measured during different time periods (Step 4). These were corrected using estimates from reference WAAS-GEO range biases measured in the same time-periods (Step 5).

To determine the differential range biases experienced by users with different receiver correlator spacings, the range biases at the WAAS reference receiver correlator spacings (0.1 L1-chips for the L1-frequency signal and 1.0 L5-chips for the L5-frequency signal) were used as the "truth" and subtracted from the range biases at all other correlator spacings (Step 3). The average of the range biases across all satellites was also subtracted from the range biases at all other correlator spacings, to mimic actual receiver output (Step 6).

These processing steps are described in detail:

1. Correlation

Points on the correlation triangle are formed by correlating the SRI-dish code waveform with ideal replicas at various delays and advances of up to 1 chip.

(In practice, given the large number of correlator output points available for the interpolated code chip waveform, the correlation is performed using the Fast Fourier Transform method.)

In the example below in Figure B-30, ideal replicas advanced and delayed by 0.1, 0.2, 0.3, and 0.4 chips are used to form early and late correlator outputs E1 and L1, E2 and L2, E3 and L3, and E4 and L4 at these chip spacings. Correlating the ideal replica without advances or delays with the received signal gives us the P (Prompt) correlator output.

P, E1-E4, and L1-L4 form discrete points on the correlation triangle (Figure B-31). Using more finely spaced advanced and delayed ideal replica chip spacings produces the entire correlation triangle. The ideal correlation triangle, formed by correlating an ideal replica code (without advances or delays) with itself, is shown in blue. Just for

illustration, shown in red is a correlation "triangle" with artificially large injected errors.
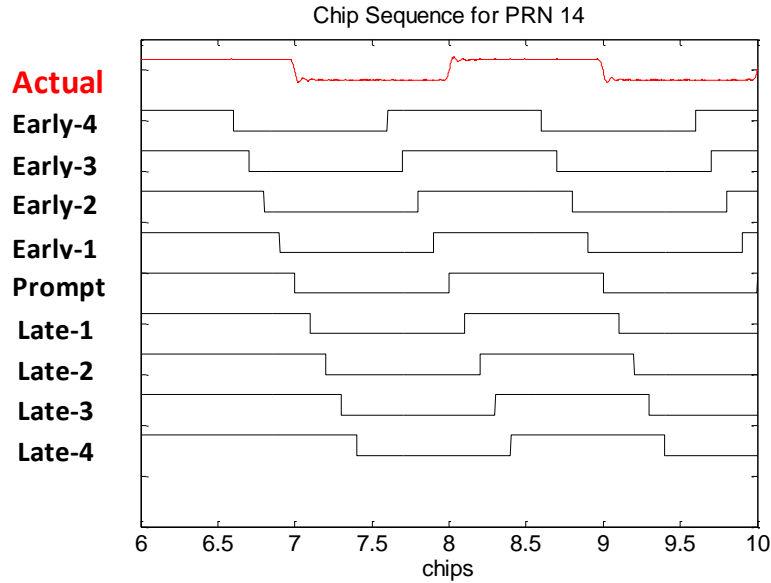
Figure B-30: Form early, prompt and late replicas at different delays/ advances and

correlate with actual code-sequence
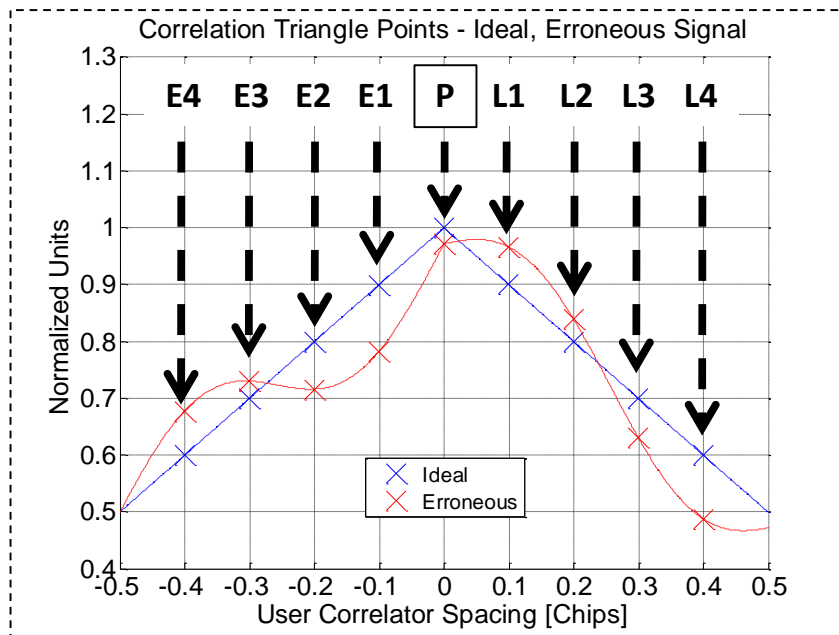
Figure B-31: Points on correlation triangle for each different delay/ advance

2. Discriminator Operation in Tracking Loop

These non-ideal correlation triangles are used to compute the resultant range biases at the output of the tracking loop. An actual early-minus-late discriminator can be used, but here a close approximation is used instead which is much more computationally efficient.

This approximation involves taking simple differences between corresponding points on the correlation triangle in Figure B-31, for example, E1 − L1, E2 − L2, E3 − L3. Next the differences are normalized and scaled. The scale factor K used to scale the normalized differences is computed as follows:

$$K = \frac{1}{2P} * \frac{1}{f_{CA}} * c \tag{1}$$

where

f_{CA}:   *frequency of GPS-L1C/A Code*

c: *speed of light*

P: *value of prompt (P) correlation*

Finally the normalized and scaled differences are plotted against the absolute horizontal distance (chips) between the points. For instance, the absolute horizontal distance between E1 and L1 is abs(-0.1 − (+0.1)) chips = 0.2 chips. Satellite signal deformation range biases at the output of the tracking loop are obtained in this way.

Figure B-32 shows the satellite signal deformation range biases for the ideal signal as well as the illustration signal with artificially large injected errors.
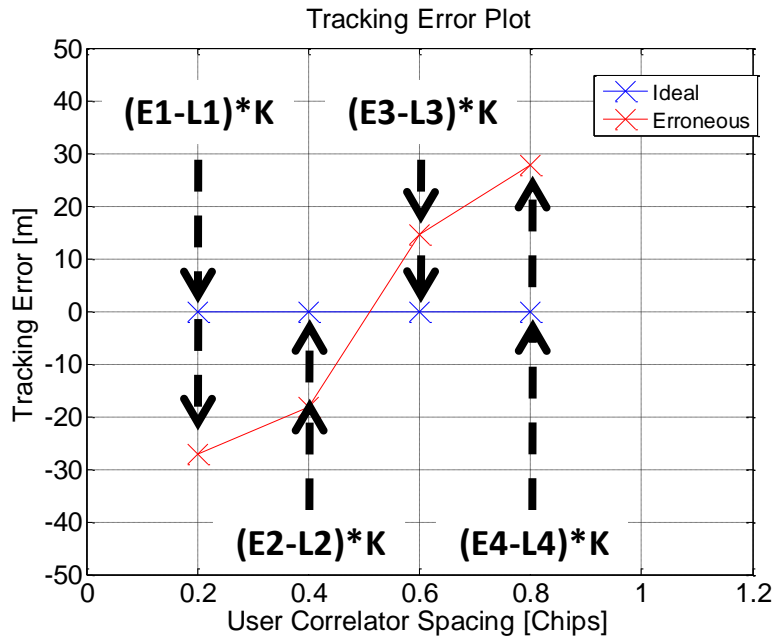
Figure B-32: Satellite signal deformation range biases for ideal and erroneous signals

3. Offset all satellite signal deformation range bias curves by their values at reference correlator spacing

This step is performed since the concern is over *differential errors* (not absolute errors) experienced by user receivers when their correlators are configured differently from reference receiver correlators. Again, these differential errors are different for different satellites and correlator spacing pairs.

The following sets of satellite signal deformation range bias curves are for reference correlator spacings of 0.1 chips and 1 chip, respectively (Figure B-33 and Figure B-34).

Since 0.1 chips is the typical reference receiver correlator spacing in the WAAS reference system setup, subsequent discussion will focus exclusively on this reference correlator spacing.
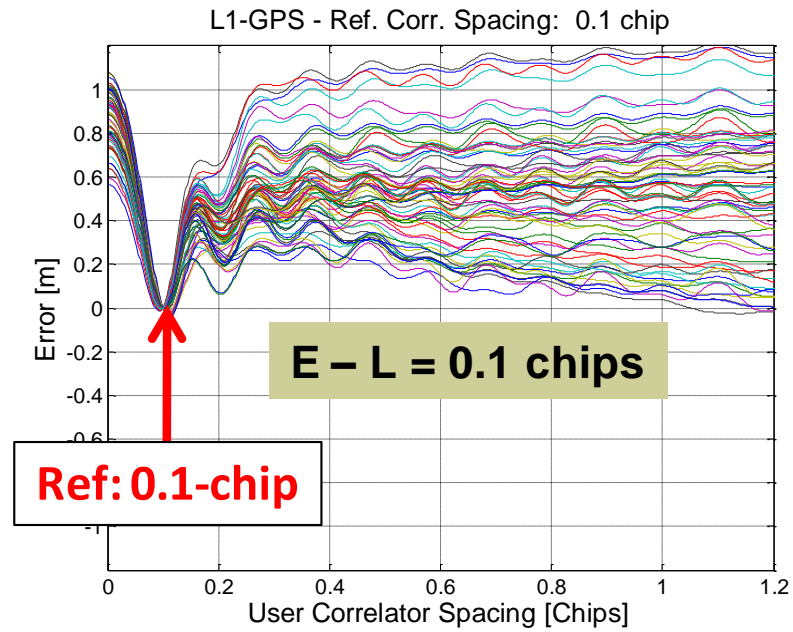
Figure B-33**:** Satellite signal deformation range biases for reference correlator spacing of 0.1 chips.
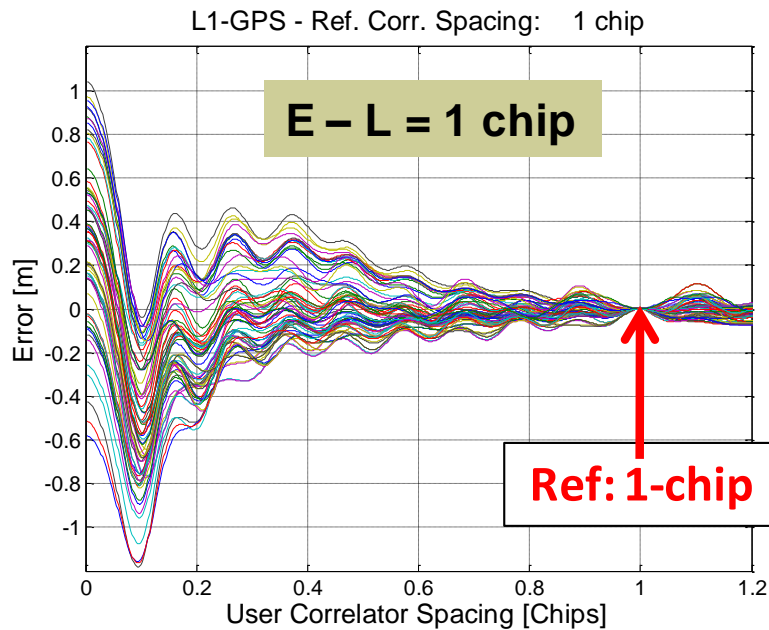
Figure B-34**:** Satellite signal deformation range biases for reference correlator spacing

of 1 chip.

These two sets of curves are virtually identical. The difference is that each set is

referenced to a reference receiver with a different correlator spacing (0.1 chip for

Figure B-33 and 1 chip for Figure B-34)**.** The curves show very similar variation from

satellite to satellite across each set.

4. Presence of Time-Varying Drifts in SRI-Dish Data

The satellite dish data was collected in four time periods on August 3-4, 2010:

1. Aug 4 UTC 0-4 hours (PST 5pm-9pm Aug 3)

2. Aug 4 UTC 7-10 hours (PST 12am-3am Aug 4)

3. Aug 4 UTC 14-16 hours (PST 7am-9am Aug 4)

4. Aug 4 UTC 21-23 hours (PST 2pm-4pm Aug 4)

The satellite signal deformation range bias curves for the different time periods appear to exhibit time-varying drifts. Figure B-35 shows these curves for a reference receiver correlator spacing of **0.1 chips**. Satellite signal deformation range biases for the entire day are in green, while satellite signal deformation range biases for the time period of interest are highlighted in red. Compared to time period 1 (Figure B-35a), satellite signal deformation range biases for time periods 2 and 3 (Figure B-35b and Figure B-35c) seem to have a positive bias at some correlator spacings, while time period 4 (Figure B-35d) seems to have a negative bias.

Figure B-35a: Time period 1 highlighted.

Figure B-35b: Time period 2 highlighted.

Figure B-35c: Time period 3 highlighted.

Figure B-35d: Time period 4 highlighted.

Figure B-35: Satellite signal deformation range biases for data collected at different times of day.
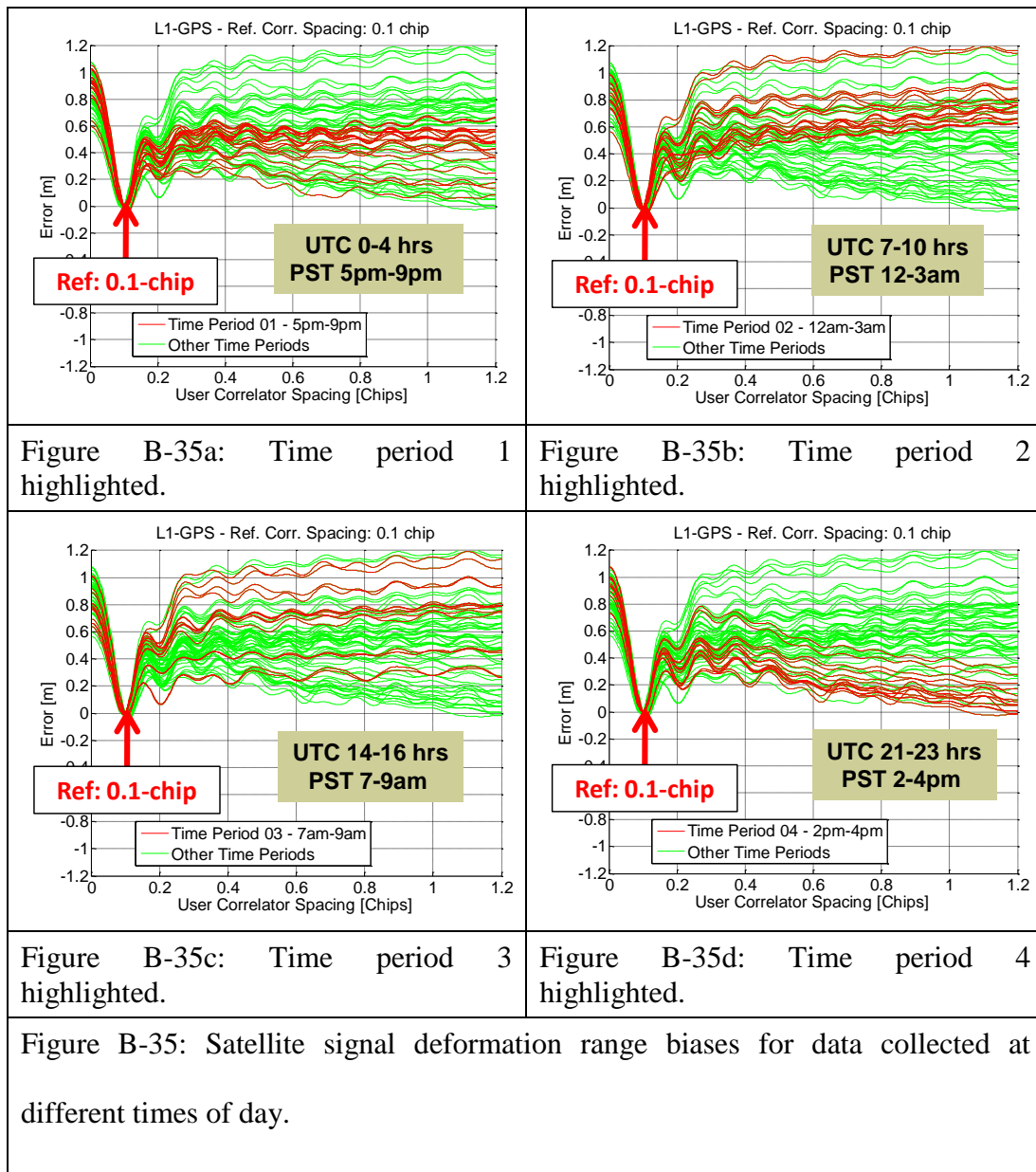
5.   Removal of Time-Varying Drifts in SRI-Dish Data

Examining the signal waveforms from the three WAAS-GEO satellites, also collected in the same time periods, confirmed the presence of these time-varying drifts. Figure B-36 shows these differences for GPS and individual WAAS-GEO satellite signals.

The time-varying drifts were estimated using the average of the three WAAS-GEO satellite signal waveforms, and used to correct the drifts in the GPS signal waveforms.

As Figure B-36 shows, the estimates of these time-varying drifts differed by up to ±0.2 m between the different WAAS-GEO satellites. This could possibly be due to time-varying thermal effects on the satellite dish, signal feedhorn, and filter, even over a short duration of minutes.

Figure B-36a: GPS signals

Figure B-36b: WAAS-GEO PRN133 signals

Figure B-36c: WAAS-GEO PRN135 signals

Figure B-36d: WAAS-GEO PRN138 signals

Figure B-36: Differences between the average over all time periods, and the satellite signal deformation range biases in different time periods.
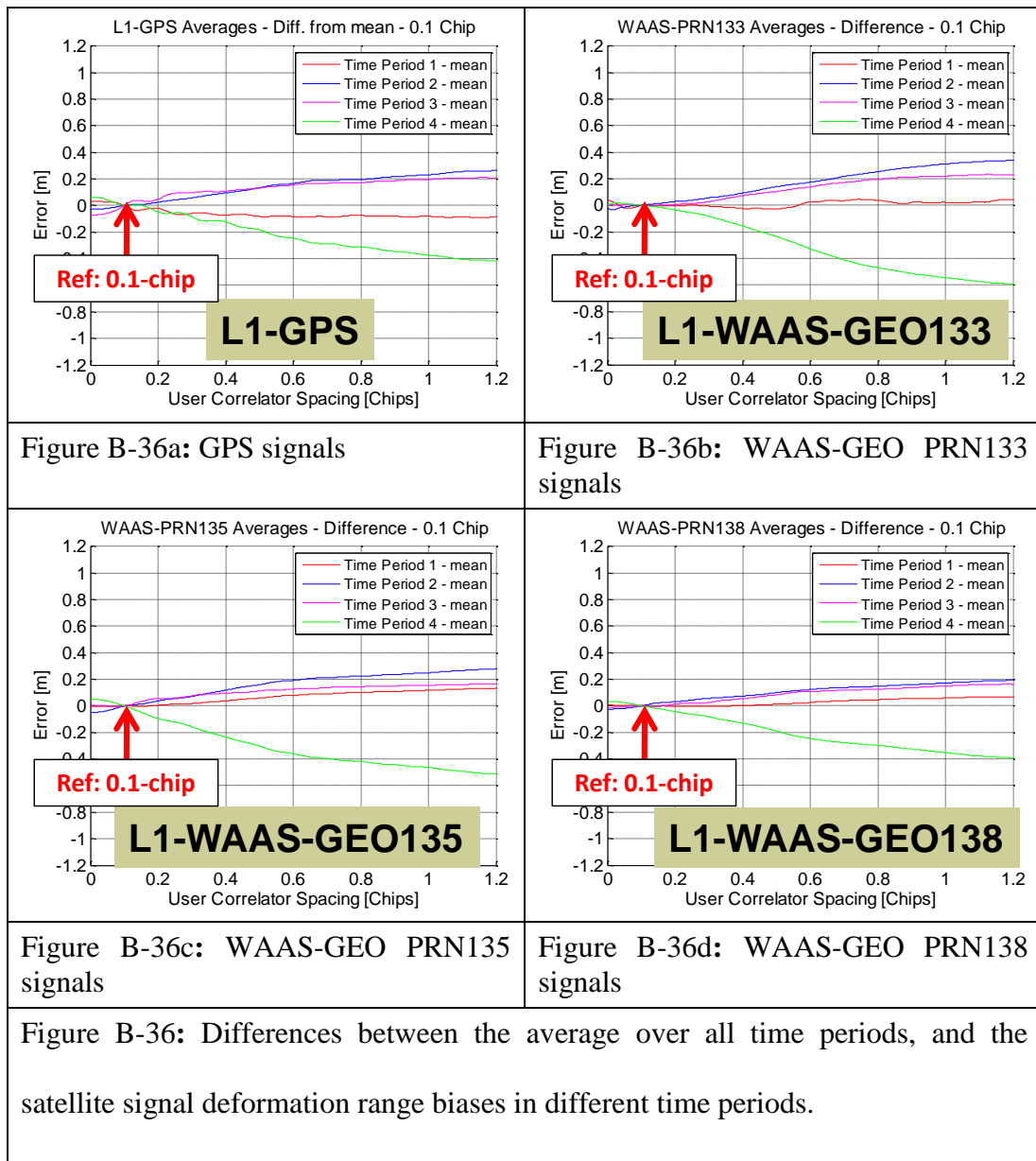
Applying these corrections yields the following satellite signal deformation range bias plots (Figure B-37). Biases for the entire day are in green, while biases for the individual time periods are highlighted in red. The time-varying drifts observed previously are substantially removed after application of the corrections from the WAAS-GEO satellites.

Figure B-37a: Time period 1 highlighted.

Figure B-37b**:** Time period 2 highlighted.

Figure B-37c**:** Time period 3 highlighted.

Figure B-37d**:** Time period 4 highlighted.

Figure B-37: Satellite signal deformation range biases for data collected at different times of day.
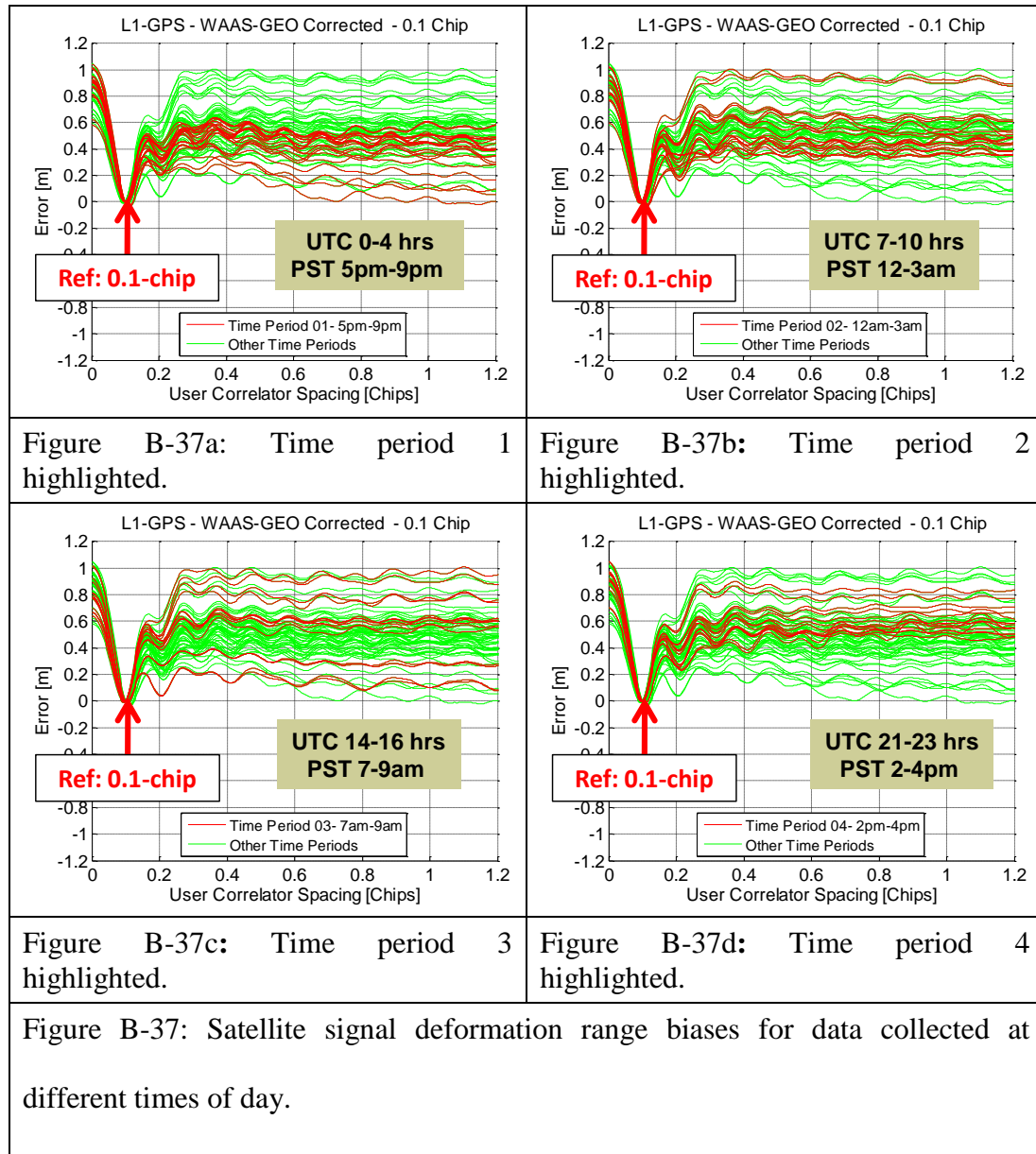
The following table shows the worst case and root-mean-square (RMS) errors for the entire set of GPS signals, before and after applying the corrections for time-varying drift. Both the worst case and RMS errors are reduced from before.

	RMS [m]	Worst Case Error [m]
Before WAAS-GEO correction	0.24	1.15
After WAAS-GEO correction	0.17	0.97

Table B-2: Worst case [m] and root-mean-square (RMS) errors [m] for the GPS

signals, before and after drift-corrections.

6.   Removal of common mean

Again, as in Step 3, the common mean is subtracted from the satellite signal

deformation range biases. This is because the concern is over inter-satellite biases and

their effect on the navigation solution. Doing so would affect only timing but not the

navigation solution. For a reference correlator spacing of 0.1 chips, the results are

shown in Figure B-38. As before, satellite signal deformation range biases for the

entire day are in green, while satellite signal deformation range biases for the

individual time periods are highlighted in red.

Figure B-38a: Time period 1 highlighted.	Figure B-38b: Time period 2 highlighted.

Figure B-38c: Time period 3 highlighted.	Figure B-38d: Time period 4 highlighted.

Figure B-38: Satellite signal deformation range biases after corrections for time-varying effects and removal of common mean.

(Reference receiver correlator spacing of 0.1 chips).
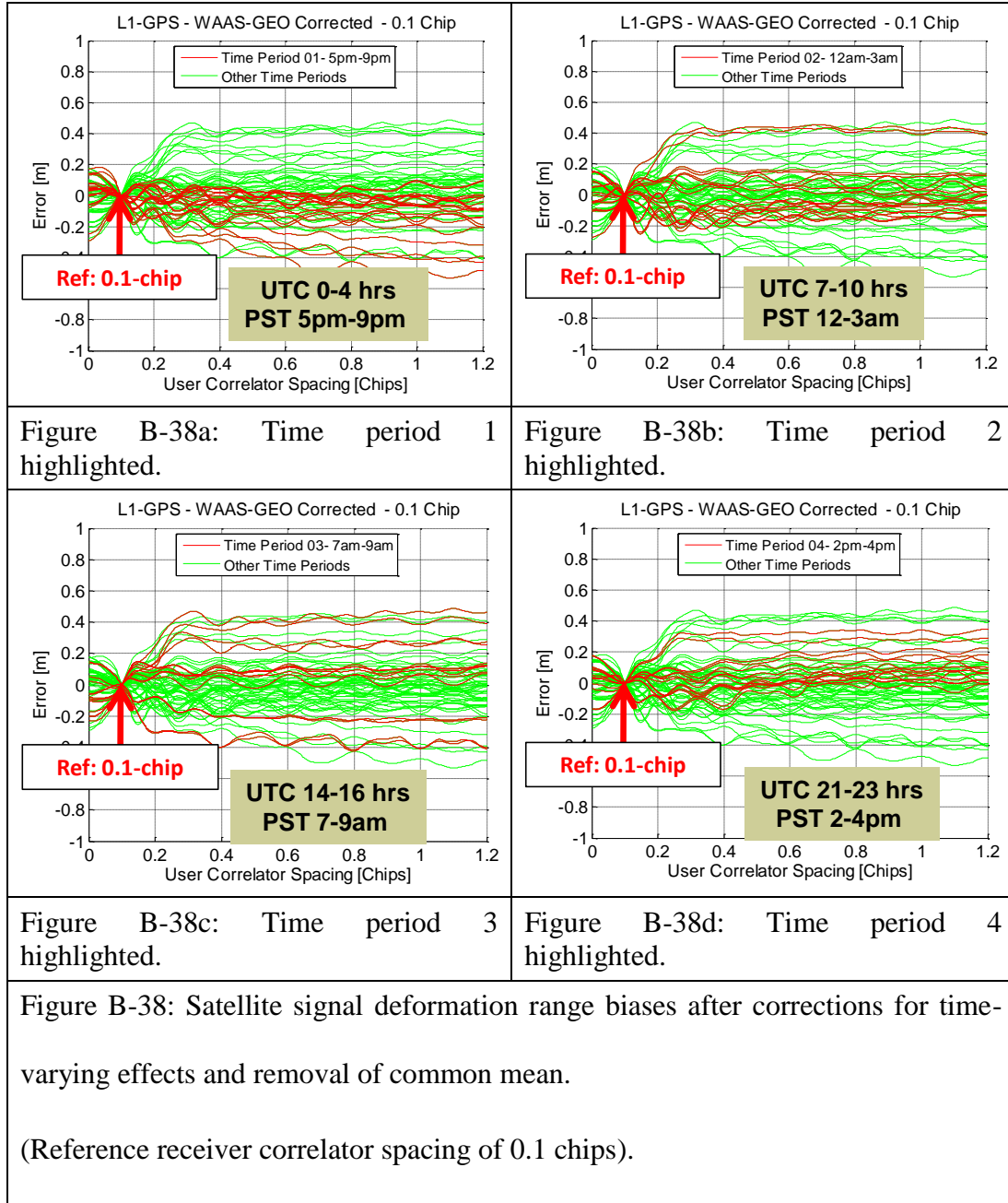
The resultant range biases from waveform distortions, as measured by the large antenna dish approach and after removal of time-dependent hardware biases, are presented in Section 3.5.1 of the main dissertation.

Appendix C

Measurement Using Controlled Pattern Reception Antenna (CRPA)

The Controlled Pattern Reception Array (CRPA) Antenna [65], in both the rooftop and lower-multipath environments, was effective in reducing strong, directed multipath and interference and maintaining high levels of signal power. However, satellite signal deformation range bias distortions on the order of 0.5-1.5 m were actually observed. These were much larger than the biases measured by other methods. Simple analysis showed that these large biases corresponded to timing errors of 1.7-5.0 ns.

The Controlled Pattern Reception Array (CRPA) approach made use of multiple antennas and inputs to form narrow beams. As the satellite signal deformation range biases of interest are 0.05-0.15 m, these different input channels must have total differential path and hardware delays not exceeding 170-500 ps. While it is easy to control cable lengths to within 0.05-0.15 m, it is much more difficult to synchronize separate pieces of hardware to timing specifications of 170-500 ps. Without sufficiently precise timing calibration, each individual antenna would form a replica with a different, non-constant delay in time, which in turn adds unintended, non-constant distortions. Coupled with the phase uncertainties associated with each COTS antenna, the overall distortions were larger than and obscured the signal deformation biases. Thus, this method was found unsuitable for measuring signal deformation range biases.

Appendix D

Detailed Availability, 95% Accuracy and Worst Case Errors for Single and Dual-Frequency WAAS Users

1   Overview

This section contains availability, accuracy, and worst case error graphs for single L1-frequency and dual L1/L5 frequency WAAS users, and for full-constellation as well as from one to five unhealthy or inaccessible satellites. These graphs are obtained based on assumptions of nominal behavior for GPS environmental errors.

2 Baseline Availability in the Absence of Satellite Signal Deformation

The use of dual-frequency L1/L5 GPS provides availability benefits especially as fewer satellites are available (Figure D-1 and corresponding Table D-1). These results are for the case of nominal ionospheric conditions. In severe ionospheric conditions, the dual-frequency benefits are likely to be increased.

	Availability Single-Frequency L1	Availability Dual-Frequency L1/L5
N - 3		
N - 4		
N - 5		
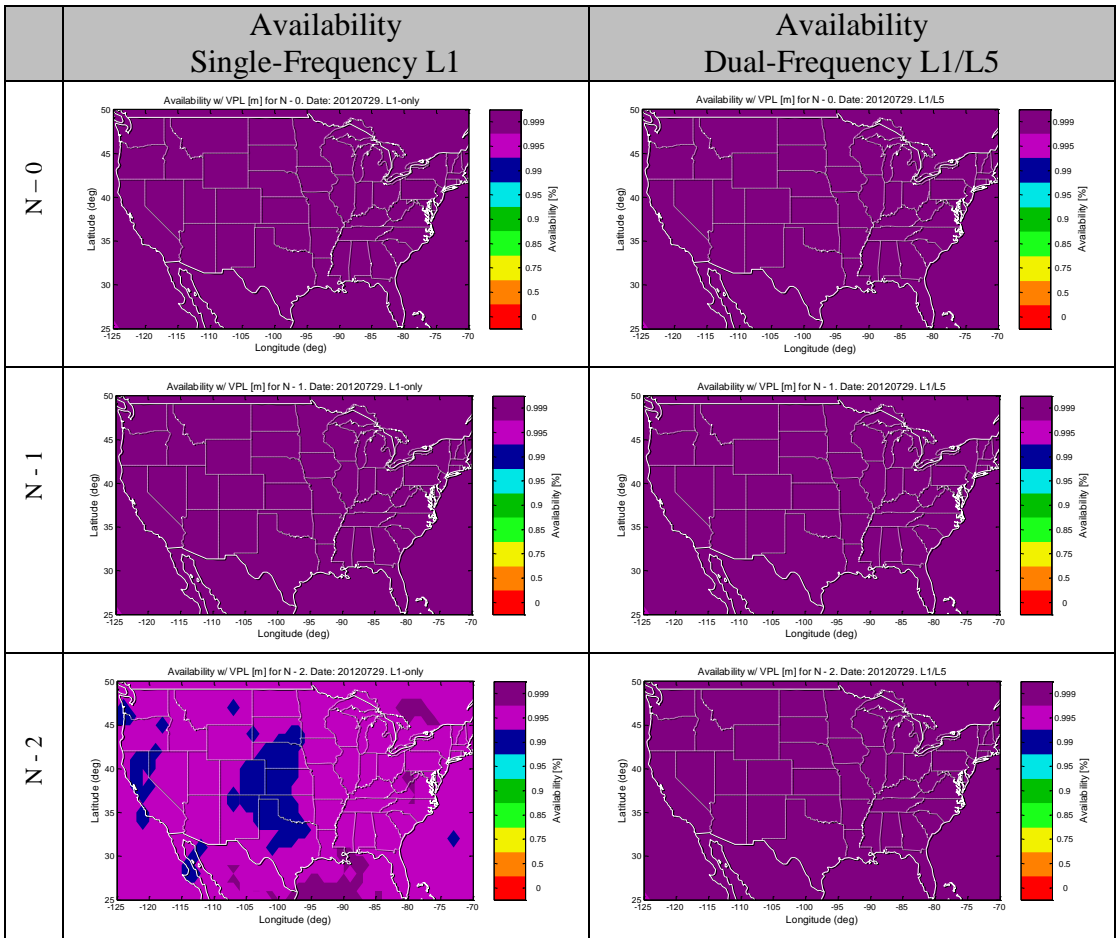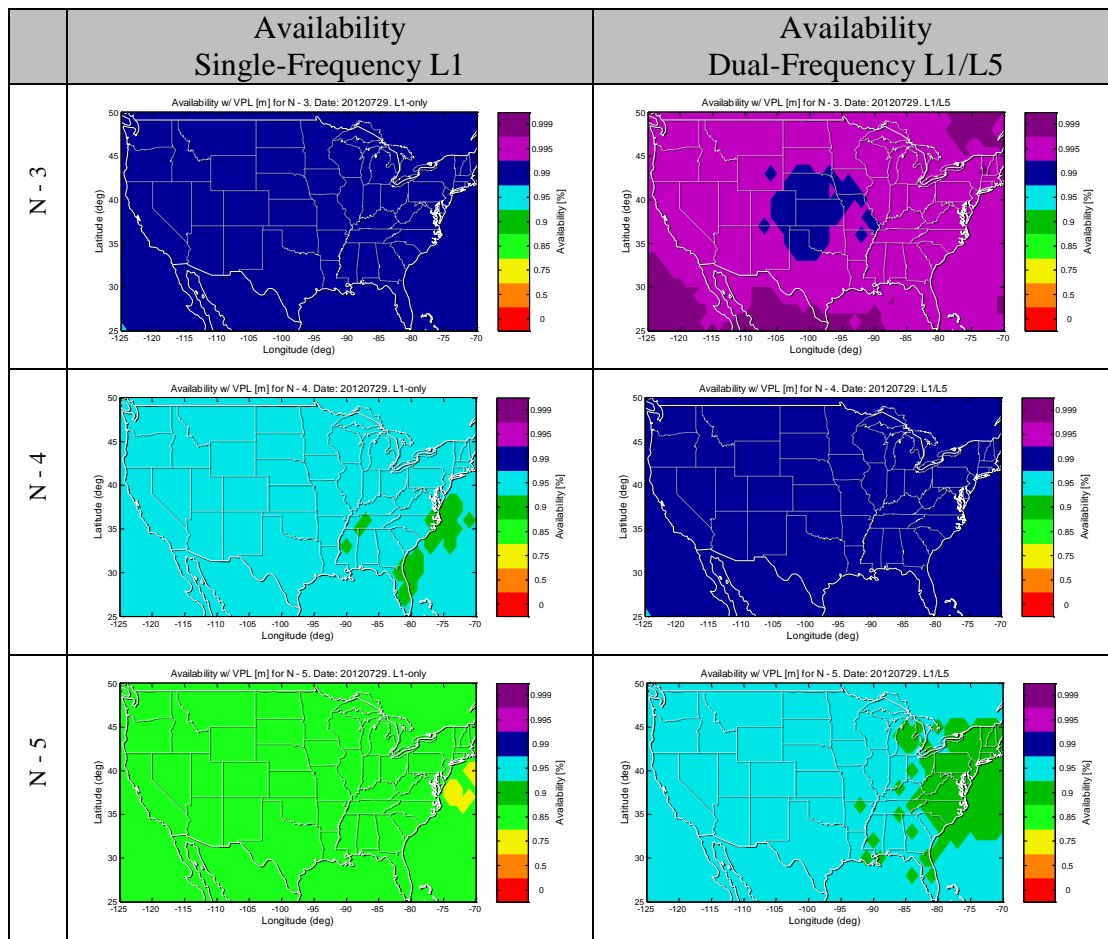
Figure D-1: Baseline Availability for Single Frequency L1-only and Dual Frequency

L1/L5 WAAS Users in the Absence of Satellite Signal Deformation

| Satellite Status | Average Availability [%] | |
	Single Frequency: L1-Only	Dual Frequency: L1/L5
N - 0	100.00%	100.00%
N - 1	99.91%	99.99%
N - 2	99.26%	99.88%
N - 3	97.01%	99.31%
N - 4	91.32%	97.15%
N - 5	80.46%	91.44%

Table D-1: Baseline Average Availability for Single Frequency L1-only and Dual

Frequency L1/L5 WAAS Users, in the Absence of Satellite Signal Deformation

3   Baseline Accuracy for Nominal WAAS Users in the Absence of Satellite Signal Deformation

Figure D-2 (and corresponding Table D-2) shows the nominal accuracy (95% 2σ) for WAAS users (excluding satellite signal deformation range biases). These figures present possibly counter-intuitive results: nominal accuracy for dual-frequency WAAS users is actually slightly worse than for single frequency users. The reason is that most of the time, the ionosphere is quiescent. In the dual-frequency system, the amplification of multipath errors by the dual-frequency ionosphere-error-removal scale factor outweighs the benefits of ionospheric error removal, leading to increased errors. Thus the increased availability of dual-frequency WAAS positioning comes at the cost of increased nominal errors.
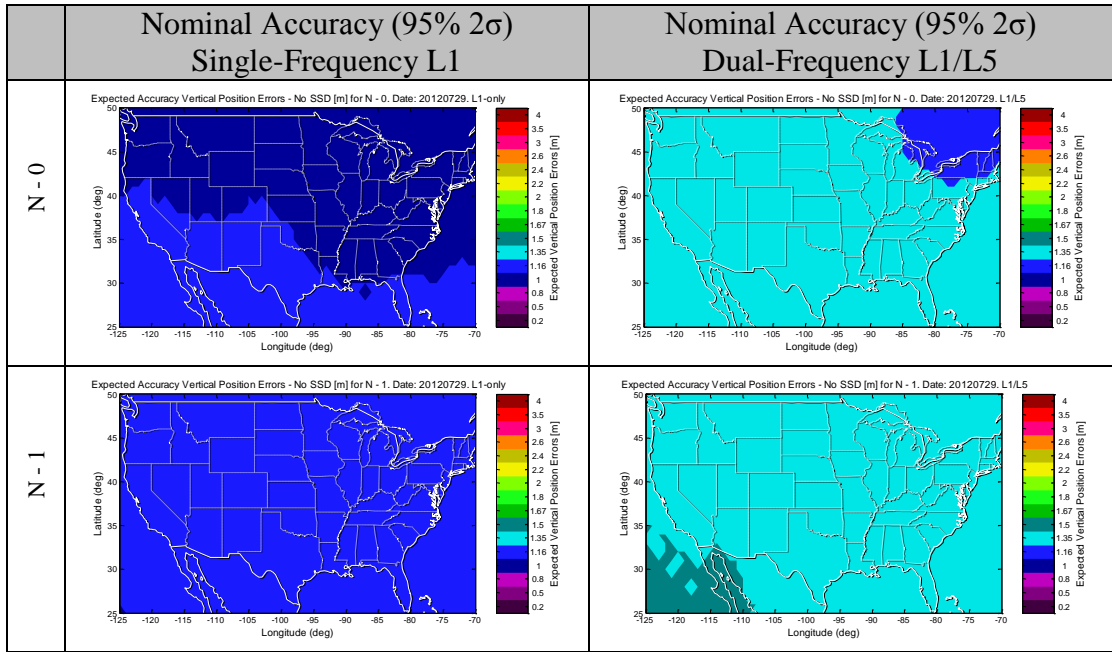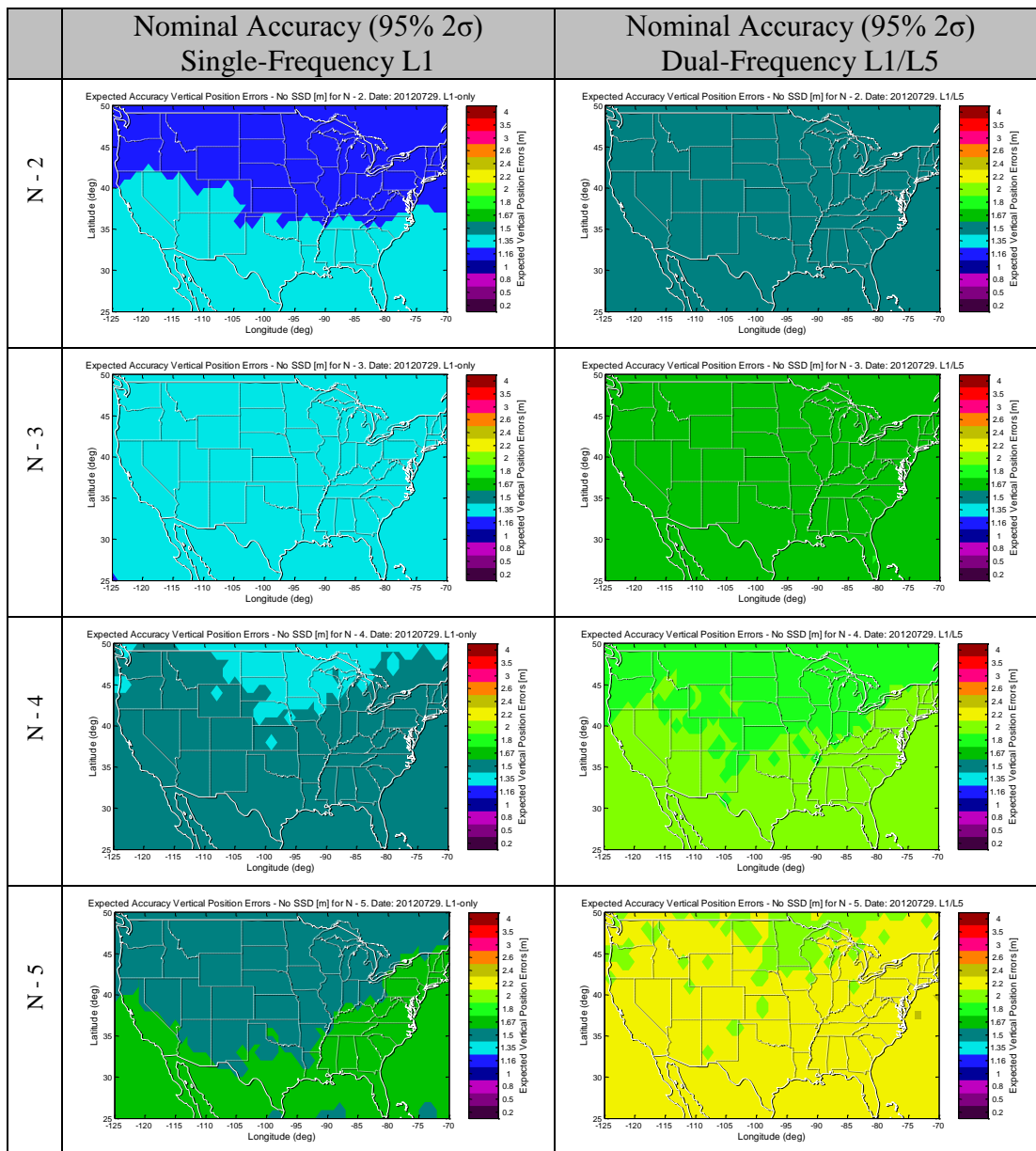
Figure D-2: Nominal Accuracy (95% 2σ) for Single Frequency L1-only and Dual Frequency L1/L5 WAAS Users, in the Absence of Satellite Signal Deformation

Satellite Status	Average Nominal Accuracy [m]	
	Single Frequency: L1-Only	Dual Frequency: L1/L5
N - 0	0.99	1.21
N - 1	1.07	1.31
N - 2	1.16	1.43
N - 3	1.27	1.61
N - 4	1.39	1.82
N - 5	1.50	2.06

Table D-2: Baseline Average Accuracy for Single Frequency L1-only and Dual Frequency L1/L5 WAAS Users, in the Absence of Satellite Signal Deformation

4 Vertical Position Errors (95%) from Satellite Signal Deformation Range Biases

For the remaining plots and tables (Figure D-3 through Figure D-14, and Table D-3 through Table D-7), the reference receiver's correlator spacing is 0.1 L1-chips. The user receiver's correlator spacing is 0.2 and 1.0 L1-chips in the unmitigated case, and 0.12 L1-chips in the mitigated case.

4.1 Unmitigated (Reference: 0.1 L1-Chips, User: 0.2 L1-Chips)
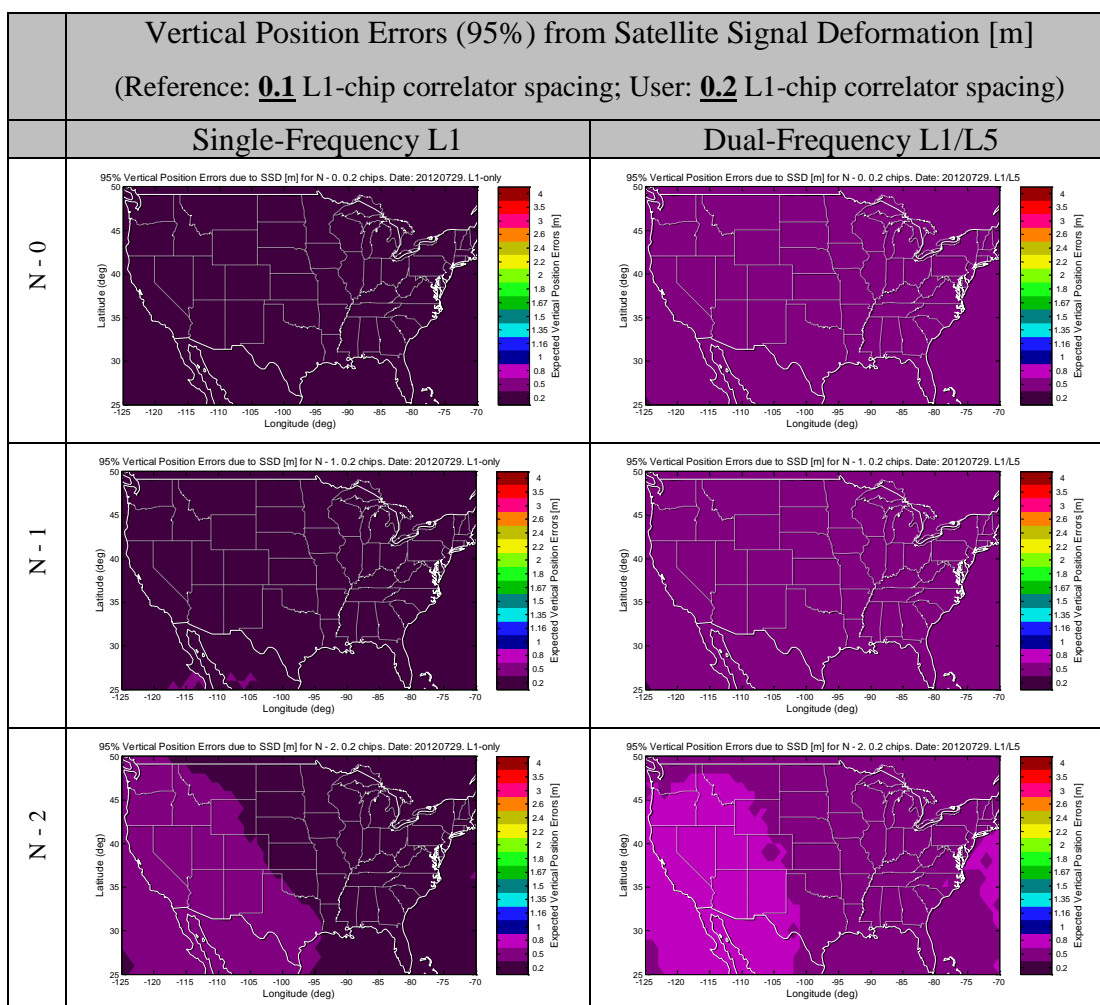
Figure D-3: Vertical Position Errors (95%) from Satellite Signal Deformation [m] for

Single Frequency L1-only and Dual Frequency L1/L5 WAAS Users

(Reference: 0.1 L1-chip correlator spacing; User: 0.2 L1-chip correlator spacing)

4.2 Unmitigated (Reference: 0.1 L1-Chips, User: 1.0 L1-Chips)

Vertical Position Errors (95%) from Satellite Signal Deformation [m] (Reference: **0.1** L1-chip correlator spacing; User: **1.0** L1-chip correlator spacing)	
Single-Frequency L1	Dual-Frequency L1/L5

Vertical Position Errors (95%) from Satellite Signal Deformation [m]
(Reference: **0.1** L1-chip correlator spacing; User: **1.0** L1-chip correlator spacing)

	Single-Frequency L1	Dual-Frequency L1/L5
N – 5		

Figure D-4: Vertical Position Errors (95%) from Satellite Signal Deformation [m] for

Single Frequency L1-only and Dual Frequency L1/L5 WAAS Users

(Reference: 0.1 L1-chip correlator spacing; User: 1.0 L1-chip correlator spacing)

4.3   Mitigated (Reference: 0.1 L1-Chips, User: 0.12 L1-Chips)

Vertical Position Errors (95%) from Satellite Signal Deformation [m]
(Reference: **0.1** L1-chip correlator spacing; User: **0.12** L1-chip correlator spacing)

	Single-Frequency L1	Dual-Frequency L1/L5
N – 0		
N – 1		

Vertical Position Errors (95%) from Satellite Signal Deformation [m]
(Reference: **0.1** L1-chip correlator spacing; User: **0.12** L1-chip correlator spacing)

	Single-Frequency L1	Dual-Frequency L1/L5
N - 2		
N - 3		
N - 4		
N - 5		

Figure D-5: Vertical Position Errors (95%) from Satellite Signal Deformation [m] for

Single Frequency L1-only and Dual Frequency L1/L5 WAAS Users

(Reference: 0.1 L1-chip correlator spacing; User: 0.12 L1-chip correlator spacing)

4.4   Summary

Satellite Status	Average Vertical Position Errors (95%) from Satellite Signal Deformation Range Biases [m]						
	Single Frequency: L1-Only				Dual Frequency: L1/L5		
	User Correlator Spacing [L1-chips]				User Correlator Spacing [L1-chips]		
	Unmitigated		Mitigated		Unmitigated		Mitigated
	0.20	1.00	0.12		0.20	1.00	0.12
N - 0	0.15	0.30	0.03		0.38	0.77	0.06
N - 1	0.18	0.34	0.03		0.43	0.87	0.07
N - 2	0.20	0.39	0.03		0.49	1.00	0.08
N - 3	0.22	0.44	0.04		0.57	1.17	0.09
N - 4	0.24	0.48	0.04		0.66	1.38	0.11
N - 5	0.26	0.52	0.05		0.75	1.56	0.13

Table D-3: Average Vertical Position Errors *(95%)* from Satellite Signal Deformation

[m] for Single Frequency L1-only and Dual Frequency L1/L5 WAAS Users

5   Vertical Position Errors (Worst Case) from Satellite Signal Deformation

Range Biases

5.1   Unmitigated (Reference 0.1 L1-Chips, User: 0.2 L1-Chips)
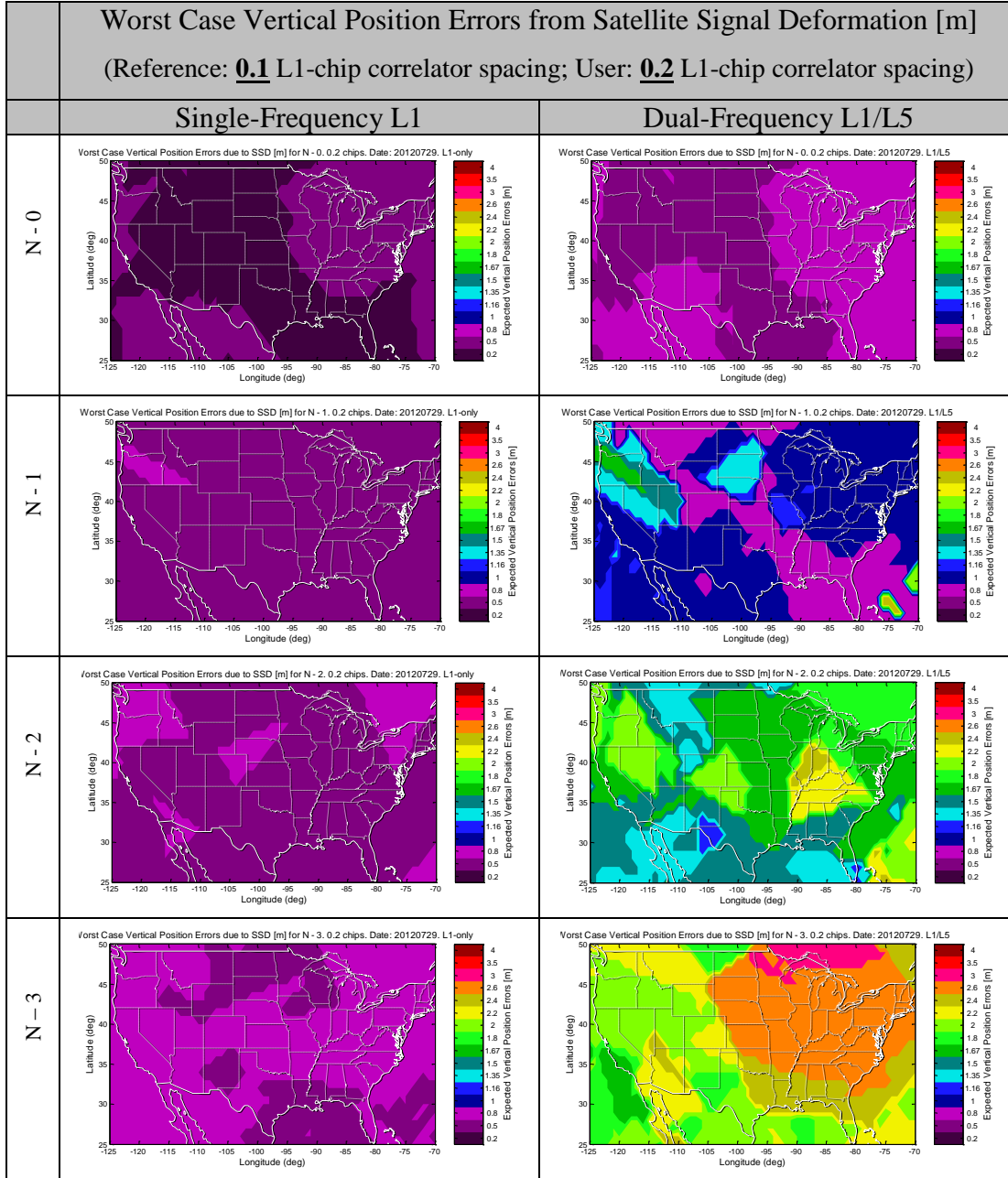
Figure D-6: Worst Case Vertical Position Errors from Satellite Signal Deformation

[m] for Single Frequency L1-only and Dual Frequency L1/L5 WAAS Users

(Reference: 0.1 L1-chip correlator spacing; User: 0.2 L1-chip correlator spacing)

5.2 Unmitigated (Reference 0.1 L1-Chips, User: 1.0 L1-Chips)

Worst Case Vertical Position Errors from Satellite Signal Deformation [m]

(Reference: **0.1** L1-chip correlator spacing; User: **1.0** L1-chip correlator spacing)

Worst Case Vertical Position Errors from Satellite Signal Deformation [m]	
(Reference: **0.1** L1-chip correlator spacing; User: **1.0** L1-chip correlator spacing)	
Single-Frequency L1	Dual-Frequency L1/L5

Figure D-7: Worst Case Vertical Position Errors from Satellite Signal Deformation

[m] for Single Frequency L1-only and Dual Frequency L1/L5 WAAS Users

(Reference: 0.1 L1-chip correlator spacing; User: 1.0 L1-chip correlator spacing)

5.3   Mitigated (Reference: 0.1 L1-Chips, User: 0.12 L1-Chips)

Worst Case Vertical Position Errors from Satellite Signal Deformation [m]	
(Reference: **0.1** L1-chip correlator spacing; User: **0.12** L1-chip correlator spacing)	
Single-Frequency L1	Dual-Frequency L1/L5

Figure D-8: Worst Case Vertical Position Errors from Satellite Signal Deformation

[m] for Single Frequency L1-only and Dual Frequency L1/L5 WAAS Users

(Reference: 0.1 L1-chip correlator spacing; User: 0.12 L1-chip correlator spacing)

5.4 Summary

Satellite Status	Average Worst Case Vertical Position Errors from Satellite Signal Deformation Range Biases [m]						
	Single Frequency: L1-Only				Dual Frequency: L1/L5		
	User Correlator Spacing [L1-chips]				User Correlator Spacing [L1-chips]		
	Unmitigated		Mitigated		Unmitigated		Mitigated
	0.20	1.00	0.12		0.20	1.00	0.12
N - 0	0.21	0.42	0.04		0.53	1.04	0.09
N - 1	0.32	0.71	0.06		0.93	1.95	0.17
N - 2	0.45	1.01	0.08		1.61	3.63	0.27
N - 3	0.54	1.16	0.09		2.19	4.25	0.36
N - 4	0.57	1.2	0.10		2.40	4.58	0.40
N - 5	0.59	1.21	0.11		2.42	4.71	0.40

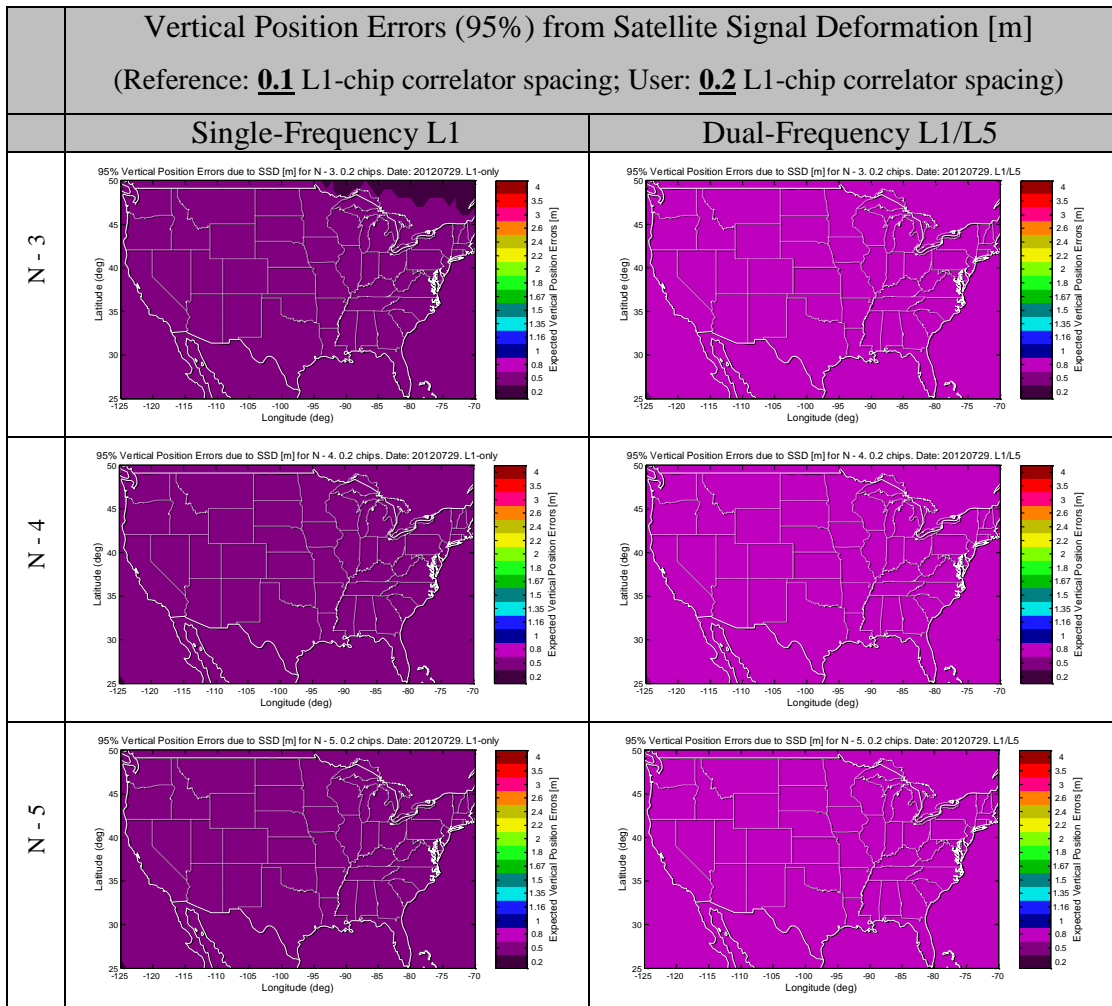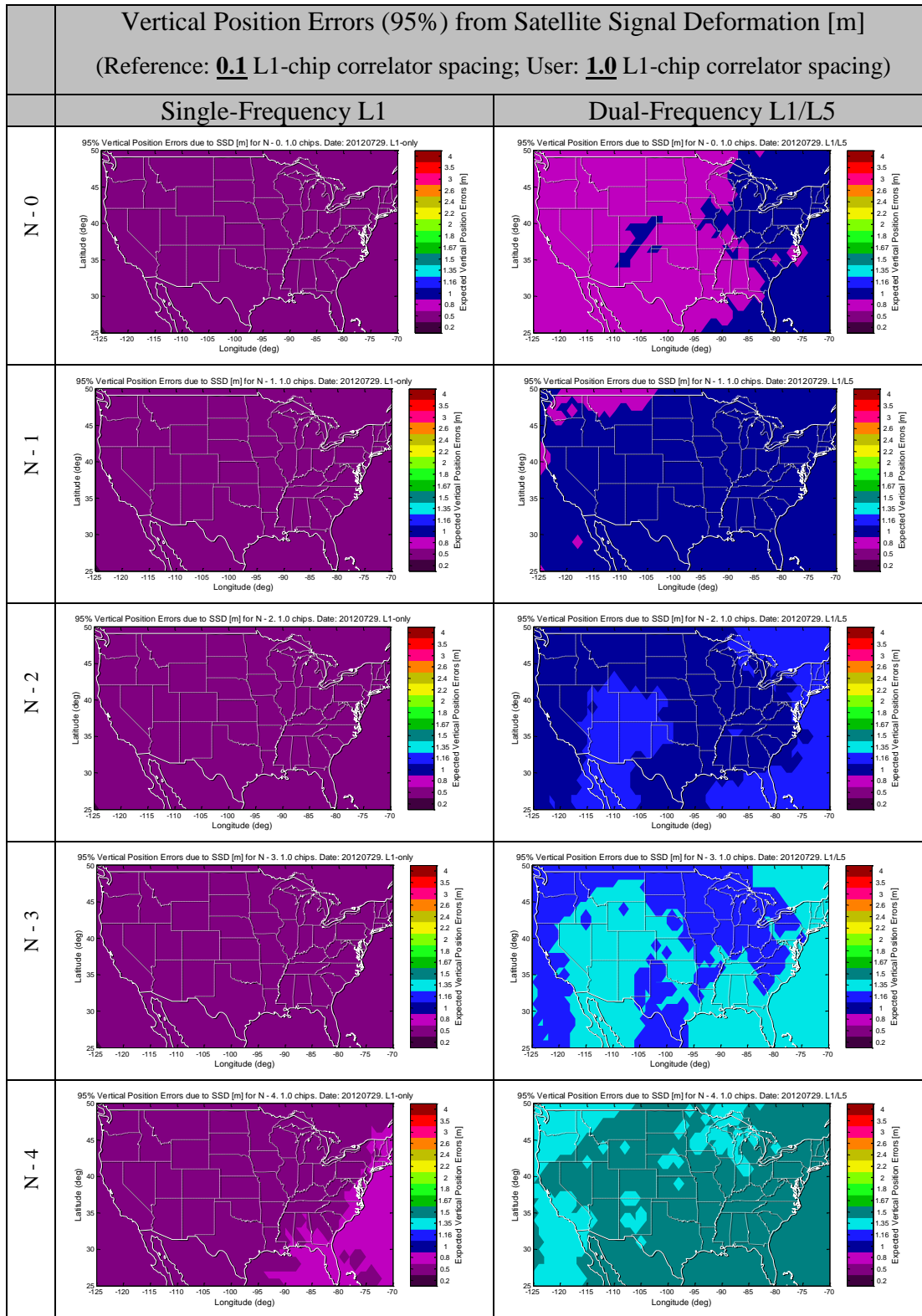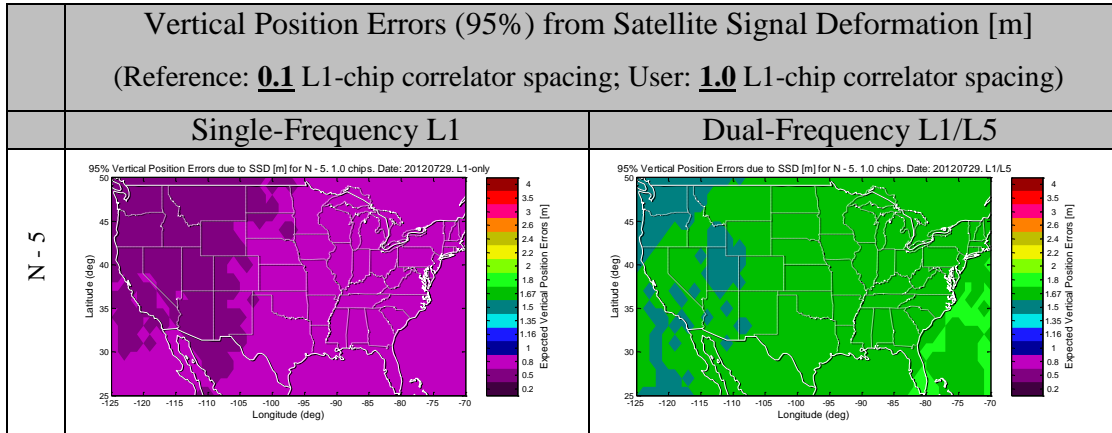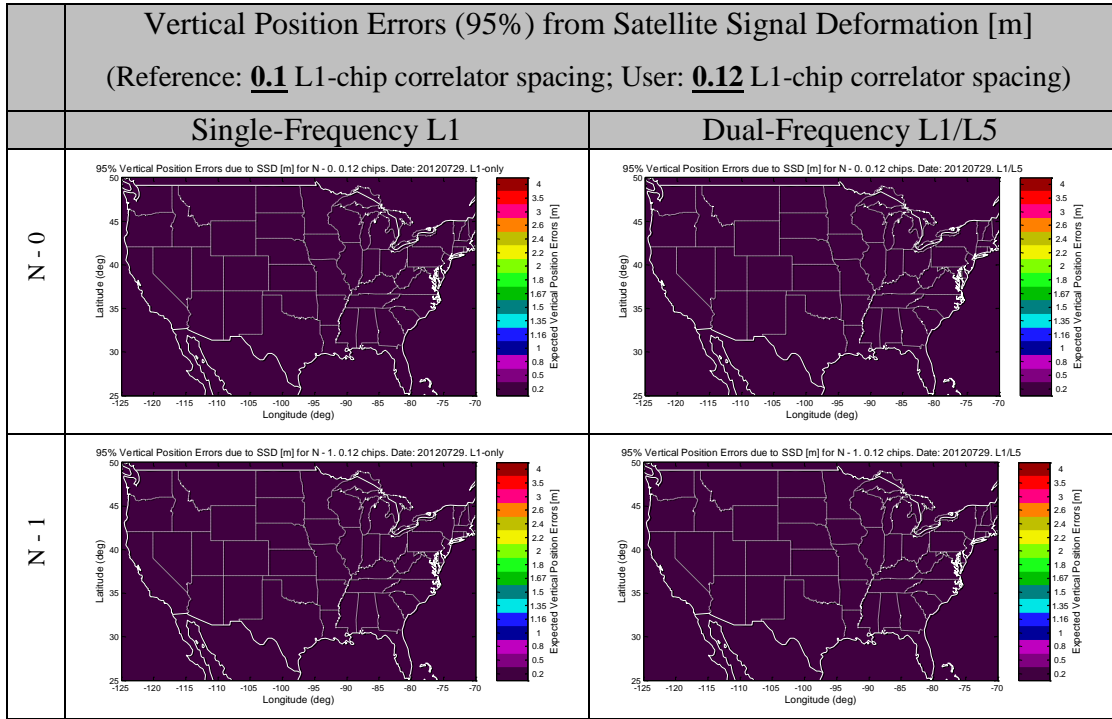Table D-4: Average Worst Case Vertical Position Errors from Satellite Signal Deformation

[m] for Single Frequency L1-only and Dual Frequency L1/L5 WAAS Users

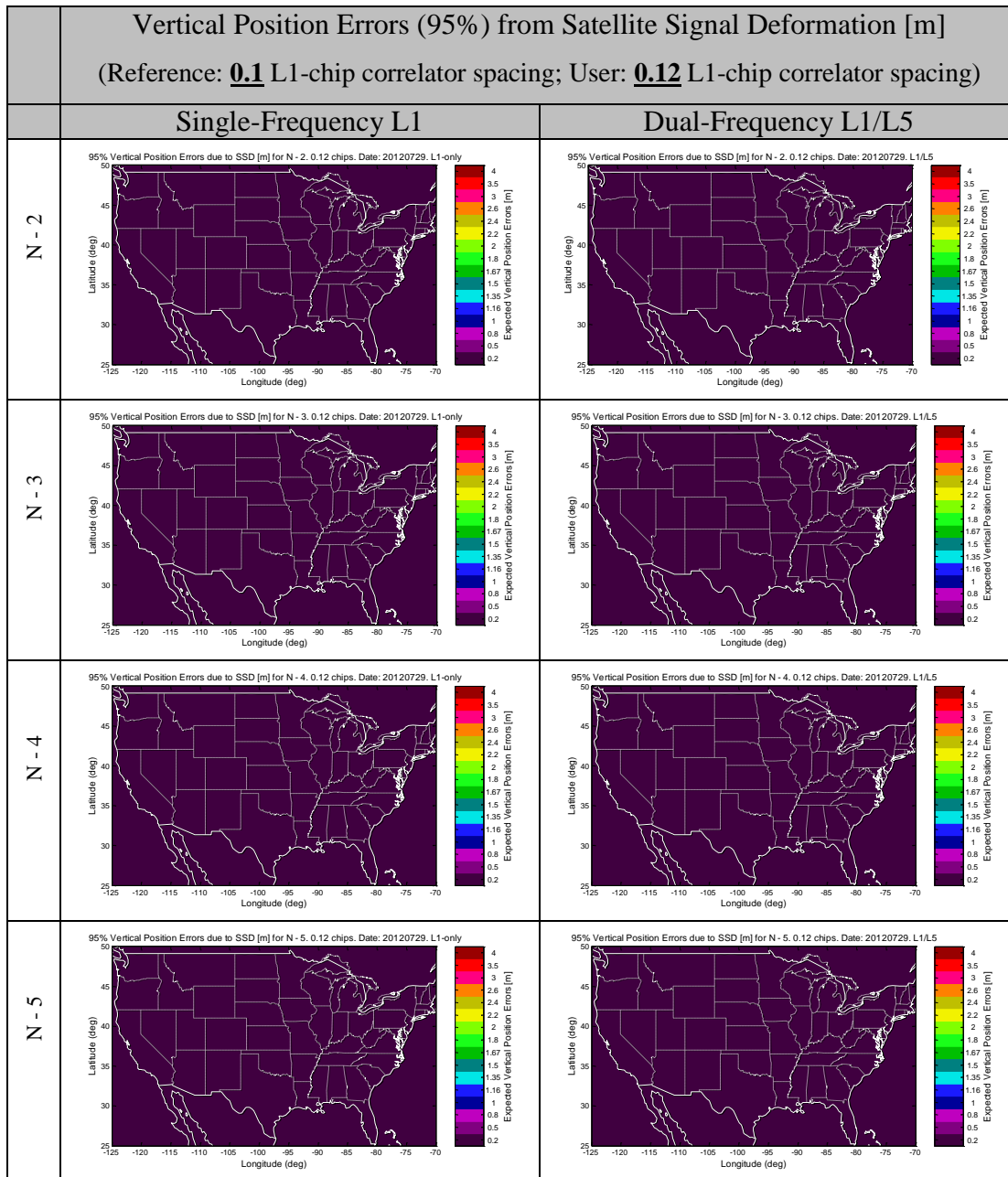| Satellite Status	Maximum Worst Case Vertical Position Errors from Satellite Signal Deformation Range Biases (Max) [m]						
	Single Frequency: L1-Only				Dual Frequency: L1/L5		
	User Correlator Spacing [L1-chips]				User Correlator Spacing [L1-chips]		
	Unmitigated		Mitigated		Unmitigated		Mitigated
	0.20	1.00	0.12		0.20	1.00	0.12
N - 0	0.28	0.90	0.06		0.80	1.99	0.16
N - 1	0.57	1.36	0.11		2.26	4.31	0.41
N - 2	0.61	1.35	0.11		2.33	4.48	0.42
N - 3	0.65	1.36	0.11		2.63	4.88	0.44
N - 4	0.70	1.53	0.13		2.81	5.59	0.46
N - 5	0.70	1.53	0.13		2.86	5.57	0.47

Table D-5: Maximum Worst Case Vertical Position Errors from Satellite Signal Deformation

[m] for Single Frequency L1-only and Dual Frequency L1/L5 WAAS Users

6   Nominal Accuracy for WAAS Users Including Vertical Position Errors from Satellite Signal Deformation Range Biases (95%)

6.1   Unmitigated (Reference: 0.1 L1-Chips, User: 0.2 L1-Chips)

Nominal Accuracy Including Vertical Position Errors (95%) from Satellite Signal Deformation Range Biases [m] (Reference: **0.1** L1-chip correlator spacing; User: **0.2** L1-chip correlator spacing)	
Single-Frequency L1	Dual-Frequency L1/L5

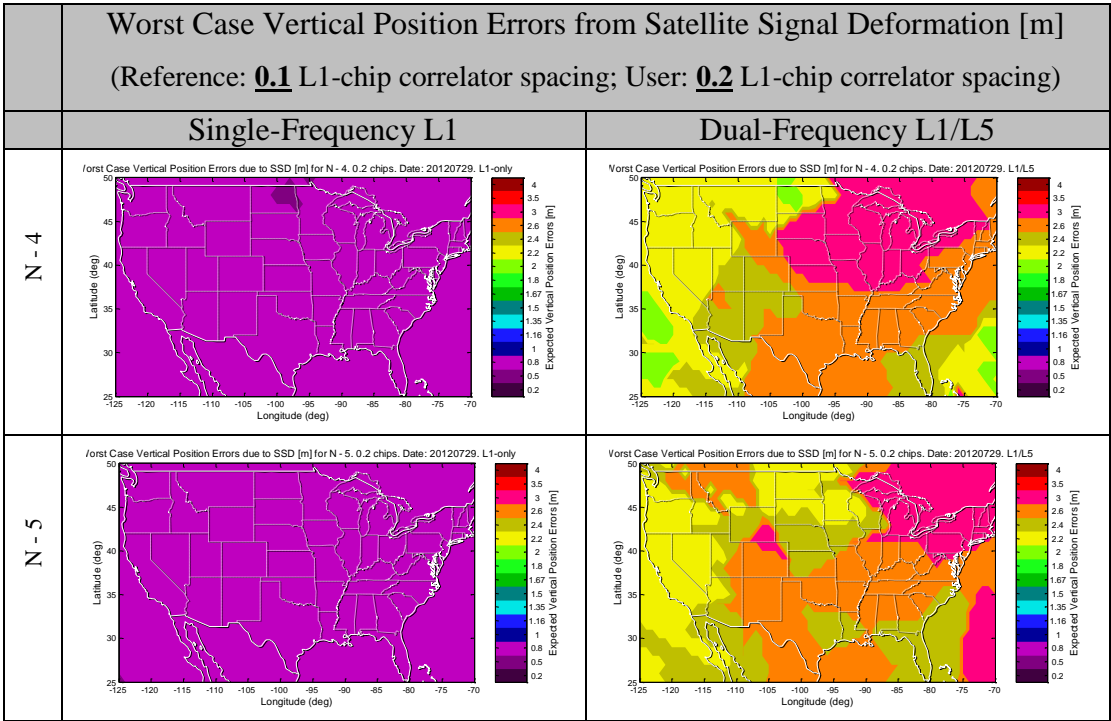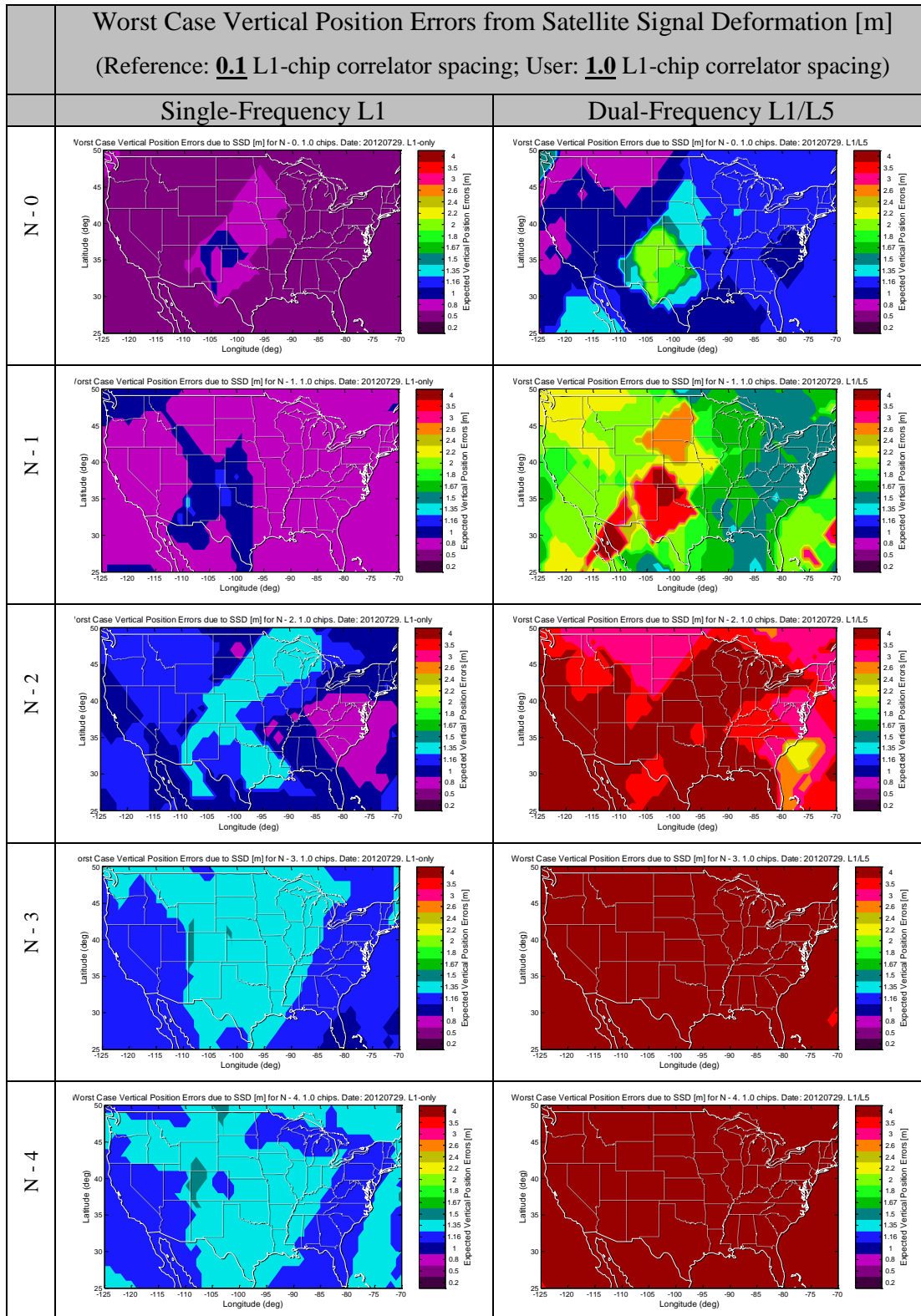|	Nominal Accuracy Including Vertical Position Errors (95%) from Satellite Signal Deformation Range Biases [m] (Reference: **0.1** L1-chip correlator spacing; User: **0.2** L1-chip correlator spacing)	
	Single-Frequency L1	Dual-Frequency L1/L5
N – 4		
N – 5		

Figure D-9: Nominal Accuracy Including Vertical Position Errors (95%) from

Satellite Signal Deformation Range Biases [m] for Single Frequency L1-only and

Dual Frequency L1/L5 WAAS Users

(Reference: 0.1 L1-chip correlator spacing; User: 0.2 L1-chip correlator spacing)

6.2   Unmitigated (Reference: 0.1 L1-Chips, User: 1.0 L1-Chips)

	Nominal Accuracy Including Vertical Position Errors (95%) from Satellite Signal Deformation Range Biases [m] (Reference: **0.1** L1-chip correlator spacing; User: **1.0** L1-chip correlator spacing)	
	Single-Frequency L1	Dual-Frequency L1/L5

Nominal Accuracy Including Vertical Position Errors (95%) from Satellite Signal Deformation Range Biases [m]

(Reference: **0.1** L1-chip correlator spacing; User: **1.0** L1-chip correlator spacing)

Figure D-10: Nominal Accuracy Including Vertical Position Errors (95%) from

Satellite Signal Deformation Range Biases [m] for Single Frequency L1-only and

Dual Frequency L1/L5 WAAS Users

(Reference: 0.1 L1-chip correlator spacing; User: 1.0 L1-chip correlator spacing)

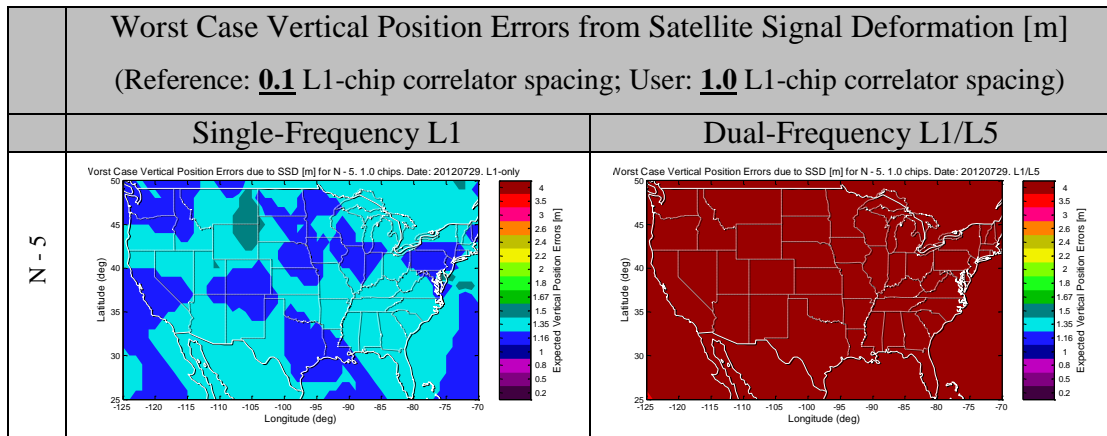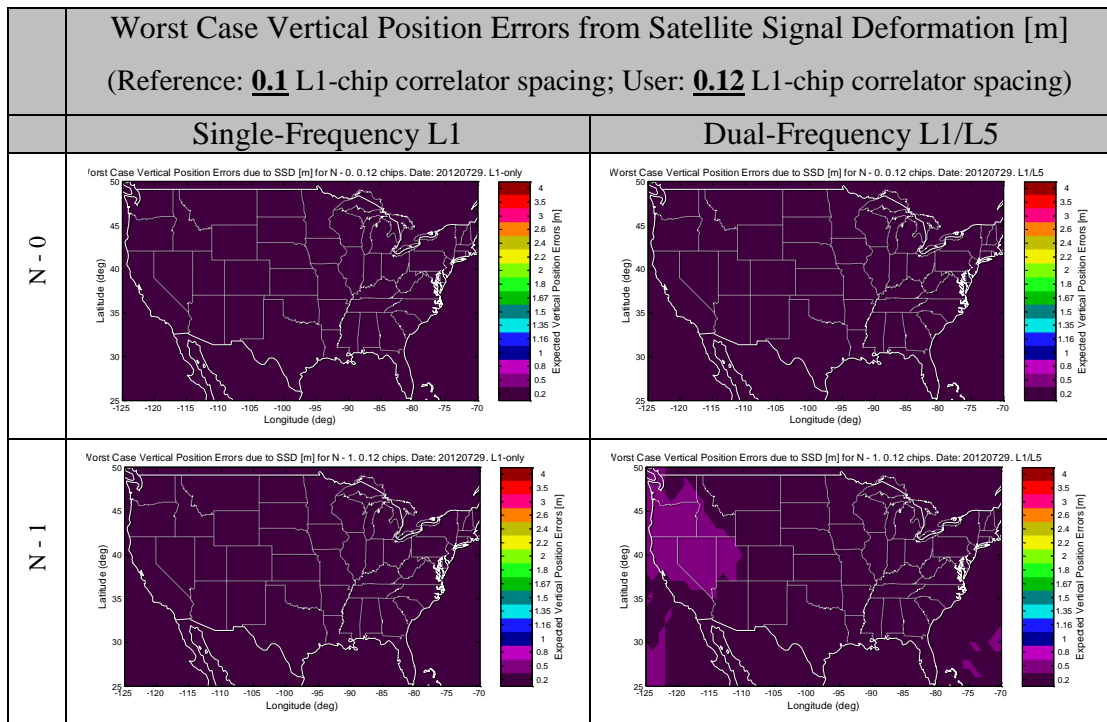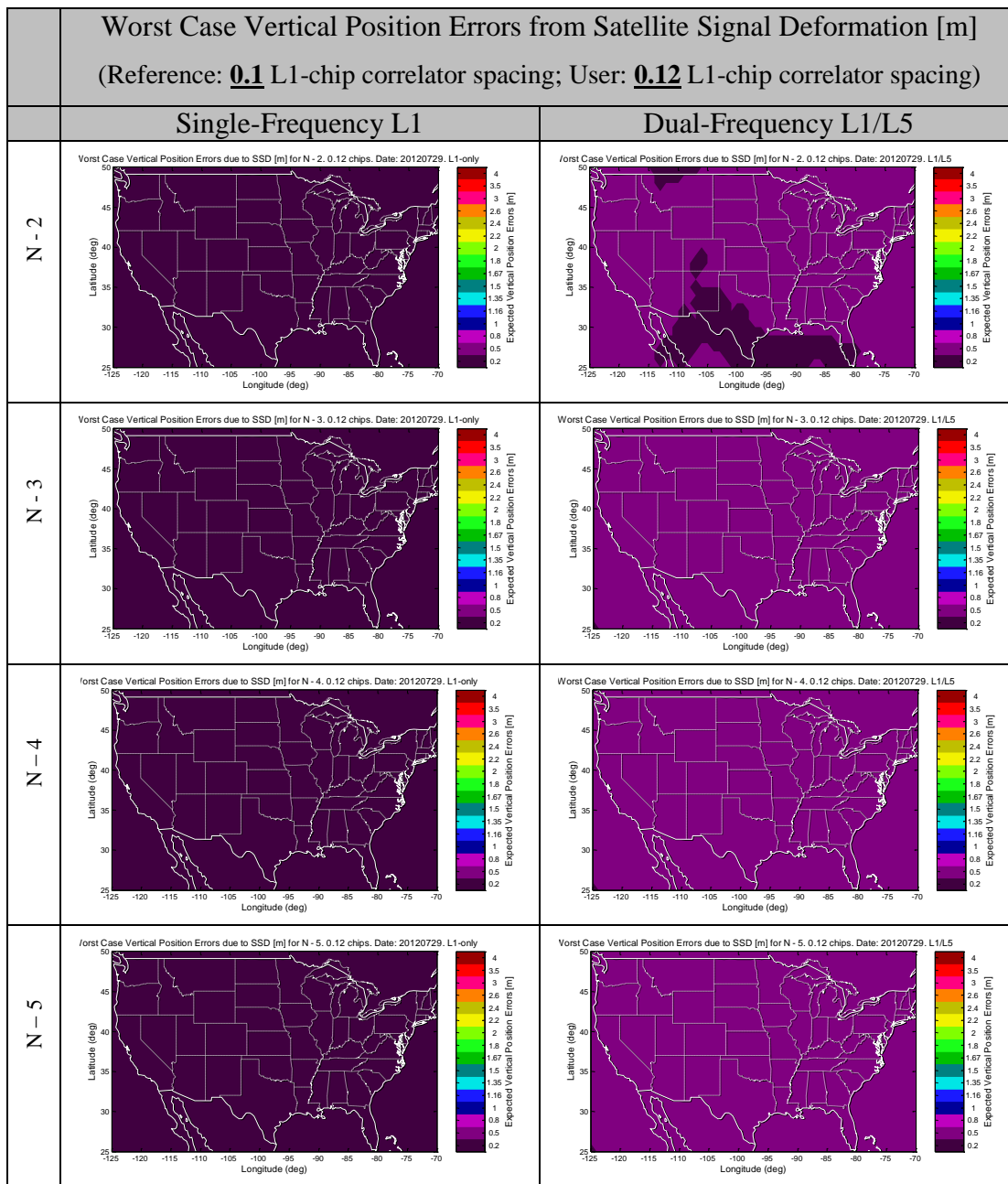## 6.3 Mitigated (Reference: 0.1 L1-Chips, User: 0.12 L1-Chips)

Figure D-11: Nominal Accuracy Including Vertical Position Errors (95%) from

Satellite Signal Deformation Range Biases [m] for Single Frequency L1-only and

Dual Frequency L1/L5 WAAS Users

(Reference: 0.1 L1-chip correlator spacing; User: 0.12 L1-chip correlator spacing)

6.4   Summary

Satellite Status	Nominal Accuracy Including Vertical Position Errors (95%) from Satellite Signal Deformation Range Biases [m]							
	Single Frequency: L1-Only				Single Frequency: L1-Only			
	User Correlator Spacing [L1-chips]				User Correlator Spacing [L1-chips]			
	No SSD	Unmitigated		Mitigated	No SSD	Unmitigated		Mitigated
	0.10	0.20	1.00	0.12	0.10	0.20	1.00	0.12
N - 0	0.99	1.15	1.29	1.02	1.21	1.59	1.98	1.27
N - 1	1.07	1.24	1.41	1.10	1.31	1.74	2.18	1.38
N - 2	1.16	1.36	1.55	1.20	1.43	1.93	2.43	1.52
N - 3	1.27	1.49	1.71	1.31	1.61	2.17	2.78	1.70
N - 4	1.39	1.63	1.87	1.43	1.82	2.48	3.20	1.93
N - 5	1.50	1.76	2.02	1.55	2.06	2.81	3.62	2.19

Table D-6: Nominal Accuracy Including Vertical Position Errors (95%) from Satellite

Signal Deformation Range Biases [m] for Single Frequency L1-only and Dual

Frequency L1/L5 WAAS Users

7 Nominal Accuracy for WAAS Users Including Vertical Position Errors from Satellite Signal Deformation Range Biases (Worst Case)

7.1 Unmitigated (Reference: 0.1 L1-Chips, User: 0.2 L1-Chips)

Nominal Accuracy Including Worst Case Vertical Position Errors from Satellite Signal Deformation Range Biases [m] (Reference: **0.1** L1-chip correlator spacing; User: **0.2** L1-chip correlator spacing)		
	Single-Frequency L1	Dual-Frequency L1/L5

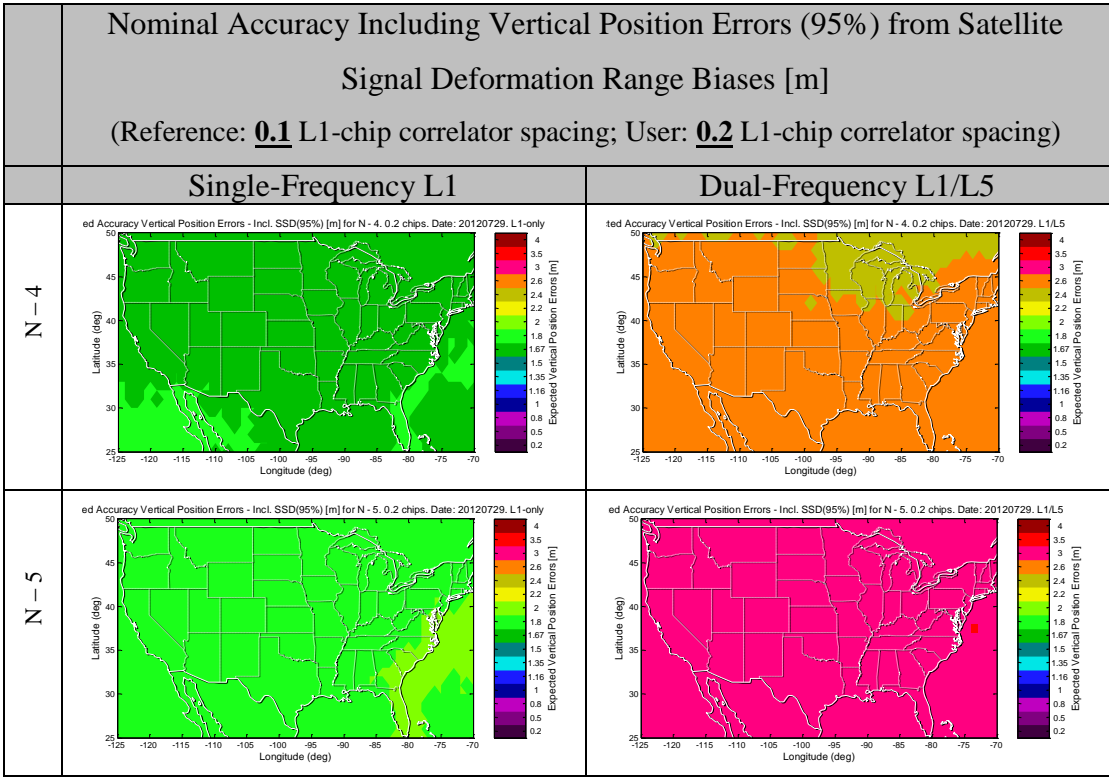| Nominal Accuracy Including Worst Case Vertical Position Errors from Satellite Signal Deformation Range Biases [m] (Reference: **0.1** L1-chip correlator spacing; User: **0.2** L1-chip correlator spacing)	
Single-Frequency L1	Dual-Frequency L1/L5

Figure D-12: Nominal Accuracy Including Worst Case Vertical Position Errors from

Satellite Signal Deformation Range Biases [m] for Single Frequency L1-only and

Dual Frequency L1/L5 WAAS Users

(Reference: 0.1 L1-chip correlator spacing; User: 0.2 L1-chip correlator spacing)

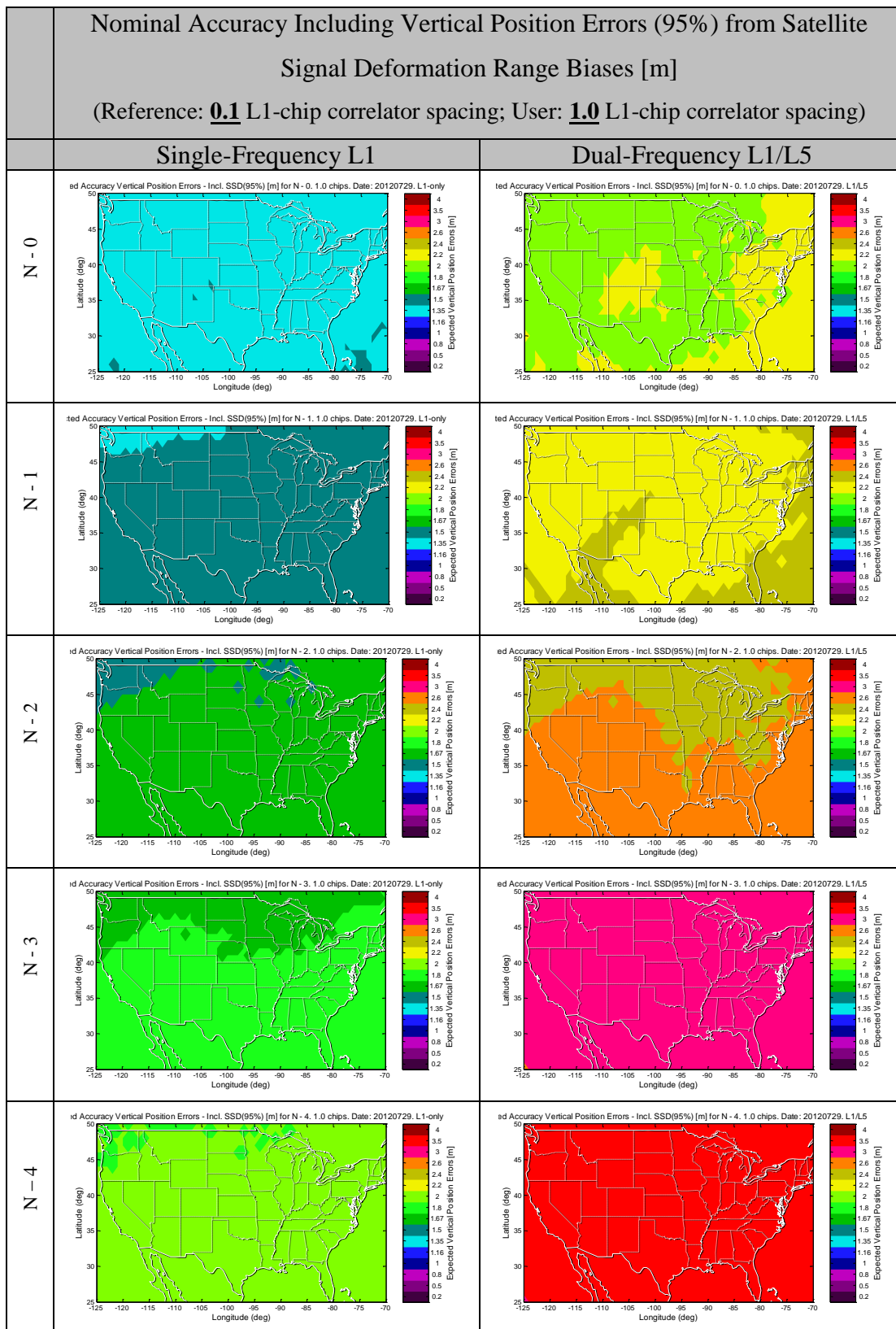## 7.2 Unmitigated (Reference: 0.1 L1-Chips, User: 1.0 L1-Chips)
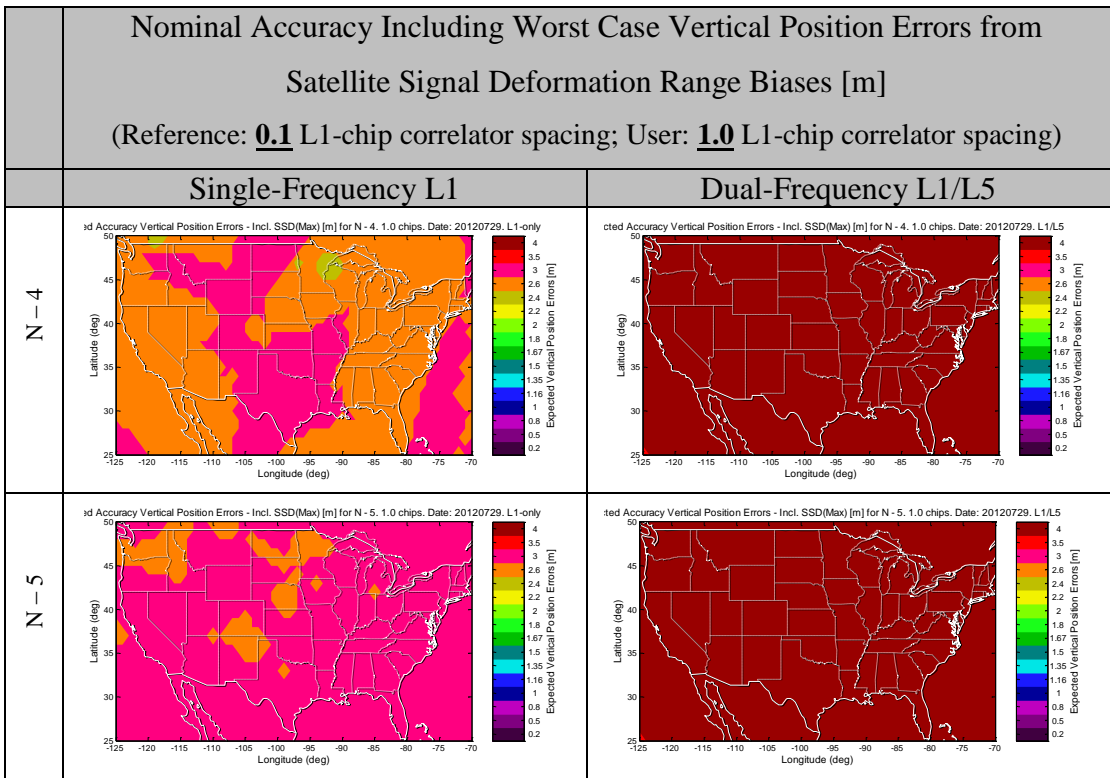
Figure D-13: Nominal Accuracy Including Worst Case Vertical Position Errors from

Satellite Signal Deformation Range Biases [m] for Single Frequency L1-only and

Dual Frequency L1/L5 WAAS Users

(Reference: 0.1 L1-chip correlator spacing; User: 1.0 L1-chip correlator spacing)

7.3   Mitigated (Reference: 0.1 L1-Chips, User: 0.12 L1-Chips)

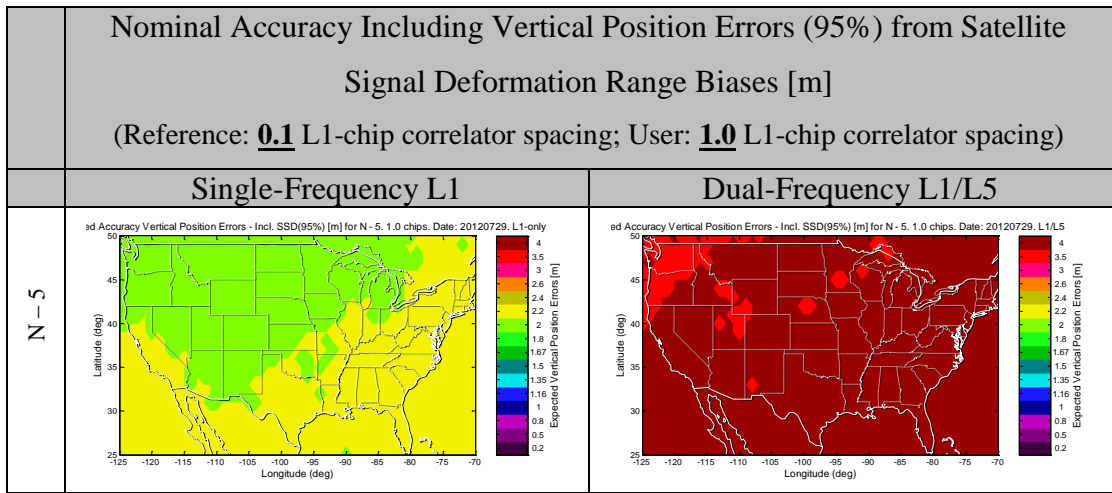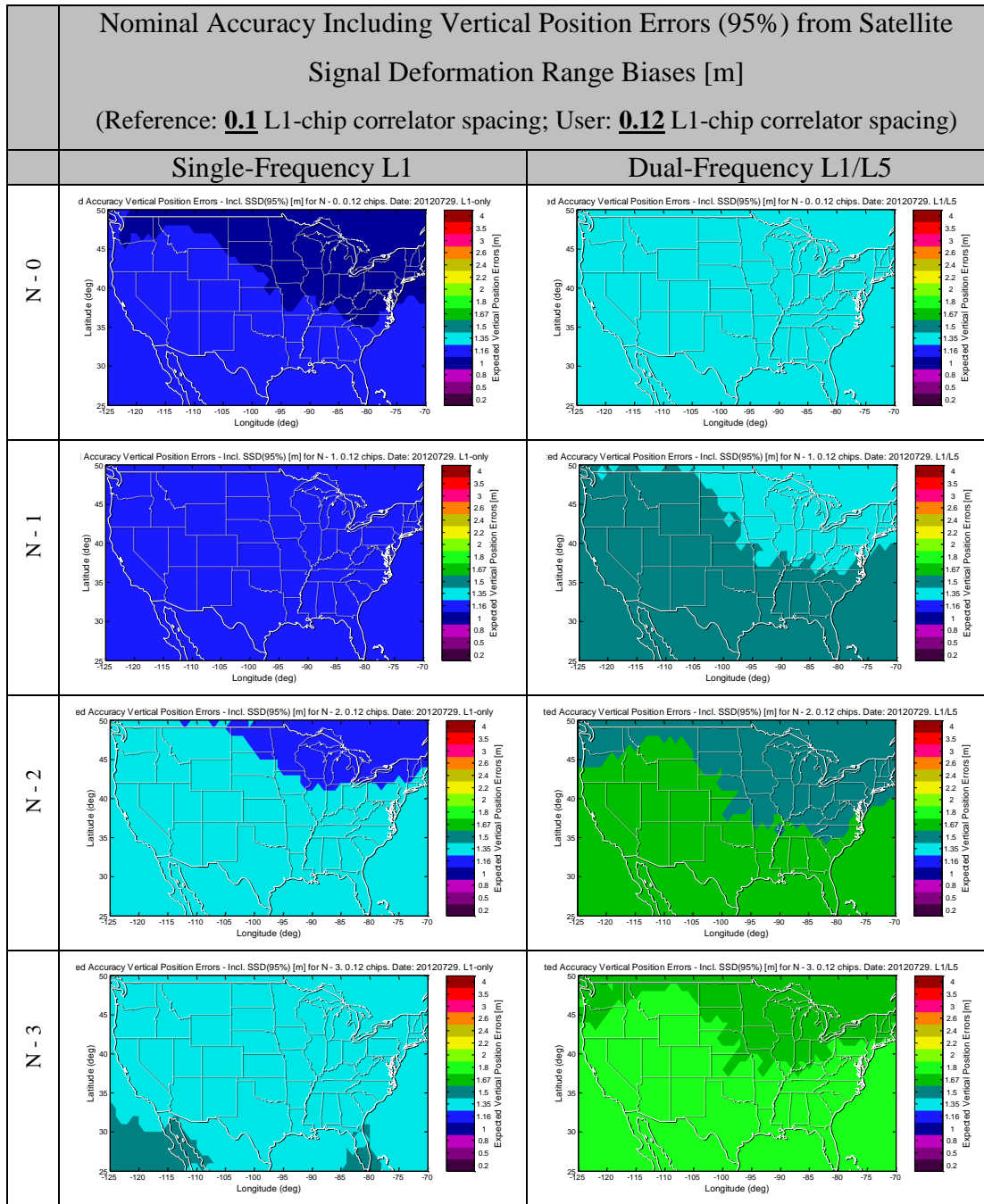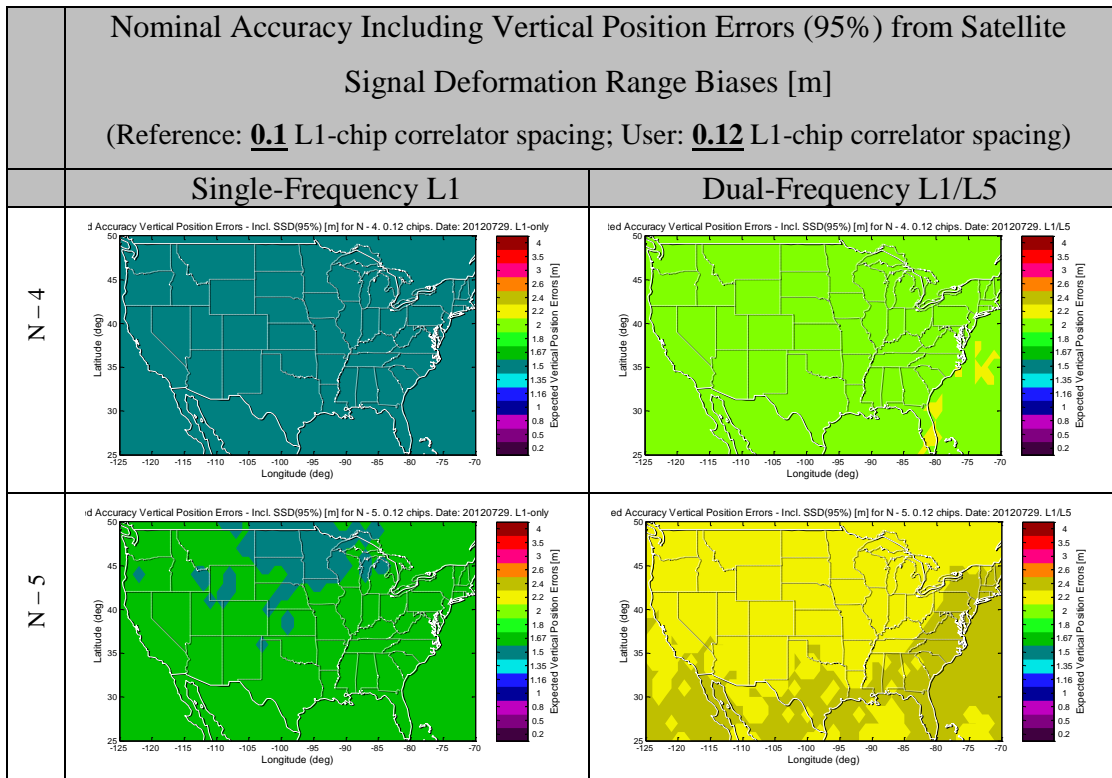|	Nominal Accuracy Including Worst Case Vertical Position Errors from Satellite Signal Deformation Range Biases [m] (Reference: **0.1** L1-chip correlator spacing; User: **0.12** L1-chip correlator spacing)	
	Single-Frequency L1	Dual-Frequency L1/L5
N – 0		
N – 1		
N – 2		
N – 3		
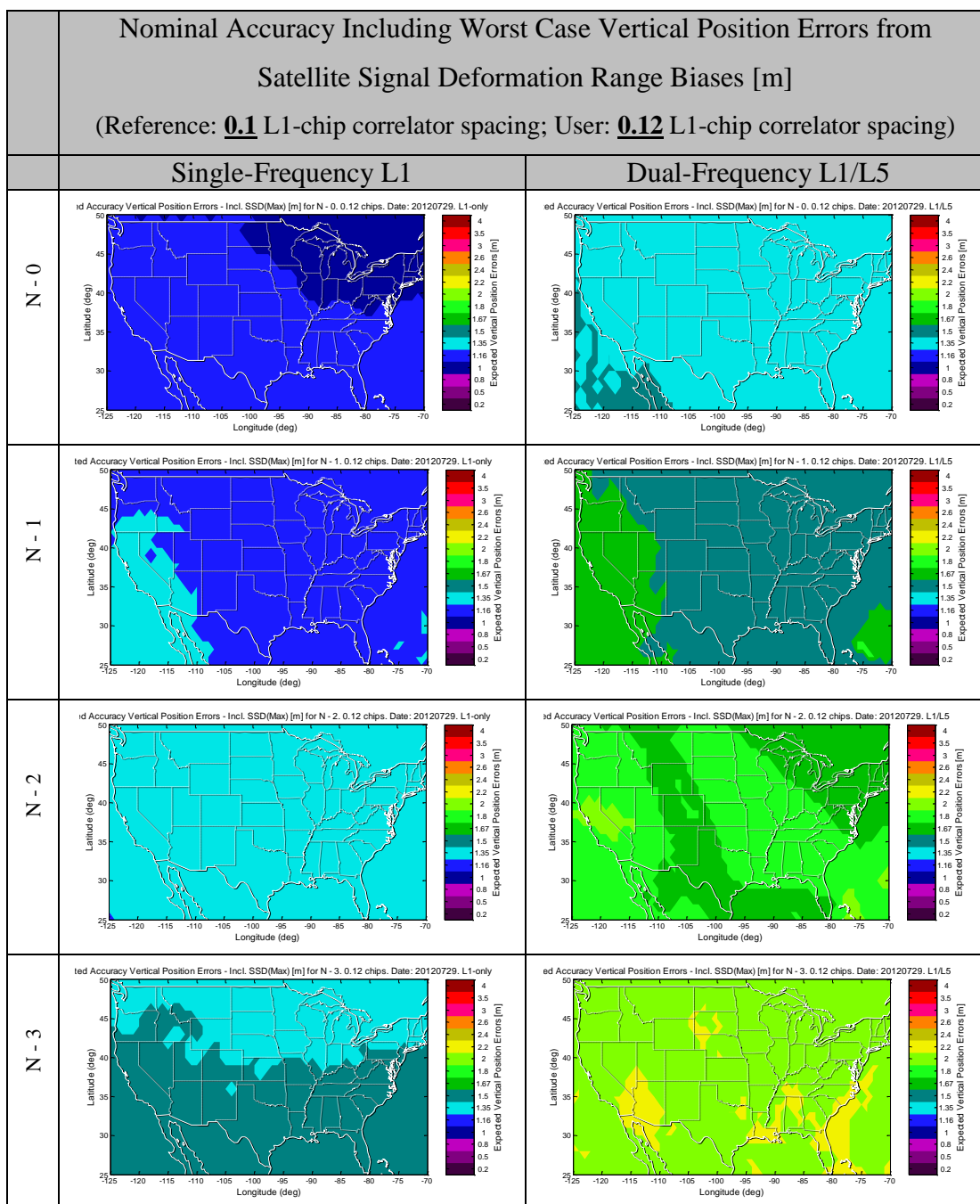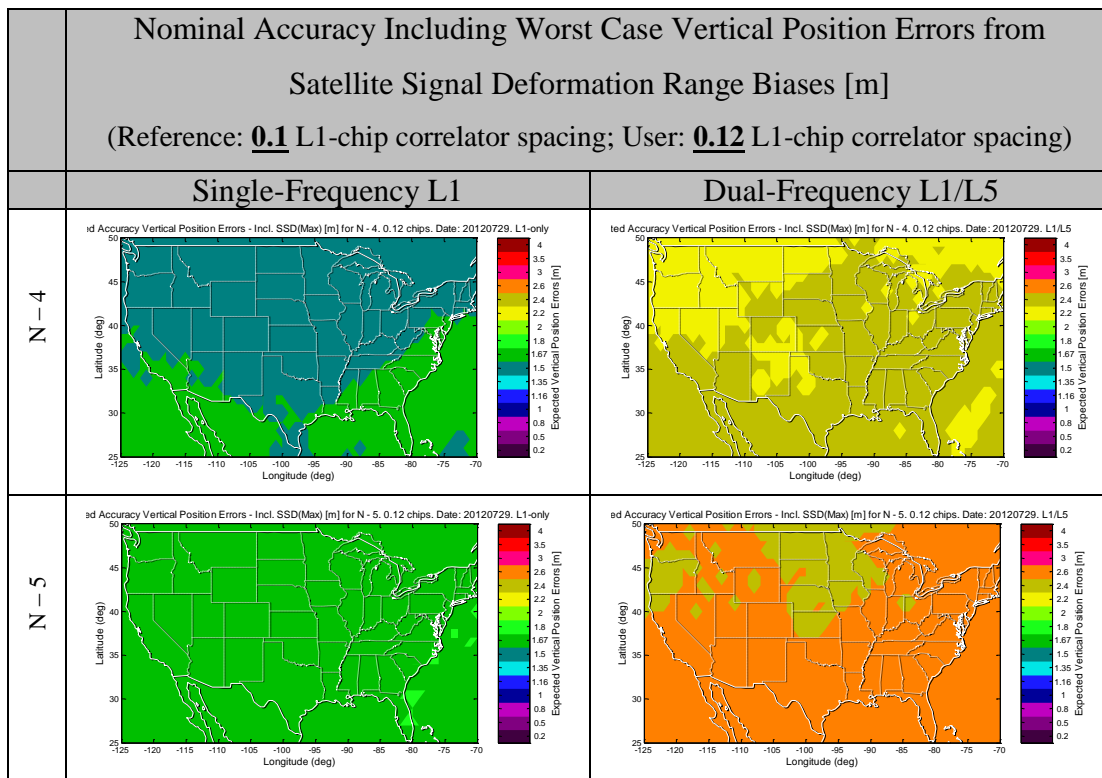
Figure D-14: Nominal Accuracy Including Worst Case Vertical Position Errors from

Satellite Signal Deformation Range Biases [m] for Single Frequency L1-only and

Dual Frequency L1/L5 WAAS Users

(Reference: 0.1 L1-chip correlator spacing; User: 0.12 L1-chip correlator spacing)

7.4 Summary

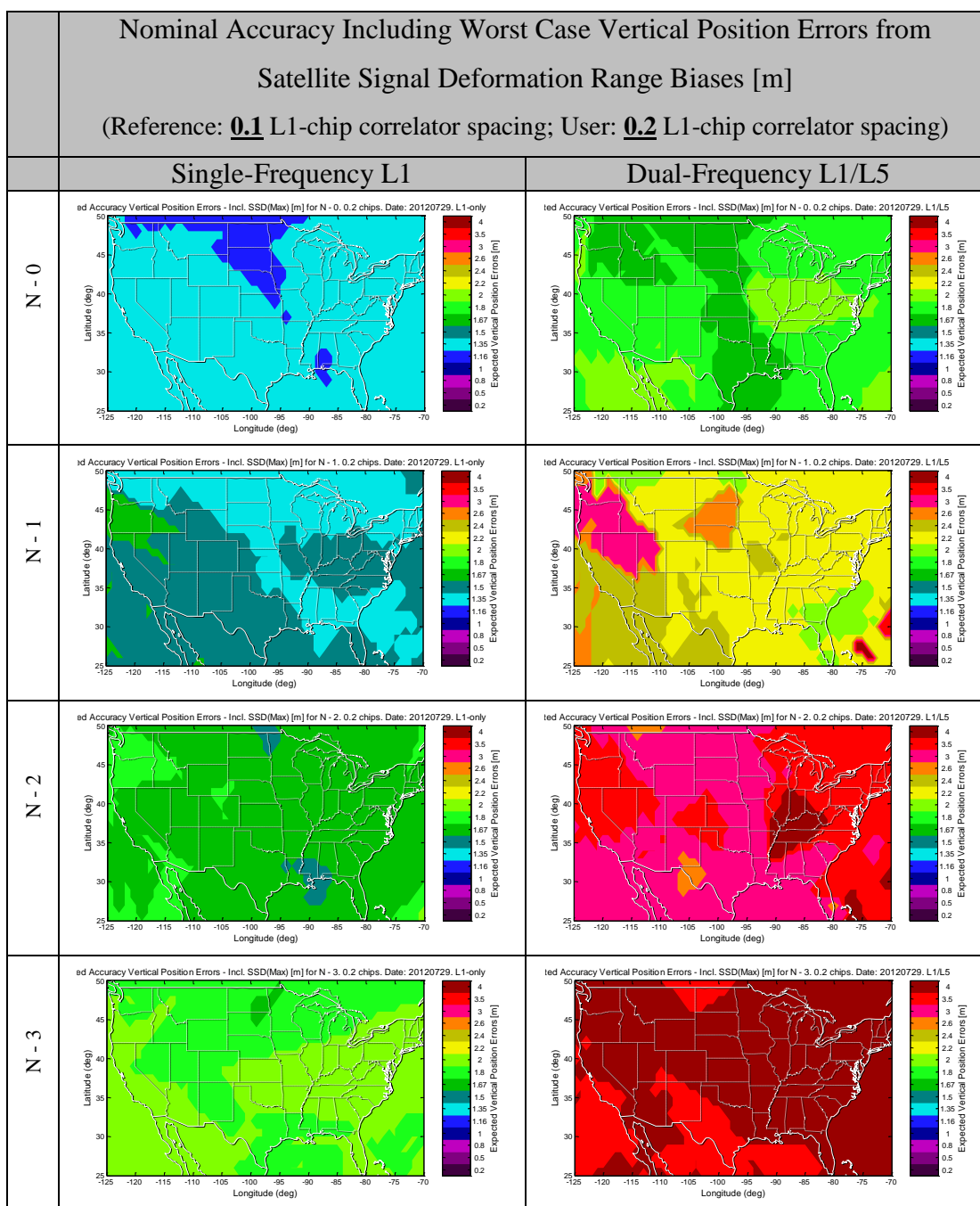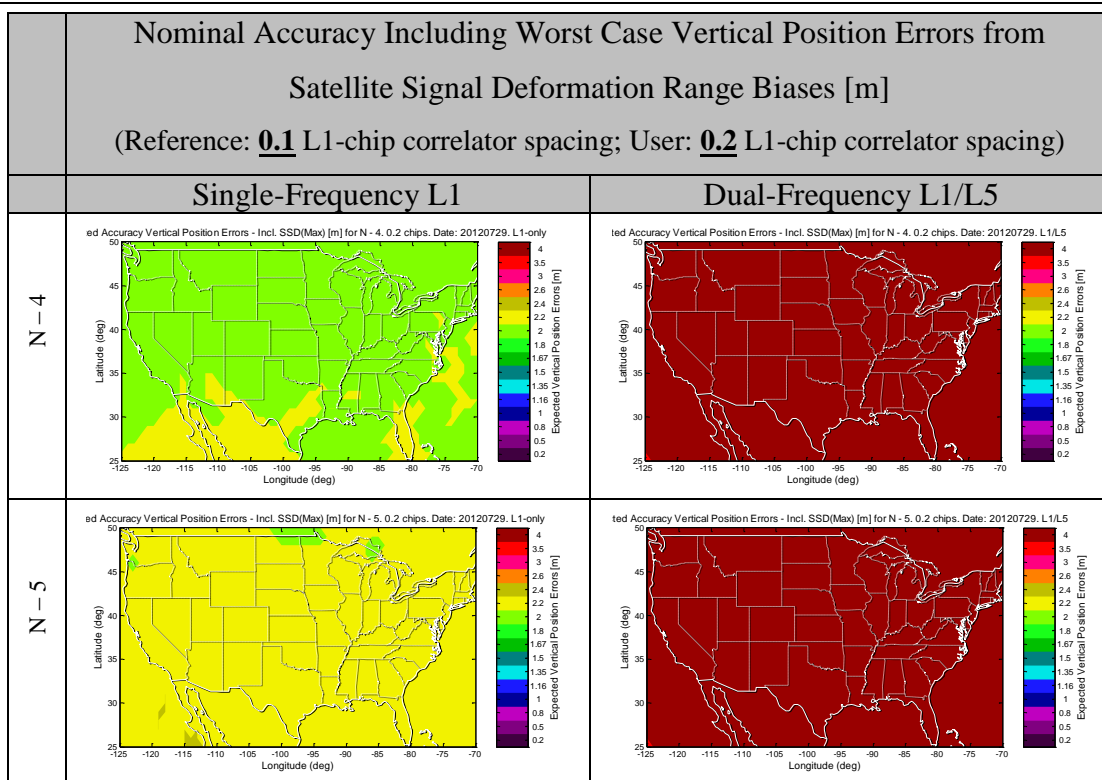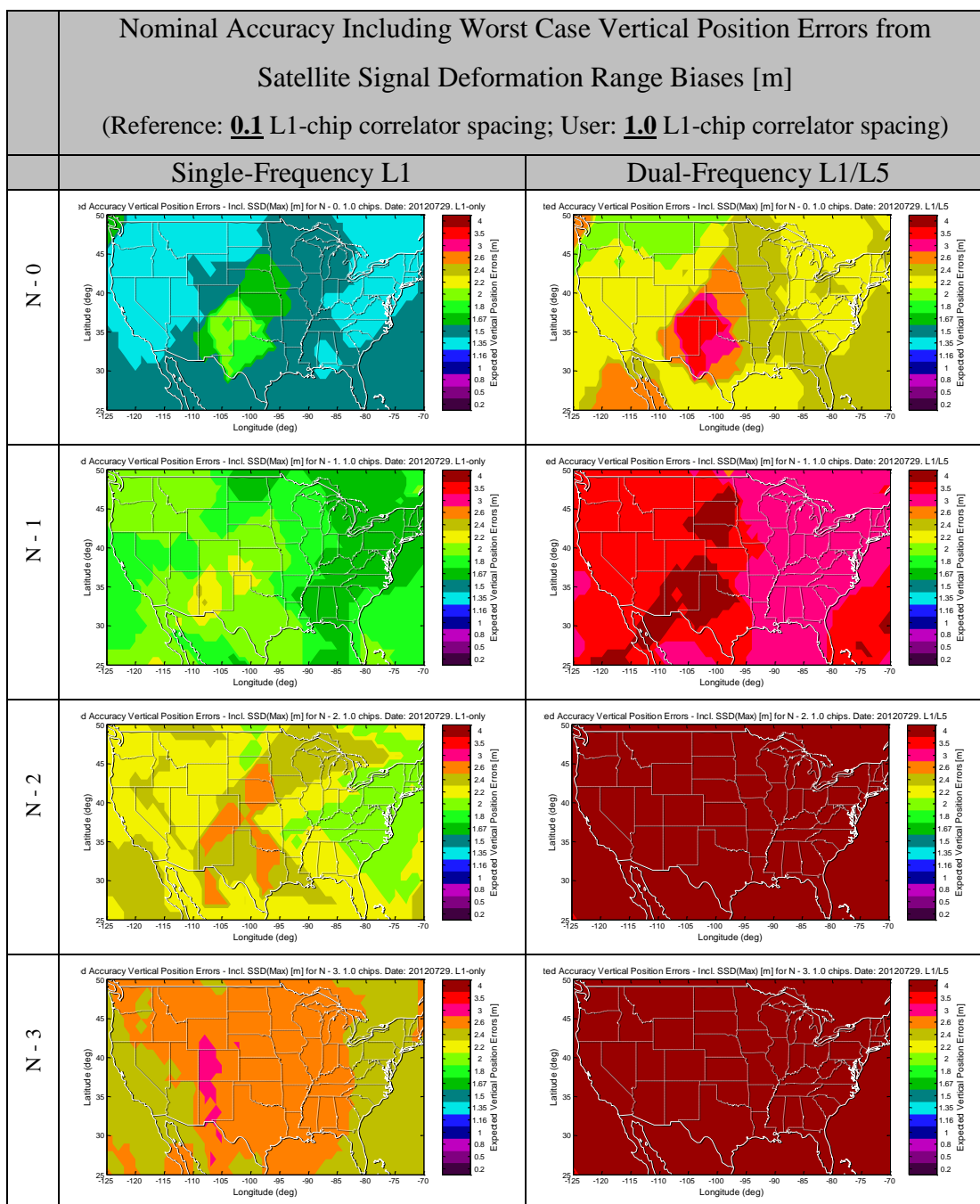| Satellite Status	Nominal Accuracy Including Worst Case Vertical Position Errors from Satellite Signal Deformation Range Biases [m]								
	Single Frequency: L1-Only					Single Frequency: L1-Only			
	User Correlator Spacing [L1-chips]					User Correlator Spacing [L1-chips]			
	No SSD	Unmitigated		Mitigated		No SSD	Unmitigated		Mitigated
	0.10	0.20	1.00	0.12		0.10	0.20	1.00	0.12
N - 0	0.99	1.20	1.41	1.03		1.21	1.74	2.25	1.30
N - 1	1.07	1.39	1.78	1.13		1.31	2.24	3.25	1.47
N - 2	1.16	1.62	2.18	1.24		1.43	3.04	5.06	1.70
N - 3	1.27	1.81	2.43	1.37		1.61	3.80	5.86	1.97
N - 4	1.39	1.96	2.59	1.49		1.82	4.22	6.40	2.22
N - 5	1.50	2.10	2.72	1.61		2.06	4.48	6.77	2.46

Table D-7: Average Nominal Accuracy Including Worst Case Vertical Position Errors

from Satellite Signal Deformation Range Biases [m] for Single Frequency L1-only

and Dual Frequency L1/L5 WAAS Users

Appendix E

Band-limited Square Wave Modulation vs Pulse Shaping

A previous study [84] compared the band-limited square wave modulation (used currently) to more efficient pulse-shaping techniques such as the Square-Root Raised-Cosine technique. Though the Square-Root Raised-Cosine technique achieves good spectral efficiency and utilization, the study concluded that the current modulation technique was much more suitable for GNSS systems.

For GNSS signal transmission, both the narrow bandwidth civil signals ($\pm$ 1 MHz about the center frequency) and the wider bandwidth military signals ($\pm$ 10 MHz about the center frequency) are transmitted in the same bandwidth of as wide as $\pm$18-20

MHz from the center frequency ([19], see also Figure 2-4 [38] and Figure 2-5 [39]). The wide transmission bandwidth allows the transmitted civil signals to maintain sharp correlation peak waveforms in the time domain. These sharp peaks in turn facilitate the use of narrow-correlator algorithms [85], which effectively reduce worst case multipath errors by factors of up to 10 or 20, providing accuracy and integrity benefits.

In contrast, the Raised-Cosine technique limits the signal transmission to a narrow bandwidth. Not only does this deny the use of the multipath-limiting narrow-correlator algorithms, the reduced transmission bandwidth signal is also more susceptible to intentional and unintentional Radio Frequency Interference. In addition, implementation of the Raised-Cosine technique results in increased complexity on the signal transmitters and receivers.

For all these reasons, the current band-limited square wave modulation is preferred to the Raised-Cosine filter modulation in the implementation of GNSS signal modulation and transmission.

Appendix F

GPS L5-Frequency Signal – Characteristics and Advantages

1   Overview

This section introduces in detail the new GPS L5-frequency signal, its characteristics and its navigation performance, advantages to its deployment, and an analysis of the ranging performance improvement over the current traditional L1-frequency signal.

2   Basic Characteristics of the GPS L5-Frequency Signal

The current L1 signal uses Direct-Sequence Spread-Spectrum (DSSS) modulation (Section 1.1.1.2) of chip rate 1.023 Mchips/sec. Past measurements using the large satellite dish showed received spectra which extended out to ± 18-20 MHz from the center frequency of 1575.42 MHz ([18]; see also Figure 2-4 [38]).

In comparison, the L5-frequency signal also uses Direct-Sequence Spread-Spectrum modulation, but has a chip rate a factor of 10 higher, 10.23 Mchips/ sec. Past large satellite dish measurements showed received spectra which also extended out to ± 18-20 MHz from the L5 center frequency of 1176.45 MHz (refer Figure 2-5 [39]).

3   Advantages of the Additional L5-Frequency Signal

This new signal provides some key advantages. It can be used for positioning on its own, providing an additional ranging signal, benefits of signal diversity, and increased navigation robustness.

Due to the higher chip rate, the new L5-frequency signal has a wider frequency spectrum and a narrower correlation peak in time. This provides additional immunity against multipath and Radio Frequency Interference, leading to a reduction in ranging errors.

The L5 frequency signal can also be used together with the current legacy L1 GPS signal to remove ionospheric errors, the largest current integrity threat and source of errors.

As of current writing (December 2013), there are four new GPS satellites which broadcast this new signal together with previous legacy signals, with more to be launched in the future. Full operational capability is expected to be reached in 2021 [86].

4   Ranging performance improvement of L5-Frequency Signal over L1-Frequency signal

This section discusses the performance of the GPS L5-frequency signal relative to the L1-frequency signal. The current L1 signal uses direct-sequence spread-spectrum modulation (Section 1.1.1) of chip rate 1.023 Mchips/sec, while the L5-frequency signal also uses direct-sequence spread-spectrum modulation, but at a chip rate 10 times higher, 10.23 Mchips/ sec.

Due to the higher chip rate, the new L5-frequency signal has a wider frequency spectrum and a narrower correlation peak in time. This provides additional immunity against multipath and Radio Frequency Interference (RFI), leading to a reduction in ranging errors.

Comparing the navigation performance of the L5 signal in a receiver with a front-end bandwidth of 20 MHz, with that of the L1 signal in a narrowband receiver with a front-end bandwidth of 2 MHz, the expected performance gain would be expected to be 10 times. However, compared to wideband L1 receivers with a front-end bandwidth of 20 MHz, the reduction may only be by a factor of approximately 3 times.

This is because the legacy L1 signal is a 1.023 Mchips/sec signal transmitted in a bandwidth much wider than the main lobe of ±1 MHz. Past satellite dish measurements showed that the transmitted frequency spectrum extended possibly beyond ±18-20 MHz (Ref: [18]; refer also Figure 2-4 [38]). In contrast, the L5 signal is a 10.23 Mchips/sec signal also transmitted in the same bandwidth (refer to Figure 2-5 [39]) rather than 10 times larger.

For the L1-frequency signal, the additional transmission bandwidth allows passage of the sidelobes in addition to the mainlobes. This results in a narrow correlation peak which is transmitted by the satellite and received by the user receiver. Established narrow-correlator code-tracking techniques are able to track the signal near the peak of the narrow correlator triangle, providing additional immunity against multipath and radio-frequency interference [85].

Unfortunately, in comparison, the same transmission bandwidth passes relatively less of the additional sidelobes of the wider-bandwidth L5-frequency signal. A more rounded correlation peak is transmitted by the satellite and received by the user

receiver. Consequently, narrow correlator code-tracking techniques would not be as useful.

Further analysis from past research showed that the L5-frequency signal had an RMS signal bandwidth three times wider than the L1-frequency signal [87]. This would result in a predicted factor of three improvement in ranging performance. Simulation results show an mprovement by a factor of 2-3 [88].

These results are similar to earlier published research comparing the GPS L1-C/A code signal with the GPS L1-P code signal, a similar signal to the GPS L5-frequency signal [89]. Prior to military encryption, the GPS L1-P code signal was unrestricted for public use. It had a chipping rate and transmission bandwidth similar to the new GPS L5 frequency signal, 10.23 Mchips/sec, or 10 times that of the GPS L1-C/A signal. Compared to a regular GPS-L1-C/A code receiver, the GPS-L1-P code did indeed have a ranging performance 10 times as good. However, when narrow-correlator technology was employed in the GPS-L1-C/A code receiver, the GPS-L1-C/A code receiver was able to achieve similar ranging performances to the GPS-L1-P code receiver. Another researcher cites improvements of a factor of 2-3 for the GPS-L1-P code compared to the GPS-L1-C/A [90].

REFERENCES

[1] FAA, "Navigation Programs - Wide Area Augmentation System (WAAS)," 16 August 2010. [Online]. Available: http://www.faa.gov/about/office_org/headquarters_offices/ato/service_units/tech ops/navservices/gnss/waas/. [Accessed 2 March 2014].

[2] R. E. Phelts and et. al, "Signal Deformation Monitoring for Dual-Frequency WAAS," in *Proceedings of the 2013 International Technical Meeting of The Institute of Navigation*, San Diego, California, 2013.

[3] P. Daly, S. Riley and P. Raby, "Recent Advances in the Implementation of GNSS," Proceedings of the 6th International Technical Meeting of the Satellite Division of The Institute of Navigation (ION GPS 1993), Salt Lake City, UT , 1993.

[4] B. D. Nordwall, "Filter Center," *Aviation Week and Space Technology, Vol. 139, No. 4,* p. 53, 26 July 1993.

[5] C. Edgar, F. Czopek and B. Barker, "A Co-operative Anomaly Resolution on PRN-19," in *Proceedings of the 12th International Technical Meeting of the Satellite Division of The Institute of Navigation (ION GPS 1999)*, Nashville, TN, 1999.

[6] R. Kalafus, "A New Error Source In Differential GNSS Operations," White Paper, Trimble Navigation, 1993.

[7] A. Mitelman, "Signal Quality Monitoring for GPS Augmentation Systems, Chapter 6," Doctoral Dissertation, Stanford University, December 2004.

[8] M. Brenner, R. Reuter and B. Schipper, "GPS Landing System Multipath Evaluation Techniques and Results," in *Proceedings of the 11th International*

Technical Meeting of the Satellite Division of The Institute of Navigation (ION GPS 1998), Nashville, TN, September 1998.

[9] C. Macabiau and E. Chatre, "Signal Quality Monitoring for Protection of GBAS Users Against Evil Waveforms," in *Proceedings of the 13th International Technical Meeting of the Satellite Division of The Institute of Navigation (ION GPS 2000)*, Salt Lake City, UT , 2000.

[10] C. Macabiau, W. Vigneau and D. Houzet, "Test-Bed for Evaluation of Impact of Evil Waveforms on Real Receivers and SQM Performance," in *Proceedings of the 15th International Technical Meeting of the Satellite Division of The Institute of Navigation (ION GPS 2002)*, Portland, OR , September 2002.

[11] A. J. Van Dierendonck and et. al, "Practical Implementation Considerations in the Detection of GPS Satellite Signal Failure," in *Proceedings of the IAIN World Congress and the 56th Annual Meeting of The Institute of Navigation*, San Diego, CA , June 2000.

[12] A. S. Bruce and et. al, "Detection of GPS Satellite Signal Failures in Satellite Based Augmentation Systems (SBAS)," in *Proceedings of the 13th International Technical Meeting of the Satellite Division of The Institute of Navigation (ION GPS 2000)*, Salt Lake City, UT , 2000.

[13] D. Akos and et. al, "Signal Quality Monitoring: Test Results," in *Proceedings of the 2000 National Technical Meeting of The Institute of Navigation*, Anaheim, CA , Jan 2000.

[14] S. Gunawardena and F. van Graas, "Analysis of GPS Pseudorange Natural Biases using a Software Receiver," in *Proceedings of the 25th International Technical Meeting of The Satellite Division of the Institute of Navigation (ION GNSS 2012)*, Nashville, TN, September 2012.

[15] P. Enge, R. E. Phelts and A. Mitelman, "Detecting Anomalous Signals from GPS Satellites for the Local Area Augmentation System (LAAS)," Presented as Working Paper 19 to GNSS Panel meeting, 18–29 October 1999.

[16] R. E. Phelts, "Multicorrelator Techniques for Robust Mitigation of Threats to GPS Signal Quality," Doctoral Dissertation, Stanford University, June 2001.

[17] D. M. Akos and et al., "High Gain Antenna Measurements and Signal Characterization of the GPS Satellites," in *Proceedings of the 17th International Technical Meeting of the Satellite Division of The Institute of Navigation (ION GNSS 2004)*, Long Beach, CA, September 2004.

[18] M. Pini and et al., "Analysis of GNSS Signals as Observed via a High Gain Parabolic Antenna," in *Proceedings of the 18th International Technical Meeting of the Satellite Division of The Institute of Navigation (ION GNSS 2005)*, Long Beach, CA , 2005.

[19] M. Pini and D. Akos, "Exploiting GNSS signal structure to enhance

observability," in *Aerospace and Electronic Systems, IEEE Transactions on, vol.43, no.4*, October 2007.

[20] A. M. Mitelman and et al., "Signal Deformations On Nominally Healthy GPS Satellites," in *Proceedings of the 2004 National Technical Meeting of The Institute of Navigation*, San Diego, CA, January 2004.

[21] C. J. Hegarty and A. J. Van Dierendonck , "Recommendations on Digital Distortion Requirements for the Civil GPS Signals," in *Proceedings of IEEE/ION PLANS 2008*, Monterey, CA , 2008.

[22] M. Brenner, P. Kline and R. Reuter, "Performance of a Prototype Local Area Augmentation System (LAAS) Ground Installation," in *Proceedings of the 15th International Technical Meeting of the Satellite Division of The Institute of Navigation (ION GPS 2002)*, Portland, OR, 2002.

[23] F. Liu, M. Brenner and C. Y. Tang, "Signal Deformation Monitoring Scheme Implemented in a Prototype Local Area Augmentation System Ground Installation," in *Proceedings of the 19th International Technical Meeting of the Satellite Division of The Institute of Navigation (ION GNSS 2006)*, Fort Worth, TX, 2006.

[24] S. Gunawardena and F. van Graas, "High Fidelity Chip Shape Analysis of GNSS Signals using a Wideband Software Receiver," in *Proceedings of the 25th International Technical Meeting of The Satellite Division of the Institute of Navigation (ION GNSS 2012)*, Nashville, TN, September 2012.

[25] UNAVCO, Formerly University NAVSTAR Consortium, "General Information - GNSS Modernization | UNAVCO," UNAVCO, Inc (non-profit university-governed consortium), 21 Apr 2014. [Online]. Available: https://facility.unavco.org/general-info/gnss-modernization/gnss-modernization.html. [Accessed 28 Apr 2014].

[26] International GNSS Service (IGS), "IGS - MGEX (International GNSS Service - Multi-GNSS Experiment)," 23 Mar 2014. [Online]. Available: http://www.igs.org/mgex/. [Accessed 28 Apr 2014].

[27] National Coordination Office for Space-Based Positioning, Navigation, and Timing, "GPS.gov: New Civil Signals," 6 Feb 2014. [Online]. Available: http://www.gps.gov/systems/gps/modernization/civilsignals/. [Accessed 2 Mar 2014].

[28] International Telecommunication Union (ITU), "Radio Regulations 2012," 2014. [Online]. Available: http://www.itu.int/pub/R-REG-RR-2012. [Accessed 2 Mar 2014].

[29] International Telecommunication Union (ITU), "Radio Regulations Edition of 2012," 2012.

[30] Agilent Technologies, Inc, "Testing and Troubleshooting Digital RF

Communications Receiver Designs," Agilent Technologies, Inc, USA, 2002.

[31] Wikipedia, "GPS Signals - Wikipedia, the free Encyclopedia," 26 February 2014. [Online]. Available: http://en.wikipedia.org/wiki/GPS_signals. [Accessed 24 March 2014].

[32] P. H. Dana, "The Global Positioning System - Signals.gif," The Geographer's Craft Project, Department of Geography, The University of Colorado at Boulder, 01 May 2001. [Online]. Available: http://www.colorado.edu/geography/gcraft/notes/gps/gif/signals.gif. [Accessed 24 March 2014].

[33] Global Positioning Systems Directorate, "IS-GPS-200G: Navstar GPS Space Segment/ Navigation User Interfaces: Systems Engineering & Integration Interface Specification," 05 September 2012. [Online]. Available: http://www.gps.gov/technical/icwg/IS-GPS-200G.pdf. [Accessed 24 March 2014].

[34] Global Positioning Systems Directorate, "IS-GPS-705C: Navstar GPS Space Segment/ User Segment L5 Interfaces: Systems Engineering & Integration Interface Specification," 05 September 2012. [Online]. Available: http://www.gps.gov/technical/icwg/IS-GPS-705C.pdf. [Accessed 24 March 2014].

[35] R. Gold, "Optimal binary sequences for spread spectrum multiplexing (Corresp.)," *IEEE Transactions on Information Theory,* vol. 13, no. 4, pp. 619-621, Oct 1967.

[36] National Coordination Office for Space-Based Positioning, Navigation, and Timing, "GPS.gov: Interface Control Documents: IS-GPS-200G: interface requirements between the GPS space and user segments for radio frequency link 1 (L1) and link 2 (L2)," 26 Feb 2014. [Online]. Available: http://www.gps.gov/technical/icwg/. [Accessed 2 Mar 2014].

[37] National Coordination Office for Space-Based Positioning, Navigation, and Timing, "GPS.gov: Interface Control Documents: IS-GPS-705C: interface requirements between the GPS space and user segments for radio frequency link 5 (L5)," 26 Feb 2014. [Online]. Available: http://www.gps.gov/technical/icwg/. [Accessed 2 Mar 2014].

[38] DLR, Stanford, Gibbons Media & Research LLC, "DLR, Stanford Track First GPS IIF Signals; Tests Begin on L5," Gibbons Media & Research LLC, 10 June 2010. [Online]. Available: http://www.insidegnss.com/node/2135. [Accessed 24 March 2014].

[39] DLR, Stanford, Gibbons Media & Research LLC, "Figure 5: On the Air," July 2010. [Online]. Available: http://www.insidegnss.com/node/2184. [Accessed 24 March 2014].

[40] J. Farrell and M. Barth, The Global Positioning System and Inertial Navigation,

McGraw-Hill, 1999.

[41] J. Johnson, "Thermal Agitation of Electricity in Conductors," *Physical Review Vol 32, American Physical Society,* vol. 32, no. 1, pp. 97-109, July 1928.

[42] P. Misra and P. Enge, "Global Positioning System: Signals, Measurements, and Performance (2nd Edition), Sections 10.6-10.7," Lincoln, MA, Ganga-Jamuna Press, 2006, pp. 417-424.

[43] A. J. Van Dierendonck, P. Fenton and T. Ford, "Theory and Performance of Narrow Correlator Spacing in a GPS Receiver," *Navigation: Journal of the Institute of Navigation,* vol. 39, no. 3, pp. 265-283, Fall 1992.

[44] V. Veitsel, A. Zhdanov and M. Zhodzishsky, "The Mitigation of Multipath Errors by Strobe Correlators in GPS/GLONASS Receivers," *GPS Solutions,* vol. 2, no. 2, pp. 38-45, Oct 01 1998.

[45] L. Garin and J. Rousseau, "Enhanced Strobe Correlator Multipath Rejection for Code & Carrier," in *Proceedings of the 10th International Technical Meeting of the Satellite Division of The Institute of Navigation*, Kansas City, MO , 1997.

[46] R. E. Phelts and P. Enge, "The Case for Narrowband Receivers," in *Proceedings of the 2000 National Technical Meeting of The Institute of Navigation*, Anaheim, CA , January 2000.

[47] R. E. Phelts and P. Enge, "The Multipath Invariance Approach for Code Multipath Mitigation," in *Proceedings of the 13th International Technical Meeting of the Satellite Division of The Institute of Navigation (ION GPS 2000)*, Salt Lake City, UT , September 2000.

[48] R. van Nee and et. al, "The multipath estimating delay lock loop: approaching theoretical accuracy limits," in *IEEE Position Location and Navigation Symposium*, Las Vegas, NV, 1994.

[49] L. Weill, "Multipath Mitigation using Modernized GPS Signals: How Good Can it Get?," in *Proceedings of the 15th International Technical Meeting of the Satellite Division of The Institute of Navigation*, Portland, OR, September 2002.

[50] Leslie, M.; Hatch, R.;Gibbons Media & Research LLC, "Ron Hatch: Searching for a Better Way," Jan-Feb 2008. [Online]. Available: http://www.insidegnss.com/node/451. [Accessed 03 Apr 2014].

[51] G. Wong and et al., "Bounding Errors Caused by Nominal GNSS Signal Deformations," in *Proceedings of the 24th International Technical Meeting of The Satellite Division of the Institute of Navigation (ION GNSS 2011)*, Portland, OR, September 2011.

[52] P. Misra and P. Enge, "Global Positioning System: Signals, Measurements, and Performance (2nd Edition), Section 5.4, Table 5.1," Lincoln, MA, Ganga-Jamuna Press, 2006, pp. 174-175.

[53] A. Komjathy and et. al, "The Ionospheric Impact of the October 2003 Storm Event on WAAS," in *Proceedings of the 17th International Technical Meeting of the Satellite Division of The Institute of Navigation*, Long Beach, CA, 2004.

[54] S. Datta-Barua and et. al, "Using WAAS Ionospheric Data to Estimate LAAS Short Baseline Gradients," in *Proceedings of the 2002 National Technical Meeting of The Institute of Navigation*, San Diego, CA, 2002.

[55] Department of Physics, Lancaster University, "Glossary of Terms," 23 May 2011. [Online]. Available: http://spears.lancs.ac.uk/glossary/. [Accessed 24 Mar 2014].

[56] E. Kaplan and C. Hegarty, Understanding GPS: Principles and Applications (1st Edition), Artech House, Feb 1996.

[57] P. Enge and et. al, "Wide area augmentation of the Global Positioning System," *Proceedings of the IEEE,* vol. 84, no. 8, pp. 1063-1088, 1996.

[58] FAA/William J. Hughes Technical Center NSTB/WAAS T&E Team, "WIDE-AREA AUGMENTATION SYSTEM PERFORMANCE ANALYSIS REPORT Report #47," Atlantic City International Airport, NJ 08405, October 1 to December 31, 2013.

[59] J. Rife, "WAAS Functions and Differential Biases," *Inside GNSS,* pp. 18-21, May/ June 2008.

[60] T. Walter, P. Enge and A. Hansen, "A Proposed Integrity Equation for WAAS MOPS," in *Proceedings of the 10th International Technical Meeting of the Satellite Division of The Institute of Navigation*, Kansas, MO, 1997.

[61] B. DeCleene, "Defining Pseudorange Integrity - Overbounding," in *Proceedings of the 13th International Technical Meeting of the Satellite Division of The Institute of Navigation*, Salt Lake City, UT, September 19 - 22, 2000.

[62] J. Rife and et. al, "Paired overbounding and application to GPS augmentation," in *IEEE Position Location and Navigation Symposium*, Monterey, CA, 2004.

[63] SC-159, Radio Technical Commission for Aeronautics (RTCA), "DO-229D Minimum Operational Performance Standards for Global Positioning System/Wide Area Augmentation System Airborne Equipment," Radio Technical Commission for Aeronautics (RTCA), 12/13/2006.

[64] S. Gleason and D. Gebre-Egziabher, "GNSS Applications and Methods, Section 10.5, Functionality of Aviation Augmentation Systems, Rife, J.," Norwood, MA, Artech House, 2009, pp. 252-257.

[65] Y.-H. Chen and et. al, "Real-Time Software Receiver for GPS Controlled Reception Pattern Antenna Array Processing," in *Proceedings of the 23rd International Technical Meeting of The Satellite Division of the Institute of Navigation (ION GNSS 2010)*, Portland, September 2010.

[66] S. Thölert, S. Erker and M. Meurer, "GNSS Signal Verification with a High Gain Antenna – Calibration Strategies and High Quality Signal Assessment," in *Proceedings of the 2009 International Technical Meeting of The Institute of Navigation*, Anaheim, CA, 2009.

[67] R. D. J. van Nee, "GPS Multipath and Satellite Interference," in *Proceedings of the 48th Annual Meeting of The Institute of Navigation*, Dayton, OH, June 1992.

[68] L. Ge, S. Han and C. Rizos, "Multipath Mitigation of Continuous GPS Measurements Using an Adaptive Filter," *GPS Solutions,* vol. 4, no. 2, pp. 19-30, 2000.

[69] S.-S. J. Jan and et. al, "Matlab Simulation Toolset for SBAS Availability Analysis," in *Proceedings of the 14th International Technical Meeting of the Satellite Division of The Institute of Navigation*, Salt Lake City, UT, 2001.

[70] T. Walter, J. Blanch and P. Enge, "Vertical Protection Level Equations for Dual Frequency SBAS," in *Proceedings of the 23rd International Technical Meeting of The Satellite Division of the Institute of Navigation*, Portland, OR, 2010.

[71] RTCA, "Minimum Operational Performance Standards for Global Positioning System/Wide Area Augmentation System Airborne Equipment,," RTCA DO-229D, 2006.

[72] T. Murphy and et. al, "Results from the Program for the Investigation of Airborne Multipath Errors," in *Proceedings of the 2005 National Technical Meeting of The Institute of Navigation*, San Diego, CA, 2005.

[73] J. P. Collins and R. B. Langley, "The residual tropospheric propagation delay: How bad can it get?," in *Proceedings of the 11th International Technical Meeting of the Satellite Division of The Institute of Navigation*, Nashville, TN, 1998.

[74] B. Wanner and D. A. Nelthropp, "Wide Area Augmentation System, LPV200 Vertical Accuracy Assessment," Presentation to ICAO NSP, October 2006.

[75] J. Seo, T. Walter and P. Enge, "Correlation of GPS signal fades due to ionospheric scintillation for aviation applications," *Advances in Space Research,* vol. 47, no. 10, p. 1777–1788, 2011.

[76] C. Carrano and et. al, "Scintillation Characteristics Across the GPS Frequency Band," in *Proceedings of the 25th International Technical Meeting of The Satellite Division of the Institute of Navigation*, Nashville, TN, September 2012.

[77] J. Betz, "Binary Offset Carrier Modulations for Radionavigation," *NAVIGATION, Journal of the Institute of Navigation,* vol. 48, no. 4, pp. 227-246, Winter 2001-2002.

[78] R. E. Phelts, "Range Biases on Modernized GNSS Codes," in *Proceedings of the European Navigation Conference GNSS/TimeNav 2007*, Geneva, Switzerland, 2007.

[79] S. Thoelert, J. Furthner and M. Meurer, "GNSS Survey - Signal Quality Assessment of the Latest GNSS Satellites," in *Proceedings of the 2013 International Technical Meeting of The Institute of Navigation*, San Diego, California , 2013.

[80] G. Wong and et. al, "Characterization of Signal Deformations for GPS and WAAS Satellites," in *Proceedings of the 23rd International Technical Meeting of The Satellite Division of the Institute of Navigation (ION GNSS 2010)*, Portland, OR , September 2010.

[81] P. Fenton and J. Jones, "The Theory and Performance of NovAtel Inc.'s Vision Correlator," in *Proceedings of the 18th International Technical Meeting of the Satellite Division of The Institute of Navigation (ION GNSS 2005)*, Long Beach, CA , September 2005.

[82] R. Phelts and D. M. Akos, "Nominal Signal Deformations: Limits on GPS Range Accuracy," in *The 2004 International Symposium on GNSS/GPS*, Sydney, Australia, December 2004.

[83] Global Positioning Systems Directorate, "IS-GPS-200G: Navstar GPS Space Segment/ Navigation User Interfaces: Systems Engineering & Integration Interface Specification, Section 3.3.1.8: Signal Coherence," 05 September 2012. [Online]. Available: http://www.gps.gov/technical/icwg/IS-GPS-200G.pdf. [Accessed 24 March 2014].

[84] J. A. A. Rodríguez, "On Generalized Signal Waveforms for Satellite Navigation, PhD Thesis," UNIVERSITY FAF MUNICH, Munich, 2008.

[85] A. van Dierendonck, P. Fenton and T. Ford, "Theory and Performance of Narrow Correlator Spacing in a GPS Receiver," *NAVIGATION, Journal of the Institute of Navigation,* vol. 39, no. 3, pp. 265 - 284, 1992.

[86] National Coordination Office for Space-Based Positioning, Navigation, and Timing, "GPS.gov: New Civil Signals," NOAA, 6 February 2014. [Online]. Available: http://www.gps.gov/systems/gps/modernization/civilsignals/. [Accessed 2 Mar 2014].

[87] C. Hegarty, "Evaluation of the Proposed Signal Structure for the New Civil GPS Signal at 1176.45 MHz, Working Note WN99W34," The MITRE Corporation, McLean, VA, 1999.

[88] M. Tran and C. Hegarty, "Receiver Algorithms for the New Civil GPS Signals," in *Proceedings of the 2002 National Technical Meeting of The Institute of Navigation*, San Diego, CA , 2002.

[89] G. Lachapelle, E. Cannon and G. Lu, "A comparison of P code and high performance C/A code GPS receivers for on the fly ambiguity resolution," *Bulletin géodésique (Journal of Geodesy),* vol. 67, no. 3, pp. 185-192, 1993.

[90] Rizos, C., University of New South Wales, School of Surveying & Spatial

Information Systems, Satellite Navigation & Positioning Laboratory (SNAP Lab), "How Good is GPS? The Civilian - Military Relationship and the Impact on GPS Performance," 1999. [Online]. Available: http://www.gmat.unsw.edu.au/snap/gps/gps_survey/chap2/243saas.htm. [Accessed 27 Apr 2014].

[91] C. Hegarty, E. Powers and B. Fonville, "Accounting for the timing bias between GPS, modernized GPS, and Galileo signals," in *Proceedings of the 36th Annual Precise Time and Time Interval (PTTI) Systems and Applications Meeting, pp. 307–317*, Washington, DC, USA, December 2004.

[92] P. Misra and P. Enge, "Global Positioning System: Signals, Measurements, and Performance (2nd Edition), Section 6.1.5," Lincoln, MA, Ganga-Jamuna Press, 2006, pp. 216-217.

[93] A. Mitelman, "Signal Quality Monitoring for GPS Augmentation Systems, Chapter 3," Doctoral Dissertation, Stanford University, December 2004.

[94] GMV, ESA, "GPS Performances," 2011. [Online]. Available: http://www.navipedia.net/index.php/GPS_Performances#cite_note-PPS-Standard-1. [Accessed 27 Apr 2014].